FimH antagonists and their therapeutic options in urinary tract infection

An example of an anti-adhesive therapy for infectious diseases

Inauguraldissertation

zur
Erlangung der Würde eines Doktors der Philosophie
vorgelegt der
Philosophisch-Naturwissenschaftlichen Fakultät
der Universität Basel

von

Anja Carina Sigl
aus Oberbipp, BE

Basel, April 2017

Genehmigt von der Philosophisch-Naturwissenschaftlichen Fakultät

auf Antrag von

Fakultätsverantwortlicher:
Prof. Dr. Beat Ernst
Institut für Molekulare Pharmazie
Universität Basel

Korreferent:
Prof. Dr. med. Niels Frimodt-Møller
Department of Clinical Microbiology
Rigshospitalet, Copenhagen/Denmark

Basel, den 10.11.15

Prof. Dr. Jörg Schibler
Dekan

“Aerodynamically, the bumble bee shouldn't be able to fly, but the bumble bee doesn't know it so it goes on flying anyway.”

Mary Kay Ash

Acknowledgement

First, I wish to express my sincerest gratitude to Prof. Dr. Beat Ernst, who offered me the opportunity to conduct this work in his research group. His constant support, scientific inputs, and guidance were most valuable and I enjoyed the fruitful and humorous discussions. I admire the never-ending energy and dedication he shows towards research, education, and the whole group.

Special thanks go to Prof. Dr. med. Niels Frimodt-Møller, who accepted to be my co-referee for this thesis. Thank you for coming to Basel.

Furthermore, I would like to thank Dr. Justyna Nowakowska and PD Dr. med. Nina Khanna for introducing me to the field of biofilms and supporting me with all these experiments. This support was very valuable.

The time at the Institute of Molecular Pharmacy is full of great memories and a great part of them are due to the fantastic group I was part of. Thank you Daniela, Pascal, and Christoph for your great company in the “Sunnestübli”. Also, I enjoyed working in the PADMET lab with Simon, Jacqueline, and Philipp, having all these (more or less) scientific discussions and your friendship.

Of course, I also want to mention all the rest of former and present group members, I really enjoyed the extremely happy, friendly, and helpful working-atmosphere. Thank you all for your friendship and the great time!

Fortunately, I could also share a lot of interesting scientific discussions and great work with my master students Manuel, Nathalie, Rachel, and Kathrin. It was very instructional to guide them through their work and share their thoughts and experiments. I learned a lot for myself and enjoyed working together in the lab, seeing all finishing their Master degree.

Thanks go to Ueli Schneider and Nicole Caviezel of the animal facility at the Department of Biomedicine, who let me perform the animal studies in their facility and supported me with help and advice. In this context, I also want to thank Prof. Dr. med. Radek Skoda for taking over responsibility for the *in vivo* studies in the first two years of my thesis. Many thanks go to Gabriele Mild and Dr. med. vet. Bettina Oswald for their help with the renewal of the application and the electronic platform. Their contributions were most appreciated for all the studies I performed.

Further acknowledgements also go to Alexia Loynton-Ferrand and Oliver Biehlmaier from the Imaging Core Facility and Janine Zankl from the FACS Core Facility of the University of Basel for their introduction into and help with microscopy and flow cytometry.

Finally, I thank my family and friends who supported me during this thesis. They always listened and encouraged me, when I needed it. It is great to have their support and knowing they will always be there.

Mostly, I owe my deepest gratitude to Michele, who has a talent for positive thinking and seeing everything in a different light. Thank you for all the jogging rounds we did together, where you listened patiently and gave advices. Thank you for all your encouragements, your understanding, and your love. Thank you for being the other half of my life.

Abstract

FimH antagonists are small molecule inhibitors, derived from α-D-mannose, which block the adhesion of uropathogenic Escherichia coli (UPEC) to bladder cells. The abolition of binding leads to clearance of the bacteria with the urine flow and prevents urinary tract infections (UTIs). Within this thesis, the merits as well as problems of an anti-adhesive therapy (in the context of the infection cycle of UTI) as an alternative approach to combat bacterial infections are described.

Previous reports showed successful applications of FimH antagonists *in vitro* and *in vivo.* The antagonists reduced bacterial attachment to cells and surfaces and decreased bladder infections in a UTI mouse model. Within this thesis, FimH antagonists from our group were screened for their minimal anti-adhesive concentration (MAC_{90}) using an *in vitro* cell infection assay. The minimal therapeutic concentration was analyzed in the context of the pharmacokinetic (PK) performance of individual antagonists. It could be shown, that a preventive application and the resulting peak concentration of a FimH antagonist in the urine relative to the MAC_{90} value is predictive for positive treatment outcome. Guided by this finding, several treatment regimens, including combination therapies with antibiotics, were successfully applied to reduce bladder infections in an experimental mouse model by up to three orders of magnitude. Furthermore, FimH antagonists were effective against catheter-associated UTI (CAUTI), assessed by a newly established 96-well screening assay, using catheter pieces and human urine. They prevented biofilm formation in concentrations as low as 6.25 µg/ml. Moreover, in all tested applications, FimH antagonists exhibited a synergistic effect with ciprofloxacin (CIP), implying the possibility of combination therapies.

Antagonizing the FimH lectin proofed cumbersome, because depending on the UPEC strain, the FimH binding pocket exhibits different affinity states towards mannose ligands. This leads to different MAC_{90} values for every individual strain and a specific antagonist. Besides, different strains vary in their infection course over longer time periods, probably related to the different affinity state of the FimH lectin.

Consequently, the differences in affinity in combination with the infection time course might strongly influence treatment regimens, which will be an important topic of future investigations.

Contents

Abbreviations

AC3	Adenylylcyclase 3
Ag43	Antigen 43
BCS	Biopharmaceutical classification system
BSA	Bovine serum albumin
CAUTI	Catheter-associated urinary tract infection
CFU	Colony forming units
CIP	Ciprofloxacin
CK2	Casein kinase 2
CNF-1	Cytotoxic necrotizing factor – 1
CRD	Carbohydrate recognition domain
CRP	cAMP-receptor protein
CV	Crystal violet
DHF-A/THF-A	di- and tetrahydrofolic acid
EPS	Extracellular polymeric substance
FAK	Focal adhesion kinase
FCS	Fetal calf serum
FSC	Forward scatter (flow cytometry)
GFP	Green fluorescent protein
Hly A	Hemolysin A
hpi	Hours post infection
HSV-2	Herpes simplex virus 2
i.v.	Intravenously
IBC	Intracellular bacterial communities
IC_{50}	Inhibitory concentration 50 (concentration that inhibits binding by 50%)
IFN-β	Interferon- β
IL-6/8	Interleukin – 6/8
LB	Luria-Bertani medium
LPS	Lipopolysaccharide
MAC_{90}	Minimal anti-adhesive concentration

MIC	Minimal inhibitory concentration
MOI	Multiplicity of infection (bacteria per cell)
OD_{600}	Optical density at 600 nm
p.o.	Per os
PABA	*Para*-aminobenzoic acid
PAMP	Pathogen associated molecular pattern
PAMPA	Parallel artificial membrane permeability assay
PBS	Phosphate buffered saline
PD	Pharmacodynamics
PI-3	Phosphatidylinositol-3 (kinase)
PK	Pharmacokinetics
PK/PD	Pharmacokinetics/pharmacodynamics
QIR	Quiescent intracellular reservoirs
rpm	Rounds per minute
rUTI	Recurrent UTI
s.c.	Subcutaneously
SSC	Side scatter (flow cytometry)
TBS	Tris-buffered saline
THP	Tamm-Horsefall Protein
TLR4	Toll-like receptor 4
TMP/SMZ	Trimethoprim/Sulfamethoxazole
UP	Uroplakin (several subunits: UP1a, UP1b, UP2, UP3a)
UPEC	Uropathogenic *Escherichia coli*
UTI	Urinary tract infection
VUR	Vesicourethral reflux

1. Introduction

1.1. Urinary tract infection

Urinary tract infection (UTI) is a highly prevalent infection worldwide, both in the community, and in hospital settings. Statistically, 50% of all women endure at least one episode of symptomatic UTI in their lifetime. Furthermore, the recurrence rate within six months is 25%, of which 3% experience a third UTI episode in the following six months.[1–3] Thereby, the strain causing a recurrent UTI (rUTI) is often genetically identical to the strain that caused the first infection.[4–6]

Particularly affected are young, sexually active women. By the age of 24, one third reported at least one physician-diagnosed UTI with medication prescription.[1,7] Although the incidence is decreasing with age - women in the age group between 55-59 have the lowest incidence rate with 6.4% - older patients show a longer symptom duration.[7,8] Overall, Foxman *et al.* estimated the annual costs of community acquired UTI in the United States to be 1.6 billion US dollars. [1,7]

A UTI episode is classified as uncomplicated or complicated. An uncomplicated UTI occurs in patients with a normal urinary tract anatomy, requires short-term treatment, and normally has no future medical consequences. Patients enduring a complicated UTI suffer from other co-morbidities, such as anatomical abnormalities in the urinary tract, diabetes, immunosuppression, pregnancy, prior pyelonephritis, catheterization, or are infected with a multi-resistant strain. Treatment of a complicated UTI is more complex and the infection can result in renal damage.[1,9,10]

In up to 90% of the uncomplicated, community-acquired cases, uropathogenic *E. coli* (UPEC) is the causing pathogen.[1,9] It is followed by *Staphylococcus saprophyticus* with incidences between 10-15%, depending on the country.[2,11] A complicated UTI can also be caused by *Klebsiella spp.*, *Enterobacter spp.*, *Serratia spp.*, and *Proteus spp.,* as well as *Staphylococci* and *Enterococci.*[2,9,10]

Uropathogenic bacteria possess several virulence factors that enhance the urologic infection potential. One of those, are the bacterial adhesins.

1.2. Adhesins as important virulence factors for UTI

UPEC possesses several distinct adhesins, providing the urinary tract colonizing advantage. Some of them are not expressed or genetically not encoded on the fecal relatives.[12]

However, type 1 pili (also termed type 1 fimbriae), the adhesin most often connected to UTI, is common within the family of Enterobacteriaceae.[13–15] Wu *et al.* were the first to report the binding of type 1 pili to uroplakin expressed on the urothelial cell surface.[16] Adhesion is the first step in the UTI infection cycle, it is mediated by the FimH lectin, located at the tip of type 1 pili.[17] *E. coli* isolates expressing type 1 fimbriae were connected to a higher disease severity compared to non-expressing bacteria, resulting in longer bacterial persistence and higher inflammatory responses in the urinary tract of children.[18]

Other important adhesins are the P pili. They are important in more advanced infection stages of UTI, especially for developing pyelonephritis.[19–21] Four genetic classes of *PapG* were discovered (I-IV).[22] Only class II PapG adhesins recognize the α-D-Gal-1-4-β-D-Gal pattern of glycolipid receptors expressed in human kidneys.[23] Therefore, class II is specifically associated with upper urinary tract infection.[24,25]

Both, type 1 and P pili were associated with bacteriuria and are responsible for the activation of the host's immune system.[18,26–30] Type 1 pili also bind to the Tamm-Horsefall-Protein (THP), the most ample glycoprotein in human urine, which contains a highly mannosylated moiety.[31–33] THP is generated by the epithelial cells lining the thick ascending loop of Henle and can be released into the urine. It is assumed to be important in the regulation of the electrolyte balance in the urine, but it also modifies immune responses and protects against UTI by binding to type 1 fimbriae and abolishing attachment to bladder cells.[33–36]

Further adhesins, such as type 3 fimbriae, S fimbriae, Dr adhesins, Ag43, curli, and F1C fimbriae can mediate adhesion in a specific infectious context, inter alia, in the urinary tract.[19–21] For some of them, the relation to UTI is ambiguous. Still, type 1

and type 3 fimbriae, Ag43, and curli are important in biofilm formation, which is a central part in the uropathogenic infection cycle (see chapter 1.7.).[19,37–39]

1.3. Type 1 pili and mannose – the discovery of the importance in UTI

In the 1970's, it was discovered that binding of bacteria to host tissue is a prerequisite for an infection. In 1972, Old characterized D-mannose and various mannose derivatives as strong inhibitors of type 1 fimbrial dependent hemagglutination of guinea pig and horse erythrocytes with *Shigella flexneri* and *Salmonella typhimurium*.[40] Only five years later, Ofek *et al.* demonstrated a D-mannose specific adhesion of *E. coli* to human mucosal cells.[41] Several reports followed confirming the mannose-dependent binding of type 1 pili; e.g., by Firon *et al*., who studied the inhibition of the binding of *E. coli* to mannan-containing yeast cells by different oligomannosides, or by Neeser *et al*., who tested plant glycoproteins for their inhibitory potential of bacterial adhesion to guinea pig erythrocytes and buccal epithelial cells.[42,43]

In 1978, the connection between type 1 pili and UTI was reported for the first time. There was a significant correlation between the presence of fimbriae on *E. coli* isolated from patients with UTI and the adhesion to human urinary tract epithelial cells, described by Eden *et al*.[44] Furthermore, over 400 *E. coli* strains were systematically tested for their ability to bind to human urinary tract epithelial cells, resulting in the hypothesis that type 1 fimbrial adhesion is a virulence factor selecting for uropathogenicity of those isolates.[45] In the same period, Aronson *et al.* used the previously established pyelonephritis mouse model by Freedman to test the potential of inhibiting a murine bladder infection caused by type 1 fimbriae producing *E. coli* with methyl α-D-mannopyranoside.[46] They were able to reduce the occurrence rate of UTI by approximately two thirds.[47] Ultimately, Hagberg *et al.* reported a detailed study about a reproducible UTI mouse model in 1982, which boosted research in the field of UTI.[48] Based on these findings and the fact that UPEC defective in type 1 fimbriae showed 100-1000 fold lower bacterial counts in the bladder, type 1 fimbriae

were confirmed as a key virulence factor for the development of UTI in mice.[49] Furthermore, Fujita *et al.* pictured the binding of *E. coli* to formalin fixed human ureteral epithelial cells from a female patient with a renal cell carcinoma and could show the inhibition of bacterial adherence with the addition of D-mannose by scanning electron microscopy.[50]

A single *E. coli* expresses between 100-500 type 1 fimbriae. They are peritrichously arranged, approximately 7 nm in diameter, and between 0.2 to 2 µm long.[14,51] Type 1 fimbriae consist of several subunits, arranged in the following order: FimA-FimF-FimG-FimH.[51] Although not necessary for the expression of type 1 fimbriae, the latter was shown to be the responsible subunit for mannose-sensitive binding to bladder epithelial cells.[52,53] Yet, type 1 fimbriae are not only the important mediator for adhesion, but also for subsequent cell entry, which was shown by Martinez *et al.* using latex beads coated with FimH to invade bladder cells via a zipper-like mechanism. Additionally, the invasion of FimH covered latex beads required reorganization of the actin skeleton, which was inhibited by the addition of D-mannose. The PapG adhesin did not lead to bead or bacterial uptake into cells.[54]

Interestingly, type 1 fimbriae are genetically encoded in uropathogenic isolates and fecal strains, but *fim* gene expression is regulated in a phase-variable manner.[12] The gene expression for the fimbrial subunits can be switched “on” or “off”. This occurs via an invertible DNA element, which contains the promotor for the expression of the main subunit of type 1 fimbriae, the FimA. The inversion is mediated by FimB or FimE, both recombinases.[19,55–57] FimB is able to switch from “on” to “off” and vice versa, whereas, FimE only switches to the “off” position.[57] During experimental murine UTI, it was demonstrated that type 1 fimbriae expression was switched “on” in all bacteria from urine, bladder, and kidneys. On the other hand, only roughly 25% express type 1 fimbriae in *in vitro* broth cultures.[56] The expression of FimB and FimE, ultimately controlling type 1 pili expression, are dependent on environmental growth factors. Low pH and high osmolarity favor the expression of FimE but repress expression of FimB, resulting in restricted expression of type 1 pili. These conditions are present in the human kidneys, whereas, in the bladder, the expression of type 1 fimbriae is favored because of neutral pH and low osmolarity.[57]

Besides pH and osmolarity, also temperature, carbon and amino acid sources, availability of oxygen, and growth media can influence type 1 fimbriae expression.[56,57] Of importance, glucose induces a cAMP-receptor protein (CRP) driven pathway leading to the inversion of *fimB*, resulting in type 1 fimbriae expression (Figure 1).[58] In summary, the presence of the *fim* gene in the bacterial genome is a prerequisite, but the expression of type 1 pili is crucial for UTI. Mutants locked in the "off" position were outcompeted by the wild-type in a mouse model of UTI in all compartments; urine, bladder, and kidneys.[59]

1.4. Cellular processes upon infection

Uroplakin 1a (UP1a), the binding partner of type 1 pili, is part of a hexagonal complex called plaques. Plaques are built of four uroplakin subunits, UP1a, UP1b, UP2, and UP3a.[20,60–63] They are important for flexibility, stability, and barrier function of the bladder and cover most of the luminal surface.[20,60] Plaques are part of lipid rafts, which are membrane domains containing high contents of lipids and proteins, such as cholesterol, sphingolipids, and caveolin-1.[61] Lipid rafts itself are membrane parts of fusiform vesicles. They undergo exocytosis when the bladder is stretched and are endocytosed when the bladder relaxes. This mechanism of membrane storage enables expansion and reduction of the bladder surface and is important to adapt to high stretching forces during urine accumulation.[61,64,65] With UPEC binding to UP1a, the bacteria are internalized within the fusiform vesicles and enter luminal surface cells upon bladder emptying.[66] Hence, UPEC employs a normal physiological mechanism for internalization, which is not only triggered by bladder extension and relaxation, but also via secondary messengers and complex signaling pathways.

Within the tetramer of the uroplakin subunits, UP1a builds a heterodimer with UP3, which has a cytoplasmic domain and functions as a signal transducer.[67] After binding of UPEC to UP1a, UP3 is phosphorylated at T244 by the casein kinase II (CK2), which leads to intracellular rising Ca^{2+} levels.[67] This triggers several downstream effects, such as increasing cAMP levels, which in turn results in cytokine production

via activation of the transcription factor CREB, or in exocytosis of fusiform vesicles, both defense mechanisms against invading UPEC (Figure 1).[62,64,66,67]

Eto *et al.* showed, that UPEC also binds to β1 and α3 integrins on the bladder cell surface. They proposed an alternative way of entering the bladder cell. Integrins contain high-mannose glycan structures similar to UP1a and appear in complexes.[68] The binding of UPEC to integrins leads to the autophosphorylation of FAK, which in turn triggers the PI-3 kinase and the activation of Rac1 Rho-family GTPase, involved in the modification of the actin skeleton of the cell. Actin rearrangement is necessary for endo- and exocytosis of fusiform vesicles.[69]

Once inside the cell, UPEC start to replicate and form intracellular bacterial communities (IBC).[65,66,70–72]

In the bladder, UPEC are also recognized by the immune system, via toll-like receptor 4 (TLR4) in complex with CD14. Thereby, TLR4 is a prominent receptor on bladder and kidney cells.[20,65,66,73] It recognizes lipopolysaccharides (LPS) and type 1 fimbriae and induces the transcription of IL-6 and IL-8, which attract neutrophils to the site of infection (Figure 1).[66,67,74–77] UPEC counteracts with the secretion of cytotoxic necrotizing factor – 1 (CNF-1), interfering with neutrophil chemotaxis.[66]

Another downstream effect of TLR4 stimulation, is the activation of the adenylyl cyclase 3 (AC3), again resulting in increased cAMP levels. As mentioned earlier, this provokes exocytosis of fusiform vesicles and simultaneously blocks their endocytosis. Thus, both GTPases, Rac-1, important for actin remodeling in lipid rafts to allow endocytosis, as well as Rab27, responsible for the delivery of fusiform vesicles to the apical surface of the bladder cells, are influenced by intracellular cAMP levels.[60,61,63,64,66,74,78]

Of interest, Ashkar *et al.* argued that the FimH protein alone is the pathogen associated molecular pattern (PAMP) that initiates the TLR4 pathway. They could show, that cells and mice infected with purified FimH protein were up-regulating the immune response resulting in IFN-β production, requiring the Trif pathway besides

the MyD88 pathway (Figure 1). Remarkably, the induced immune response provided protection against a subsequent herpes simplex virus (HSV-2) infection in mice.[79]

Furthermore, binding of FimH to UP1a leads to the activation of caspase 3 and subsequent apoptosis and exfoliation of infected bladder cells, which is an attempt of the immune system to eliminate infected cells.[20,67] However, secreted CNF-1 and hemolysins (HlyA) also induce apoptosis via the same pathway (Figure 1), providing access to underlying immature bladder cells.[66,80] Therefore, it is questionable, if cell shedding is advantageous or disadvantageous to clear the infection.

Overall, UPEC developed an elegant way to survive the harsh conditions in the bladder. Besides employing a normal physiological process to enter the cells via fusiform vesicles, UPEC also secretes virulence factors, which modulate the immune responses.

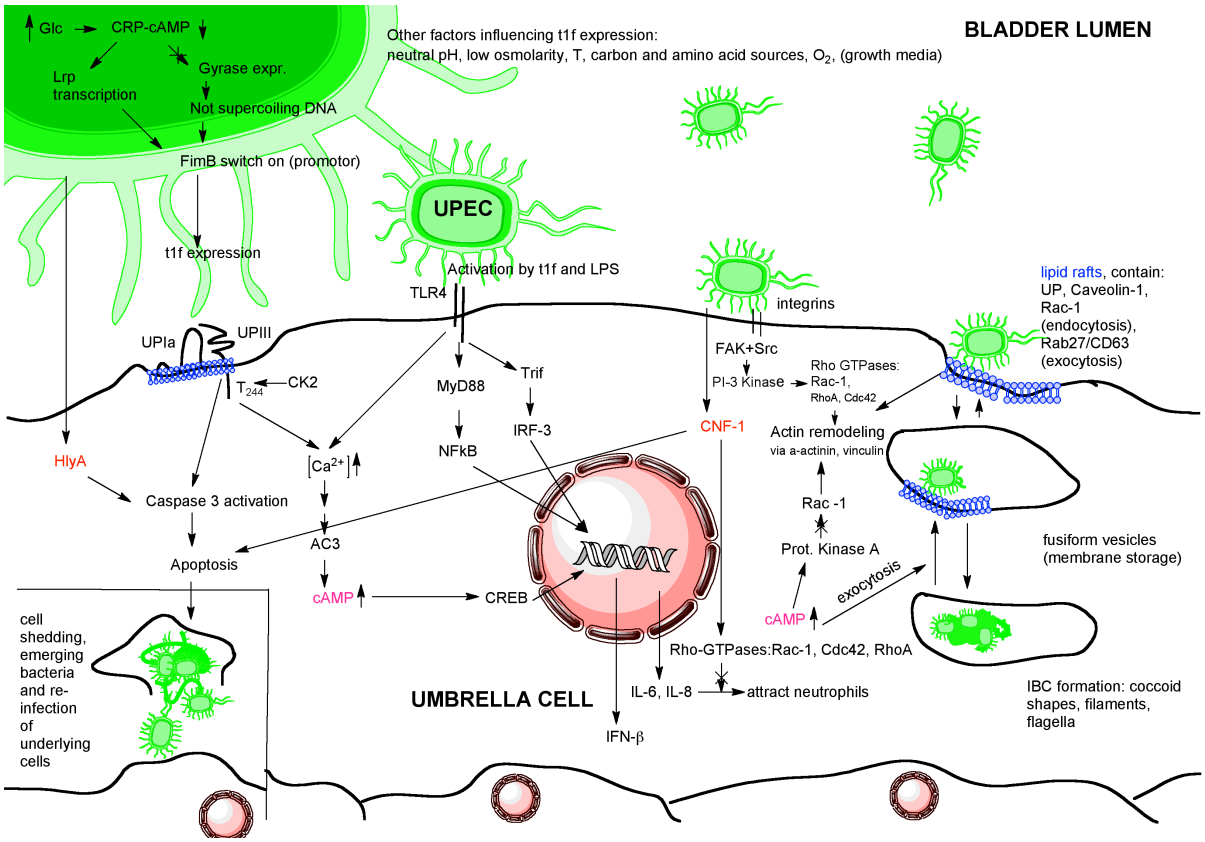

Figure 1. Synopsis of the mechanisms described for the cellular infection cycle and growth conditions for FimH expression.

1.5. The prototypic infection cycle

The UTI cycle has been classified in early, middle and late IBCs (Figure 2).[77,81] The ***early IBC*** stage is mainly characterized by the attachment and invasion of UPEC to and into bladder cells and occurs up to 3 hours post infection (hpi).[82,83] In this stage, bacteria adapt a normal rod-shaped morphology and double approximately every 30 minutes (Figure 2, 1. and 2.).[77,81] Bladder cell invasion and formation of IBC represent a natural selection process for UPECs. An IBC is a clonal population arising from one individual bacterium, limiting genetic diversity for further infection stages (bottleneck).[83] The time between 4-8 hpi, is termed ***middle IBC***.[81,84] Bacteria reduce their length and adapt a coccoid morphology with an estimated doubling time of more than one hour. An average IBC contains around 10^3-10^5 colony forming units (CFU).[81,83,85] Middle IBCs have also been named pods, because of their visible extension into the bladder lumen.[72] Starting at 12 hpi, bacterial pods burst and bacteria re-enter the bladder lumen for a new infection round (***late IBC*** stage).[81,82] Bacteria change back from their coccoid shape to the normal rod-shape and regain motility.[81] Many bacteria adapt a filamentous state during growth in IBCs, where they replicate without separation, growing as long as 70 µm. Upon fluxing, they divide and adapt their normal rod-shaped form.[77,82,81,85,84] Most importantly, Andersen *et al.* could show that bacteria were able to restore their type 1 pili after escaping from cells and attach to further cells.[85]

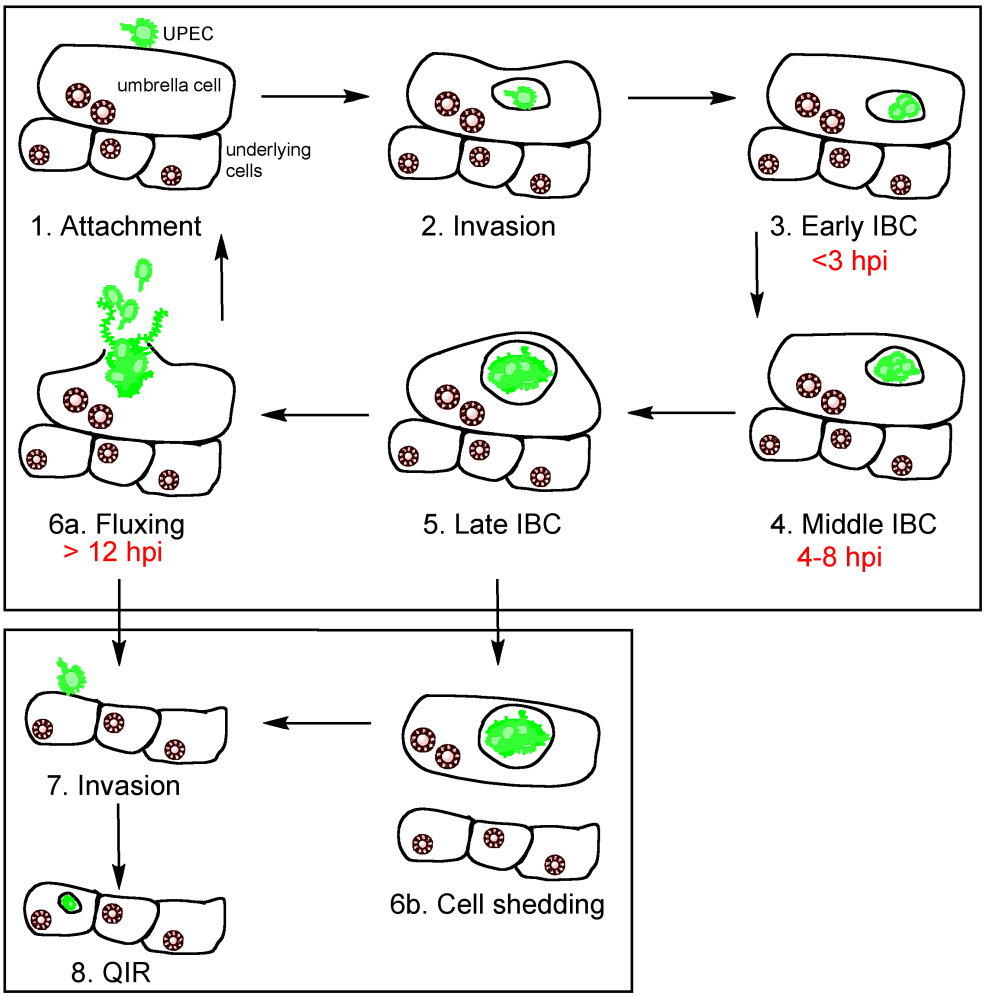

Figure 2. UTI infection cycle showing the phases of the different infection stages. 1. Attachment of bacteria; 2. Invasion into the umbrella bladder cell; 3.-5. Early, middle, and late IBC; 6a. Cell burst and bacterial fluxing, which can lead to a new infection round. 6b. Cell shedding of infected cells, a defense mechanism of the host. Both, fluxing and cell shedding (6a and 6b) allow access to underlying immature bladder cells for the bacteria, leading to cell invasion (7) and the formation of quiescent intracellular reservoirs (8, QIRs). Approximate time span for the appropriate steps are indicated in red and apply to the first infection round.

The intracellular replication is a fundamental process for the persistence of bacteria in the urinary tract. Bacteria invading, but lacking the ability to form IBCs, are rapidly cleared.[86] By invading bladder cells, bacteria escape urinal voiding. Furthermore, within the intracellular biofilm-like state formed in an IBC, bacteria are protected from several immune measures. For example, granulocytes recruited to the infected cells cannot access bacteria, due to the protective effect of the biofilm polysaccharide matrix and the surrounding uroplakin shell.[70,72] Moreover, granulocytes are not able to engulf filamentous bacteria.[81] The importance of IBC formation is also shown by the fact that the genes for the establishment of an IBC are under positive

selection.[86,87] Besides, IBCs as part of the uropathogenic infection cycle have been detected in cultured bladder cells, in mice, and in humans.[71,88,89] Nonetheless, the high decrease of bacterial CFU within the first 12 hours of an infection is attributed to immune responses, such as neutrophil influx and cell shedding.[82]

After apoptosis or bacterial outburst of superficial bladder cells, underlying immature basal and intermediate bladder cells become exposed to the infection.[70,82] Yet, bacteria infecting these cells remain in a latent state and are not replicating. This so-called quiescent intracellular reservoir (QIR, Figure 2, 8.) is often composed of only very few bacteria and remains undetected by the immune system, responsible for bacterial persistence. In mice, at 24 hpi, remaining bacteria in the bladder originate from IBCs, whereas, at 48 hpi, they originate from QIR.[83]

Bacteria in immature cells are kept in a cellular compartment similar to a late endosome, which is tightly surrounded by actin filaments. Possibly, these filaments form a barrier for exchange of nutrients or growth factors from the cytosol to and from the endosomal compartment, which restricts bacterial growth. Eto *et al.* could show that as soon as the actin was destroyed, the bacteria started to replicate. They hypothesized that the progress from the QIR state into an active IBC state is triggered by the turnover rate of the bladder cells.[90] During differentiation of immature cells into umbrella cells, changes in size, morphology, cytokeratin profile, and actin network, as well as the expression of UPs occur, enabling bacterial transition form QIR to IBC.[91] The formation of QIRs together with maturation into IBCs upon cell differentiation would explain the frequently occurring recurrent infections after a specific time length.[65,77,82,90,92]

1.6. UTI: Treatment standard and resistance rates

Although UTI is a self-limiting disease, treatment of symptoms and decrease of disease burden is often necessary. The antimicrobial therapy of choice is most frequently, either trimethoprim/sulfamethoxazole (TMP/SMZ) or fluoroquinolones for three days, or β-lactams or nitrofurantoin for five days.[93–97]

Although a treatment for three days was shown to be less effective than a 5-10 days therapy, antibiotic intake should be minimized to reduce antibiotic resistance rates.[98,99] Also, a single dose of fosfomycin parallels the effect of other treatment options in terms of microbiological and clinical success in uncomplicated UTI and is associated with low resistance rates.[100,101]

Figure 3 is an overview about the mode of actions of the mentioned antibiotics. All exhibit a bactericidal or bacteriostatic effect, resulting in a selection pressure for bacterial survival.[102,103] In contrast, targeting FimH does not exhibit such selective pressure, implying no or less occurrence of resistances.

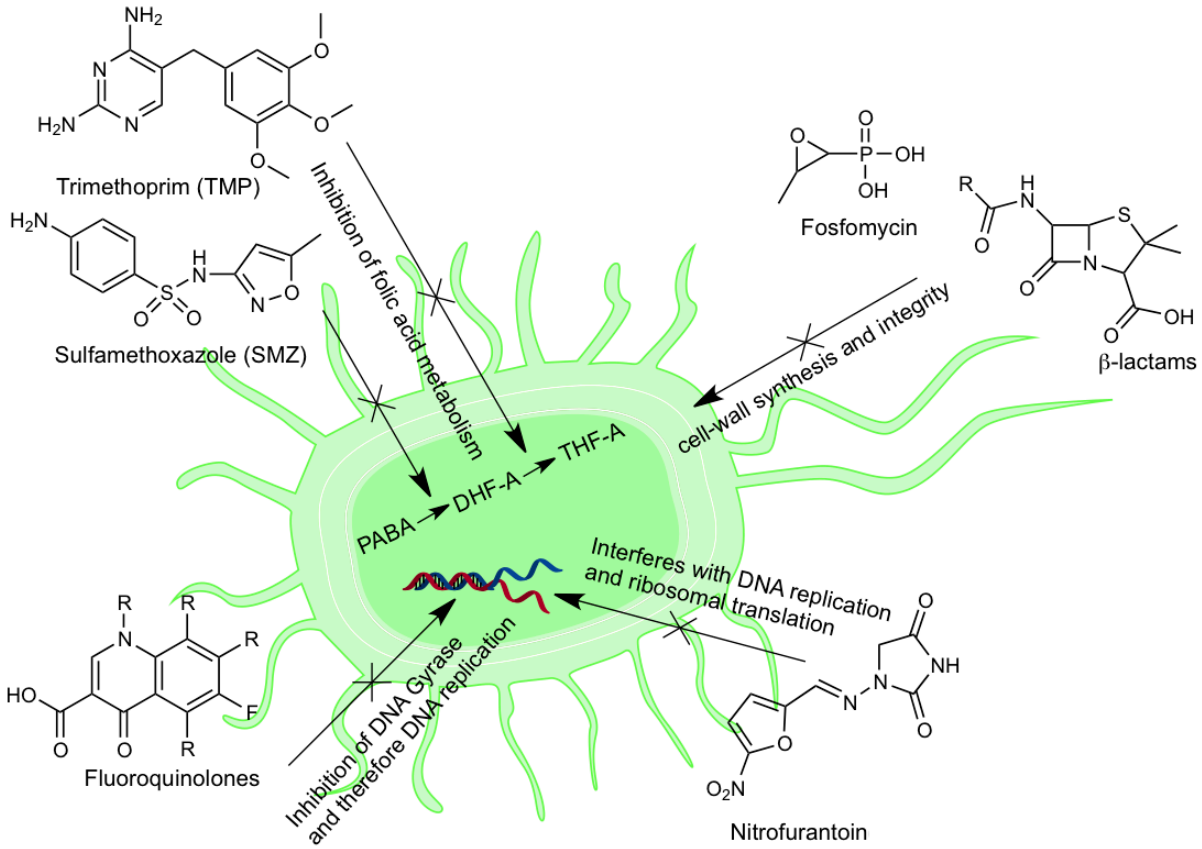

Figure 3. Schematic modes of action of antibiotics mostly used in the treatment of UTI.[102,103] PABA: *para*-aminobenzoic acid, DHF-A and THF-A: dihydrofolic acid and tetrahydrofolic acid, respectively. The mode of action of nitrofurantoin is not completely revealed, but it interferes with DNA replication and ribosomal translation.[104,105]

Increasing resistance rates are a worldwide threat and include the majority of available antibiotics. Accordingly, resistant UTI pathogens were confirmed for several antibiotic classes like β-lactams, quinolones, aminoglycosides, and

tetracyclines and differ depending on countries and regions. For UTI treatment, only nitrofurantoin and fosfomycin lack high resistance rates so far.[106,107]

Other possibilities for treating UTI are limited and include preventive options, such as increasing daily fluid uptake, changing hygiene procedures, or frequent urination. Also, the preventive intake of antibiotics is suggested in some cases.[108,109] The latter is critical for the development of resistant strains, as a preventive intake of TMP/SMZ for one month results in resistant bacterial colonies in the intestine, which is a frequent source for uropathogenic bacteria.[108] Also, a long-term prophylactic intake (daily, for approximately two years) of antibiotics in children at risk of rUTI showed that *E. coli*, the most common isolated uropathogen, developed a multidrug resistance in 55.5%, most often with cephalosporins and TMP/SMZ.[110] Furthermore, it was revealed recently that subinhibitory concentrations of antibiotics, which result from low-dose preventive intakes, trigger the expression of adhesins, leading to an increase in biofilm formation and more extensive colonization of murine bladders of UPEC and *Staphylococcus saprophyticus*. Thus, recurrence was not prevented and infections were worse than the primary infection.[111]

Another prominent preventive option is the intake of cranberry products. However, the usefulness is controversial. A meta-analysis by Jepson *et al.* reported no significant effect of cranberries compared to placebo groups in the occurrence of symptomatic UTI, neither in preventing rUTI.[112] Contrarily, Wang *et al.* reported a positive correlation of cranberry product intake and the reduction of UTI incidences.[113]

1.7. Biofilm

1.7.1. Biofilms in the face of UTI

Costerton *et al.* described a biofilm as “matrix-enclosed bacterial populations adherent to each other and/or to surfaces or interfaces”.[114] A microbial biofilm starts with attachment of individual bacterial cells with subsequent cell multiplication and production of extracellular polymeric substance (EPS).[115,116]

Biofilms provide an advantageous way of growth for bacteria, offering protection from antimicrobial agents and the immune system of the host.[117–123] Antibiotic tolerance increases by approximately 1000-fold when comparing planktonic bacteria with bacteria in biofilms.[124] Consequently, biofilm-related infections are difficult to resolve by the host and also by antibiotic treatment.[125,126] Thus, the ability for biofilm formation is considered as another important virulence factor for UTI. There, biofilms are not only important during IBC growth, but can also form on the surface of medical devices, such as catheters.

1.7.2. Surface adhesion and biofilm formation – many factors involved

The ability for biofilm formation depends on several factors. The most important factors described in literature, are discussed in Table 1.

Table 1. Overview of important proteins and structures involved in biofilm formation and promotion.

Protein/Structure	Role in biofilm formation
Type 1 fimbriae	Type 1 fimbriae mediate primary attachment to both, abiotic and biotic surfaces. They are required for aggregation and microcolony formation, a prelude for biofilm development.[124,127–133] Type 1 fimbriae are up-regulated in biofilms and especially in CAUTIs or CAUTI mimicking conditions.[37,134–137] The invertible DNA element responsible for the expression of type 1 fimbriae, is predominantly in the "on" position in strains isolated from catheterized patients.[138] Mutants deficient in type 1 pili expression have diminished biofilm formation capacities.[129,133,138,139] Guiton *et al.* observed a 20-fold attenuation of biofilm of a FimH mutant strain on silicone tubing after 24h.[137]
Curli	Curli were first detected on the surface of *E. coli* and were described as coiled, thin auto-aggregative structures.[140] They mediate initial surface adhesion and cell-to-cell contacts, because they only extend between 0.5-1 µm from the cell.[14,141,130,142–144] Curli are important for the integrity of an initial pellicle formation, as they form a dense cellulose-containing network around the bacteria.[133] They were shown to be vital for biofilm growth and *in vivo* fitness.[145]
Antigen 43 (Ag43)	The Ag43 is an autotransporter protein encoded by the *flu* gene, which is present in 83% of UPEC strains.[14,39,146] It mediates auto-aggregation through intracellular Ag43-Ag43 recognition and is important for biofilm formation on abiotic surfaces.[39,130,14,146–150] Similar to type 1 fimbriae, also this adhesin shows a phase-variable expression.[19] The presence of Ag43 was associated with long-term persistence in the urinary tract, since it was found in IBCs within bladder cells.[39,72,141]
Flagella	Flagella are responsible for the movement in liquid environments and along surfaces. They allow deposition of bacteria at the right spot for the initiation of a biofilm.[151,152] Although important for spreading and biofilm initiation, they are not required *per se* for adhesion and are absent in later biofilm stages.[124,129,133,136,142] While it was reported that lacking flagella led to a defective biofilm formation, the catheter colonization ability of mutants lacking flagella compared to wild-type bacteria was not significantly different.[129,138]

Type 3 fimbriae	Type 3 fimbriae were described for *Klebsiella pneumonia* and related to biofilm formation, both on catheters and other surfaces.[37,38,141,153] Type 3 fimbriae are encoded on a conjugative plasmid by the *mrkABCDF* operon and were transferred to many Enterobacteriaceae including UPEC.[38,153] Similar to type 1 fimbriae, mutants defective of type 3 fimbriae show decreased biofilm formation.[38] Type 1 and 3 fimbriae were not detected in planktonic cells grown in urine, but are highly expressed in biofilms on catheters.[37] Additionally, type 3 fimbriae were not expressed when cultured in Luria-Bertani medium (LB).[38]
EPS	The production of an EPS matrix is crucial for the establishment and development of a biofilm.[154] The EPS consists of proteins, lipids, LPS, and bacterial DNA, but composition can vary between different species.[116,124] Even the EPS itself was proposed to be important for bacterial adhesion.[155,156] Interestingly, also mannose is an essential part of the EPS.[157,158] Rodriguez and Elimelech reported that upon addition of 1% of D-mannose to their growth medium, biofilm production was increased. Higher concentrations of D-mannose decreased the biofilm mass. They hypothesized that type 1 fimbriae are important for recognition of mannose and the build-up of the EPS.[139]

In fact, the involvement of the factors described in Table 1 in biofilm formation might depend on the specific environmental conditions. For instance, many of the factors (type 1 pili, flagella, curli, and Ag43) are dispensable for an F plasmid promoted biofilm.[115] Also, the list is not final and there might be more factors important for biofilm formation under specific conditions, for example F9 fimbriae.[159]

During biofilm formation, the described adhesins and proteins act in a distinct interplay, depending on biofilm stage and environmental influences. For example, although expression of Ag43 is not inhibited by type 1 fimbriae, the latter is longer and hinders the Ag43 in mediating close cell-to-cell contact. Not only type 1 fimbriae can prevent Ag43-mediated aggregation, also flagella, LPS or capsule expression.[149,160–163] Thus it was shown that upon deletion of the capsule gene, biofilm formation was greatly improved.[38] Also, curli and flagella have an inverse

relationship concerning their expression.[164,165] Similarly, type 1 fimbriae are not expressed when type 3 fimbriae are present, which is also true vice versa. Still, both types may be genetically encoded.[37]

In summary, biofilms are the result of a distinct interplay of many factors and depend on environmental conditions, resulting in different morphological biofilm structures.

1.7.3. Biofilms in catheter-associated UTI (CAUTI)

Catheter-associated urinary tract infections (CAUTI) are a high health burden in hospitals and other health care institutions. In the United States, CAUTI is responsible for over one million cases yearly of nosocomial bacteriuria.[166] In general hospitals, approximately 15-25% of patients have need for an urinary catheter during their hospital stay.[167] CAUTI involves several bacterial species, such as *Pseudomonas spp*., *Klebsiella spp*., *Staphylococcus epidermidis*, *Enterococcus faecalis*, and *Escherichia coli*.[168,169] The latter is responsible for approximately 30% of CAUTIs.[170,171]

Silicone-latex catheters are prone for colonization and biofilm formation by UPEC.[172] Although strains causing asymptomatic bacteriuria (ABU) outcompete UPEC regarding their growth rate in urine, UPEC strains are better biofilm formers on silicone-latex Foley catheters.[172–175] To prevent biofilm formation of uropathogenic bacteria on catheter surfaces, bacterial colonization is inhibited by coating with antibiotics or other antimicrobial agents. However, the effect lasts only for a short period of time.[176–183]

Biofilm on a catheter surface, but also on drainage bags and in the uroepithelium itself, provide a constant source for bacteriuria. Therefore, the ability for biofilm formation characterizes strains causing rUTIs.[167]

1.8. The FimH anti-adhesive approach

Already more than three decades ago, Aronson *et al.* proposed an anti-adhesive therapy targeting type 1 pili.[47] However, it was only in 1997 when Langermann *et al.* proposed a FimH adhesin vaccination.[184] Today, several studies using FimH antagonists as an anti-adhesive approach for the treatment of UTI have been published. An overview of the FimH antagonists proposed by different research groups and the obtained results are summarized in Figure 4 and Table 2.

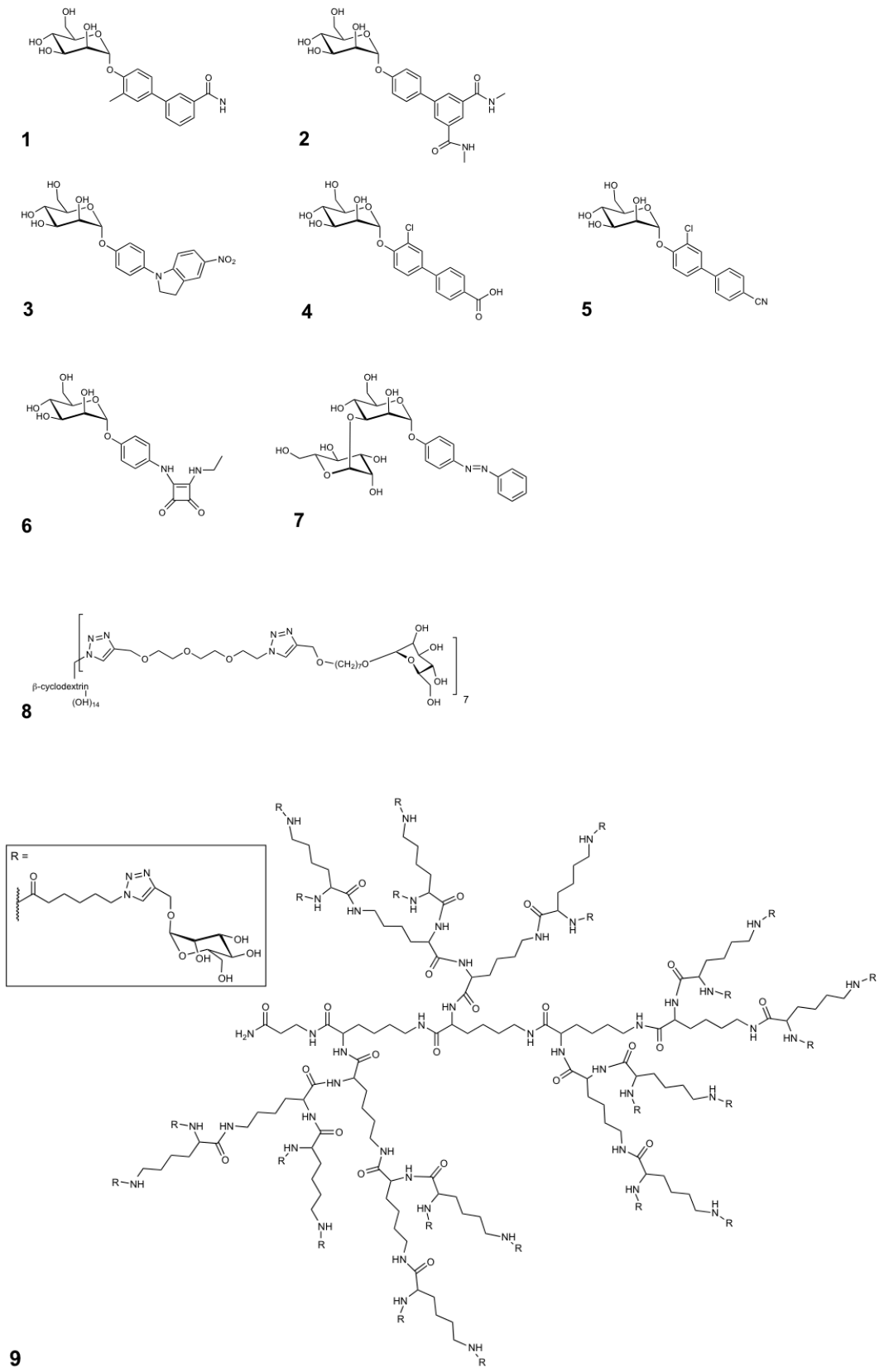

Figure 4. Structures of FimH antagonists designed and tested by different research groups. **1, 2:** Hultgren *et al.*[137,185–187], **3, 4, 5**: Ernst *et al.*[188–190], **6**, **7**: Lindhorst *et al.*[191,192], **8**: Boukaert *et al.*[193], **9**: Roy *et al.*[194]

Table 2: Results of **1**-**9** reported by the corresponding research groups.

Group and antagonist number	Summary of published results	Ref
Hultgren *et al.* Antagonists **1** & **2**	Biphenyl-mannopyranoside derivatives showed improved activity in *in vitro* hemagglutination and biofilm assays combined with good pharmacokinetic (PK) properties *in vivo*. With modifications on the biaryl structure, the previous lead structure could be improved, increasing its' potency by approximately 5-fold and showing higher overall plasma and urine concentrations (**1**).	185
	An orally available FimH antagonist (**1**) was effective in the murine model of UTI. Furthermore, the potential of FimH antagonists in preventing acute UTI and treating chronic UTI (Log_{10} 3 CFU/ml reduction in the bladder) caused by a multidrug-resistant *E. coli* strain was shown. Also, the study provided insight into the long-term pathogenic mechanisms in the bladder.	186,187
	An orally applied mannoside (**2**) prevented a CAUTI infection in mice and potentiated the effect of TMP/SMZ.	137
Ernst *et al.* Antagonists **3**-**5**	Orally available FimH antagonists were successfully applied *in vitro* and *in vivo.* Various studies explored different aglycones. The best antagonists were applied intravenously (i.v., **3**) and orally (p.o., **4** & **5**) and reached a reduction of Log_{10} 3 CFU/ml in the bladder of the UTI mouse model. With a bioisosteric replacement of the carboxylate in the *para*-position of the outer aromatic ring of the biphenyl aglycone with cyanide, the PK properties of **4** were markedly improved (**5**).	188–190

Lindhorst *et al.* Antagonists **6** & **7**	The group investigated the inhibition of binding of type 1-fimbriated *E. coli* to mannoside- and mannan-coated surfaces by squaric acid monoamide mannosides (**6**). Docking studies revealed a specific binding of the glycon moiety to the carbohydrate recognition domain (CRD) of FimH, with the aglycon moiety interacting with the entrance of the FimH CRD.	[191]
	Photoswitchable azobenzene mannobiosides (**7**) showed promising binding to the FimH CRD *in silico*. This could be useful in developing photoswitchable adhesive surfaces for glycoarrays.	[192]
Bouckaert *et al.* Antagonist **8**	Mono- and heptavalent gylcoconjugates connected to β-cyclodextrin were tested as FimH antagonists in the mouse model of UTI. Instilling 2 µg of the heptavalent antagonist together with bacteria directly into the bladder of mice led to a decrease of the CFU of approximately 1 to 2 Log_{10} units. Furthermore, the glycoconjugates were shown to rapidly reach the mouse bladder upon intravenous application and retaining urine levels over 2 µg for 24 hours.	[193]
Roy *et al.* Antagonist **9**	Mannosylated dendrimers were tested in the hemagglutination assay. A 500-fold increase in potency compared to methyl α-D-mannopyranoside was achieved.	[194]

1.9. FimH shows a catch bond behavior

The FimH of UPEC has different natural variants exhibiting different binding characteristics. Mutations in the FimH gene are pathoadaptive, i.e., they provide an advantage for uropathogenic isolates in colonizing the urinary tract compared to their fecal relatives.[195,196] Fecal strains show very low adhesion capacities to mannosylated surface structures opposed to uropathogenic strains.[195] However, not all UPEC isolates show the same binding pattern. Some are able to adhere to monomannosylated structures, whereas most of the strains are only able to bind trimannosylated structures. Yet, the binding of monomannosylated structures correlates with the binding to uroepithelial cells.[197–199]

The lectin FimH at the tip of type 1 fimbriae is composed of an N-terminal lectin domain, containing the CRD, and the C-terminal pilin domain (Figure 5), connecting the FimH to the other subunits of the type 1 fimbriae (FimG, FimF, and the multiple subunits FimA anchored into the cell membrane).[200,201] Upon spatial separation of the lectin and pilin domains, the affinity of the CRD to mannose is strongly enhanced, due to a β-sheet twist in the lectin domain, leading to a tighter binding pocket (Figure 5, green loop). This is the case either in the natural course of infection, where urine flow leads to a shear induced separation, or when the FimH has a structural mutation leading to a constant separation of both domains. The strengthening of binding upon domain separation due to shear force is called a catch-bond mechanism.[198,201–204] Thus, the pilin domain functions as an allosteric inhibitor of mannose binding of the lectin domain. Furthermore, it was proposed that the binding of a ligand in the lectin domain in some strains mediates a change from the native, low affinity form of FimH to a medium affinity binding with slightly superior affinity, which is further enhanced upon complete domain separations induced by shear force (high affinity state).[199,201]

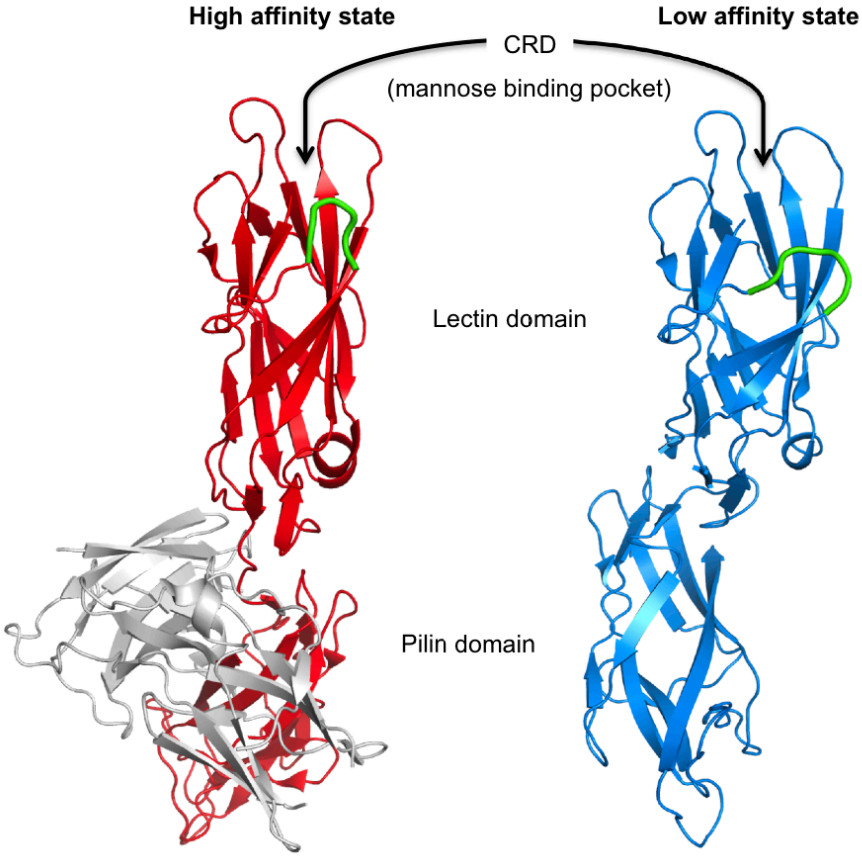

Figure 5. High and low affinity states of FimH and the differences in the overall structure of the two domains. For the high affinity state (red), the protein was crystallized with the FimC chaperone, interrupting the interaction of both domains. The β-sheet twist leads to the closing of the binding pocket (indicated in green) and enhanced binding of mannose. The structures were created with PyMol Software by Deniz Eris (PDB codes: 1QUN and 3JWN).

The differences in binding strength to monomannosylated structures of different UPEC can be explained by different mutations in the *fim* gene. Although 90% of the amino acids in the FimH structure are conserved in UPEC strains, a few can influence the conformations of the lectin domain, or the interaction between the lectin and pilin domain.[86] Systematical analyses of mutational changes within different structural regions of the lectin domain and in the inter-domain region revealed the influences upon the affinity state of the binding pocket towards mannose. By expressing different residual mutations in an *E. coli* K-12 background, it was shown that several regions within the two domains are important in the allosteric switch from low to high affinity.[199] Importantly, different combinations of amino acids at positions 27, 62, and 163 were implied to increase or decrease virulence in the murine mouse model by influencing the affinity state of the FimH.[86,205]

Overall, the FimH protein represents an elaborate catch-bond mechanism system, providing a dynamic attachment of UPEC to the bladder epithelium. The concept of the different binding states of FimH is schematically displayed in Figure 6. It is important to consider not only two different states, but include the intermediate state, induced by ligand binding.

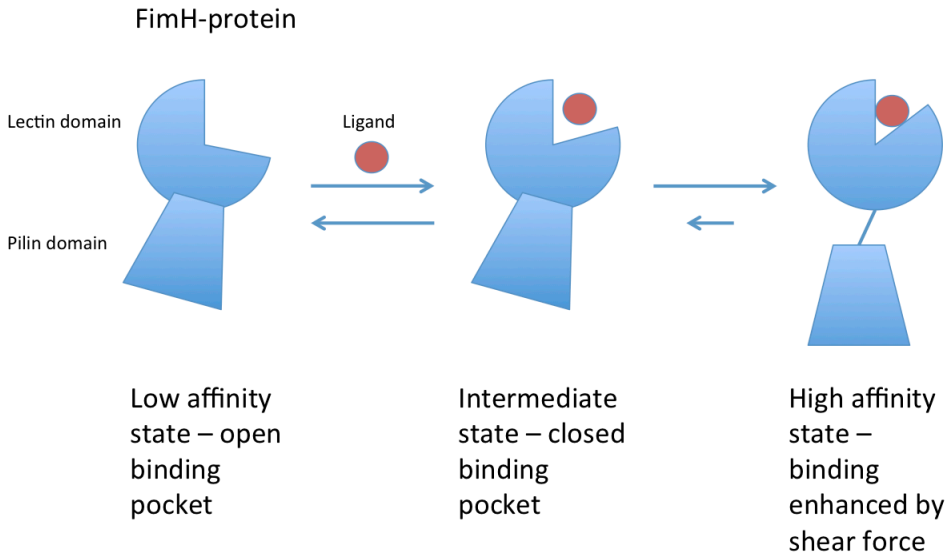

Figure 6. Schematic representation of the different affinity states (low-medium-high) of FimH towards ligand binding.

Soluble FimH antagonists are not able to benefit from shear force enhanced binding, but compete with a ligand that does (UP1a, fixed on bladder cell surface). Therefore, antagonists should target the low and intermediate state FimH to completely abolish binding to bladder epithelial cells.

1.10. Summary and Outlook

Because of a very high prevalence as well as increasing resistance rates, there is an urgent need for new therapeutic options to treat UTI. However, since the infection cycle is the result of a complex bacterial and cellular interplay and frequent rUTI are common, it is a challenging task. Nevertheless, blocking FimH has shown promising results so far. This therapy could proof successful in preventing rUTI and could

possibly replace an antibiotic prophylaxis also in CAUTI. Likewise, it could reduce the use of antibiotics in UTI therapy, by applying FimH antagonists in combination. Consequently, it could help to delay resistance development of frequently used antibiotics against UTI.

FimH antagonists do not directly exert a selection pressure for bacterial survival and the receptors on bladder cells are also unlikely to evolutionarily change their mannosylated surface. Therefore, resistance development against FimH antagonists is doubtful, since this would require a mutational change in the FimH CRD, which would also abolish binding to natural receptors. Yet, it could be that the bacteria employ other adhesins suitable for establishing contact with the host cell and initiating infection.

In a wider perspective, not only the therapy for UTI could profit from an anti-adhesive approach. Many bacteria and viruses use a carbohydrate binding-epitope for adhesion and initiation of infection. Therefore, glycomimetics could become a new class of therapeutics to treat infectious diseases.[206]

2. Aim of the thesis

Aim of the thesis

In the past few years, FimH antagonists showed promising results in several *in vitro* and *in vivo* assays (see Table 2), were successfully used against chronic cystitis in mice, and were applied against CAUTI in a mouse model.[137,187] However, nor the appropriate PK/PD index for the application of FimH antagonists, neither an optimal application regimen was yet established.

The aim of this thesis was to assess treatment applications of FimH antagonists in the context of the complex infection cycle of UTI. Therefore, preventive and therapeutic applications were studied in different set-ups. Variations included treatment time, inoculum, time of infection, and application routes. Moreover, the potency of FimH antagonists for the prevention of biofilm formation in relation to CAUTI was investigated. Overall, this thesis aimed at guiding treatment regimens for future applications in patients.

Besides, within different optimization projects, newly synthesized antagonists were characterized for their PK and pharmacodynamic (PD) performance *in vitro* and *in vivo*.

Furthermore, the influence of the FimH affinity states of different UPECs upon antagonist binding was investigated. Yet, further studies are needed, as this will be an important and inevitable step towards general treatment finding.

3. Methodology

This section shortly discusses the most important methods used for the results gained in this thesis. Thereby, the focus lies on reporting of advantages and disadvantages of assay systems regarding the interpretation of their outcome, rather than reporting detailed assay protocols. However, protocols that are no part of a manuscript or paper, but results are shown in this thesis (microscopy and PCR), are also described here in detail.

3.1. Bacterial cultivation

Generally, bacteria were cultivated in type 1 pili inducing conditions, i.e., in 10 ml LB medium, static, at 37°C for the designated time length important for the assays.[82] The expression of type 1 pili under these conditions was confirmed with fluorescence microscopy (Figure 7A).

3.2. In vitro cell infection assay

The *in vitro* cell infection assay was performed as previously described, however with some modifications.[207] The assay was used to determine the minimal anti-adhesive concentrations (MAC_{90}) of several antagonists and different UPEC strains.

The detailed assay procedures were published in **PAPER I**. In general, cells were infected with green fluorescent protein (GFP) expressing bacteria and incubated for 1.5 h (or indicated time lengths). Then, cells were washed to remove non-attached bacteria, detached from wells and analyzed using flow cytometry. Living cells were gated selectively via side scatter (SSC) and forward scatter (FSC), and analyzed for their GFP intensity. This reflects the amount of bacteria either binding to or internalized into the individual cells (Figure 7).

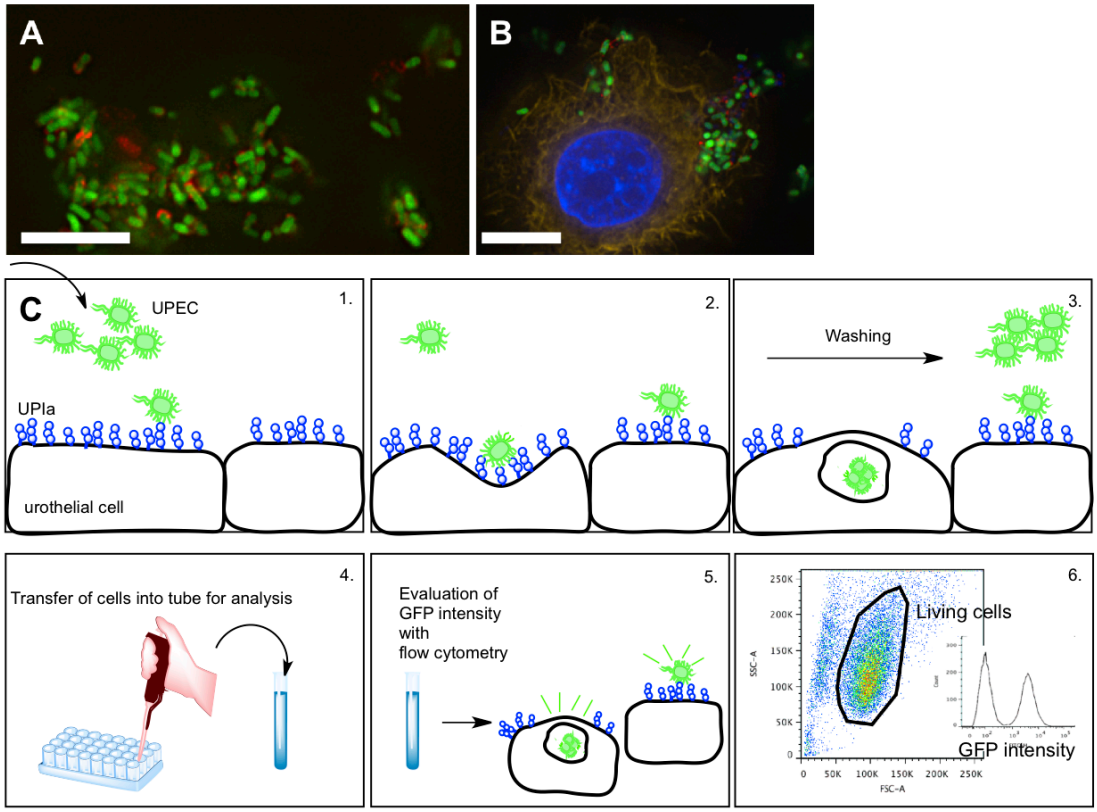

Figure 7. (A) GFP-expressing J96 with stained type 1 pili (Alexa 647, red), which proofs the expression of type 1 pili on the surface of J96 bacteria. (B) 5637 bladder cell after three hours of infection with J96. The cell nucleus (blue, DAPI) and the F-actin skeleton are labeled (orange, rhodamine-phalloidin). Bacteria cluster on the cell surface, partly within the cell. The red stain of type 1 pili is only weakly visible. (A) and (B) were pictured with fluorescence microscopy at 100X and 60X magnification, respectively. Bars represent 10 µm. (C) Schematic explanation of the *in vitro* cell infection assay. Cells were infected with UPEC and incubated at 37°C (1. and 2.). After incubation, cells were washed to remove non-adherent bacteria (3.). After cell transfer from wells into tubes, living cells were gated within flow cytometry and analyzed for their GFP intensity (4.-6.)

The human bladder carcinoma cell line 5637 is widely used for the assessment of pathogenicity of UPEC strains and infection cycle studies.[54,61,64,68,208,209] They show typical characteristics of the *in vivo* infection, such as bacterial attachment, invasion, and fluxing.[54,82] Also, they express UP1a, integrin receptors, as well as TLR4, and type 1 pili provoke a cytokine response. [61,68,74,210] Therefore, the 5637 cell line offers a good model for the screening of antagonists, most closely mimicking *in vivo* infection events. Yet, the assay is very delicate. Within the master thesis of Nathalie Lüdin and Rachel Zimmermann, the assay was optimized in several respects. First, the bacterial load for infection was reduced to optimize the multiplicity of infection (MOI). This is an indication for the ratio of bacteria per cell. Second, the assay procedure was refined, e.g., cells were detached using trypsin (Invitrogen) and

dissolved in phosphate buffered saline (PBS) containing 2% fetal calf serum (FCS, Invitrogen) to increase the number of living cells. Third, to reduce cell clumping, the samples were filtered before measurement to eliminate false negative exclusions while gating for living single cells. Also, the analysis within the flow cytometer was refined, i.e., to accept a result, minimally 10'000 living cells had to be recorded and cell viability was related to all measured events. The viability should be minimally 20% for valuable sample analysis.

Despite these refinements and optimizations, the assay system remains sensitive. Although the number of seeded cells per well was constant, after two days of growth, it varied between 5 x 10^4 and 3 x 10^5. The bacterial numbers ranged from 2 x 10^7 to 1.7 x 10^8 CFU/well. This results in MOIs from 400 to 3400, a factor of 8.5. Furthermore, Rachel Zimmermann found that the amount of pili expressed by different UPECs using immunostaining varied considerably. Also, the GFP intensity of the individual strains was different, although they harbor the same plasmid and were grown in the same culture conditions. During the assay, which is quite labor intensive, the time frame used for specific steps also influences cell viability and ultimately the assay outcome. These reasons are most likely responsible for the variability of the assay results.

Moreover, a crucial point of the natural infection cycle is the detachment of umbrella bladder cells, either by natural immune reactions or by bursting after extensive intracellular replication of bacteria. This renders the underlying immature cells exposed to the bacteria.[20,66,67,80] Yet, this effect cannot be studied with the present *in vitro* model, as the cells grow in a monolayer and lack multi-dimensions. Therefore, they are only representative for the initial infection events, such as attachment and invasion. Therefore, the 3D-organoid bladder model, as presented by Smith *et al.* would be promising to study the whole infection cycle of UTI *in vitro*.[209]

3.3. The C3H/HeN mouse strain for PK studies and infection

The exact procedures for PK studies and infection studies are described in **PAPER I/PAPER II/PAPER III/ MANUSCRIPT I**. The different treatment schemes are discussed in Chapter 4.3.1 and **MANUSCRIPT I**.

The mouse model of ascending UTI was originally described by Hagberg *et al*. and is an established model for studying antibiotic treatment regimens in UTI.[48,211] The mouse model offers several advantages. Mice express the Gal(α1-4)Galβ glycolipid binding-motif for kidney infections, which is also expressed in humans, but not in rats.[48,212] In parallel to human infections, mice are infected via the ascending, transurethral route and are able to clear the urine of bacteria without treatment after some time.[211] Furthermore, mice also show IBCs, similar to the human pathogenesis.[71]

On the other hand, Lanne *et al.* argued that C3H/HeN mice show different isoreceptor patterns regarding glycolipids and glycoproteins in the urinary tract compared to human or monkey.[213] Also, C3H are susceptible to vesicourethral reflux (VUR), allowing fast kidney infections.[214] Since VUR is critical for the assessment of kidney infections, transurethral inoculation was performed carefully, injecting 50 µl over a time-span of 30s with a Hamilton syringe.[215] However, this does not completely rule out the possibility of VUR.[216,217] Although the activity of FimH antagonists is focused on bladder infections, one should consider these facts analyzing kidney infections.

3.4. Biofilm

The classical biofilm assay using crystal violet (CV) staining was first described by Christensen *et al.* and was later modified in several studies.[218] Most prominent were the modifications by O'Toole *et al.,* which served as the basic protocol for the studies in this thesis.[219] The detailed assay procedures employed for this work are described in **MANUSCRIPT II.**

Crystal violet is basic and binds to extracellular, negatively charged molecules on the cell surface or in the polysaccharide matrix of biofilms.[220] In general, the assay is easy to perform, widely used, cheap, and delivers reproducible results in most cases.[221]
Nonetheless, CV-staining is not suited for distinguishing living from dead cells and strongly depends on washing steps within the assay, which makes it difficult to compare results between laboratories or even between individuals.[221,222] Therefore, CV assays should be used for a general screening, but must be accompanied by enumeration of bacteria for detailed information about the amount of living bacteria within a biofilm.

The assay format used for the testing of biofilm on a catheter surface, as presented in **MANUSCRIPT II**, offers a reproducible and robust method to test strains, catheter material, and therapeutics. It allows a simultaneous screening of different conditions in a 96-well plate and is only moderately time consuming.

3.5. Microscopy

Microscopic experiments were performed aiming at revealing cell infection processes, morphological changes of bacteria (i.e., pili expression, bacterial form), and analysis of biofilm structures. Ultimately, visualization should help to assess type 1 pili expression within the infection cycle and might determine treatment possibilities with FimH antagonists.

Pictures of the cell infection assay and of the biofilm were obtained by fluorescence microscopy, which included the following steps:
Cells or biofilms were cultured on 8-well µ-slides (ibidi, Germany). For the staining of bacterial type 1 pili, 200 µl of a highly concentrated bacterial solution from a washed overnight culture (optical density (OD_{600}) of 2) was mixed with 100 µl of an anti-type 1-pili rabbit antibody (1:250 in 2% bovine serum albumin (BSA) in PBS, kindly provided by Dr. Carsten Struve and Prof. Karen Krogfelt, Statens Serum Institut, Denmark) and incubated for 30 min at room temperature, before centrifugation

(13000 rounds per minute (rpm) for 1 min) and washing of the bacterial pellet (3x in PBS). Then, the pellet was dissolved in 100 µl of the secondary antibody, Alexa 647 chicken anti-rabbit IgG (Invitrogen) and incubated for 30 min at room temperature. After a further centrifugation and washing step, the bacterial pellet was dissolved to the desired OD_{600} and used for the assay.

For staining, cells or biofilms were washed two times with PBS at room temperature before fixation with paraformaldehyde (3.7%, Sigma-Aldrich) for 5 min at 37°C. After fixation, wells were washed with PBS and 200 µl Triton 0.1% (Sigma-Aldrich, in PBS) were added for overall 10 minutes at 37°C. Thereby, the Triton solution was exchanged after 5 min incubation. After washing, a 5% BSA (Sigma-Aldrich) solution was added for 1h. Following removal of BSA and washing with PBS (2x), rhodamine-phalloidin 1U (Invitrogen) was added at room temperature for 20 min. Anew washing with TBS Triton 0.1% (3x) followed before staining with DAPI (Sigma-Aldrich) for another 5 min. After washing of the DAPI solution with Tris-buffered saline (TBS, 1x), mounting media (Vectashield H1000) was added to protect fluorescence before wells were sealed with the coverslip. For picture caption and analysis, the widefield Delta Vision Core System and the SoftWorx software at the Imaging Core Facility of the University of Basel was used. Images were prepared with Imaris x64.

3.6. PCR of FimH

For PCR of the lectin domain of FimH from different UPECs, the bacteria were cultured overnight and DNA was purified using the Wizard® Genomic DNA Purification Kit. Then, PCR was performed adding dNTP mix (Sigma Aldrich), Polymerase (iProof, BioRad) and the following primers: FimH seq Fwd, ACCGCGCAAAACATCCAGTT and FimH seq rev, CCGGTGGCGCTTTATTTG (Microsynth). After PCR (BioRad iCycler®), the products were analyzed in a 1.25% agarose gel (Sigma Aldrich) with electrophoresis. To purify DNA, the Gen Elute PCR Glean up Kit (Sigma Aldrich) was used. Sequenzing of purified DNA was done by Microsynth AG, Switzerland.

4. Results and Discussion

The following sub-chapters summarize the central investigations and achievements of this thesis. They are grouped into main project areas and are more or less extensive, depending on the focus of this thesis. Publications and manuscripts resulting from these projects are indicated and numbered within the text and are included in chapter 5.

4.1. Optimization of pharmacokinetic and pharmacodynamic properties (PAPER I and PAPER II)

PAPER I

As mentioned in chapter 1.8 „The FimH anti-adhesive approach“, numerous antagonists have been published over the last few years. However, to reach therapeutic efficacy, high doses were needed, mainly because of insufficient PK properties. Therefore, starting from a biphenyl α-D-mannopyranoside, new antagonists were synthesized using a bioisosteric replacement strategy, striving towards higher oral bioavailability and renal excretion, while maintaining the high pharmacodynamic activity of the antagonists. The results were published in **PAPER I**:

„FimH Antagonists: Bioisosteres To Improve the *in Vitro* and *in Vivo* PK/PD Profile“

Simon Kleeb,# Lijuan Pang,# Katharina Mayer,# Deniz Eris,# Anja Sigl,# Roland C. Preston, Pascal Zihlmann, Timothy Sharpe, Roman P. Jakob, Daniela Abgottspon, Aline S. Hutter, Meike Scharenberg, Xiaohua Jiang, Giulio Navarra, Said Rabbani, Martin Smiesko, Nathalie Lüdin, Jacqueline Bezençon, Oliver Schwardt, Timm Maier, Beat Ernst
# equally contributed

Journal of Medicinal Chemistry, February 2015

My contributions:

- Conducting some of the PK studies and their evaluations, as well as all infection studies and their analysis.
- Taking part in project discussions, manuscript preparations, and in the review process.

PAPER II

In another project, previously tested ester-prodrugs of biphenyl α-D-mannopyranosides were synthesized in order to increase oral bioavailability resulting from an increased permeation in the gut. However, by this modification, solubility decreased dramatically. Disrupting the molecular planarity and symmetry of the biphenyl aglycone increased solubility and at the same time retained high permeability. This was achieved by introducing heteroatoms in the outer aromatic ring of the biphenyl aglycone. Also, the molecules of this new series proofed to be metabolically stable and were excreted unchanged. One of the antagonists resulted in urine concentrations over 1 µg/ml for 6 hours after oral application. The results are reported in **PAPER II**:

"FimH Antagonists – solubility vs. permeability"

Lijuan Pang,[#] Jacqueline Bezençon[#], Simon Kleeb[#], Said Rabbani, Anja Sigl, Martin Smiesko, Christoph P. Sager, Oliver Schwardt, and Beat Ernst[*]

# equally contributed

Journal of Carbohydrate Chemistry, October 2016

My contributions:

- Performing the *in vivo* PK study and providing the according text for the manuscript.

4.2. Optimization of oral bioavailability via prodrug approach (PAPER III)

PAPER III

The most practical and simplest way for drug application for patients suffering from UTI, is via the oral route, which would also allow for easy frequent dosing. Therefore, the ideal FimH antagonist should be orally available. Although several mannosides were identified with high affinities, promising a good therapeutic effect, many suffer from low solubility. This restricts oral availability not only by limiting the maximally applicable dose in a given volume, but also by limiting drug dissolution within the intestines, a prerequisite for permeation. Therefore, the oral bioavailability of FimH antagonists belonging to the biopharmaceutical classification system (BCS) class II (low solubility, high permeability), could be markedly improved if intestinal fluids were saturated and high doses could be applied.[223] A prodrug approach was studied to increase solubility of potent FimH antagonists. Inspired by marketed drugs, such as Fosamprenavir, phosphate prodrugs were synthesized and analyzed regarding their PK parameters *in vitro* and *in vivo*.[224,225] The results are presented in **PAPER III**:

"FimH Antagonists - Phosphate Prodrugs Improve Oral Bioavailability"

Simon Kleeb,[#] Xiaohua Jiang,[#] Priska Frei,[#] Anja Sigl, Jacqueline Bezençon, Karen Bamberger, Oliver Schwardt, and Beat Ernst[*]

# equally contributed

Journal of Medicinal Chemistry, March 2016

My contributions:

- Performing and evaluating all *in vivo* PK studies and discussing results for further development
- Providing the text for the *in vivo* part and assisting in editing part of the text.

4.3. Application of FimH antagonists in UTI and CAUTI

4.3.1. Finding the optimal treatment regimen for UTI (MANUSCRIPT I)

MANUSCRIPT I

Anti-adhesive therapies pose a new challenge regarding an optimal treatment regimen. The basis for a successful anti-adhesive therapy is the exactly timed and dosed application in regard of the natural infection events. The different stages of the infection described in chapter 1.5., would suggest a preventive application, i.e., before bacteria attach to bladder cells, or after fluxing, when re-expressing type 1 fimbriae. The attempts for conventional PK/PD index finding, as it is performed in other areas, failed, most likely because of a missing preventive dose (internal data). Therefore, treatment finding started from the basic assessment of a preventive application, using the reference *n*-heptyl α-D-mannopyranoside (**1**, Figure 10). Thereafter, three antagonists from the internal collection were chosen based upon their *in vitro* minimal anti-adhesive concentration (MAC_{90}) and PK results. The most promising candidate was selected to study the long-term preventive effect of a single-dose, (see **MANUSCRIPT I**). The basic workflow and the antagonist structures are shown in Figure 8 and Figure 10, respectively.

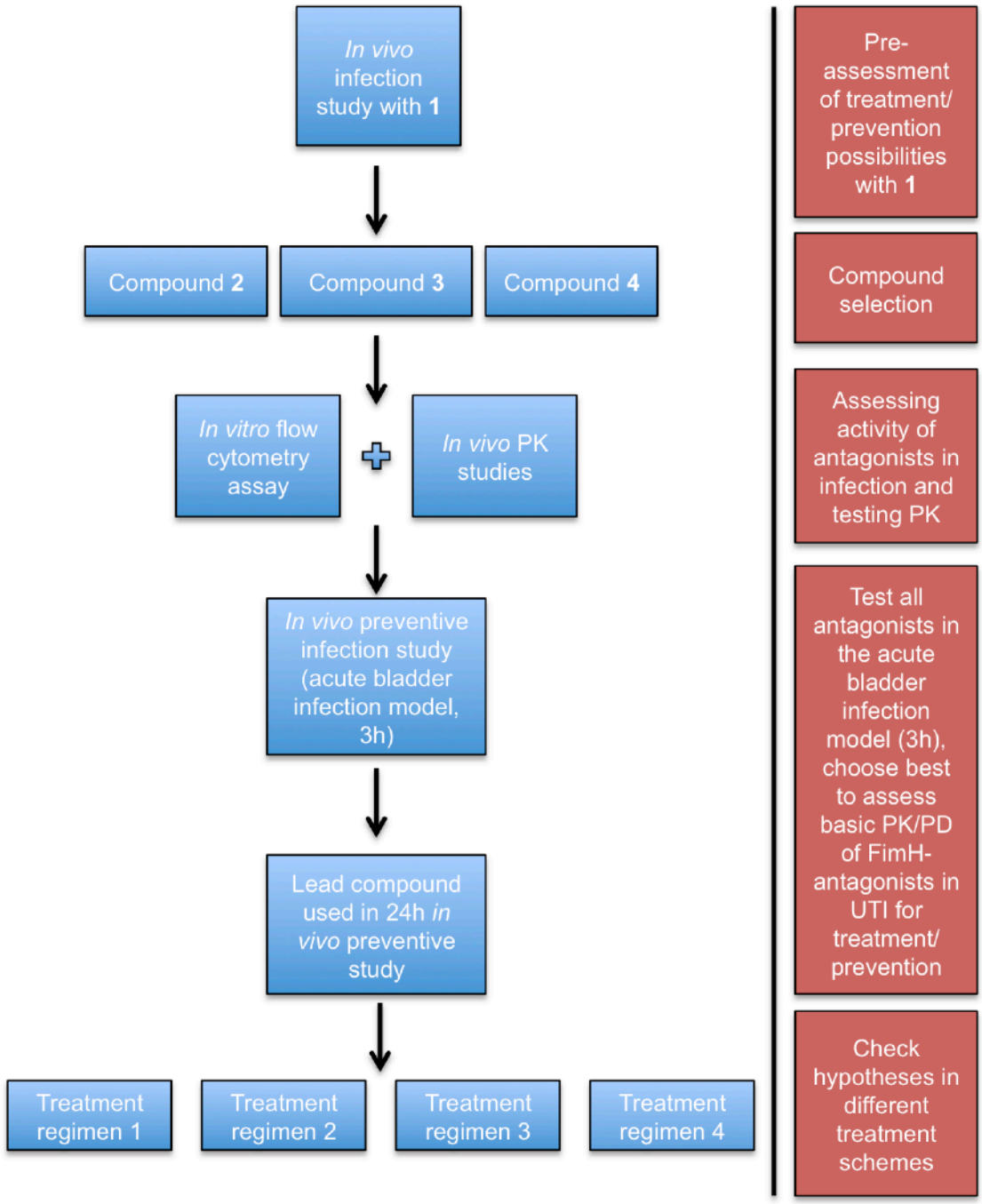

Figure 8. Basic workflow for the identification of the optimal application of FimH antagonists in UTI infection. Blue rectangles show the performed studies, red rectangles display the reasoning for the studies. The antagonist structures are displayed in Figure 10.

4.3.1.1. Pre-assessment of treatment/prevention possibilities

For all infection studies, the previously used and established murine infection model was used.[48,188,211,226] For the validation of antagonists, a short-term infection (up to 3 hours) was employed as described in previous publications from our group.[188–190]

The model is valuable to determine the potency of inhibiting the initial attachment and reducing the acute bladder infection. In a first step, different time points of addition of the antagonist relative to the infection time was studied. This should explain the importance of the timing of antagonist application and its availability within the short-term infection, which mainly includes attachment and invasion. The reference **1** was applied intravenously at a dose of 20 mg/kg at four different times (Figure 9). The effect of **1** is clearly most potent in a preventive application, as shown by the 1-3 Log_{10} reduction in all compartments after a preventive application (-30 min and -15 min). Most prominent is the bacterial reduction in the bladder of group 1 (-30 min).

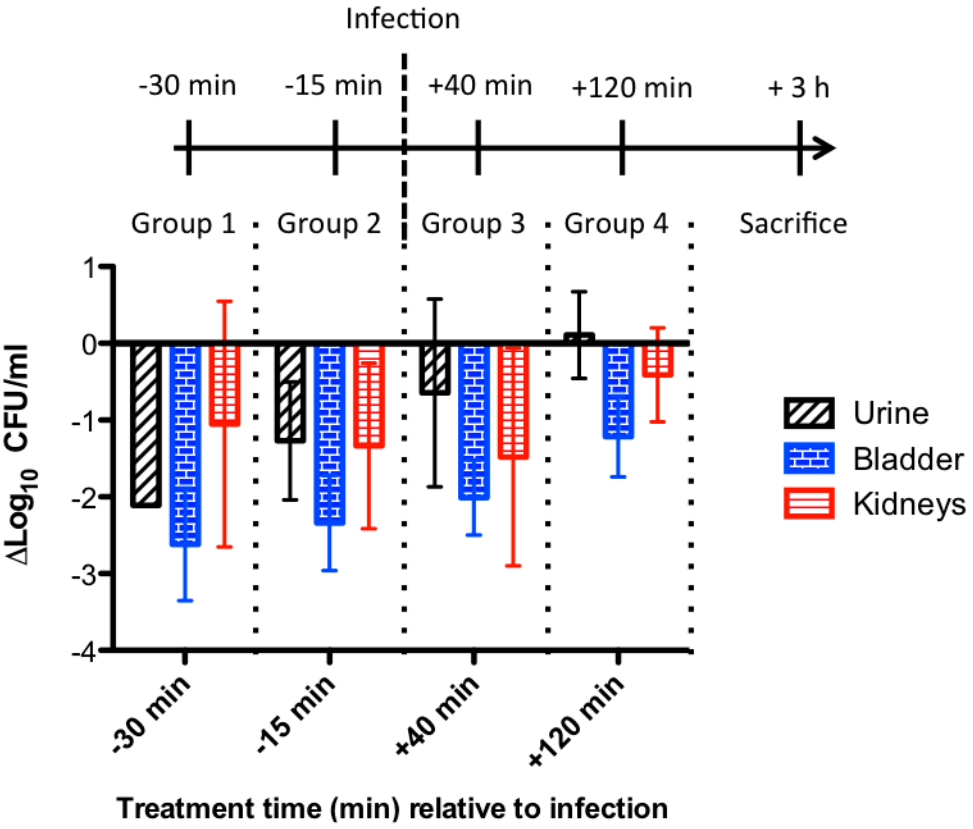

Figure 9. Log_{10} CFU/ml compared to the untreated control group (zero level line) depending on treatment time relative to infection. Bars represent mean Log_{10} reduction of treated groups compared to the mean Log_{10} of controls with SD in urine, bladder, and kidneys (n=4, control values of 6 mice).

The later the antagonist was applied (group 1 to 4) the higher the recovered bacterial burden. First, urine counts increased upon later treatment, then bladder counts, whereas the kidney counts showed an opposite trend. There was a reduction in the kidney counts even when the antagonist was added 40 min after infection, but there was no effect when applied later. The increasing bacterial counts with time may be

explained by the ascending nature of the infection. To avoid attachment to bladder cells, the antagonist must rapidly reach a high concentration in urine. Application of antagonist at a later time point showed therefore a lower effect, reflected in the increasing bladder counts. The infection in the kidneys is a slower process, as bacteria need time to ascend from the bladder. This explains the prolonged effect of antagonist in the kidneys compared to the effect in the bladder or urine, even when antagonist **1** was added after the infection.

Overall, the time point of antagonist addition is crucial for the development of the infection and depends on antagonist availability in urine, i.e., the PK characteristics of the individual antagonists. Clearly, FimH antagonists have the highest effect upon a preventive application in acute bladder infection.

4.3.1.2. Compound selection

Three FimH antagonists were selected for comparison of potency upon a preventive application in the acute bladder infection mouse model. For a future application in patients, antagonists should be orally available. Therefore, testing was performed by oral application only and high solubility and reasonable permeability were preliminary criteria. The selected antagonists represent two distinct chemical classes, the indolinylphenyl mannopyranoside derivatives, **2**[188] and **3,** and the biphenyl mannopyranoside derivatives **4**[190] (Figure 10).

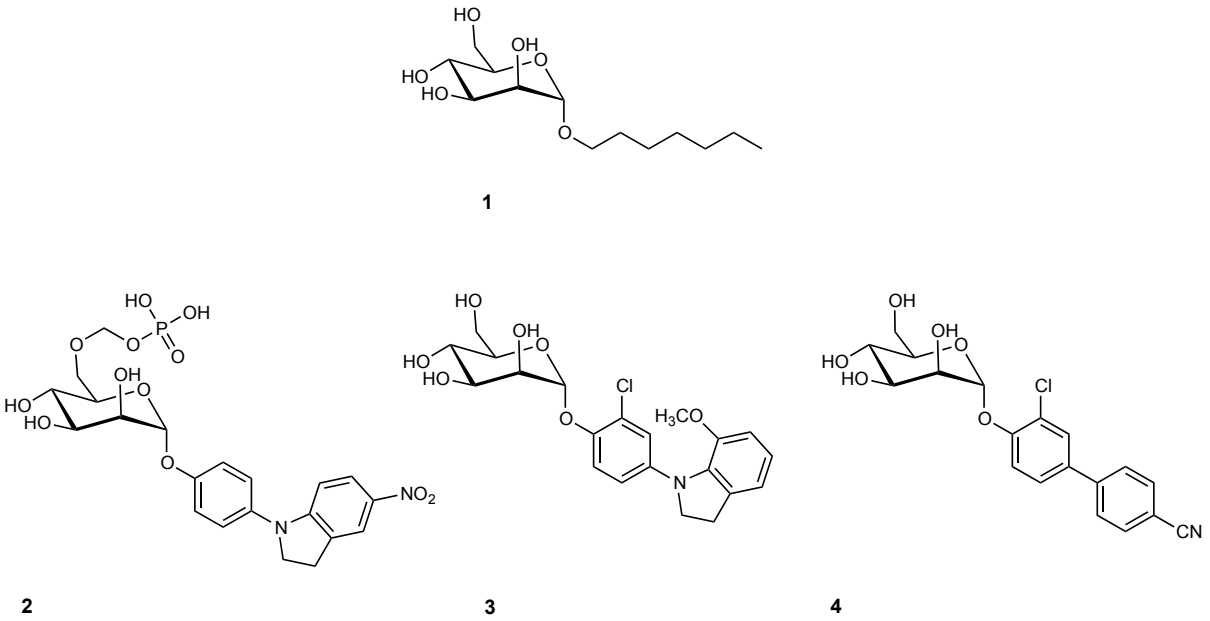

Figure 10. The reference *n*-heptyl α-D-mannopyranoside (**1**), two indolinylphenyl-mannopyranoside derivatives (**2** & **3**), and a biphenyl mannopyranoside derivative (**4**) were chosen for the evaluation of their effect in a murine UTI infection model. The phosphate-prodrug **2**, with a phosphate in position 6 of the mannose moiety was used to increase solubility (**PAPER III**).

For an appropriate treatment regimen, a minimal local concentration of a FimH antagonist in the bladder is required. Similar to the minimal inhibitory concentration (MIC) used as reference level for activity of antibiotics, the minimal anti-adhesive concentration (MAC_{90}) was defined, representing the minimal therapeutic concentration in urine required to inhibit 90% of bacterial adhesion. It is measured using *in vitro* bladder cell cultures and evaluated by flow cytometry (chapter 3.2.).[188,207]

Antagonist **2** is a potent FimH antagonist, which showed a three Log_{10} units reduction in bladder infection counts upon intravenous administration in the murine infection model (48a from Jiang *et al.*).[188] Since antagonist **2** has very low intrinsic water solubility (24 µg/ml), it was not suitable for oral application. A prodrug strategy using phosphate derivatives for improving water solubility (**PAPER III**) was effective in increasing solubility over 3000 µg/ml. Yet, **2** resulted in a MAC_{90} value of 0.5 µg/ml.[188]

Antagonist **3** was selected because of higher intrinsic water solubility (>250 µg/ml), and best membrane permeability within this series (PAMPA Log P_e -4.6 cm/s, measured by Jacqueline Bezençon), although it showed lower activity in the cell infection assay (MAC_{90} 11.18 µg/ml).[207] Antagonist **4**, representing the biphenyl mannopysanoside derivatives, was chosen because of acceptable water solubility

(192 µg/ml, Jacqueline Bezençon) and high activity in the cell infection assay (MAC_{90} 0.09 µg/ml).[190]

To investigate the significance of the MAC_{90} as a guideline for an effective therapeutic concentration and establishment of an appropriate treatment regimen, the MAC_{90} was evaluated in the context of the PK of the individual antagonists.

4.3.1.3. In vivo pharmacokinetic studies

The three FimH antagonists were orally applied, each to three mice, and urine concentrations were measured over time (Figure 11). Antagonist **3** was investigated twice, with a dose of 1.25 mg/kg, based on solubility, and 10 mg/kg, resulting of the improved solubility when formulated with 5% DMSO and 1% Tween 80 in PBS (see **PAPER I**).[190]

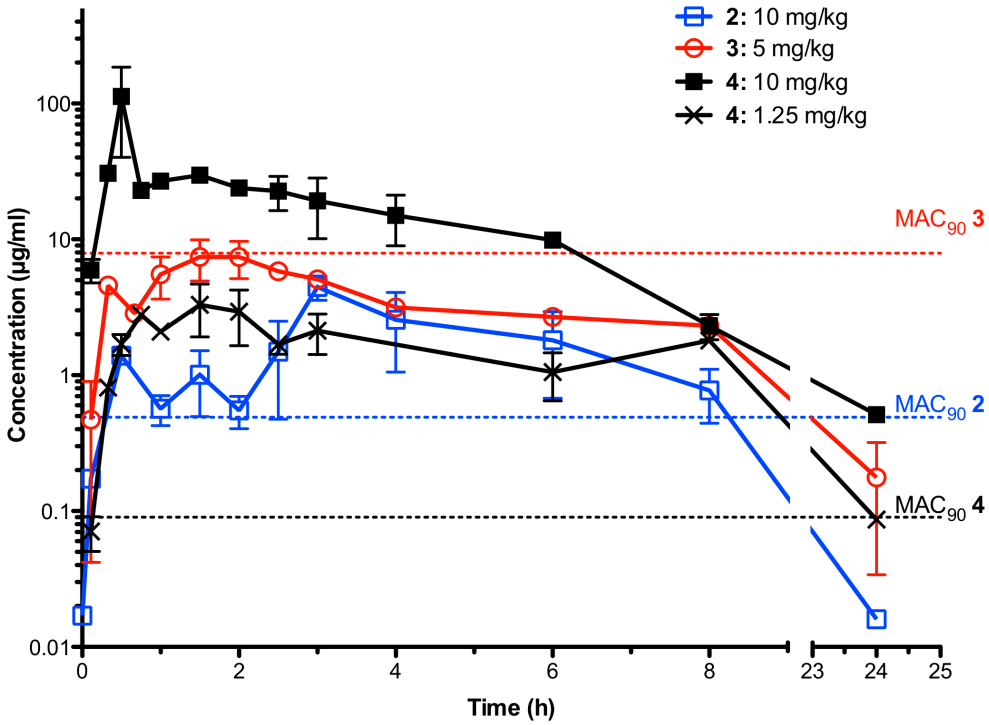

Figure 11. Urine levels of **2**, **3** and **4** over time after oral application. The MAC_{90} levels are indicated by a dashed line and colored according to the corresponding antagonist. The doses were: **2** (blue): 10 mg/kg**, 3** (red): 5 mg/kg, **4** (black): 1.25 mg/kg and 10 mg/kg.

Generally, all three antagonists showed prolonged concentrations above 0.5 µg/ml in urine starting from approximately 30 min after application and extending up to

8 hours after application. The antagonists accumulated in urine and led to high urine levels, which was considered beneficial for antagonizing bacterial attachment in the bladder. The indolinylphenyl derivative **2** showed a fast increase in urine levels within the first few minutes, but reached the C_{max} of 4.5 µg/ml at 3 hours post application resulting in a C_{max}/MAC_{90} ratio of circa 9. The overall $T>MAC_{90}$ was approximately 6 hours (2 to 8 hours after application).

For antagonist **3**, urine levels also maximized between 1.5 and 2 hours post application (7.4 µg/ml) and slowly decreased to 2.3 µg/ml after eight hours. Despite the high intrinsic solubility, the best permeation results in the PAMPA assay, and the highest urine levels in the mouse, the MAC_{90} was never reached. Therefore, it will probably only have minor effects in an infection treatment.

FimH antagonist **4** also showed an accumulation in urine for both dosages (1.25 mg/kg and 10 mg/kg). Both curves parallel nicely, yet, the dose increase of a factor eight (from 1.25 mg/kg to 10 mg/kg) increased the C_{max} from 3.3 µg/ml (1.5h) for the low dose to 112.6 µg/ml for the high dose (0.5h), which is a factor of approximately 37. This indicates that the formulation effectively increased drug levels in urine, not only because of an improvement of solubility, but also because of the inhibition of efflux transporters in the intestines by Tween 80.[227,228] Both doses result in urine levels of roughly 2 µg/ml at 8 hours after application. The $T>MAC_{90}$ for antagonist **4** with 10 mg/kg and 1.25 mg/kg was 24 hours, corresponding to 100% of the time measured. Therefore, although the formulation increased the C_{max} of antagonist **4**, it did not markedly prolong the $T>MAC_{90}$. The C_{max}/MAC_{90} ratio was approximately 30 for the low and over 1000 for the higher dosage.

In a next step, the three antagonists were applied in the acute bladder infection model (3 hours infection) to test the validity of combining the previously determined MAC_{90} value with the PK study results for an effect prediction. All antagonists were preventively applied.

4.3.1.4. Acute bladder infection inhibition potential

The short infection time of 3 hours allows to study initial adhesion and invasion starting immediately after bacteria (experimentally) entered the bladder.[81] The antagonists were orally applied 40 min before infection with the bacterial strain UTI89. This guarantees that the experimental infection is initiated when high antagonist concentrations in urine are available. Based on the pre-assessments ($T>MAC_{90}$ and/or C_{max}/MAC_{90}), antagonist **3** was expected to result in the lowest effect in terms of bacterial load reduction, whereas both, antagonists **2** and **4** (at 1.25 and 10 mg/kg) should result in a more pronounced bacterial reduction and antagonist **4** (10 mg/kg) should be the most effective. In Figure 12 the numbers of colony forming units (CFU) at 3 hpi after a preventive treatment with the three antagonists as well as the antibiotic ciprofloxacin (CIP, applied s.c., 8 mg/kg, 10 min before infection) are compared to an untreated control group in bladder (A) and kidneys (B).

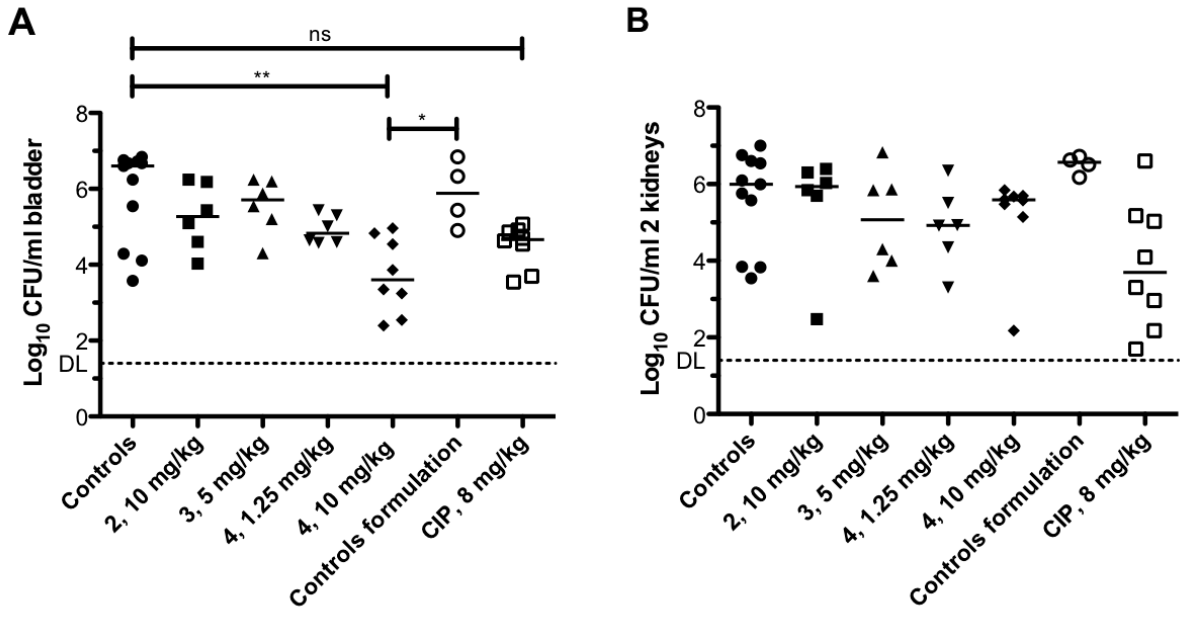

Figure 12. CFU/ml of homogenized bladder (A) and kidneys (B) of infected mice treated either with different antagonists or ciprofloxacin (CIP). Results were compared to untreated controls or a control group, which received the vehicle formulation of antagonist **4** (5% DMSO in PBS containing 1% Tween 80), termed controls formulation. Bars represent median values. N=11 for controls, n=6 for the antagonists **2**, **3**, and **4** 1.25 mg/kg, n=8 for **4** 10 mg/kg, and CIP, and n=4 for controls formulation. (Significance testing: Kruskal-Wallis test, Dunn's post-test, $P < 0.05$). DL: detection limit (dashed line).

Compared to the median CFU/ml of Log_{10} 6.6 in the control group, bladder colony counts were reduced in the groups treated with the antagonists **2** and **4** as well as with CIP, but only moderately with **3**. However, only treatment with antagonist **4** (10 mg/kg) showed a statistically significant reduction of bladder counts (Kruskal-Wallis test, Dunn's post-test, $P< 0.05$) compared to the control group and the controls formulation. With antagonist **4,** a 3 Log_{10} CFU/ml reduction was achieved, compared to a 2 Log_{10} CFU/ml reduction for the CIP treatment group. No significant decrease of CFU counts was observed in kidneys, indicating that the primary compartment of action of the FimH antagonists is the bladder. Although not significant, CIP decreased kidney colony counts by 2.3 Log_{10} units.

The results of the PK study and the acute bladder infection study with antagonist **4** were published in **PAPER I**.[190]

Overall, these results indicate that the MAC_{90} determined in the *in vitro* assay together with *in vivo* PK indeed provide a reference for an effective reduction of bacteria within the first three hours in the bladder. Antagonist **3**, which did not reach MAC_{90} levels in PK studies, showed nearly no effect in the bladder compared to the controls. On the other hand, both, antagonists **2** and **4** (in the higher dose), showed reasonable (Log_{10} 1.4) to excellent (Log_{10} 3) CFU/ml reductions in the bladder compartment. Furthermore, the therapeutic effect is mirrored in the C_{max}/MAC_{90} ratio. As mentioned earlier, antagonist **2** exceeded the MAC_{90} by approximately a factor of 9 at the maximum concentration levels (3 h post application), which is within the infection time studied. Antagonist **4** exceeded the MAC_{90} by approximately 300-fold in a dose of 10 mg/kg. Besides, the bacterial reduction of **4** in the bladder was approximately doubled when the higher dose (10 mg/kg) instead of the lower (1.25 mg/kg) was applied. Therefore, an effective treatment needs concentrations exceeding MAC_{90}, with the magnitude of C_{max}/MAC_{90} being important.

Bacterial loads in the kidneys were only moderately reduced by antagonist **3** (-0.93 Log_{10} CFU/ml) and antagonist **4** at the lower dose (-1.1 Log_{10} CFU/ml). In the kidneys, α-D-gal-1-4-β-D-gal globosides are important for UPEC binding via PapG class II adhesins.[23] PapG is therefore not targeted by FimH antagonists. In addition, as discussed in chapter 3.3., C3H mice are susceptible towards vesicourethral reflux,

which allows a fast development of kidney infections.[214] Nevertheless, the clearance of bacteria from the bladder should also limit the number of ascending bacteria in later infection stages.

The infection itself might influence the PK properties of FimH antagonists. Therefore, urine concentrations of antagonists at two time-points during the infection were analyzed (0.6 and 3.67 h after application). The urine concentrations matched previously determined PK concentrations for all antagonists (data not shown). These results are an indication that the infection does not influence the PK properties of the tested antagonists.

Since antagonist **4** proofed to be the most effective in the acute bladder infection, it was chosen for further evaluations, which are presented in **MANUSCRIPT I**:

"Treatment regimens of FimH antagonists against urinary tract infection – PK/PD of an anti-adhesive therapy"

Anja Sigl, Priska Frei, Katharina Mayer, and Beat Ernst

Shall be submitted to *Antimicrobial Agents and Chemotherapy*

My contributions:

- The designing, planning, and performing of all studies and their evaluations.
- Writing of the entire manuscript.

4.3.2. Application of FimH antagonists in CAUTI (MANUSCRIPT II)

MANUSCRIPT II

Since type 1 pili are important for biofilm formation (see Chapter 1.7.) FimH antagonists could be therapeutically useful to prevent biofilm formation of UPEC on catheter surfaces and reduce the risk for CAUTI. Therefore, FimH antagonists were screened for their potential to prevent biofilm in a conventional CV-staining assay and proofed to be effective. The assay format was further adjusted to more closely mimic human situation. This ultimately led to the deep-well catheter assay, which allows the screening of antagonists against biofilm formation on the surface of catheters in pooled human urine. The results are summarized in **MANUSCRIPT II**:

“The preventive effect of FimH antagonists on biofilms formed on a catheter surface”

Anja Sigl, Justyna Nowakowska*, Oliver Schwardt, Lijuan Pang, Priska Frei, Nina Khanna*, and Beat Ernst

*Infection Biology Laboratory, Department of Biomedicine, University and University Hospital of Basel, Switzerland

Shall be submitted to *Antimicrobial Agents and Chemotherapy*

My contribution:

- Expand and amend the preliminary experiments of Justyna Nowakowska, e.g., testing antagonists in the same set-up in LB medium.
- Adapt the testing of antagonists in human urine.
- Develop and perform the catheter assay.
- Writing the entire manuscript.

4.4. The influence of the FimH affinity state upon in vivo infection (parts of master theses of Manuel Starck, Nathalie Lüdin, and Rachel Zimmermann)

Several mutations can influence the binding pocket of the FimH lectin domain of UPEC and affect the affinity of the bacteria towards soluble or fixed ligands (see Chapter 1.9.).[86,199,205] Most of the published work so far was performed using UTI89, which has a FimH locked in the high affinity state, resulting in a residence time of antagonists on the FimH CRD of approximately 3.6 hours, which is atypical for carbohydrate-lectin interactions.[229]

When interfering with the binding to the bladder epithelium, soluble FimH antagonists are confronted with all three naturally occurring FimH conformations (affinity states, chapter 1.9.). Therefore, several antagonists were screened against different UPEC strains using the established *in vitro* cell infection assay (chapter 3.2. and **PAPER I**) and IC_{50} and MAC_{90} were recorded (Table 3).[207] Additionally to UTI89, also J96 (kindly received from Prof. James R. Johnson, University of Minnesota Medical School), and CFT073 (kindly received from Prof. Harry L.T. Mobley, University of Michigan Medical School) were used.[230,231] Both strains were transformed with the pBR322GFP plasmid using electroporation to express GFP. The procedure was described by Scharenberg *et al.* and was previously used for UTI89.[207]

Table 3: IC_{50} and MAC_{90} of several antagonists against UTI89, J96, and CFT073 determined in the *in vitro* cell infection assay. Part of these experiments were performed by Nathalie Lüdin and Rachel Zimmermann, two former master students. Indicated are mean values of individual measurements with SD. For evaluation, only living cells were analyzed. N.d., not determined, *[1] Resulting cell viability below 20%, *[2] Cell viability below 20% in a few samples.

Antagonist name	Structure	UTI89		J96 *[1]		CFT073	
		IC_{50}	MAC_{90}	IC_{50}	MAC_{90}	IC_{50}	MAC_{90}
n-heptyl α-D-mannopyranoside	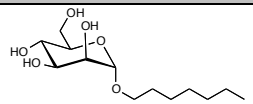	6.9± 3.9 µM	14.8 ±11.5 µM	2.1 ± 1.5 µM	18.8 ± 13.6 µM	17.4 ± 6.2 µM	156.4 ± 55.6 µM
JXH-III-047 (**3** in 4.3.1.)	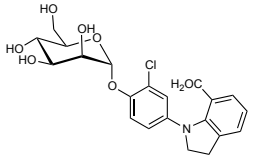	3.9 ± 2.8 µM	18.1 ± 12.3 µM	n.d.		n.d.	
MH17 (**2** in 4.3.1.)	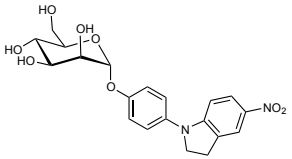	0.21 ± 0.13 µM	3.1 ± 1.6 µM	n.d.		n.d.	
JXH-III-029	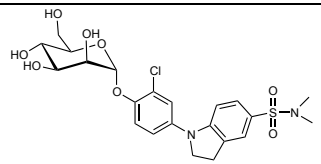	95 ± 63 nM	395 ± 370 nM	21 ± 3.4 nM	188 ± 31 nM	18.9 ± 5.4 nM	170 ± 49 nM
JXH-IV-084	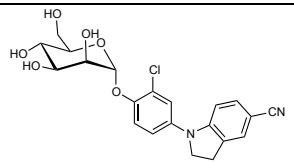	147 nM	1.8 µM	0.25 ± 0.11 nM	2.2 ± 1 nM	58 ± 55 nM	530 ± 500 nM

Antagonist name	Structure	UTI89		J96 *[1]		CFT073	
		IC_{50}	MAC_{90}	IC_{50}	MAC_{90}	IC_{50}	MAC_{90}
JXH@087	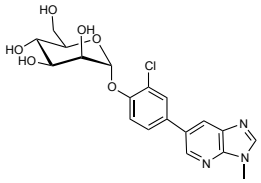	57 nM	880 nM	1.3 ± 1.3 nM	12.2 ± 11 nM	28 ± 15 nM	319 ± 51 nM
WS495	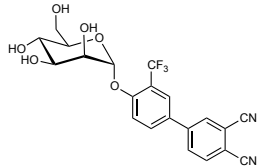	n.d.		39 nM	17 µM	n.d.	
KMFH58 (**4** in 4.3.1., **10j** in **PAPER I**, **MANUSCRIPT I**, **5** in **MANUSCRIPT II**)	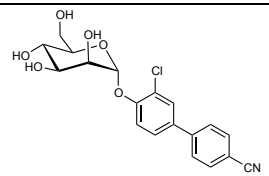	0.11 ± 0.1 µM	0.95 ± 1 µM	0.56 ± 0.3 µM	4 ± 5.4 µM	1.26 ± 0.73 µM *[2]	18 ± 22 µM *[2]

Clearly, affinities of individual antagonists vary between strains, likely due to the affinity state of the FimH. Although J96 showed the best affinities for many of the antagonists, the values are biased. J96 accounted for the highest cell toxicity and resulted in low viable cell counts in many samples. Often, fewer than 20% of all cells were still alive and could be evaluated, which might have decreased the GFP signal and led to a lower IC_{50} or MAC_{90}. This might account to some extent for the high standard deviations reported for J96 in Table 3. Further difficulties of the assay, contributing to the high variations of the reported values, are discussed in chapter 3.2.

JXH@087 resulted in the highest affinity for all three tested strains, but suffers from low solubility (2.4 µg/ml, determined by Jacqueline Bezençon). Applied in the acute bladder infection model (3h infection), JXH@087 failed to reduce the bacterial load of UTI89, J96, and CFT073 (results not shown). It remains unclear, whether this is due to the low solubility, limiting availability of JXH@087 in the urine, or its low residence time. More likely, the outcome of the *in vivo* experiment is resulting from a combination of the above parameters and not only a single reason.

Within another master thesis, Manuel Starck sequenced all FimH of the strains used in this thesis and compared the amino acid mutations. Figure 13 shows a crystal structure of the FimH protein in the low affinity state (*E. coli* K-12), where the positions of amino acid differences within the lectin domain of the strains of interest are marked. In the adjacent table, the mutations are indicated.

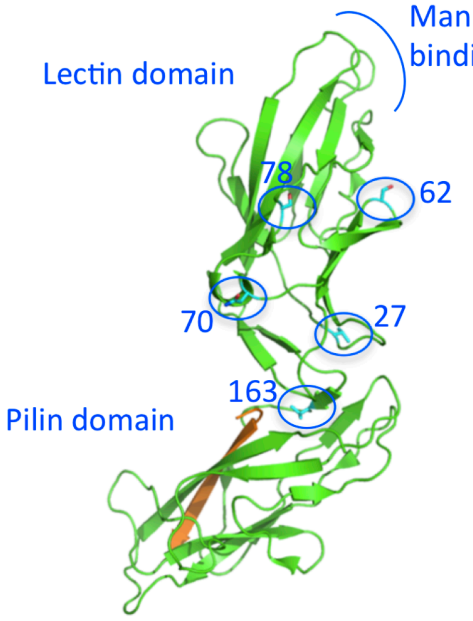

Strain	Amino acid differences in position...				
	27	**62**	**70**	**78**	**163**
UTI89	A	A	S	N	V
J96	V	S	N	S	V
CFT073	A	S	S	N	A
C175-94	A	S	N	S	V

Figure 13. The protein structure of FimH (E. coli K-12, PDB code 4J3O) with the indicated positions of the mutated amino acids summarized in the table on the right. Only the differences within the lectin domain are shown. The picture was kindly provided by Christoph Sager (PyMol).

As introduced in chapter 1.9., single mutations can have an allosteric effect upon affinity of the mannose binding site by influencing the tertiary structure of the protein, which ultimately leads to a more shallow or tighter binding pocket. This affinity may influence the initial binding strength to the uroplakin on bladder cells of UPEC in the first step of the infection. It was estimated that the K_d of the low affinity state to D-mannose is approximately 300 µM compared to 1.2 µM of the high affinity state.[198]

Figure 13 represents the differences in amino acid residues between four strains (UTI89, J96, CFT073, and C175-94, the latter was provided by Dr. Carsten Struve, Statens Serum Institut, Denmark) within the FimH lectin domain. Among those mutations, positions 27, 62, and 163 were previously described as important for mannose binding. Typically, A27V in combination with V163A resulted in decreased CFU counts in the bladder *in vivo*. Furthermore, both A62S or A27V together with V163A resulted in fewer IBCs in the bladder of mice.[86] Likewise, A62S was also associated with a reduced binding to mannose and diminished biofilm formation.[86,232] However, the authors also concluded that the mannose binding ability does not represent *in vivo* fitness.[86] On the other hand, the combinations of A/A/V (UTI89) and A/S/A (CFT073) on positions 27, 62, and 163 were not found in healthy feces, where

A/S/V (C175-94) was most common.[205] Therefore, these positions were proposed to be subject to positive selection for an increased fitness in the urinary tract.[86,233]

The affinity state influences initial binding to surfaces and consequently also the ability for surface exploration. All factors in combination, i.e., binding strength, residence time, and exploration of a surface can have advantages or disadvantages in certain circumstances, which creates a natural selective mechanism. As presented in **MANUSCRIPT II**, the ability for strong mannose binding selects for good biofilm formers, which was also confirmed by Hung *et al*.[133] Since attachment and biofilm formation is an important part in UTI, the virulence of different strains might partly be connected to the affinity state of their FimH. To test the virulence of different strains, mice were infected with UTI89, *Δfim*UTI89 J96, and C175-94 and their bacterial load at 24 hpi and 72 hpi was analyzed (Figure 14).

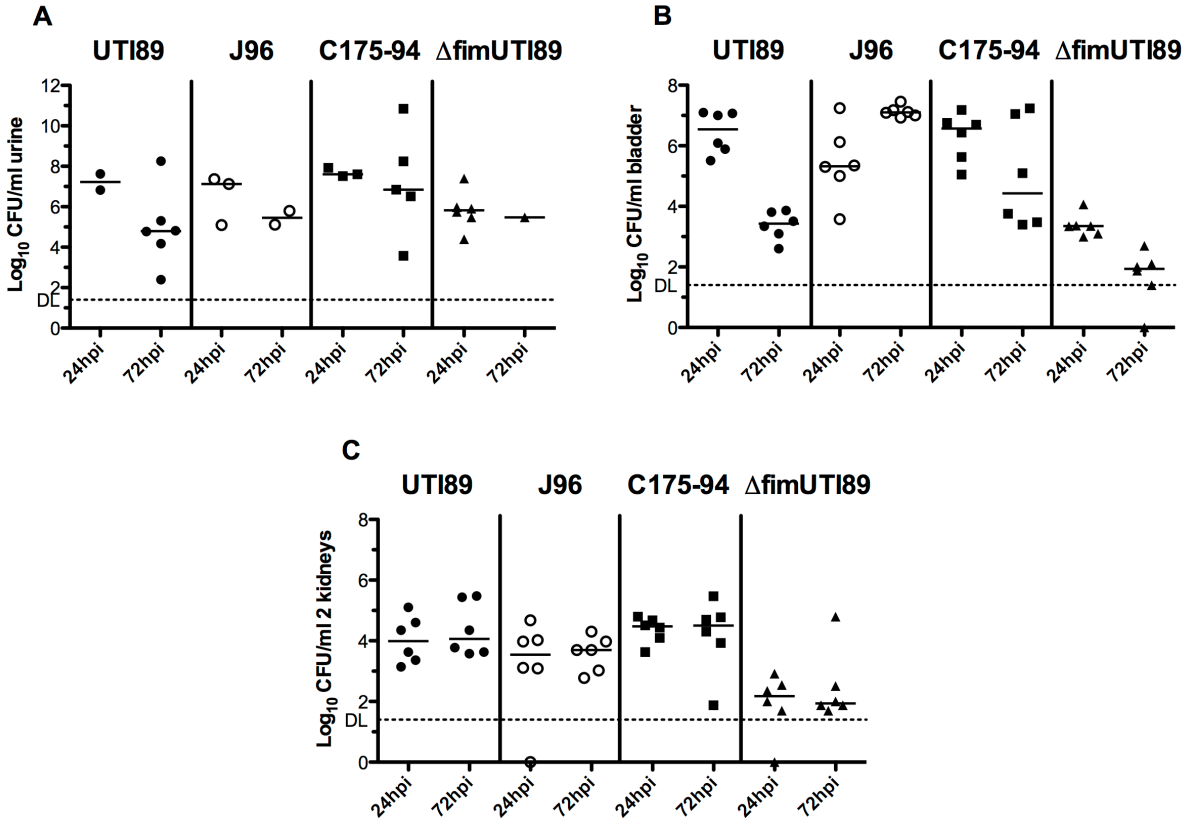

Figure 14. CFU in urine (A), bladder (B), and kidneys (C) after 24 or 72 hours of infection with different bacterial strains indicated on the x-axis. A line in each group indicates the median.

UTI89 resulted in high urine and bladder CFU counts at 24 hpi (7 and 6.5 Log_{10} CFU/ml, respectively), but bacterial loads dropped markedly at 72 hpi, with bladder counts at 3.4 Log_{10} CFU/ml (Figure 14A and 14B). Thus, UTI89 caused a rapid bladder infection with initial high bacterial burden, which greatly decreased over time. Instead, J96 resulted in an opposite infection course with low bacterial loads in the bladder at 24 hpi (5.3 Log_{10} CFU/ml), which dramatically increased at 72 hpi, with 7.1 Log_{10} CFU/ml (Figure 14B). Thereby, it caused uniformly high bacterial counts in the bladder of all six mice tested. C175-94 resembled the course of UTI89, with high counts in urine and bladder at 24 hours (7.6 and 6.6 $Log1_0$ CFU/ml, respectively) and low counts at 72 hpi with a median of 4.4 Log_{10} CFU/ml in the bladder. However, the bladder colony counts of C175-94 were scattered over a broad range within the six mice tested (Figure 14B).

In the kidneys (Figure 14C), all strains reached similarly high counts, which were stable over the 72 hours of infection, and leveled at approximately 4 Log_{10} CFU/ml. The mutant strain *Δfim*UTI89, lacking functional type 1 pili, resulted in low bladder and kidney infections (Figure 14B and 14C), which was not stable over time. This shows the importance of type 1 pili for the establishment of a UTI, but also for persistence.

Overall, since bacterial adhesion is a crucial step in UTI, the affinity state of FimH might be of great importance and governs the infection course not only at the beginning, but likely for the whole duration of the infection. All tested strains showed a different trend concerning bacterial loads, most obviously seen in the bladder. All strains established a similarly high kidney infection, which was stable over time. Kidney infection is independent of FimH. Totsika *et al.* reported a chronic cystitis in 40% of C3H/HeN mice after two weeks of infection with EC958.[187] Conceivably, also this course of infection might be specific for EC958 and different in human beings. Of course, it is not possible to completely assess the infection course of all tested bacteria based on only two time points, but it indicates that every bacterium has a different time course of infection, which might require a different treatment scheme with FimH antagonists.

Yet, the infection time course is not only dependent on the FimH state, but on other virulence genes and on the host's health state, for example. In any case, revealing the influence of the FimH mutations upon treatment options and affinities of FimH antagonists remains the subject of future investigations.

5. Papers and manuscripts

5.1. PAPER I

„FimH Antagonists: Bioisosteres To Improve the *in Vitro* and *in Vivo* PK/PD Profile“

Simon Kleeb,# Lijuan Pang,# Katharina Mayer,# Deniz Eris,# Anja Sigl,# Roland C. Preston, Pascal Zihlmann, Timothy Sharpe, Roman P. Jakob, Daniela Abgottspon, Aline S. Hutter, Meike Scharenberg, Xiaohua Jiang, Giulio Navarra, Said Rabbani, Martin Smiesko, Nathalie Lüdin, Jacqueline Bezençon, Oliver Schwardt, Timm Maier, Beat Ernst

# equally contributed

Journal of Medicinal Chemistry, February 2015

Journal of Medicinal Chemistry

Article

pubs.acs.org/jmc

FimH Antagonists: Bioisosteres To Improve the in Vitro and in Vivo PK/PD Profile

Simon Kleeb,[†,∥] Lijuan Pang,[†,∥] Katharina Mayer,[†,∥] Deniz Eris,[†,∥] Anja Sigl,[†,∥] Roland C. Preston,[†] Pascal Zihlmann,[†] Timothy Sharpe,[§] Roman P. Jakob,[‡] Daniela Abgottspon,[†] Aline S. Hutter,[†] Meike Scharenberg,[†] Xiaohua Jiang,[†] Giulio Navarra,[†] Said Rabbani,[†] Martin Smiesko,[†] Nathalie Lüdin,[†] Jacqueline Bezençon,[†] Oliver Schwardt,[†] Timm Maier,[‡] and Beat Ernst*[,†]

[†]Institute of Molecular Pharmacy, Pharmacenter, University of Basel, Klingelbergstrasse 50, CH-4056 Basel, Switzerland

[‡]Structural Biology, Biocenter, University of Basel, Klingelbergstrasse 70, CH-4056 Basel, Switzerland

[§]Biophysical Facility, Biocenter, University of Basel, Klingelbergstrasse 70, CH-4056 Basel, Switzerland

Supporting Information

ABSTRACT: Urinary tract infections (UTIs), predominantly caused by uropathogenic *Escherichia coli* (UPEC), belong to the most prevalent infectious diseases worldwide. The attachment of UPEC to host cells is mediated by FimH, a mannose-binding adhesin at the tip of bacterial type 1 pili. To date, UTIs are mainly treated with antibiotics, leading to the ubiquitous problem of increasing resistance against most of the currently available antimicrobials. Therefore, new treatment strategies are urgently needed. Here, we describe the development of an orally available FimH antagonist. Starting from the carboxylate substituted biphenyl α-D-mannoside **9**, affinity and the relevant pharmacokinetic parameters (solubility, permeability, renal excretion) were substantially improved by a bioisosteric approach. With 3′-chloro-4′-(α-D-mannopyranosyloxy)biphenyl-4-carbonitrile (**10j**) a FimH antagonist with an optimal in vitro PK/PD profile was identified. Orally applied, **10j** was effective in a mouse model of UTI by reducing the bacterial load in the bladder by about 1000-fold.

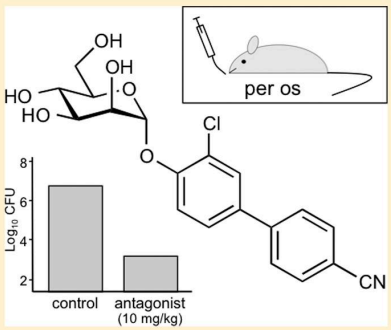

INTRODUCTION

Urinary tract infection (UTI) is one of the most frequent infectious diseases worldwide and affects millions of people every year.[1] In more than 70% of the reported cases, uropathogenic *Escherichia coli* (UPEC) is the causal pathogen.[2] Acute, uncomplicated lower urinary tract infection, commonly referred to as cystitis, requires an antibiotic treatment for symptom relief (i.e., reduction of dysuria, frequent and urgent urination, bacteriuria, pyuria) and for prevention of more devastating or even life threatening complications like pyelonephritis and urosepsis.[3,4] However, the repeated use of antibacterial chemotherapeutics provokes antimicrobial resistance leading to treatment failure.[5] Hence, a new approach for the prevention and treatment of UTI with orally applicable therapeutics is urgently needed.[6]

UPEC undergo a well-defined infection cycle within the host.[7] The key step in pathogenesis is bacterial adhesion to the epithelial cells in the lower urinary tract.[8] This interaction prevents UPEC from clearance by the bulk flow of urine and enables the bacteria to colonize the epithelial cells. The adhesion is mediated by the virulence factor FimH located at the tip of bacterial type 1 pili.[9,10] FimH consists of two immunoglobulin-like domains: the N-terminal lectin domain and (connected by a short linker) the C-terminal pilin domain.[11] The lectin domain encloses the carbohydrate recognition domain (CRD) that binds to the oligomannosides of the glycoprotein uroplakin Ia on the epithelial cell surface.[12] The pilin domain anchors the adhesin to the pilus and regulates the switch between two conformational states of the CRD with high and low affinity for mannosides, respectively.

More than 3 decades ago, Sharon and co-workers described various oligomannosides and aryl α-D-mannosides as potential antagonists of the FimH-mediated bacterial adhesion.[13,14] However, only weak interactions in the milli- to micromolar range were observed. In recent years, several high-affinity monovalent mannose-based FimH antagonists with various aglycones like *n*-alkyl,[15] phenyl,[16] dioxocyclobutenylaminophenyl,[17] umbelliferyl,[16] biphenyl,[18−22] indol(in)-ylphenyl,[23] triazolyl,[24] and thiazolylamino[25] have been reported. In addition, different multivalent presentations of the mannose have been synthesized[26−32] and a heptavalent presentation of *n*-heptyl α-D-mannoside (**1**) tethered to β-cyclodextin proved to be highly effective when applied together with the UTI89 bacterial strain through a catheter into the bladder of C3H/HeN mice.[32] Importantly, adverse side effects resulting from nonselective binding of FimH antagonists (they are all α-D-mannopyrano-

Received: October 3, 2014
Published: February 10, 2015

DOI: 10.1021/jm501524q
J. Med. Chem. 2015, 58, 2221−2239

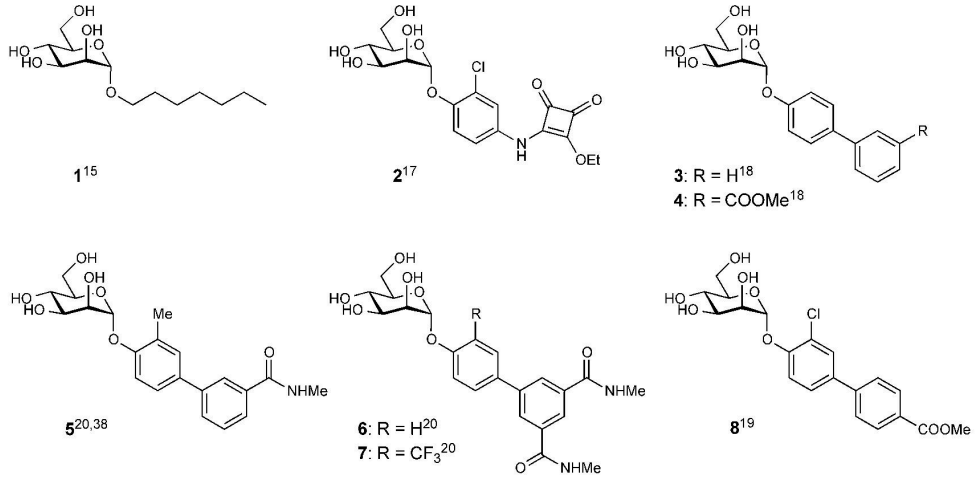

Figure 1. Monovalent FimH antagonists **1**–**4** acting as reference compounds and **5**–**8** which have been orally explored in in vivo disease models.

sides) to mannose receptors of the human host system have recently been ruled out.[33]

The high affinities of the monovalent α-D-mannopyranosides are based on optimal interactions with the main structural features of the CRD:[34−37] first, the mannose binding pocket accommodating the mannose moiety by means of an extended hydrogen bond network and, second, the entrance to the binding site composed of three hydrophobic amino acids (Tyr48, Tyr137, and Ile52) and therefore referred to as "tyrosine gate" hosting aliphatic and aromatic aglycones. As an example, *n*-heptyl α-D-mannopyranoside (**1**) exhibits nanomolar affinity due to hydrophobic contacts of the alkyl aglycone with the hydrophobic residues of the tyrosine gate.[15] Furthermore, aromatic aglycones, such as present in mannosides **2** and **3** (Figure 1), provide strong π−π stacking interactions with the tyrosine gate. This interaction is further favored by the addition of an electron withdrawing substituent on the terminal ring of the biaryl portion (→**4**).[18,19]

Recent in vivo PK studies in mice proved the high potential of the biphenyl α-D-mannosides **5**−**8** for an oral treatment, although high doses (≥50 mg/kg) were necessary to achieve the minimal concentrations required for the antiadhesive effect in the urinary bladder.[19−21] Moreover, the therapeutic effect could only be maintained for a few hours, i.e., 4 h for a po (per os) single-dose application of **7** (50 mg/kg), because of rapid elimination by glomerular filtration and low reabsorption from the primary urine in the renal tubules.[20]

To date, the physicochemical properties affecting the rate of renal excretion, i.e., lipophilicity and plasma protein binding (PPB), or metabolic liabilities promoting nonrenal elimination pathways have been barely investigated for FimH antagonists. The goal of the present study was to optimize the biphenyl α-D-mannoside with respect to oral bioavailability and renal excretion. Starting from antagonist **9**[19] (Figure 2), we synthesized new biphenyl derivatives, characterized their affinity to the CRD, structurally investigated their binding mode, and determined physicochemical and pharmacokinetic parameters predictive for intestinal absorption and renal elimination. Furthermore, we determined in vivo PK (pharmacokinetics) of the most promising new antagonists in a mouse model. After oral administration, the compound with the best PK profile proved effective in reducing the bacterial loads upon bladder infection in a mouse model of UTI.

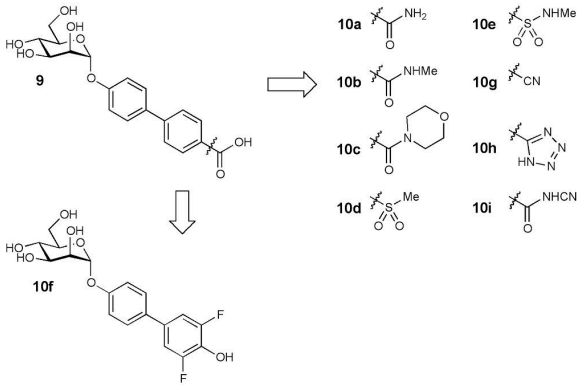

Figure 2. Bioisosteric replacement of the carboxylic acid substituent of biphenyl α-D-mannopyranoside **9**.

■ RESULTS AND DISCUSSION

As previously reported, the carboxylate substituent present in the biphenyl mannoside **9** (its electron withdrawing potential being essential for an enhanced drug target interaction) strongly decreases the lipophilicity of the antagonist (log $D_{7.4} < -1.5$ [19]) in comparison to the *n*-heptyl (→**1**, log P = 1.7 [19]) or the unsubstituted biphenyl aglycone (→**3**, log P = 2.1 [22]). Since low lipophilicity is a major reason for low intestinal absorption and rapid renal excretion of the systemically available antagonist,[19,23] we aspired to improve oral bioavailability as well as renal excretion by replacing the carboxylate in **9** with various bioisosteric groups[39] (Figure 2).

Synthesis. Iodide **11** was prepared from peracetylated mannose and 4-iodophenol in the presence of $BF_3{\cdot}Et_2O$.[22] In a palladium-catalyzed Miyaura−Suzuki coupling[40] with the boronic acid or boronate derivatives **12a**−**g**, the biphenyl derivatives **13a**−**g** were obtained in good to excellent yields. Final deprotection yielded the test compounds **10a**−**g**. When microwave-assisted reaction conditions[41] were utilized, the conversion of arylnitrile **13g** to tetrazole **14** proceeded rapidly and with good yield. After deprotection of **14** using Zemplén conditions, the test compound **10h** was obtained (Scheme 1).

The cyanobenzamide derivative **10i** (Scheme 2) was obtained from **9** by peracetylation (→**15**) followed by conversion of the

DOI: 10.1021/jm501524q
J. Med. Chem. 2015, 58, 2221−2239

Scheme 1[a]

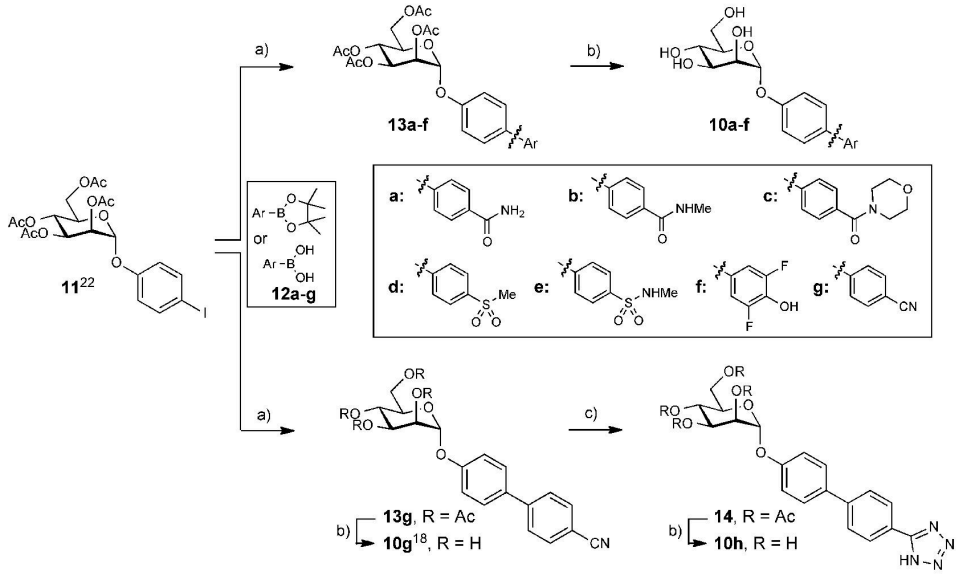

[a](a) $Pd(Cl_2)dppf{\cdot}CH_2Cl_2$, K_3PO_4, DMF, 80 °C, 4 h (**13a–g**, 44–99%); (b) NaOMe, MeOH, rt, 4 h (**10a–h**, 29–86%); (c) $TMSN_3$, $Bu_2Sn(O)$, DME, 150 °C, microwave, 10 min (81%).

Scheme 2[a]

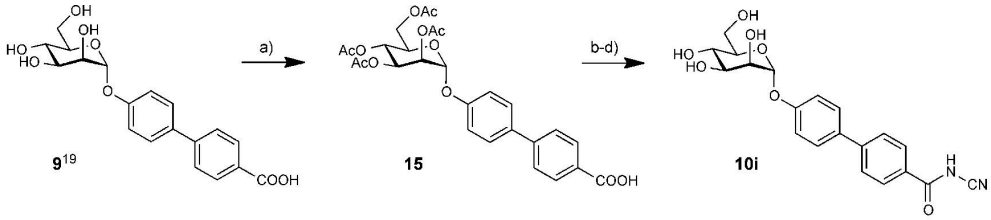

[a](a) (i) Ac_2O, DMAP, pyridine, 0 °C to rt, overnight; (ii) sat. $NaHCO_3$ aq, DCM, rt, 2 h (**15**, 53%); (b) 1-chloro-*N*,*N*,2-trimethyl-1-propenylamine, toluene, 0 °C to rt, 2 h; (c) NaH, NH_2CN, DMF, 0 °C to rt, overnight; (d) NaOMe, MeOH, rt, 4 h (**10i**, 21% for three steps).

Scheme 3[a]

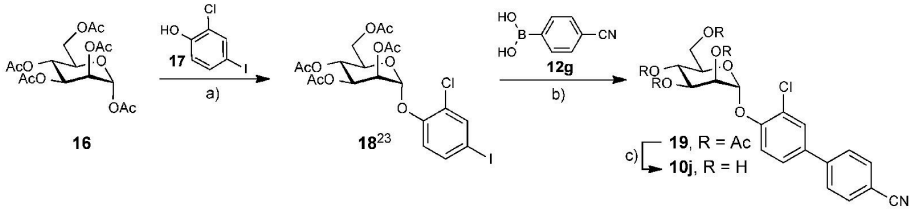

[a](a) $BF_3{\cdot}Et_2O$, CH_2Cl_2, 40 °C (76%); (b) $Pd(Cl_2)dppf{\cdot}CH_2Cl_2$, K_3PO_4, DMF, 80 °C (75%); (c) NaOMe, MeOH, rt, 4 h (48%).

carboxylic acid into its acid chloride with 1-chloro-*N*,*N*,2-trimethyl-1-propenylamine.[42] Without isolation, the acid chloride was reacted with sodium hydrogen cyanamide in DMF followed by deacetylation under Zemplén conditions to yield the test compound **10i**.

Finally, to further improve the pharmacokinetic properties of mannoside **10g**[18] (see Table 3), a chloride substituent was introduced to the ortho-position of the aromatic ring adjacent to the anomeric oxygen. For its synthesis, peracetylated α-D-mannose (**16**) was coupled with 2-chloro-4-iodophenol (**17**) using $BF_3{\cdot}Et_2O$ as promotor (→**18**, 76%). After the introduction of the second aromatic ring by Miyaura–Suzuki coupling (→**19**, 75%), deprotection yielded mannoside **10j** (Scheme 3).

Binding Affinity. The binding affinity of heptyl mannoside **1**, the biphenyl mannosides **3**, **9**, **20**,[18] and the bioisosteres **10a–j** was determined in a competitive fluorescence polarization assay (FP assay) and with isothermal titration calorimetry (ITC). A protein construct consisting of the CRD with a C-terminal His-tag with a thrombin cleavage site (FimH-CRD-Th-His_6) was used for all experiments.[43]

Competitive Fluorescence Polarization Assay. For the rapid evaluation of binding affinity, we established a competitive

DOI: 10.1021/jm501524q
J. Med. Chem. 2015, 58, 2221–2239

Scheme 4[a]

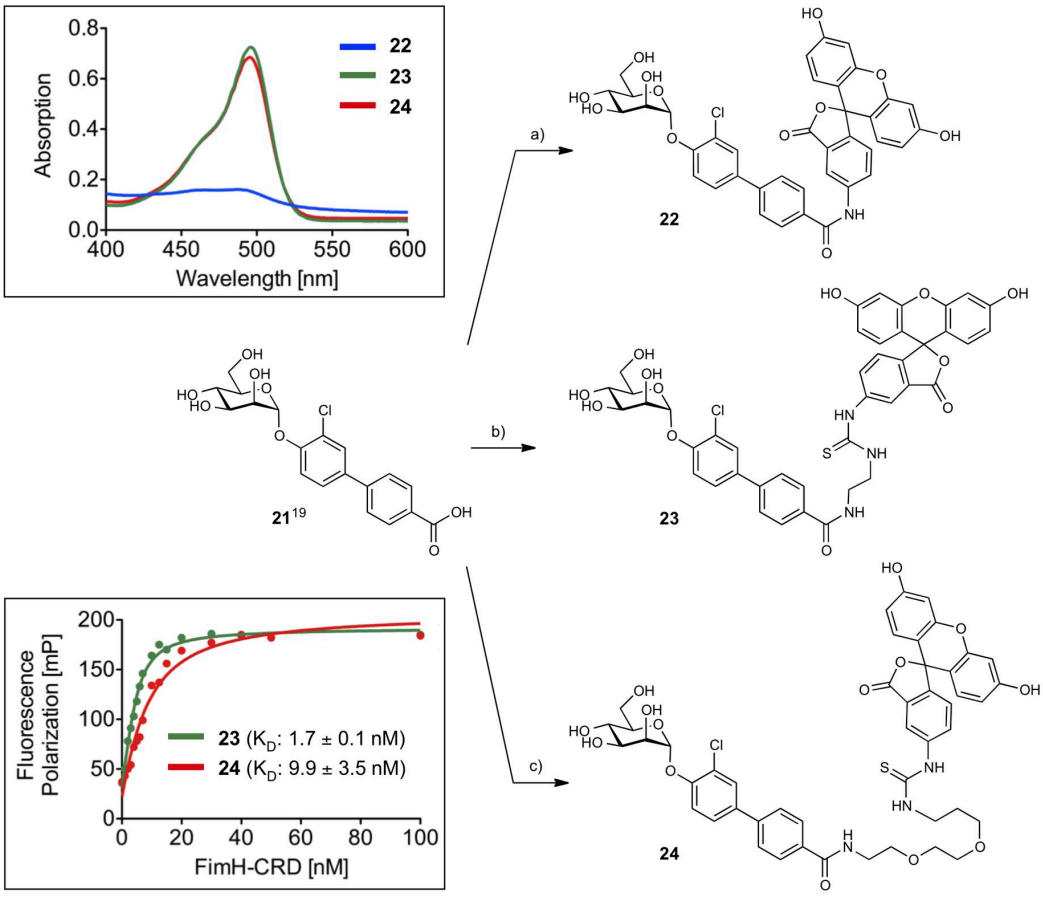

[a](a) 1-[(1-(Cyano-2-ethoxy-2-oxoethylideneaminooxy)dimethylaminomorpholinomethylene)]methanaminium hexafluorophosphate (COMU), NEt_3, fluoresceinamine, DMF, rt, 7 h (**22**, 19%); b) (i) DIC, NHS, *N*-Boc-ethylenediamine, DMF, rt, 12 h; (ii) TFA, DCM, rt, 10 min (68% over two steps), (iii) fluorescein isothiocyanate (FITC), NEt_3, DMF, rt, 3 h (**23**, 48%); (c) (i) DIC, NHS, *N*-Boc-PEG2-NH_2, DMF, rt, 14 h; (ii) TFA, DCM, rt, 30 min (62% over two steps); (iii) FITC, DMF, rt (**24**, 65%).

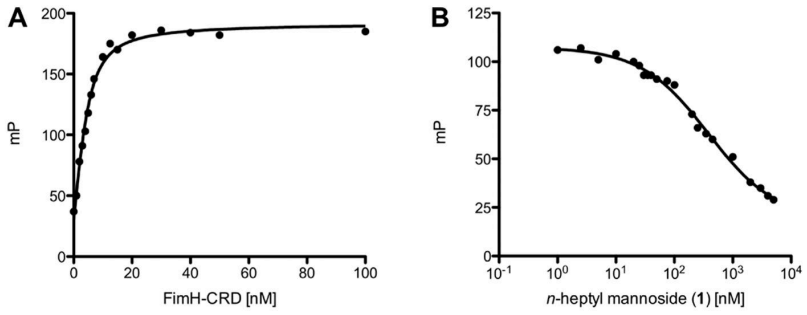

Figure 3. (A) Direct binding curve of the labeled competitor **23** obtained by adding a linear dilution of FimH-CRD (0−100 nM) and a constant concentration of competitor **23** (5 nM). The K_D was determined by fitting the experimental data to a single-site binding fit that accounts for ligand depletion. In three FP based direct binding experiments the K_D of competitor **23** was determined to be 1.7 nM. (B) Inhibition curve of *n*-heptyl mannoside (**1**) from the competitive FP assay. The IC_{50} value was determined by nonlinear least-squares fitting to a standard four-parameter equation. A modified Cheng−Prusoff equation[45] was used to calculate the corresponding K_D value (K_D = 28.3 nM).

binding assay based on fluorescence polarization (FP). Similar formats have been applied before for the detection of carbohydrate−lectin interactions.[18,44] In this assay, the antagonist of interest displaces a fluorescently labeled competitor from the binding site, thereby causing a reduction in fluorescence polarization.[45] To identify the optimal competitor, fluorescein isothiocyanate (FITC) was connected to the FimH ligand **21** by three linkers of different lengths (→**22**−**24**, Scheme 4). For

DOI: 10.1021/jm501524q
J. Med. Chem. 2015, 58, 2221−2239

optimal sensitivity and signal-to-noise ratio, three main parameters need to be considered: (i) the affinity of the competitor should not be impaired by the fluorescent label; (ii) the conformational flexibility of the label upon binding of the competitor to the CRD should be low; (iii) the fluorescence properties of the label should not be affected by the connected ligand.[46−48] A change in fluorescence properties was observed for reporter ligand **22** in which the label was linked to the biphenyl agylcone by an amide bond. The absorption spectrum revealed a lack of the characteristic fluorescein absorption peak at 494 nm (Scheme 4), likely due to an extension of the conjugated system to the biphenyl moiety of the ligand. The elongated saturated spacer groups in competitors **23** and **24** ensured that the expected spectral properties of the dye were retained (Scheme 4).

For the determination of their binding affinity, fixed concentrations of the reporter ligands **23** and **24** were incubated for 24 h with a linear dilution of the FimH-CRD (0−100 nM). FP was measured using a plate reader, with polarized excitation at 485 nm and emission at 528 nm measured through appropriately oriented polarizers. Fitting the single-site binding function of Cooper[49] to the observed FP data resulted for compound **23** in a dissociation constant (K_D = 1.7 nM, Figure 3A) similar to that of the unlabeled parent compound **21**,[19] whereas **24** showed a 5-fold lower affinity (9.9 nM) (Scheme 4). Therefore, the reporter ligand **23** fulfills all characteristics as an optimal competitor and was used for the FP assay.

For the test compounds **1**, **3**, **9**, **20**, and **10a−j**, a 24 h incubation time was applied before FP was measured because of the long residence time of FimH antagonists ($t_{1/2}$ > 3.5 h, Figure 3B[50]). The 24 h incubation period was empirically determined to be necessary to reach equilibrium between reporter ligand and compound of interest. IC_{50} values were obtained by nonlinear least-squares regression (standard four-parameter dose−response curve) and converted to K_D values using a modified Cheng−Prusoff equation.[45] This equation accounts for the ligand depletion effect in competitive titrations involving high-affinity interaction partners present in similar concentrations. Under these conditions, the free concentration of an interacting species cannot be assumed to equal the total concentration.

The K_D values determined for the test compounds **1**, **3**, **9**, **20**, and **10a−j** are summarized in Table 1. Against our expectations, the biphenyl mannosides **3** and **9** exhibit similar affinities (Table 1), despite the presence of an electron withdrawing carboxylate substituent in antagonist **9**. According to the crystal structure of FimH cocrystallized with the sulfonamide derivative **10e** (Figure 4A), the outer aromatic ring of the biphenyl aglycone forms $\pi-\pi$ interactions with the electron rich Tyr48, which is part of the tyrosine gate of FimH.[15] A reduction of electron density of the aglycone by the electron withdrawing carboxylate was expected to enforce these $\pi-\pi$ stacking interactions and lead to improved affinity. However, this beneficial effect might be compensated by an entropic penalty originating from the improved $\pi-\pi$ stacking to Tyr48 that might lead to the reduced flexibility of both protein and antagonist. Furthermore, a beneficial enthalpy effect might be partially compensated by an enthalpy penalty originating from the desolvation of the charged carboxylate in **9**[51] (see also Experimental Section). Although this substituent is solvent exposed, at least a partial desolvation may be necessary upon antagonist binding. To prove this assumption, we replaced the carboxylate by the corresponding methyl ester (→**20**)[18] in order to reduce the desolvation penalty and, as predicted by the Hammett constant σ_p,[52] to further improve the $\pi-\pi$ stacking.

Table 1. Affinities (K_D) of FimH Antagonists to FimH-CRD-Th-His$_6$[b]

Entry	Compd		Affinity K_D [nM]
1	**1**		28.3 ± 5.0
2	**3**		15.1 ± 2.2
3	**9**	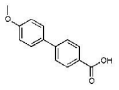	17.9 ± 1.5
4	**20**	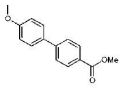	3.6 ± 0.9
5	**10a**	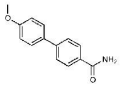	2.8 ± 0.3
6	**10b**	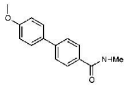	2.9 ± 0.5
7	**10c**	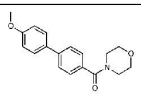	3.0 ± 0.1
8	**10d**	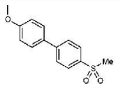	1.7 ± 0.2
9	**10e**	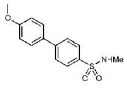	2.7 ± 0.4
10	**10f**	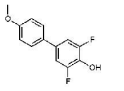	3.7 ± 0.2
11	**10g**	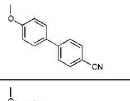	2.0 ± 0.6
12	**10h**	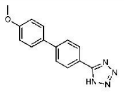	5.7 ± 0.1
13	**10i**	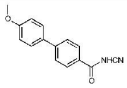	8.4 ± 0.3
14	**10j**	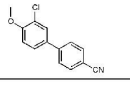	< 1[a]

[a]The K_D value of **10j** was approximated to be in the subnanomolar range. The IC_{50} value obtained in the competitive FP assay was equal to the lowest value that can be resolved by the assay, indicating stoichiometric titration of **10j** due to its high affinity. Consequently, its K_D must be below the K_D of competitor **23**. [b]Dissociation constants (K_D) were determined in a competitive fluorescence polarization assay.

DOI: 10.1021/jm501524q
J. Med. Chem. 2015, 58, 2221−2239

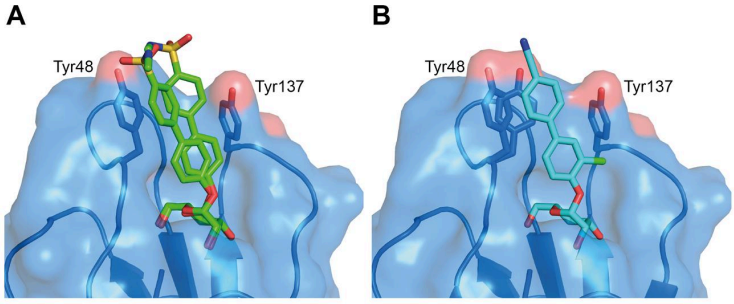

Figure 4. Ligand binding poses determined by X-ray cocrystallization with compounds **10e** resolved to 1.07 Å (A) and **10j** resolved to 1.10 Å (B). The electron density surrounding the aglycone of **10e** indicates flexibility of the aglycone and was modeled in two poses. Both compounds bind in a similar pose with a well-defined hydrogen network surrounding the mannose moiety and $\pi-\pi$ stacking interactions between the second aromatic ring and Tyr48 side chain (A). In contrast, in the FimH-CRD/**10j** structure the amino acid side chain of Y48 can be modeled in two distinct rotamers, suggesting flexibility also of the receptor (B).

Indeed, a 6-fold improvement in affinity was achieved. However, since the methyl ester undergoes rapid enzyme-mediated hydrolysis in vivo,[19] it will not be available at the place of action in the urinary bladder. The methyl ester was therefore replaced by metabolically stable bioisosteres[39] exhibiting comparable electron withdrawing properties[52] (Table 1, entries 5−13). The most potent derivatives **10d**, **10e**, and **10g** showed affinities in the low nanomolar range.

As previously reported,[22] a chloro substituent in the ortho-position of the aromatic ring adjacent to the anomeric oxygen is favorable for affinity and improves the physicochemical properties relevant for oral bioavailability. Indeed, the corresponding antagonist **10j** was the most potent compound tested in this study.

Isothermal Titration Calorimetry (ITC). To further confirm our hypothesis regarding $\pi-\pi$ stacking and desolvation, we performed ITC experiments with the reference compound **1**, the unsubstituted biphenyl mannoside **3**, the carboxylic acid **9**, and the bioisosteres **10b−e,g,j** (Table 2). ITC allows the simultaneous determination of the stoichiometry (N), the change in enthalpy (ΔH) and the dissociation constant (K_D) for ligand−protein binding.[53,54] The reliable determination of these three parameters requires well-defined sigmoidal titration curves characterized by the dimensionless Wiseman parameter c (c = Mt(0) K_D^{-1}, where Mt(0) is the initial macromolecule concentration).[55] To be sure that data can be fitted with confidence, the c-value should be between 1 and 1000 (ideally between 5 and 500),[56] which could be achieved for the antagonists **3** and **9**. For titrations involving low micromolar Mt(0) and interactions in the low nanomolar or picomolar range, as suggested for the bioisosteres **10b−j**, c-values above 1000 were expected. Since these conditions lead to steep titration curves that do not allow the determination of the curve slope representing $1/K_D$, we applied an alternative, competitive format referred to as displacement assay.[57,58] First, FimH-CRD-Th-His$_6$ was preincubated with the low affinity antagonist *n*-heptyl 2-deoxy-α-D-mannopyranoside (**25**, for synthesis see Supporting Information). The high-affinity bioisosteres of interest were titrated into the protein−ligand complex giving well-defined sigmoidal titration curves.

The resulting K_D values (Table 2) correspond well with the data obtained from the FP assay (Table 1). A comparison of the thermodynamic fingerprints of antagonists **3** and **9** reveals that the more favorable enthalpic contribution resulting from facilitated $\pi-\pi$ stacking leads to a net enthalpy gain ($\Delta\Delta H$ = −3.7 kJ/mol). However, an even greater increase in enthalpy is likely countered by the enthalpy costs for desolvation of the electron withdrawing carboxylate.

The gain in enthalpy is in turn compensated by an unfavorable entropy ($-T\Delta\Delta S$ = 3.2 kJ/mol) as a result of the reduced flexibility of both the antagonist and the Tyr48 side chain caused by the improved interaction. This is not entirely outweighed by the beneficial entropy contribution related to the partial desolvation of the carboxylate and the related release of water into the bulk. Added together, the enthalpy and entropy contributions of antagonists **3** and **9** result in similar affinities (K_D of 17.7 and 15.0 nM, respectively).

In contrast, the replacement of the carboxylate group by various neutral bioisosteres (entries 4−7) reduces the enthalpy costs for desolvation (see calculated free energies of desolvation, Experimental Section) and therefore leads to a markedly improved enthalpy ($\Delta\Delta H$ from −3.5 to −5.8 kJ/mol). As a result, an up to 5-fold improvement of the K_D values was achieved. Finally, with a cyano substituent (entries 8 and 9), the enthalpy term was further improved ($\Delta\Delta H$ = −3.7 kJ/mol) because of a reduced desolvation penalty and improved $\pi-\pi$ stacking interactions. However, this beneficial component is again partially compensated by a decrease in entropy. This can be attributed, first, to the loss of flexibility of the tightly bound ligand (Figure 4B) and, second, to the smaller surface area of the cyano substituent compared to amide, sulfonamide, and sulfone, which results in a smaller number of water molecules being released to bulk upon binding.

X-ray Crystallography. To determine the binding poses of the bioisosters, we cocrystallized the compounds **10e** and **10j** with the FimH-CRD (Figure 4). Atomic resolution crystal structures were obtained at 1.07 Å (**10e**) and 1.10 Å (**10j**). As observed in previous mannoside cocrystal structures,[15,18,36] the mannose moiety forms an extensive hydrogen bond network to the well-defined binding site with all of its hydroxyl groups. The biphenyl aglycone is located between the tyrosine gate residues (Tyr48/Tyr137). The $\pi-\pi$ stacking of the second aromatic ring of the aglycone to the side chain of Tyr48 contributes most to the interaction energy of the aglycone moiety. Interactions to the Tyr137 side chain on the other hand are only limited. Whereas a previously published crystal structure of a biphenyl mannoside in complex with FimH-CRD suffers from crystal contacts of binding site residues (Tyr48 side chain to backbone oxygen of Val27) possibly causing the distortion of the binding site,[18] the binding sites of our structures are mostly solvent exposed. This

DOI: 10.1021/jm501524q
J. Med. Chem. 2015, 58, 2221−2239

Table 2. Thermodynamic Parameters from ITC for Selected FimH Antagonists Binding to FimH-CRD-Th-His_6[d]

Entry	Compd		K_D[a] [nM]	ΔG [kJ/mol]	ΔH[a] [kJ/mol]	$-T\Delta S$ [kJ/mol]	n	Type of measurement
1	**1**[b,c]	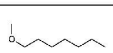	28.9 (25.8 – 32.3)	-43.0	-50.3 (-50.2 – -50.7)	7.3	1.00	direct
2	**3**[b]		17.7 (14.1 – 22.3)	-44.2	-45.0 (-44.5 – -45.6)	0.8	1.07	direct
3	**9**	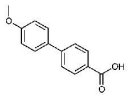	15.0 (13.4 – 16.7)	-44.7	-48.7 (-48.4 – -49.0)	4.0	1.05	direct
4	**10b**	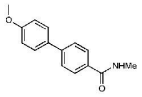	4.3 (3.2 – 5.6)	-47.8	-54.5 (-54.1 – -54.9)	6.7	1.02	competitive vs. **25**
5	**10c**	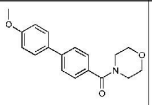	5.0 (3.8 – 6.6)	-47.4	-54.5 (-54.1 – -54.8)	7.1	0.97	competitive vs. **25**
6	**10d**	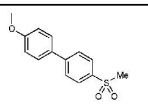	3.0 (2.1 – 4.2)	-48.7	-52.3 (-51.5 – -53.1)	3.6	0.99	competitive vs. **25**
7	**10e**	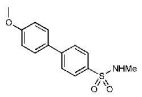	3.5 (2.9 – 4.3)	-48.2	-52.2 (-51.6 – -52.8)	3.9	1.06	competitive vs. **25**
8	**10g**	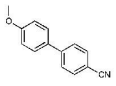	2.8 (2.3 – 3.3)	-48.8	-58.2 (-57.8 – -58.6)	9.4	1.00	competitive vs. **25**
9	**10j**	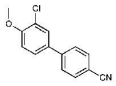	1.3 (1.1 – 1.6)	-50.7	-60.9 (-60.4 – -61.4)	10.1	1.01	competitive vs. **25**
10	**25**	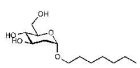	9'386 (8'555 – 10'287)	-28.7	-19.5 (-19.1 – -20.0)	-9.1	1.00	direct

[a]95% confidence interval from fitting in parentheses. [b]Global fit including two direct titration measurements. [c]ITC data were previously published with an n-value of 0.82.[37] [d]n, stoichiometric correction factor.

revealed the flexibility of the aglycone in the FimH-CRD/**10e** structure, since the electron density toward the solvent-exposed sulfonamide indicates that there is not one single orientation. Therefore, the aglycone was modeled in two distinct poses. In contrast, in the FimH-CRD/**10j** structure the amino acid side chain of Y48 can be modeled in two distinct rotamers, suggesting flexibility also of the receptor.

Physicochemical Properties and in Vitro Pharmacokinetics. Intestinal absorption and renal excretion are prerequisites for a successful oral treatment of UTI with FimH antagonists. Furthermore, reabsorption of antagonist from the renal ultrafiltrate is desirable for maintaining the minimal antiadhesive concentration in the target organ, namely, the bladder, over an extended period of time. To estimate the influence of the bioisostere approach on oral bioavailability and the rate of renal excretion, we determined lipophilicity by means of the octanol–water distribution coefficient (log $D_{7.4}$),[59] aqueous solubility, and membrane permeability in the artificial membrane permeability assay (PAMPA)[60] and the colorectal adenocarcinoma (Caco-2) cell monolayer model.[61]

DOI: 10.1021/jm501524q
J. Med. Chem. 2015, 58, 2221–2239

Table 3. Physicochemical and in Vitro Pharmacokinetic Parameters[h]

compd	pK_a[a]	log $D_{7.4}$[b]	solubility [μg/mL]/pH[c]	PAMPA log P_e [cm/s]/pH[d]	Caco-2 P_{app} [10^{-6} cm/s][e] a → b	Caco-2 P_{app} [10^{-6} cm/s][e] b → a	PPB f_b [%][f]	metabolic stability $t_{1/2}$ [min][g]
1		1.65	>3000	−4.89	7.0 ± 0.6	9.4 ± 0.2	81	13
3		2.1 ± 0.1	21 ± 1/7.4	−4.7 ± 0.1/7.4	10.0 ± 0.9	19.0 ± 1.2	93 ± 1	nd
20		2.14	33.8/6.51	−4.7	4.23	nd	93	1.0
9	3.88	<−1.5	>3000/6.61	no permeation	nd	nd	73	>60
10a		0.5 ± 0.1	12 ± 1/7.4	−6.8 ± 0.3/7.4	0.12 ± 0.01	0.61 ± 0.03	nd	nd
10b		0.8 ± 0.0	122 ± 13/7.4	−9.2 ± 1.4/7.4	1.10 ± 0.82	0.87 ± 0.15	nd	nd
10c		0.2 ± 0.1	>250/7.4	−7.8 ± 0.3/7.4	0.18 ± 0.07	1.30 ± 0.03	48 ± 2	>60
10d		0.4 ± 0.0	246 ± 17/7.4	−7.2 ± 0.0/7.4	0.36 ± 0.01	1.76 ± 0.12	99 ± 1	>60
10e		0.7 ± 0.1	>250/7.4	−8.6 ± 0.2/7.4	0.28 ± 0.23	1.82 ± 0.14	>99	>60
10f	6.5	1.1 ± 0.0	>150/3.0	−7.7 ± 0.8/5.0	0.40 ± 0.02	1.90 ± 0.17	nd	nd
			>150/7.4	−8.8 ± 0.1/7.4				
10g		1.4 ± 0.0	186 ± 4/7.6	−5.7 ± 0.0/7.4	2.0 ± 0.1	13.2 ± 2.1	99 ± 0	>60
10h	3.7	−1.4 ± 0.1	11 ± 0/3.0	−9.3 ± 1.4/5.0	0.17 ± 0.00	0.22 ± 0.01	nd	nd
			273 ± 2/7.4	−8.8 ± 1.4/7.4				
10i	2.5	−1.1 ± 0.1	>150/3.0	−6.8 ± 0.2/5.0	0.22 ± 0.14	0.29 ± 0.03	nd	nd
			>150/7.4	−7.0 ± 0.1/7.4				
10j		2.1 ± 0.0	192 ± 5/7.4	−5.2 ± 0.0/7.4	2.2 ± 0.4	22.1 ± 1.5	89 ± 1	>60

[a] pK_a values were determined by NMR spectroscopy. [b] Octanol−water distribution coefficients (log $D_{7.4}$) were determined by a miniaturized shake-flask procedure at pH 7.4. Values represent the mean ± SD of sextuplicate measurements.[59] [c] Kinetic solubility was measured in a 96-well format using the μSOL Explorer solubility analyzer at the indicated pH in triplicate. [d] P_e = effective permeability. Passive permeation through an artificial membrane was determined by the parallel artificial membrane permeation assay (PAMPA). Values represent the mean ± SD of quadruplicate measurements performed at the indicated pH.[60] [e] P_{app} = apparent permeability. Permeation through a Caco-2 cell monolayer was assessed in the absorptive (a → b) and secretory (b → a) directions in triplicate.[61] [f] Plasma protein binding (PPB) was determined by equilibrium dialysis in triplicate.[62] [g] Metabolic stability was determined by incubating the compounds (2 μM) with pooled rat liver microsomes (RLM, 0.5 mg/mL) in the presence of NADPH (1 mM, compounds **1**, **9**, **10c−e,g,j**) or without NADPH (compound **20**).[63] [h] nd = not determined.

Oral Bioavailability. Oral bioavailability of a compound relies on solubility, permeation through the membranes lining the intestine, and stability against first pass metabolism.[64,65] As discussed by Lipinski[66] and Curatolo,[67] dose and permeability define the minimum aqueous solubility required for oral administration. Thus, a dose of 1 mg/kg of a moderately permeable compound requires a solubility of at least 52 μg/mL. Whereas sufficient aqueous solubility (>3000 μg/mL) was reported for *n*-heptyl α-mannopyranoside (**1**),[19] the unsubstituted biphenyl α-D-mannopyranoside **3** and the antagonists bearing a methylcarboxylate, carboxamide, or tetrazole substituent (compounds **20**, **10a**, and **10h**) were found to be scarcely soluble.[22] As proposed by Ishikawa,[68] a possible reason is the apolar and planar aglycone. By contrast, the polar carboxylic acid moiety present in antagonist **9** or the substituents in the bioisosteres **10b−j** enhance solubility to 122−273 μg/mL, a level sufficient for in vivo PK studies. For in vivo disease studies, however, dosages of up to 10 mg/kg were foreseen (see below), requiring a solubility of 520 μg/mL.[66,67] For this reason, surfactant Tween 80 (1%) had to be added.

Furthermore, permeability data derived from PAMPA[69] and the Caco-2 model[70] suggest moderate to high permeation of the moderately lipophilic antagonists **1**, **3**, and **20** (log $D_{7.4}$ > 1.6) through the intestinal membranes. The bioisosteres **10a−f,h,i**, although slightly more permeable than the strongly hydrophilic carboxylic acid derivative **9**, show only low values of permeability compared to *n*-heptyl α-D-mannopyranoside (**1**) or the unsubstituted biphenyl mannoside **3**. However, the *p*-cyanobiphenyl derivatives **10g** and **10j** display elevated log $D_{7.4}$ and effective permeability (log P_e) in the range for successful intestinal absorption. Regarding both sufficient aqueous solubility and elevated membrane permeability, the *p*-cyano substituted bioisosteres **10g** and **10j** are thus the most promising candidates for oral absorption. Moreover, combining the bioisosteric replacement with the addition of a chloro substituent in the ortho-position of the aromatic ring adjacent to the anomeric oxygen (→**10j**)[22] resulted in the most advantageous physicochemical profile for oral bioavailability.

Renal Excretion. The rate of renal excretion depends on the rate of glomerular filtration and the propensity to tubular secretion and reabsorption of an antagonist.[71] Only the fraction that is not bound to plasma proteins is expected to enter the glomerular filtrate.[72] Plasma protein binding (PPB) data indicating the fraction bound (f_b) are listed in Table 2.[62] The biphenyls **9** and **10c** were identified as moderate binders to plasma proteins ($f_b \leq 65\%$), which suggests a low impact of PPB on antagonist filtration. The f_b values of the antagonists **1**, **3**, **20**, and **10j** were between 80% and 93%, whereas the bioisosteres **10d,e,g** showed particularly high protein binding ($f_b \geq 99\%$) implying slow compound entry into the primary urine. However, the kinetic aspects of PPB, that is, association and dissociation rate constants, remain to be determined to quantify precisely the influence of PPB on filtration.[73]

Furthermore, log $D_{7.4}$ was identified as key determinant of tubular reabsorption.[74−76] Accordingly, lipophilic compounds are predominantly reabsorbed from the renal filtrate. Given that renal clearance is the major route of elimination, this will result in a slow but steady excretion into the bladder. In contrast, hydrophilic compounds are poorly reabsorbed and thus quickly renally eliminated, which leads to high initial compound levels in the urine but narrows the time range where the minimal antiadhesive concentration is maintained. Consequently, low log $D_{7.4}$ as shown for the antagonists **9**, **10h**, and **10i** implies low tubular reabsorption and rapid elimination of the filtered molecules by the urine. Otherwise, log $D_{7.4}$ between 0.2 and 0.7, such as determined for the bioisosteres **10a-e**, suggests

DOI: 10.1021/jm501524q
J. Med. Chem. 2015, 58, 2221−2239

Table 4. Pharmacokinetic Parameters Determined after a Single iv Application of Compounds 9, 10c, 10e, and 10j in Female C3H/HeN Mice[a]

	plasma						
compd	C_0 (μg/mL)	dose (mg/kg)	V_z (mL)	$t_{1/2}$ (h)	AUC_{0-inf} (μg·h/mL)	CL_{tot} (mL/h)	urine, C_{max} (μg/mL)
9	40	50	25.2	0.33	23.5	53.1	300
10c	109.7	50	28.3	0.4	25.3	49.4	4611
10e	151.6	50	19.5	1.9	175.1	7.1	387
10j	0.36	0.625	52.8	0.17	0.07	218	10

[a]Values were calculated using PKSolver.[78] C_0, initial concentration; V_z, volume of distribution in terminal phase; AUC, area under the curve; CL_{tot}, total clearance; C_{max}, maximal concentration.

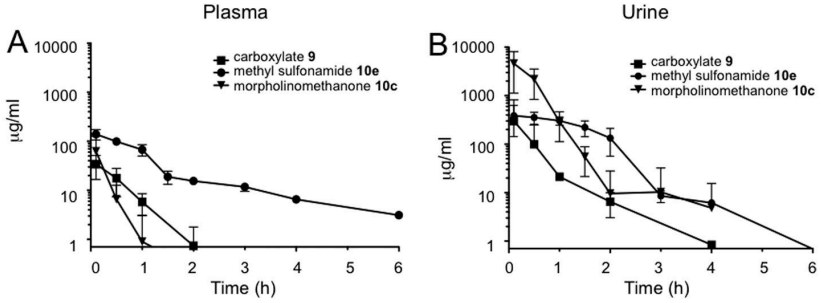

Figure 5. Antagonist concentrations in (A) plasma and (B) urine after a single iv application of **9**, **10c**, and **10e** (50 mg/kg).

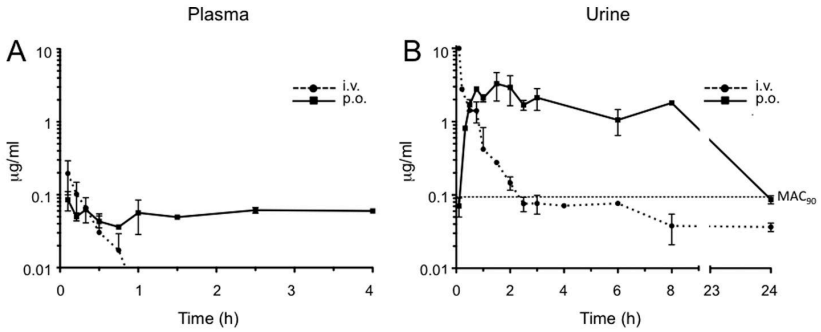

Figure 6. Antagonist concentrations in (A) plasma and (B) urine after a single iv and po application of compound **10j** (iv, 0.625 mg/kg; po, 1.25 mg/kg). MAC_{90} is the minimal antiadhesive concentration to inhibit 90% adhesion (0.094 μg/mL).

increasing propensity to tubular reuptake, whereas log $D_{7.4} > 1$ as shown for heptyl mannoside **1** and the biphenyl mannosides **3**, **20**, **10g**, **10f**, and **10j** is optimal for tubular reabsorption from the glomerular filtrate and thus for slow renal clearance.

Metabolic Stability. Increasing lipophilicity is usually paralleled by increasing susceptibility to metabolism.[77] Liabilities toward metabolic clearance pathways that prevent the intact antagonist from reaching the target in the bladder were therefore of interest. To assess their propensity to cytochrome P450 (CYP450) mediated metabolism, heptyl mannoside **1**, the carboxylic acid derivative **9**, and the bioisosteres **10c–e,g,j** were incubated with rat liver microsomes (RLM, 0.5 mg/mL) in the presence of the cofactor β-nicotinamide adenine dinucleotide phosphate (NADPH).[63] To confirm the high propensity of the methyl ester present in antagonist **20** to carboxylesterase (CES) mediated hydrolysis, this antagonist was incubated with RLM only. The profiles of unchanged compound versus time revealed high susceptibility of heptyl mannoside **1** to CYP450-mediated metabolism ($t_{1/2}$ = 13 min) and rapid hydrolysis of the ester **20** by the hepatic CES ($t_{1/2}$ = 1.0 min). Otherwise, the bioisosteres **10c–e,g,j** were stable against enzyme-mediated bioconversion ($t_{1/2}$ > 60 min), suggesting lower propensity to metabolic, nonrenal elimination pathways.

Considering PPB, lipophilicity, and metabolic stability data, we therefore expected (i) a steady release of compounds **10d,e,g,j** into the bladder because of high PPB decelerating glomerular filtration (**10d,e,g**) and/or high log $D_{7.4}$ supporting tubular reabsorption (**10g,j**), (ii) a fast excretion of antagonists **9** and **10c** via the urine due to low PPB and low log $D_{7.4}$, and (iii) a rapid clearance of heptyl mannoside **1** from the body by renal and metabolic pathways. Compounds featuring high propensity to renal excretion as major route of elimination (**10c**, **10e** and **10j**) were selected for in vivo PK studies in a mouse model.

Pharmacokinetic Studies in C3H/HeN Mice. This first part of our study explored the predicted effects of lipophilicity, PPB, and metabolic stability on antagonist disposition and elimination upon a single dose iv application (50 mg/kg) of compounds **10c** and **10e**. The PK parameters of these applications and those of the previously published carboxylate **9** are summarized in Table 4. The table also contains the results of the iv administration of compound **10j** (0.625 mg/kg).

DOI: 10.1021/jm501524q
J. Med. Chem. 2015, 58, 2221–2239

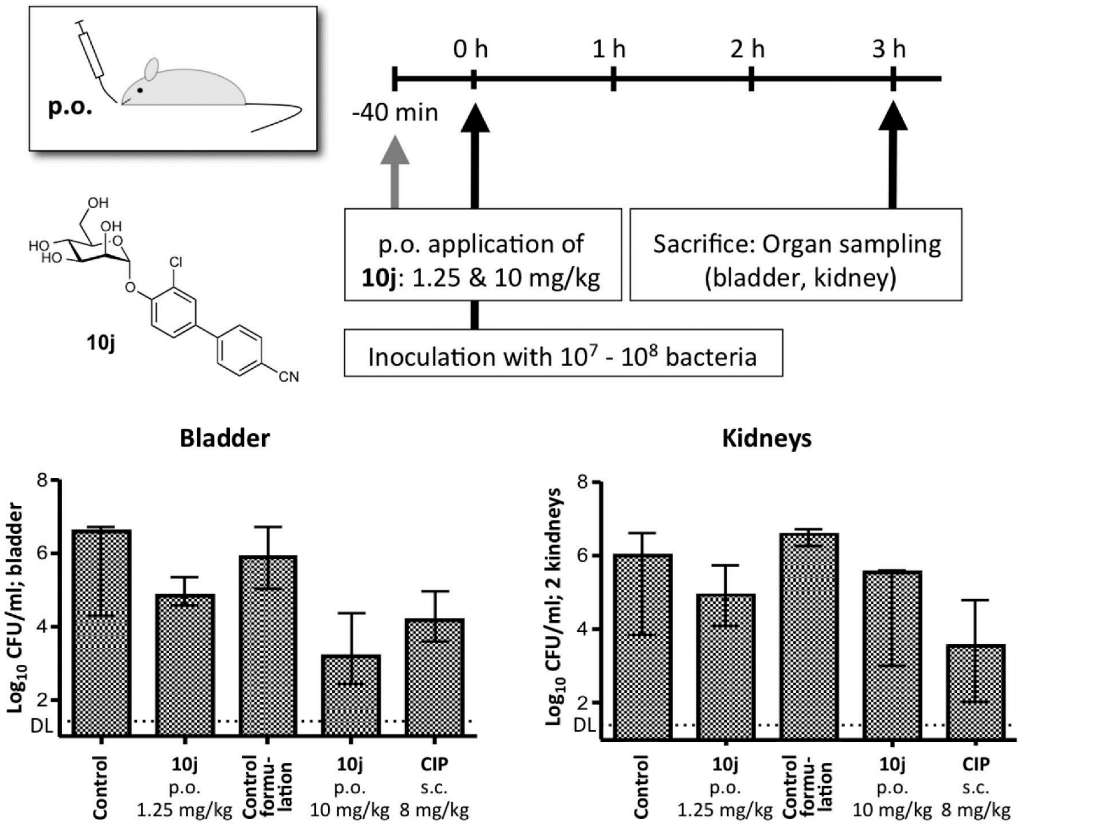

Figure 7. Preventive efficacy of **10j** in the UTI mouse model 3 h after infection. The bars depict the median bacterial load with the interquartile range in the different study groups. Shown are the results of the control group (PBS), control group formulation (5% DMSO in PBS containing 1% Tween 80), and the intervention groups with the preventive applications of either 1.25 or 10 mg/kg **10j** po or 8 mg/kg CIP sc (representing the murine dose equivalent to a human standard dose).[81] DL, detection limit. CFU, colony forming units.

In contrast to the fast plasma clearance of antagonists **9** and **10c** (Figure 5A), the methylsulfonamide bioisostere **10e** attained higher initial concentration in plasma (C_0) and lower total clearance (CL_{tot}). Therefore, it could be detected until 6 h after application, resulting in markedly higher plasma AUC. The observed high C_0 of compound **10e** may be attributed to a small volume of distribution (V_z) resulting from the high PPB ($f_b \geq 99\%$).[72] In urine (Figure 5B), the carboxylic acid **9** and the morpholinomethanone **10c** displayed high levels immediately following administration and a rapid concentration decrease within the first 2 h, reflecting the rapid elimination from plasma. Fast renal excretion as major route of elimination can be rationalized by the physicochemical properties of the antagonists **9** and **10c**, that is, moderate PPB and log $D_{7.4}$, as well as high metabolic stability. Otherwise, the methylsulfonamide bioisostere **10e** showed sustained compound levels in urine over a period of 2 h and subsequent slow decrease until 6 h after administration. This sustained renal excretion is a result of the interplay of the antagonist's elevated PPB and log $D_{7.4}$.

In a second study, the *p*-cyano bioisostere **10j**, characterized by a high oral absorption potential, was administered as a single dose iv (0.625 mg/kg) and po (1.25 mg/kg). The plasma concentration curve upon iv dosing displays a steep decline within the first hour after application, while the po curve shows a prolonged period where absorption and elimination are in equilibrium (Figure 6A). The urine concentration profiles (Figure 6B) parallel the plasma curves obtained by the two modes of application; i.e., high plasma clearance upon iv bolus injection led to high initial antagonist levels in urine and a rapid concentration decline. By contrast, sustained plasma concentrations upon po administration resulted in prolonged urine levels.

As a result, urine concentrations exceed the minimum level required for the antiadhesive effect as estimated from the in vitro cell infection model[79] (minimal antiadhesion concentration,[23] $MAC_{90} = 0.094\ \mu g/mL$) for more than 8 h upon oral single-dose administration (Figure 6B).

Infection Study in C3H/HeN Mice. In a preventive study, six mice were inoculated with UTI89 following an oral application of **10j** (1.25 mg/kg) 40 min prior to infection. Three hours after inoculation, the animals were sacrificed and bladder and kidneys were removed. Organs were homogenized and analyzed for bacterial counts. The effect of the FimH antagonist was compared to a 8 mg/kg dose of ciprofloxacin (CIP), applied subcutaneously (sc) 10 min before infection. CIP is used as standard antibiotic therapy in humans for the treatment of UTI.[80] In mice, the dose of 8 mg/kg sc was shown to mimic the standard human dose regarding peak levels and the AUC_{24} in serum.[81] The median reductions in bacterial counts in mice treated with **10j** and CIP compared to the control group 3 h after infection are displayed in Figure 7.

DOI: 10.1021/jm501524q
J. Med. Chem. 2015, 58, 2221−2239

The median value in the untreated control group showed bacterial counts of 6.6 $\log_{10}$ colony forming units (CFU) in the bladder and 6 $\log_{10}$ CFU in the kidneys. After oral application of 1.25 mg/kg **10j**, bacterial loads in the bladder decreased by 1.78 $\log_{10}$ CFU and 1.07 $\log_{10}$ CFU in the kidneys. The lower reduction in the kidneys is most likely due to the differing adhesion mechanisms between bladder and kidneys (type 1 pili vs P-pili), which is not targeted by **10j**.[82] With CIP (8 mg/kg sc) a substantial reduction in both bladder and kidneys (median reductions of 2.44 $\log_{10}$ and 2.47 $\log_{10}$, respectively) was observed. Despite the low oral dose of **10j** (1.25 mg/kg), the approximately 100-fold reduction of CFU in the bladder promised an even higher effect upon dose increase to 10 mg/kg. Since the solubility of **10j** for this increased dose is too low (192 μg/mL), we used 5% DMSO and surfactant Tween 80 (1%) as solubilizer. To effectively compare the effect of a higher dose of **10j**, a control group receiving the formulation only (5% DMSO in PBS containing 1% Tween 80, termed control group formulation) was tested in parallel. When 10 mg/kg **10j** was applied, bacterial loads in the bladder decreased by 2.68 $\log_{10}$ CFU/mL compared to the control group formulation, clearly exceeding the effect of CIP with a reduction of 2.44 $\log_{10}$ CFU/mL. However, only a moderate reduction of 1.04 $\log_{10}$ CFU was achieved in the kidneys.

■ SUMMARY AND CONCLUSION

Recently, numerous monovalent alkyl and aryl α-D-mannopyranosides have been described as potent FimH antagonists. However, most of them suffer from insufficient pharmacokinetic properties, i.e., modest bioavailability and short duration of the therapeutic effect in the bladder, their site of action. As a consequence, high doses at short intervals are required to achieve antiadhesive effects over an extended period of time. Therefore, the goal of the present study was an appropriate optimization of the pharmacokinetic profile of biphenyl α-D-mannopyranosides while keeping their high affinity to the CRD of FimH. The starting point was the biphenylcarboxylate **9** where the critical carboxylate was replaced by bioisosteres.[39,83]

With a series of bioisosteres, a 3- to 5-fold improvement of affinity was achieved compared to **9**. Although binding necessitates only partial desolvation of the carboxylate and its bioisosteric replacements, a reduction of the enthalpy penalty for desolvation[51] was identified as the source of the improved affinity exhibited by the bioisosteres. Thermodynamic evaluation of antagonists **10b–e** revealed almost identical enthalpy contribution to binding. However, for antagonists with the *p*-cyano substituent (**10g** and **10j**) an enhancement of up to −8.7 kJ/mol was observed, indicating a reduced desolvation penalty and an improved stacking as derived from the crystal structure of **10j** cocrystallized with the CRD of FimH (Figure 4B). On the other hand, higher affinity originating from a reduction of conformational flexibility of ligand and protein resulted in a concomitant entropy penalty of up to 6.5 kJ/mol.

In addition to the improved pharmacodynamics, the relevant pharmacokinetic parameters (solubility, permeability, renal excretion) were substantially improved. With 3′-chloro-4′-(α-D-mannopyranosyloxy)biphenyl-4-carbonitrile (**10j**), a FimH antagonist with an optimal in vitro PK/PD profile was identified. The *p*-cyano substituent conferred lipophilicity and high binding to plasma proteins, which slowed the rate of renal excretion. Despite higher lipophilicity, antagonist **10j** was insusceptible to CYP450-mediated metabolism and therefore predominantly eliminated via the renal pathway. In vivo experiments confirmed the excellent PK profile of **10j** with steady renal excretion for more than 8 h after oral application (1.25 mg/kg), suggesting a long-lasting antiadhesive effect. Finally, the preventive oral application of **10j** (10 mg/kg) reduced the bacterial load in the bladder by almost 1000-fold 3 h after infection. Although the first 3 h of the infection do not represent the complete infection cycle, they represent the time span of bacteria adhering and invading urothelial cells.[84,85] Nevertheless, the effect of FimH antagonist **10j** within a longer infection time and at higher dosing will be the subject of future investigations.

■ EXPERIMENTAL SECTION

Synthesis. The synthesis of compounds **10a–d**, **10f**, **10g**, **10i**, **13a–d**, **13f**, **13g**, **15**, **18**, and **25**, including compound characterization data, can be found in the Supporting Information.

General Methods. NMR spectra were recorded on a Bruker Avance DMX-500 (500.1 MHz) spectrometer. Assignment of ^{1}H and ^{13}C NMR spectra was achieved using 2D methods (COSY, HSQC, HMBC). Chemical shifts are expressed in ppm using residual $CHCl_3$, CHD_2OD, or HDO as references. Optical rotations were measured using PerkinElmer polarimeter 341. Electron spray ionization mass spectra were obtained on a Waters micromass ZQ. The LC/HRMS analyses were carried out using a Agilent 1100 LC equipped with a photodiode array detector and a Micromass QTOF I equipped with a 4 GHz digital time converter. Microwave-assisted reactions were carried out with a CEM Discover and Explorer. Reactions were monitored by TLC using glass plates coated with silica gel 60 F_{254} (Merck) and visualized by using UV light and/or by charring with a molybdate solution (a 0.02 M solution of ammonium cerium sulfate dihydrate and ammonium molybdate tetrahydrate in aqueous 10% H_2SO_4). MPLC separations were carried out on a CombiFlash Companion or Rf (Teledyne Isco) equipped with RediSep normal-phase or RP-18 reversed-phase flash columns. LC–MS separations were done on a Waters system equipped with sample manager 2767, pump 2525, PDA 2525, and Micromass ZQ. All compounds used for biological assays are at least of 95% purity based on HPLC analytical results. Commercially available reagents were purchased from Fluka, Aldrich, Alfa Aesar, or abcr GmbH & Co. KG (Germany). Solvents were purchased from Sigma-Aldrich or Acros and were dried prior to use where indicated. Methanol (MeOH) was dried by refluxing with sodium methoxide and distilled immediately before use. Dimethoxyethane (DME) was dried by filtration over Al_2O_3 (Fluka, type 5016 A basic).

4′-(2,3,4,6-Tetra-*O*-acetyl-α-D-mannopyranosyloxy)-*N*-methylbiphenyl-4-sulfonamide (13e). A Schlenk tube was charged with aryl iodide **11**[22] (116 mg, 0.21 mmol), 4-(*N*-methylsulfamoyl)-phenylboronic acid (**12e**, 50 mg, 0.23 mmol), $Pd(dppf)Cl_2 \cdot CH_2Cl_2$ (5 mg, 0.006 mmol), K_3PO_4 (67 mg, 0.32 mmol), and a stirring bar. The tube was closed with a rubber septum and was evacuated and flushed with argon. This procedure was repeated once, and then anhydrous DMF (1 mL) was added under a stream of argon. The mixture was degassed in an ultrasonic bath and flushed with argon for 5 min and then stirred at 80 °C overnight. The reaction mixture was cooled to rt, diluted with EtOAc (50 mL), and washed with water (50 mL) and brine (50 mL). The organic layer was dried over Na_2SO_4 and concentrated in vacuo. The residue was purified by MPLC on silica gel (petroleum ether/EtOAc) to afford **13e** (105 mg, 84%) as a white solid. $[\alpha]_D^{20}$ +56.4 (*c* 0.50, MeOH). ^{1}H NMR (500 MHz, $CDCl_3$): δ = 7.92–7.90 (m, 2H, Ar–H), 7.70–7.68 (m, 2H, Ar–H), 7.57–7.55 (m, 2H, Ar–H), 7.21–7.19 (m, 2H, Ar–H), 5.60–5.57 (m, 2H, H-1, H-3), 5.48 (dd, J = 1.8, 3.4 Hz, 1H, H-2), 5.40 (t, J = 10.0 Hz, 1H, H-4), 4.38 (dd, J = 5.4, 10.8 Hz, 1H, NH), 4.30 (dd, J = 4.9, 12.3 Hz, 1H, H-6a), 4.13–4.08 (m, 2H, H-5, H-6b), 2.72 (d, J = 5.4 Hz, 3H, NCH_3), 2.22, 2.07, 2.05, 2.04 (4 s, 12H, 4 $COCH_3$). ^{13}C NMR (126 MHz, $CDCl_3$): δ = 170.55, 170.06, 170.03, 169.75 (4 CO), 155.97, 144.81, 137.16, 134.09, 128.62, 127.85, 127.39, 117.01 (Ar–C), 95.78 (C-1), 69.34 (C-5), 69.31 (C-2), 68.81 (C-3), 65.86 (C-4), 62.07 (C-6), 29.44 ($NHCH_3$), 20.92, 20.74, 20.72 (4C, 4 $COCH_3$). ESI-MS *m*/*z*, calcd for $C_{27}H_{31}NNaO_{12}S$ $[M + Na]^+$: 616.1. Found: 616.1.

DOI: 10.1021/jm501524q
J. Med. Chem. 2015, 58, 2221–2239

4′-(α-D-Mannopyranosyloxy)-*N*-methylbiphenyl-4-sulfonamide (10e). To a solution of **13e** (40 mg, 0.07 mmol) in dry MeOH (5 mL) was added freshly prepared 1 M NaOMe/MeOH (0.1 equiv) under argon. The mixture was stirred at rt until the reaction was complete (monitored by TLC), then neutralized with Amberlyst-15 (H^+) ion-exchange resin, filtered, and concentrated in vacuo. The residue was purified by MPLC on silica gel (DCM/MeOH, 10:1 to 7:1) to afford **10e** (22 mg, 76%) as white solid. $[\alpha]_D^{20}$ +105.7 (*c* 0.30, MeOH). ^{1}H NMR (500 MHz, CD_3OD): δ = 7.90−7.88 (m, 2H, Ar−H), 7.80−7.79 (m, 2H, Ar−H), 7.66−7.64 (m, 2H, Ar−H), 7.26−7.25 (m, 2H, Ar−H), 5.58 (d, *J* = 1.7 Hz, 1H, H-1), 4.06 (dd, *J* = 1.8, 3.3 Hz, 1H, H-2), 3.96 (dd, *J* = 3.4, 9.5 Hz, 1H, H-3), 3.79−3.74 (m, 3H, H-4, H-6a, H-6b), 3.63 (ddd, *J* = 2.5, 5.2, 9.7 Hz, 1H, H-5), 2.57 (s, 3H, $NHCH_3$). ^{13}C NMR (126 MHz, CD_3OD): δ = 158.34, 146.13, 138.67, 134.55, 129.53, 128.82, 128.21, 118.29 (Ar−C), 100.09 (C-1), 75.53 (C-5), 72.42 (C-3), 71.96 (C-2), 68.32 (C-4), 62.68 (C-6), 29.31 ($NHCH_3$). HRMS *m*/*z*, calcd for $C_{19}H_{23}NNaO_8S$ $[M + Na]^+$: 448.1037. Found: 448.1038.

5-(4′-(2,3,4,6-Tetra-*O*-acetyl-α-D-mannopyranosyloxy)-biphenyl-4-yl)-1*H*-tetrazole (14). A Schlenk tube was charged with **13g** (30 mg, 0.06 mmol), trimethylsilyl azide (16 μL, 0.12 mmol), dibutyltin oxide (2 mg, 0.006 mmol), DME (1 mL), and a stirring bar. The mixture was heated to 150 °C for 10 min by microwave irradiation. The reaction mixture was cooled to rt and then concentrated in vacuo. The residue was purified by MPLC on silica gel (DCM/MeOH, 9:1 to 8:1) to afford **14** (26 mg, 81%) as a colorless oil. $[\alpha]_D^{20}$ +56.1 (*c* 0.3, MeOH). ^{1}H NMR (500 MHz, $CDCl_3$): δ = 8.25−8.15 (m, 2H, Ar−H), 7.75−7.65 (m, 2H, Ar−H), 7.60−7.55 (m, 2H, Ar−H), 7.20−7.17 (m, 2H, Ar−H), 5.64−5.55 (m, 2H, H-1, H-3), 5.49 (dd, *J* = 1.7, 3.3 Hz, 1H, H-2), 5.40 (t, *J* = 10.1 Hz, 1H, H-4), 4.31 (dd, *J* = 5.3, 12.4 Hz, 1H, H-6a), 4.17−4.06 (m, 2H, H-5, H-6b), 2.22, 2.07, 2.06, 2.05 (4 s, 12H, 4 $COCH_3$). ^{13}C NMR (126 MHz, $CDCl_3$): δ = 170.67, 170.14, 170.11, 169.81 (4 CO), 155.61, 128.36, 127.84, 127.49, 116.93 (Ar−C), 95.78 (C-1), 69.36 (C-5), 69.26 (C-2), 68.90 (C-3), 65.89 (C-4), 62.12 (C-6), 20.92, 20.76, 20.73 (4 $COCH_3$). ESI-MS *m*/*z*, calcd for $C_{27}H_{28}N_4NaO_{10}$ $[M + Na]^+$: 591.2. Found: 591.1.

5-(4′-(α-D-Mannopyranosyloxy)biphenyl-4-yl)-1*H*-tetrazole (10h). Prepared according to the procedure described for **10e** from **14** (26 mg, 0.03 mmol). Yield: 18 mg (quant) as a white solid. $[\alpha]_D^{20}$ +112.1 (*c* 0.1, MeOH/H_2O, 2:1). ^{1}H NMR (500 MHz, CD_3OD): δ = 7.98−7.96 (m, 2H, Ar−H), 7.72−7.71 (m, 2H, Ar−H), 7.58−7.54 (m, 2H, Ar−H), 7.16−7.13 (m, 2H, Ar−H), 5.46 (d, *J* = 1.7 Hz, 1H, H-1), 3.94 (dd, *J* = 1.9, 3.5 Hz, 1H, H-2), 3.83 (dd, *J* = 3.4, 9.5 Hz, 1H, H-3), 3.68−3.61 (m, 3H, H-4, H-6a, H-6b), 3.52 (ddd, *J* = 2.5, 5.4, 9.7 Hz, 1H, H-5). ^{13}C NMR (126 MHz, CD_3OD): δ = 158.19, 145.07, 134.97, 129.29, 128.74, 128.55, 118.26 (Ar−C), 100.13 (C-1), 75.52 (C-5), 72.42 (C-3), 71.98 (C-2), 68.33 (C-4), 62.69 (C-6). HRMS *m*/*z*, calcd for $C_{19}H_{21}N_4O_6$ $[M + H]^+$: 401.1456. Found: 401.1450.

4′-(2,3,4,6-Tetra-*O*-acetyl-α-D-mannopyranosyloxy)-3′-chlorobiphenyl-4-carbonitrile (19). Prepared according to the procedure described for **13e** from aryl iodide **18**[23] (79 mg, 0.135 mmol), **12g** (22 mg, 0.15 mmol), $Pd(dppf)Cl_2{\cdot}CH_2Cl_2$ (3.3 mg, 4 μmol), and K_3PO_4 (57 mg, 0.27 mmol). Yield: 57 mg (75%) as a white solid. $[\alpha]_D^{20}$ +77.7 (*c* 0.5, $CHCl_3$). ^{1}H NMR (500 MHz, $CDCl_3$): δ = 7.72 (d, *J* = 8.3 Hz, 2H, Ar−H), 7.63 (m, 3H, Ar−H), 7.43 (dd, *J* = 2.2, 8.6 Hz, 1H, Ar−H), 7.27 (d, *J* = 8.6 Hz, 1H, Ar−H), 5.64−5.59 (m, 2H, H-1, H-2), 5.54 (dd, *J* = 1.9, 3.2 Hz, 1H, H-3), 5.41 (t, *J* = 10.1 Hz, 1H, H-4), 4.28 (dd, *J* = 5.2, 12.3 Hz, 1H, H-6a), 4.17 (ddd, *J* = 2.1, 5.1, 10.0 Hz, 1H, H-5), 4.10 (dd, *J* = 2.2, 12.3 Hz, 1H, H-6b), 2.21 (s, 3H, $COCH_3$), 2.12- 2.00 (m, 9H, 3 $COCH_3$). ^{13}C NMR (126 MHz, $CDCl_3$): δ = 170.54, 170.08, 169.90, 169.84, (4C, CO) 151.67, 143.61, 135.29, 132.87, 129.41, 127.53, 126.60, 125.20, 118.79, 117.36, 111.47 (Ar−C, CN), 96.72 (C-1), 70.00 (C-5), 69.39 (C-3), 68.82 (C-2), 65.86 (C-4), 62.16 (C-6), 20.98, 20.81, 20.79, 20.78 (4 $COCH_3$). ESI-MS *m*/*z*, calcd for $C_{27}H_{26}ClNNaO_{10}$ $[M + Na]^+$: 582.1. Found: 582.1.

3′-Chloro-4′-(α-D-mannopyranosyloxy)biphenyl-4-carbonitrile (10j). Prepared according to the procedure described for **10e** from **19** (36 mg, 0.06 mmol). Yield: 12 mg (48%) as a white solid. $[\alpha]_D^{20}$ +109.4 (*c* 0.23, MeOH). ^{1}H NMR (500 MHz, CD_3OD): δ = 7.80−7.72 (m, 5H, Ar−H), 7.59 (dd, *J* = 2.2, 8.6 Hz, 1H, Ar−H), 7.48 (d, *J* = 8.7 Hz, 1H, Ar−H), 5.62 (d, *J* = 1.4 Hz, 1H, H-1), 4.12 (dd, *J* = 1.8, 3.3 Hz, 1H, H-2), 4.00 (dd, *J* = 3.4, 9.5 Hz, 1H, H-3), 3.83−3.68 (m, 3H, H-4, H-6a, H-6b), 3.63 (ddd, *J* = 2.3, 5.4, 9.6 Hz, 1H, H-5). ^{13}C NMR (126 MHz, CD_3OD): δ = 153.65, 145.15, 135.42, 133.86, 129.82, 128.53, 127.87, 125.47, 119.70, 118.59 (Ar−C), 111.97 (CN), 100.66 (C-1), 76.05 (C-5), 72.39 (C-3), 71.80 (C-2), 68.20 (C-4), 62.65 (C-6). IR (KBr), ν = 3400 (OH), 2227 (C≡N), 1606, 1487 (Ar−C=C) cm^{-1}. HRMS *m*/*z*, calcd for $C_{19}H_{18}ClNNaO_6$ $[M + Na]^+$: 414.0715. Found: 414.0721.

3′-Chloro-*N*-(3′,6′-dihydroxy-3-oxo-3*H*-spiro-[isobenzofuran-1,9′-xanthen]-5-yl)-4′-(α-D-mannopyranosyloxy)biphenyl-4-carboxamide (22). Compound **21** (10.0 mg, 0.024 mmol), fluoresceinamine isomer I (12.7 mg, 0.037 mmol), and COMU (20.9 mg, 0.049 mmol) were dissolved in dry DMF (1 mL). Then NEt_3 (10 μL, 0.073 mmol) was added and the mixture was stirred at rt for 7 h. 1 N HCl in DMF was added until acid reaction on pH paper and the mixture was concentrated. The residue was dissolved in DCM/MeOH (3:1) and loaded onto a silica gel column. The complex mixture of compounds was only partially resolved. The fractions containing the product were collected, concentrated, and purified by preparative HPLC (gradient H_2O/MeCN, +0.2% HCO_2H) to afford compound **22** (5 mg, 19%). $[\alpha]_D^{20}$ +21.1 (*c* 0.10, MeOH). ^{1}H NMR (500 MHz, CD_3OD): δ = 8.26 (d, *J* = 8.4 Hz, 2H, Ar−H), 7.88−7.74 (m, 3H, Ar−H), 7.66 (dd, *J* = 2.2, 8.6 Hz, 1H, Ar−H), 7.51 (d, *J* = 8.7 Hz, 1H, Ar−H), 7.29 (dd, *J* = 1.9, 5.3 Hz, 2H, Ar−H), 7.19 (dd, *J* = 2.1, 8.3 Hz, 1H, Ar−H), 7.08−6.99 (m, 2H, Ar−H), 6.95 (d, *J* = 8.7 Hz, 1H, Ar−H), 6.72 (dd, *J* = 5.5, 10.6, Hz, 2H, Ar−H), 6.61 (dd, *J* = 2.3, 8.7 Hz, 1H, Ar−H), 5.65 (s, 1H, H-1), 4.15 (dd, *J* = 1.8, 3.2 Hz, H-2), 4.03 (dd, *J* = 3.4, 9.5, Hz, H-3), 3.87−3.72 (m, 3H, H-4, H-6a, H-6b), 3.65 (m, 1H, H-5). ^{13}C NMR (126 MHz, CD_3OD): δ = 137.50, 136.01, 131.90, 130.24, 130.20, 129.87, 129.24, 128.03, 127.91, 125.79, 125.46, 124.73, 118.99, 118.76, 118.65 (Ar−C), 100.73 (C-1), 76.06 (C-5), 72.42 (C-3), 71.85 (C-2), 68.24 (C-4), 62.69 (C-2). ESI-MS *m*/*z*, calcd for $C_{39}H_{31}ClNO_{12}$ $[M + H]^+$: 740.2. Found: 740.2.

3′-Chloro-*N*-(2-(3-(3′,6′-dihydroxy-3-oxo-3*H*-spiro-[isobenzofuran-1,9′-xanthen]-5-yl)thioureido)ethyl)-4′-(α-D-mannopyranosyloxy)biphenyl-4-carboxamide (23). To a stirred solution of compound **21** (25 mg, 0.061 mmol) in dry DMF (1 mL), NHS (21 mg, 0.183 mmol) was added, followed by DIC (9.2 mg, 0.073 mmol). The mixture was stirred at rt for 2 h. Then *N*-Boc-ethylendiamine (10.7 mg, 0.067 mmol) was added and the reaction was stirred for 10 h. It was then cooled down to 0 °C, diluted with water, and concentrated. Chromatography on silica gel (DCM/MeOH) yielded 23 mg (0.042 mmol, 68%) of *tert*-butyl (3′-chloro-4′-(α-D-mannopyranosyloxy)biphenyl-4-yl-carboxamido)ethyl)carbamate. This product was dissolved in DCM (3 mL), and TFA (1 mL) was added. The solid dissolved during addition of TFA. After 10 min the reaction was complete. The mixture was evaporated, and excess TFA was removed in high vacuum. The intermediate *N*-(2-aminoethyl)-3′-chloro-4′-(α-D-mannopyranosyloxy)biphenyl-4-carboxamide TFA salt (23 mg, 0.042 mmol, quant) was used directly in the next step. It was dissolved in dry DMF (0.5 mL), and NEt_3 (12.8 mg, 0.127 mmol) was added. The mixture was cooled to 0 °C. Then FITC (14.8 mg, 0.038 mmol) was added and the mixture was stirred for 3 h in the dark. The mixture was then coevaporated with water, taken up in MeOH/10% aq acetic acid and evaporated. Chromatography on silica gel (DCM/MeOH) yielded compound **23**, contaminated with triethylammonium acetate. The compound was then redissolved in MeOH, and 0.5 N HCl in MeOH was added. The mixture was evaporated and chromatographed on silica gel to yield pure **23** (15 mg, 47%). $[\alpha]_D^{20}$ +12.1 (*c* 0.30, MeOH). ^{1}H NMR (500 MHz, CD_3OD): δ = 8.12 (s, 1H), 7.92 (d, *J* = 8.3 Hz, 2H, Ar−H), 7.70 (dd, *J* = 5.0, 13.1 Hz, 2H, Ar−H), 7.64 (d, *J* = 8.3 Hz, 2H, Ar−H), 7.54 (dd, *J* = 2.2, 8.6 Hz, 1H, Ar−H), 7.46 (d, *J* = 8.7 Hz, 1H, Ar−H), 7.09 (d, *J* = 8.2 Hz, 1H, Ar−H), 6.74 (s, 2H), 6.69 (d, *J* = 1.4 Hz, 2H, Ar−H), 6.55 (d, *J* = 8.4 Hz, 2H, Ar−H), 5.63 (d, *J* = 1.3 Hz, H-1), 4.15 (dd, *J* = 1.8, 3.1 Hz, H-2), 4.03 (dd, *J* = 3.4, 9.5 Hz, H-3), 3.94 (s, 2H, CH_2), 3.86−3.64 (m, 6H, H-4, H-5, H-6, CH_2). ^{13}C NMR (126 MHz, CD_3OD): δ = 153.21, 143.84, 136.41, 129.66, 129.18, 127.76, 127.70, 125.37, 118.64, 103.62 (Ar−C), 100.75 (C-1), 76.00 (C-5), 72.41 (C-3), 71.86 (C-2), 68.24 (C-4), 62.69 (C-6), 40.76 (CH_2). ESI-MS *m*/*z*, calcd for $C_{42}H_{37}ClN_3O_{12}S$ $[M + H]^+$: 842.2. Found: 842.2.

DOI: 10.1021/jm501524q
J. Med. Chem. 2015, 58, 2221−2239

3′-Chloro-*N*-(2-(2-(2-(3-(3′,6′-dihydroxy-3-oxo-3*H*-spiro[isobenzofuran-1,9′-xanthen]-5-yl)thioureido)ethoxy)ethoxy)ethyl)-4′-(α-D-mannopyranosyloxy)biphenyl-4-carboxamide (24). Compound **21** (280 mg, 0.68 mmol) was dissolved in dry DMF (5 mL) under argon. Then NHS (235 mg, 2.04 mmol) was added, followed by DIC (0.12 mL, 0.78 mmol) and the mixture was stirred at rt for 4 h. Then Boc-PEG2-NH_2 (186 mg, 0.75 mmol) was added, and the mixture was stirred at rt under argon for 10 h. It was then slowly diluted with water and concentrated. The residue was purified by chromatography on silica gel (DCM/MeOH) to give *tert*-butyl (2-(2-(2-(3′-chloro-4′-(α-D-mannopyranosyloxy)biphenyl-4-ylcarboxamido)ethoxy)ethoxy)ethyl)-carbamate (300 mg, 0.468 mmol, 69%). Then the carbamate was suspended in DCM (3 mL), and TFA (1 mL) was added dropwise at rt. After 30 min, the solvents were evaporated and the crude mixture was dissolved in $CHCl_3$/MeOH (6:4, +0.5% conc NH_4OH) and transferred to a silica gel column, eluting with the same solvent mixture, to yield *N*-(2-(2-(2-aminoethoxy)ethoxy)ethyl)-3′-chloro-4′-(α-D-mannopyranosyloxy)biphenyl-4-carboxamide (228 mg, 90%). A fraction of the amine (10 mg, 0.018 mmol) was dissolved in dry DMF (0.5 mL) and cooled to 0 °C. FITC (6.5 mg, 0.017 mmol) was added, and the mixture was stirred for 1 h. The mixture was concentrated and the residue was purified by chromatography on silica (DCM/MeOH) to yield **24** (10 mg, 65%). ^{1}H NMR (500 MHz, CD_3OD): δ = 8.21 (d, J = 1.4 Hz, 1H, Ar−H), 7.88 (d, J = 8.3 Hz, 2H, Ar−H), 7.68 (d, J = 2.2 Hz, 2H, Ar−H), 7.63 (d, J = 8.3 Hz, 2H, Ar−H), 7.53 (dd, J = 2.2, 8.6 Hz, 1H, Ar−H), 7.43 (d, J = 8.7 Hz, 1H, Ar−H), 7.09 (d, J = 8.2 Hz, 1H, Ar−H), 6.68 (d, J = 2.3 Hz, 2H, Ar−H), 6.65 (dd, J = 2.6, 8.6 Hz, 2H, Ar−H), 6.53 (dd, J = 1.6, 8.7 Hz, 2H, Ar−H), 5.61 (d, J = 1.3 Hz, 1H, H-1), 4.14 (dd, J = 1.8, 3.2, Hz, 1H, H-2), 4.03 (dd, J = 3.4, 9.5 Hz, 1H, H-3), 3.93−3.53 (m, 16H), 3.37 (s, 2H, NCH_2), 1.30 (s, 2H, CH_2). ^{13}C NMR (126 MHz, CD_3OD): δ = 170.01 (CO), 153.17, 143.72, 136.37, 134.37, 130.39, 129.69, 129.04, 127.78, 127.73, 125.35, 118.60, 103.60 (Ar−C), 100.72 (C-1), 75.97 (C-5), 72.41 (C-3), 71.86, 71.40, 70.59 (5C, C-2, OCH_2), 68.23 (C-4), 62.64 (C-6), 49.88, 45.49, 40.97 (CH_2). ESI-MS m/z, calcd for $C_{46}H_{45}ClN_3O_{14}S$ $[M + H]^+$: 930.2. Found: 930.4.

Competitive Fluorescence Polarization Assay. *Expression and Purification of CRD of FimH.* A recombinant protein consisting of the CRD of FimH linked to a 6His-tag via a thrombin cleavage site (FimH-CRD-Th-His_6) was expressed in *E. coli* strain HM125 and purified by affinity chromatography as previously described.[43]

K_D Determination of FITC-Labeled Ligands. The functionalized ligands (**23**, **24**) were prepared as a 10 mM stock solution in pure DMSO (Sigma-Aldrich, Buchs, Switzerland). All further dilutions of compounds and FimH-CRD-Th-His_6 protein were prepared in assay buffer (20 mM HEPES, 150 mM NaCl, 50 μg/mL BSA, pH 7.4). BSA was added to the assay buffer to prevent nonspecific binding of protein to the plastic surface. Binding isotherms for the fluorescent ligands were obtained in direct binding studies by adding a constant concentration of ligand (final concentration 5 nM) and a linear dilution of protein (final concentration 0−100 nM) to a final volume of 200 μL in 96-well, black, flat bottom NBS plates (Corning Inc., Corning, NY, USA). After incubation of the plate for 24 h at rt with gentle shaking, the fluorescence polarization was measured with the Synergy H1 hybrid multimode microplate reader (BioTek Instruments Inc., Winooski, VT, USA) with polarized excitation at 485 nm and emission measured at 528 nm through polarizing filters parallel and perpendicularly oriented to the incident polarized light. K_D values were determined by plotting the FP readout as a function of the protein concentration and applying the following single-site binding equation (eq 1) that accounts for ligand depletion:

$$S_{obs} = S_F + (S_B - S_F) \times \left(\frac{C_P + C_L + K_D - \sqrt{(C_P + C_L + K_D)^2 - 4C_PC_L}}{2C_L} \right) \quad (1)$$

where S_{obs} is the observed signal from the ligand, S_F is the signal from free ligand, S_B is the signal from bound ligand, C_P is the total concentration of protein, and C_L is the total concentration of ligand.[49]

K_D Determination of FimH Antagonists. The fluorescently labeled ligand **23** was used for the competitive fluorescence polarization assay. A linear dilution of nonlabeled FimH antagonist with final concentrations ranging from 0 to 10 μM was titrated into 96-well, black, flat-bottom NBS plates (Corning Inc.) to a final volume of 200 μL containing a constant concentration of protein (final concentration 25 nM) and FITC-labeled ligand which was fixed at a higher concentration in competitive binding assays than in direct binding experiments to obtain higher fluorescence intensities (final concentration 20 nM). Prior to measuring the fluorescence polarization, the plates were incubated on a shaker for 24 h at rt until the reaction reached equilibrium. The IC_{50} value was determined with Prism (GraphPad Software Inc., La Jolla, CA, USA) by applying a standard four-parameter IC_{50} function. The obtained IC_{50} values were converted into their corresponding K_D values using the derivation of the Cheng−Prusoff equation.[45] This variation of the Cheng−Prusoff equation is applied to competition assays with tight-binding inhibitors and includes terms to correct for ligand depletion effects. However, the K_D for antagonists having a higher affinity toward FimH than the labeled ligand could not be accurately determined.[45]

Isothermal Titration Calorimetry (ITC). All ITC experiments were performed with the FimH-CRD-Th-His_6 protein using a VP-ITC instrument from MicroCal, Inc. (Malvern Instruments, Worcestershire, U.K.) with a sample cell volume of 1.4523 mL. The measurements were performed with 0−5% DMSO at 25 °C, a stirring speed of 307 rpm, and 10 μcal s^{-1} reference power. The protein samples were dialyzed in assay buffer prior to all experiments. Because of the high protein consumption of ITC, only the experiments for the reference compounds (**1**, **3**, and **25**) were measured in duplicates. Compounds **1**, **3**, **9**, and **25** were measured in a direct fashion by titration of ligand (100−2,000 μM) into protein (8.6−55 μM) with injections of 3−8 μL at intervals of 10 min to ensure nonoverlapping peaks. The quantity c = Mt(0) K_D^{-1}, where Mt(0) is the initial macromolecule concentration, is of importance in titration microcalorimetry. The c-values of the direct titrations were below 1000 and thus within the reliable range. For the compounds **10b−e**, **10g**, and **10j** additional competitive ITC experiments were performed because of their high affinity resulting in c-values above 1000 for direct titrations. These ligands (600 μM) were titrated into protein (30 μM), which was preincubated with compound **25** (300 μM) resulting in sigmoidal titration curves. Because of slow reaction kinetics, titration intervals of 20 min were used.

Baseline correction and peak integration were performed using the Origin 7 software (OriginLab, Northampton, MA, USA). An initial 2 μL injection was excluded from data analysis. Baseline subtraction and curve-fitting with the three variables N (concentration correction factor), K_D (dissociation constant), and ΔH° (change in enthalpy) were performed with the SEDPHAT software, version 10.40 (National Institutes of Health).[86] A global fitting analysis was performed for the competition titration (**10b−e**, **10g**, or **10j** competing for the protein binding site with compound **25**) and the direct titration of the competitor (compound **25** binding to protein) to fit for K_D. ΔH° and N were fitted from direct titrations of **10b−e**, **10g**, or **10j** into protein. For the compounds **3**, **9**, and **25** binding to protein all variables could be determined from a global analysis of the direct titration.

The thermodynamic parameters were calculated with the following equation (eq 2):

$$\Delta G^\circ = \Delta H^\circ - T\Delta S^\circ = RT \ln K_D = -RT \ln K_A \quad (2)$$

where ΔG°, ΔH°, and ΔS° are the changes in free energy, enthalpy, and entropy of binding, respectively, T is the absolute temperature, and R is the universal gas constant (8.314 J mol^{-1} K^{-1}). The 95% confidence intervals of the measurements were calculated for the two variables K_D and ΔH° with the one-dimensional error surface projection within the SEDPHAT software.

Calculation of the Free Energy of Desolvation. The three-dimensional representation for each of the aglycons (4-methoxybiphenyl scaffold, Figure 8) was built in the Maestro[87] modeling environment, and the global minimum conformation was identified by performing 500 iterations of the mixed torsional/low-mode conformational sampling in combination with the OPLS-2005 force-field and the implicit solvent model (water) as implemented in the Macromodel

DOI: 10.1021/jm501524q
J. Med. Chem. 2015, 58, 2221−2239

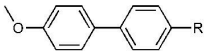

Figure 8. 4-Methoxybiphenyl scaffold of aglycons.

9.9.[88] The global minimum structures were used as input for the AMSOL 7.1 program[89] to obtain the free energy of desolvation ΔG_{des} (Table 5) with the SM5.4A solvation model[90] and the AM1[91] level of theory (used keywords "AM1 SM5.4A SOLVNT=WATER TRUES").

Table 5. Aqueous Free Energy of Desolvation

R	ΔG_{des} [kJ/mol]
neutral	
H	15.6
$CONHCH_3$	39.9
$COOCH_3$	23.0
SO_2NHCH_3	65.5
SO_2CH_3	56.4
4-morpholineamide	45.3
CN	22.0
deprotonated	
COO^-	298.2
SO_2-N^--Me	342.0

Determination of the MAC_{90} by Flow Cytometry. The MAC_{90} was determined in principle as in the previously published flow cytometry assay[79] but with some modifications. The human epithelial bladder carcinoma cell line 5637 (DSMZ, Braunschweig, Germany) was grown in RPMI 1640 medium, supplemented with 10% fetal calf serum (FCS), 100 U/mL penicillin, and 100 μg/mL streptomycin at 37 °C, 5% CO_2. All solutions were purchased from Invitrogen (Basel, Switzerland). The cells were subcultured 1:6 twice per week [using trypsin/EDTA (Sigma-Aldrich) for the detachment]. Two days before infection, 1.8×10^5 cells were seeded in each well of a 24-well plate in RPMI 1640 containing 10% FCS without antibiotics. The cell density was approximately $(3-5) \times 10^5$ cells/well at the assay day.

For infection, the GFP-expressing clinical *E. coli* isolate UTI89[92] (UTI89 wt) and the GFP-expressing FimA-H knockout strain UTI89 Δ*fimA-H* were used (strains were provided by Prof. Urs Jenal, Biocenter, University of Basel, Switzerland).[79] Bacteria were cultivated at 37 °C in 10 mL Luria–Bertani (LB) broth (Becton, Dickinson and Company) overnight, harvested by centrifugation (3800 rpm, 10 min), and washed three times in phosphate buffered saline (PBS, Sigma-Aldrich), and a bacterial solution of OD_{600} of 0.75 in RPMI + 10% FCS was prepared. For the determination of the MAC_{90} value, the IC_{90}, linear dilutions of the FimH antagonist were prepared in 5% DMSO and PBS. Bacteria and antagonists were preincubated for 10 min at 37 °C, before cells were infected with either only 200 μL of bacterial solution of UTI89 or UTI89 Δ*fimA-H* (positive and negative controls), or 225 μL of the preincubated bacteria–antagonist mixture. Infection lasted for 1.5 h. During this time infected cells were incubated at 37 °C. Then, cells were washed with PBS and detached from wells by the addition of 150 μL of trypsin and incubation at 37 °C for 10 min, before flushing from wells PBS containing 2% FCS and transferred to tubes. To dilute the trypsin, cells were centrifuged at 13 000 rpm, 1 min, 600 μL of the supernatant was discarded, and the pellet was resuspended in the remaining 300 μL of PBS containing 2% FCS. Samples were stored on ice until measurement. Before analysis with the flow cytometer (Becton Dickinson, FACSCanto II), the samples were gently mixed and filtered using a 35 μm nylon mesh (Corning Life Sciences) to prevent cellular aggregation. Cells were gated with linear scaling for side scatter (SSC) and forward scatter (FSC) and GFP intensity of live cells was evaluated. IC_{90} values were determined by plotting the concentration of the antagonist in a logarithmic mode versus the mean fluorescence intensity (MFI) of living cells and by fitting a dose–response curve (variable slope, four parameters) with the Prism software (GraphPad Prism).

X-ray Analysis of the Antagonists 10e and 10j Cocrystallized with FimH-CRD. *FimH-CRD/**10e** Cocrystallization.* Initial FimH-CRD (18 mg/mL in 20 mM HEPES, pH 7.4) crystals were obtained in complex with 4-(5-nitroindolin-1-yl)phenyl α-D-mannopyranoside (5 mM).[23] Crystals were grown in sitting-drop vapor diffusion at 20 °C with 200 nL of protein–antagonist mixture together with 200 nL of precipitant solution in well D3 (0.2 M sodium phosphate monobasic monohydrate, 20% w/v PEG 3,350) of the PEG/Ion HT screen (Hampton Research, CA, USA). Cubic crystals appeared within 1 week, which served as cross-seeding crystals. A solution of FimH-CRD (20 mg/mL) and **10e** (5 mM) was mixed with 0.2 M sodium phosphate monobasic monohydrate, 20% w/v PEG 400 with 0.5 μL of each solution. Streak-seeding was performed after 1 day of incubation. Cubic FimH-CRD/**10e** crystals formed within 24 h. Crystals were flash cooled to 100 K with perfluoropolyether cryo oil (Hampton Research, CA, USA) as cryoprotectant. Data were collected with synchrotron radiation (λ = 0.999 99 Å) at the PXIII beamline, Swiss Light Source, Switzerland.

*FimH-CRD/**10j** Cocrystallization.* Cocrystals were initially grown in sitting-drop vapor diffusion at 20 °C with 0.5 μL of a mixture of FimH-CRD (20 mg/mL) and **10j** (5 mM) together with 0.5 μL of 0.1 M HEPES, pH 7.5, 2 M ammonium sulfate. Platelike crystals formed within 2 weeks and were used as seeds for subsequent crystallization. Diffraction quality crystals were grown by streak-seeding in 0.5 μL of FimH-CRD (10 mg/mL) with **10j** (2.5 mM) and 0.5 μL of 0.1 M HEPES, pH 7.5, 1.25 M ammonium sulfate. The drops were covered with perfluoropolyether cryo oil prior to flash cooling to 100 K. Data were collected with synchrotron radiation (λ = 1.000 03 Å) at the PXIII beamline, Swiss Light Source, Switzerland.

Structure Determination and Refinement. Data were indexed and integrated with the XDS package[93] for the FimH-CRD/**10e** cocrystal structure, and with mosflm[94] for the FimH-CRD/**10j** cocrystal structure (Table 6). Scaling was performed with XDS and SCALA included in the CCP4 suite, respectively.[95] Structures were solved by molecular

Table 6. Data Collection and Refinement Statistics for FimH-CRD/10e and FimH-CRD/10j Cocrystals

	FimH-CRD/**10e**	FimH-CRD/**10j**
PDB code	4CSS	4CST
space group	$P2_12_12_1$	$P2_12_12_1$
no. of molecules in the asymmetric unit	1	1
Cell Dimensions		
a, *b*, *c* (Å)	48.38, 56.23, 61.59	48.84, 55.89, 61.00
α, β, γ (deg)	90, 90, 90	90, 90, 90
Data Collection		
beamline	Swiss Light Source PXIII	Swiss Light Source PXIII
resolution range (Å)[a]	30.0–1.07 (1.13–1.07)	23.5–1.10 (1.12–1.10)
unique observations[a]	72000 (9354)	66470 (2500)
average multiplicity[a]	10.9 (3.7)	5.4 (2.4)
completeness (%)	96.1 (78.0)	97.2 (76.5)
R_{merge} [a]	0.056 (0.57)	0.051 (0.305)
mean $I/\sigma(I)$ [a]	21.5 (2.22)	15.5 (2.9)
Refinement		
resolution range (Å)	15.7–1.07	23.5–1.10
R, R_{free}	11.2, 13.2	11.4, 13.0
rms deviation from ideal bond length (Å)	0.010	0.010
rms deviation from ideal bond angle (deg)	1.170	1.420

[a]Values in parentheses are for highest-resolution shell.

DOI: 10.1021/jm501524q
J. Med. Chem. 2015, 58, 2221–2239

replacement with PHASER[96] using the FimH-CRD-butyl α-D-mannopyranoside complex (PDB code 1UWF) as search model. The structures were iteratively built using the COOT software[97] and refined with the PHENIX software.[98] Geometric restraints for **10e** and **10j** were generated with PRODRG.[99] The models were validated using molprobity.[100] Residues 113−115 were not modeled in the **10e** structure because of disorder. Furthermore, the ligand was modeled in two possible conformations. For both ligands, electron density is reduced on the second aromatic ring because of flexibility of the ligand.

Physicochemical and in Vitro Pharmacokinetic Studies. *Materials.* Dimethyl sulfoxide (DMSO), 1-propanol, 1-octanol, Dulbecco's modified Eagle medium (DMEM)−high glucose, L-glutamine solution, penicillin−streptomycin solution, Dulbecco's phosphate buffered saline (DPBS), trypsin−EDTA solution, magnesium chloride hexahydrate, and reduced nicotinamide adenine dinucleotide phosphate (NADPH) were purchased from Sigma-Aldrich. MEM nonessential amino acid (MEM-NEAA) solution, fetal bovine serum (FBS), and DMEM without sodium pyruvate and phenol red were bought from Invitrogen (Carlsbad, CA, USA). PRISMA HT universal buffer, GIT-0 Lipid Solution, and Acceptor Sink Buffer were ordered from pIon (Woburn, MA, USA). Human plasma was bought from Biopredic (Rennes, France), and acetonitrile (MeCN) and methanol (MeOH) were from Acros Organics (Geel, Belgium). Pooled male rat liver microsomes were purchased from BD Bioscience (Franklin Lakes, NJ, USA). Tris(hydroxymethyl)aminomethane (TRIS) was obtained from AppliChem (Darmstadt, Germany). The Caco-2 cells were kindly provided by Prof. G. Imanidis, FHNW, Muttenz, and originated from the American Type Culture Collection (Rockville, MD, USA).

pK_a. The pK_a values were determined as described elsewhere.[101] In brief, the pH of a sample solution was gradually changed and the chemical shift of protons adjacent to ionizable centers was monitored by ^{1}H nuclear magnetic resonance (NMR) spectroscopy. The shift was plotted against the pH of the respective sample, and the pK_a was read out from the inflection point of the resulting sigmoidal curve.

log $D_{7.4}$. The in silico prediction tool ALOGPS[102] was used to estimate log *P* values of the compounds. Depending on these values, the compounds were classified into three categories: hydrophilic compounds (log *P* below zero), moderately lipophilic compounds (log *P* between zero and one), and lipophilic compounds (log *P* above one). For each category, two different ratios (volume of 1-octanol to volume of buffer) were defined as experimental parameters (Table 7).

Table 7. Compound Classification Based on Estimated log *P* Values

compd type	log *P*	ratio (1-octanol/buffer)
hydrophilic	<0	30:140, 40:130
moderately lipophilic	0−1	70:110, 110:70
lipophilic	>1	3:180, 4:180

Equal amounts of phosphate buffer (0.1 M, pH 7.4) and 1-octanol were mixed and shaken vigorously for 5 min to saturate the phases. The mixture was left until separation of the two phases occurred, and the buffer was retrieved. Stock solutions of the test compounds were diluted with buffer to a concentration of 1 μM. For each compound, six determinations, that is, three determinations per 1-octanol/buffer ratio, were performed in different wells of a 96-well plate. The respective volumes of buffer containing analyte (1 μM) were pipetted to the wells and covered by saturated 1-octanol according to the chosen volume ratio. The plate was sealed with aluminum foil, shaken (1350 rpm, 25 °C, 2 h) on a Heidolph Titramax 1000 plate-shaker (Heidolph Instruments GmbH & Co. KG, Schwabach, Germany), and centrifuged (2000 rpm, 25 °C, 5 min, 5804 R Eppendorf centrifuge, Hamburg, Germany). The aqueous phase was transferred to a 96-well plate for analysis by LC−MS.

The log $D_{7.4}$ coefficient was calculated from the 1-octanol/buffer ratio (o/b), the initial concentration of the analyte in buffer (1 μM), and the concentration of the analyte in buffer (c_B) with eq 3:

$$\log D_{7.4} = \log\left(\frac{1\,\mu\text{M} - c_B}{c_B}\,\frac{1}{o/b}\right) \quad (3)$$

Aqueous Solubility. Solubility was determined in a 96-well format using the μSOL Explorer solubility analyzer (pIon, version 3.4.0.5). For each compound, measurements were performed at pH 3.0 and 7.4 in triplicate. For this purpose, six wells of a deep well plate, that is, three wells per pH value, were filled with 300 μL of PRISMA HT universal buffer, adjusted to pH 3.0 or 7.4 by adding the requested amount of NaOH (0.5 M). Aliquots (3 μL) of a compound stock solution (10−50 mM in DMSO) were added and thoroughly mixed. The final sample concentration was 0.1−0.5 mM, and the residual DMSO concentration was 1.0% (v/v) in the buffer solutions. After 15 h, the solutions were filtered (0.2 μm 96-well filter plates) using a vacuum to collect manifold (Whatman Ltd., Maidstone, U.K.) to remove the precipitates. Equal amounts of filtrate and 1-propanol were mixed and transferred to a 96-well plate for UV/vis detection (190−500 nm, SpectraMax 190). The amount of material dissolved was calculated by comparison with UV/vis spectra obtained from reference samples, which were prepared by dissolving compound stock solution in a 1:1 mixture of buffer and 1-propanol (final concentrations 0.017−0.083 mM).

Parallel Artificial Membrane Permeation Assay (PAMPA). Effective permeability (log P_e) was determined in a 96-well format with the PAMPA.[60] For each compound, measurements were performed at pH 5.0 and 7.4 in quadruplicates. Eight wells of a deep well plate, that is, four wells per pH value, were filled with 650 μL of PRISMA HT universal buffer adjusted to pH 5.0 or 7.4 by adding the requested amount of NaOH (0.5 M). Samples (150 μL) were withdrawn from each well to determine the blank spectra by UV/vis spectroscopy (190−500 nm, SpectraMax 190). Then analyte dissolved in DMSO was added to the remaining buffer to yield 50 μM solutions. To exclude precipitation, the optical density was measured at 650 nm, with 0.01 being the threshold value. Solutions exceeding this threshold were filtered. Afterward, samples (150 μL) were withdrawn to determine the reference spectra. Further 200 μL was transferred to each well of the donor plate of the PAMPA sandwich (pIon, P/N 110163). The filter membranes at the bottom of the acceptor plate were infused with 5 μL of GIT-0 lipid solution, and 200 μL of Acceptor Sink Buffer was filled into each acceptor well. The sandwich was assembled, placed in the GutBox, and left undisturbed for 16 h. Then it was disassembled and samples (150 μL) were transferred from each donor and acceptor well to UV plates for determination of the UV/vis spectra. Effective permeability (log P_e) was calculated from the compound flux deduced from the spectra, the filter area, and the initial sample concentration in the donor well with the aid of the PAMPA Explorer software (pIon, version 3.5).

Colorectal Adenocarcinoma (Caco-2) Cell Permeation Assay. Caco-2 cells were cultivated in tissue culture flasks (BD Biosciences) with DMEM high glucose medium, containing L-glutamine (2 mM), nonessential amino acids (0.1 mM), penicillin (100 U/mL), streptomycin (100 μg/mL), and fetal bovine serum (10%). The cells were kept at 37 °C in humidified air containing 5% CO_2, and the medium was changed every second day. When approximately 90% confluence was reached, the cells were split in a 1:10 ratio and distributed to new tissue culture flasks. At passage numbers between 60 and 65, they were seeded at a density of 5.3×10^5 cells per well to Transwell six-well plates (Corning Inc.) with 2.5 mL of culture medium in the basolateral and 1.8 mL in the apical compartment. The medium was renewed on alternate days. Permeation experiments were performed between days 19 and 21 after seeding. Prior to the experiment, the integrity of the Caco-2 monolayers was evaluated by measuring the transepithelial electrical resistance (TEER) with an Endohm tissue resistance instrument (World Precision Instruments Inc., Sarasota, FL, USA). Only wells with TEER values higher than 250 Ω cm^2 were used. Experiments were performed in the apical-to-basolateral (absorptive) and basolateral-to-apical (secretory) directions in triplicate. Transport medium (DMEM without sodium pyruvate and phenol red) was withdrawn from the donor compartments of three wells and replaced by the same volume of compound stock solution (10 mM in DMSO) to reach an initial sample concentration of 62.5 μM. The Transwell plate was then shaken (600 rpm, 37 °C) on a Heidolph

DOI: 10.1021/jm501524q
J. Med. Chem. 2015, 58, 2221−2239

Titramax 1000 plate-shaker. Samples (40 μL) were withdrawn from the donor and acceptor compartments 30 min after initiation of the experiment, and the compound concentrations were determined by LC−MS (see below). Apparent permeability (P_{app}) was calculated according to eq 4:

$$P_{app} = \frac{dQ}{dt}\frac{1}{Ac_0} \quad (4)$$

where dQ/dt is the compound flux (mol s^{-1}), A is the surface area of the monolayer (cm^2), and c_0 is the initial concentration in the donor compartment (mol cm^{-3}).[60] After the experiment, TEER values were assessed again for each well and results from wells with values below 250 Ω cm^2 were discarded.

Plasma Protein Binding (PPB). PPB was determined in a 96-well format using a high throughput dialysis block (HTD96b; HTDialysis LCC, Gales Ferry, CT, USA). For each compound, measurements were performed in triplicate. Dialysis membranes (MWCO 12-14 K; HTDialysis LCC) were hydrated according to the instructions of the manufacturer and placed into the dialysis block. Human plasma was centrifuged (5800 rpm, 5 °C, 10 min), the pH of the supernatant (without floating plasma lipids) was adjusted to 7.4 by adding the requested amount of HCl (4 M), and analyte was added to yield a final concentration of 10 μM. Equal volumes (150 μL) of plasma containing the analyte or TRIS-HCl buffer (0.1 M, pH 7.4) were transferred to the compartments separated by the dialysis membrane. The block was covered with a sealing film and left undisturbed (5 h, 37 °C). Afterward, samples (90 μL) were withdrawn from the buffer compartments and diluted with plasma (10 μL). From the plasma compartments, samples (10 μL) were withdrawn and diluted with TRIS-HCl buffer (90 μL). The solutions were further diluted with ice-cooled MeCN (300 μL) to precipitate the proteins and centrifuged (3600 rpm, 4 °C, 10 min). The supernatants (50 μL) were retrieved, and the analyte concentrations were determined by LC−MS (see below). The fraction bound (f_b) was calculated as follows (eq 5):

$$f_b = 1 - \frac{c_b}{c_p} \quad (5)$$

where c_b is the concentration of the analyte withdrawn from the buffer compartment before dilution and c_p is the concentration in the plasma compartment. The values were accepted if the recovery of analyte was between 80% and 120% of the initial amount.

Cytochrome P450 Mediated Metabolism. Incubations consisted of pooled male rat liver microsomes (0.5 mg microsomal protein/mL), test compound (2 μM), $MgCl_2$ (2 mM), and NADPH (1 mM) in a total volume of 300 μL TRIS-HCl buffer (0.1 M, pH 7.4) and were performed in a 96-well plate on a Thermomixer Comfort (Eppendorf). Compounds and microsomes were preincubated (37 °C, 700 rpm, 10 min) before NADPH was added. Samples (50 μL) at $t = 0$ min and after an incubation time of 5, 10, 20, and 30 min were quenched with 150 μL of ice-cooled MeOH, centrifuged (3600 rpm, 4 °C, 10 min), and 80 μL of supernatant was transferred to a 96-well plate for LC−MS analysis (see below). The metabolic half-life ($t_{1/2}$) was calculated from the slope of the linear regression from the log percentage remaining compound versus incubation time relationship. Control experiments without NADPH were performed in parallel.

LC−MS Measurements. Analyses were performed using an 1100/1200 series HPLC system coupled to a 6410 triple quadrupole mass detector (Agilent Technologies, Inc., Santa Clara, CA, USA) equipped with electrospray ionization. The system was controlled with the Agilent MassHunter Workstation Data Acquisition software (version B.01.04). The column used was an Atlantis T3 C18 column (2.1 mm × 50 mm) with a 3 μm particle size (Waters Corp., Milford, MA, USA). The mobile phase consisted of eluent A (H_2O containing 0.1% formic acid (for **10a**−**f**,**h**,**i**), or 10 mM ammonium acetate, pH 5.0 in 95:5, H_2O/MeCN (for **10g**,**j**)) and eluent B (MeCN containing 0.1% formic acid). The flow rate was maintained at 0.6 mL/min. The gradient was ramped from 95% A/5% B to 5% A/95% B over 1 min and then held at 5% A/95% B for 0.1 min. The system was then brought back to 95% A/5% B, resulting in a total duration of 4 min. MS parameters such as fragmentor voltage, collision energy, polarity were optimized individually for each analyte, and the molecular ion was followed for each compound in the multiple reaction monitoring mode. The concentrations of the analytes were quantified by the Agilent Mass Hunter Quantitative Analysis software (version B.01.04).

In Vivo Studies. *Animals.* Female C3H/HeN mice weighing between 19 and 25 g were obtained from Charles River Laboratories (Sulzfeld, Germany) or Harlan (Venray, The Netherlands) and were housed three or four per cage. The mice were kept under specific pathogen-free conditions in the Animal House of the Department of Biomedicine, University Hospital of Basel, and animal experimentation guidelines according to the regulations of the Swiss veterinary law were followed. After 7 days of acclimatization, 9- to 10-week-old mice were used for the studies. Animals had free access to chow and water at any time and were kept in a 12 h/12 h light/dark cycle. For administration volumes and sampling the good practice guidelines were followed.[103]

Pharmacokinetic Studies. The single-dose studies for the first experiment set were performed by intravenous application of FimH antagonists at a dosage of 50 mg/kg body weight, followed by plasma and urine sampling. Antagonists were diluted in PBS (Sigma-Aldrich) for injection into the tail vein. Blood and urine samples (10 μL) were taken at 6 and 30 min and at 1, 2, 4, 6, and 8 h after injection. For the PK studies with **10j**, the antagonist was dissolved in PBS with 5% DMSO (Sigma-Aldrich) and injected into the tail vain (0.625 mg/kg) or given orally (1.25 mg/kg) using a gavage (syringes from BD Micro Fine, U-100 Insuline, 30 G with BD Microlance 3, 25 G needles, Becton Dickinson and Soft-Ject, 1 mL syringes from Henke Sass Wolf; gavage from Fine Science Tools). Blood and urine were sampled (10 μL) after 7, 13, 20, 30, 45 min and after 1, 1.5, 2, 2.5, 3, 4, 6, 8, and 24 h. Both blood and urine samples were directly diluted after sampling with MeOH (Acros Organics) to precipitate the proteins and centrifuged for 11 min at 13 000 rpm. The supernatants were transferred to a 96-well plate (Agilent Technologies, 0.5 mL, polypropylene), and the analyte concentrations were determined by LC−MS (see above).

Infection Study. For all infection studies, the drinking water of the mice was replaced by water containing 5% glucose (monohydrate from AppliChem, BioChemica), 3 days before the start of the experiment. **10j** was dosed at 1.25 mg/kg (in 5% DMSO and PBS) and 10 mg/kg (in 5% DMSO in PBS containing 1% Tween 80, all purchased from Sigma-Aldrich) and applied orally via gavage to six and four mice, respectively, as described in the section Pharmacokinetic Studies, 40 min prior to infection. Ciprofloxacin (Ciproxin solution, 2 mg/mL, Bayer) was dosed with 8 mg/kg, which would correspond to a human dose of 500 mg,[81] subcutaneously 10 min prior to infection with UTI89 to 4 mice. The values for the control group (PBS, po) resulted from the infection of 11 mice. Four mice were orally treated with the formulation vehicle for **10j** (5% DMSO in PBS containing 1% Tween 80) and termed controls formulation. Before infection, remaining urine in the bladder was expelled by gentle pressure on the abdomen. Mice were anesthetized in 2.5 vol % isoflurane/oxygen mixture (Attane, Minrad Inc., USA) and placed on their back. Infection was performed transurethrally using a polyethylene catheter (Intramedic polyethylene tubing, inner diameter 0.28 mm, outer diameter 0.61 mm, Becton Dickinson), on a syringe (Hamilton Gastight Syringe 50 μL, removable 30G needle, BGB Analytik AG, Switzerland). After gentle insertion of the catheter into the bladder, 50 μL of bacterial suspension of UTI89 (5.5×10^9 to 2.25×10^{10} CFU/mL) was slowly injected. This corresponded to approximately 10^7−10^8 CFU per mouse. Mice were killed by CO_2 3 h after inoculation, and bladder and kidneys were aseptically removed. Organs were homogenized in 1 mL of PBS using a tissue lyser (Retsch, Germany). Serial dilutions of bladder and kidneys were plated on Levine Eosin Methylene Blue Agar plates (Becton Dickinson), and CFUs were counted after overnight incubation at 37 °C.

■ ASSOCIATED CONTENT

Supporting Information

HPLC data and chromatograms of target compounds and ^1H NMR spectra of the synthetic compounds. This material is available free of charge via the Internet at http://pubs.acs.org.

DOI: 10.1021/jm501524q
J. Med. Chem. 2015, 58, 2221−2239

AUTHOR INFORMATION

Corresponding Author

*Phone: +41 61 267 15 51. Fax: +41 61 267 15 52. E-mail: beat.ernst@unibas.ch.

Author Contributions

‖S.K., L.P., K.M., D.E., and A.S. contributed equally to the project.

Notes

The authors declare no competing financial interest.

ACKNOWLEDGMENTS

The authors thank Prof. Dr. med. Radek Skoda, Department of Biomedicine, University Hospital Basel, Switzerland, for giving us access to the animal facility. The financial support by the Swiss National Science Foundation (SNF Interdisciplinary Grant K-32K1-120904) is gratefully acknowledged.

ABBREVIATIONS USED

ΔH, change in enthalpy; ΔS, change in entropy; AUC, area under the curve; BSA, bovine serum albumin; C_{max}, maximal concentration; Caco-2, colorectal adenocarcinoma; CFU, colony forming unit; CL_{tot}, total clearance; CRD, carbohydrate recognition domain; C_0, initial concentration; DL, detection limit; FITC, fluorescein isothiocyanate; FP, fluorescence polarization; ITC, isothermal titration calorimetry; iv, intravenous; K_D, dissociation constant; MAC_{90}, minimal antiadhesion concentration to inhibit 90% adhesion; PAMPA, parallel artificial membrane permeation assay; P_{app}, apparent permeability; PD, pharmacodynamics; P_e, effective permeability; PK, pharmacokinetics; po, per os; sc, subcutaneous; UPEC, uropathogenic *Escherichia coli*; UTI, urinary tract infection; V_z, volume of distribution in terminal phase

REFERENCES

(1) Foxman, B.; Barlow, R.; D'Arcy, H.; Gillespie, B.; Sobel, J. D. Urinary tract infection: self-reported incidence and associated costs. *Ann. Epidemiol.* **2000**, *10*, 509−515.

(2) Ronald, A. The etiology of urinary tract infection: traditional and emerging pathogens. *Am. J. Med.* **2002**, *113* (Suppl. 1A), 14S−19S.

(3) Fihn, S. D. Acute uncomplicated urinary tract infection in women. *N. Engl. J. Med.* **2003**, *349*, 259−266.

(4) Hooton, T. M.; Besser, R.; Foxman, B.; Fritsche, T. R.; Nicolle, L. E. Acute uncomplicated cystitis in an era of increasing antibiotic resistance: a proposed approach to empirical therapy. *Clin. Infect. Dis.* **2004**, *39*, 75−80.

(5) Sanchez, G. V.; Master, R. N.; Karlowsky, J. A.; Bordon, J. M. In vitro antimicrobial resistance of urinary *Escherichia coli* isolates among U.S. outpatients from 2000 to 2010. *Antimicrob. Agents Chemother.* **2012**, *56*, 2181−2183.

(6) Clatworthy, A. E.; Pierson, E.; Hung, D. T. Targeting virulence: a new paradigm for antimicrobial therapy. *Nat. Chem. Biol.* **2007**, *3*, 541−548.

(7) Mulvey, M. A.; Schilling, J. D.; Martinez, J. J.; Hultgren, S. J. Bad bugs and beleaguered bladders: interplay between uropathogenic *Escherichia coli* and innate host defenses. *Proc. Natl. Acad. Sci. U.S.A.* **2000**, *97*, 8829−8835.

(8) Schilling, J. D.; Mulvey, M. A.; Hultgren, S. J. Structure and function of *Escherichia coli* type 1 pili: new insight into the pathogenesis of urinary tract infections. *J. Infect. Dis.* **2001**, *183* (Suppl. 1), S36−S40.

(9) Wiles, T. J.; Kulesus, R. R.; Mulvey, M. A. Origins and virulence mechanisms of uropathogenic *Escherichia coli*. *Exp. Mol. Pathol.* **2008**, *85*, 11−19.

(10) Capitani, G.; Eidam, O.; Glockshuber, R.; Grütter, M. G. Structural and functional insights into the assembly of type 1 pili from *Escherichia coli*. *Microbes Infect.* **2006**, *8*, 2284−2290.

(11) Le Trong, I.; Aprikian, P.; Kidd, B. A.; Forero-Shelton, M.; Tchesnokova, V.; Rajagopal, P.; Rodriguez, V.; Interlandi, G.; Klevit, R.; Vogel, V.; Stenkamp, R. E.; Sokurenko, E. V.; Thomas, W. E. Structural basis for mechanical force regulation of the adhesin FimH via finger trap-like β sheet twisting. *Cell* **2010**, *141*, 645−655.

(12) Sharon, N. Carbohydrates as future anti-adhesion drugs for infectious diseases. *Biochim. Biophys. Acta* **2006**, *1760*, 527−537.

(13) Firon, N.; Itzhak, O.; Sharon, N. Interaction of mannose-containing oligosaccharides with the fimbrial lectin of *Escherichia coli*. *Biochem. Biophys. Res. Commun.* **1982**, *105*, 1426−1432.

(14) Firon, N.; Ofek, I.; Sharon, N. Carbohydrate specificity of the surface lectins of *Escherichia coli*, *Klebsiella pneumoniae*, and *Salmonella typhimurium*. *Carbohydr. Res.* **1983**, *120*, 235−249.

(15) Bouckaert, J.; Berglund, J.; Schembri, M.; De Genst, E.; Cools, L.; Wuhrer, M.; Hung, C.-S.; Pinkner, J.; Slättegard, R.; Zavialov, A.; Choudhury, D.; Langermann, S.; Hultgren, S. J.; Wyns, L.; Klemm, P.; Oscarson, S.; Knight, S. D.; De Greve, H. Receptor binding studies disclose a novel class of high-affinity inhibitors of the *Escherichia coli* FimH adhesin. *Mol. Microbiol.* **2005**, *55*, 441−455.

(16) Firon, N.; Ashkenazi, S.; Mirelman, D.; Ofek, I.; Sharon, N. Aromatic alpha-glycosides of mannose are powerful inhibitors of the adherence of type 1 fimbriated *Escherichia coli* to yeast and intestinal epithelial cells. *Infect. Immun.* **1987**, *55*, 472−476.

(17) Sperling, O.; Fuchs, A.; Lindhorst, T. K. Evaluation of the carbohydrate recognition domain of the bacterial adhesin FimH. Design, synthesis and binding properties of mannoside ligands. *Org. Biomol. Chem.* **2006**, *4*, 3913−3922.

(18) Han, Z.; Pinkner, J. S.; Ford, B.; Obermann, R.; Nolan, W.; Wildman, S. A.; Hobbs, D.; Ellenberger, T.; Cusumano, C. K.; Hultgren, S. J.; Janetka, J. W. Structure-based drug design and optimization of mannoside bacterial FimH antagonists. *J. Med. Chem.* **2010**, *53*, 4779−4792.

(19) Klein, T.; Abgottspon, D.; Wittwer, M.; Rabbani, S.; Herold, J.; Jiang, X.; Kleeb, S.; Lüthi, C.; Scharenberg, M.; Bezençon, J.; Gubler, E.; Pang, L.; Smiesko, M.; Cutting, B.; Schwardt, O.; Ernst, B. FimH antagonists for the oral treatment of urinary tract infections: from design and synthesis to in vitro and in vivo evaluation. *J. Med. Chem.* **2010**, *53*, 8627−8641.

(20) Cusumano, C. K.; Pinkner, J. S.; Han, Z.; Greene, S. E.; Ford, B. A.; Crowley, J. R.; Henderson, J. P.; Janetka, J. W.; Hultgren, S. J. Treatment and prevention of urinary tract infection with orally active FimH inhibitors. *Sci. Transl. Med.* **2011**, *3*, 109ra115.

(21) Han, Z.; Pinkner, J. S.; Ford, B.; Chorell, E.; Crowley, J. M.; Cusumano, C. K.; Campbell, S.; Henderson, J. P.; Hultgren, S. J.; Janetka, J. W. Lead optimization studies on FimH antagonists: discovery of potent and orally bioavailable ortho-substituted biphenyl mannosides. *J. Med. Chem.* **2012**, *55*, 3945−3959.

(22) Pang, L.; Kleeb, S.; Lemme, K.; Rabbani, S.; Scharenberg, M.; Zalewski, A.; Schädler, F.; Schwardt, O.; Ernst, B. FimH antagonists: structure−activity and structure−property relationships for biphenyl α-D-mannopyranosides. *ChemMedChem* **2012**, *7*, 1404−1422.

(23) Jiang, X.; Abgottspon, D.; Kleeb, S.; Rabbani, S.; Scharenberg, M.; Wittwer, M.; Haug, M.; Schwardt, O.; Ernst, B. Anti-adhesion therapy for urinary tract infections—a balanced PK/PD profile proved to be key for success. *J. Med. Chem.* **2012**, *55*, 4700−4713.

(24) Schwardt, O.; Rabbani, S.; Hartmann, M.; Abgottspon, D.; Wittwer, M.; Kleeb, S.; Zalewski, A.; Smiesko, M.; Cutting, B.; Ernst, B. Design, synthesis and biological evaluation of mannosyl triazoles as FimH antagonists. *Bioorg. Med. Chem.* **2011**, *19*, 6454−6473.

(25) Brument, S.; Sivignon, A.; Dumych, T. I.; Moreau, N.; Roos, G.; Guérardel, Y.; Chalopin, T.; Deniaud, D.; Bilyy, R. O.; Darfeuille-Michaud, A.; Bouckaert, J.; Gouin, S. G. Thiazolylaminomannosides as potent antiadhesives of type 1 piliated *Escherichia coli* isolated from Crohn's disease patients. *J. Med. Chem.* **2013**, *56*, 5395−5406.

(26) Lindhorst, T. K.; Kieburg, C.; Krallmann-Wenzel, U. Inhibition of the type 1 fimbriae-mediated adhesion of *Escherichia coli* to erythrocytes by multiantennary D-mannosyl clusters: the effect of multivalency. *Glycoconjugate J.* **1998**, *15*, 605−613.

DOI: 10.1021/jm501524q
J. Med. Chem. 2015, 58, 2221−2239

(27) Nagahori, N.; Lee, R. T.; Nishimura, S.-L.; Pagé, S.; Roy, R.; Lee, Y. C. Inhibition of adhesion of type 1 fimbriated *Escherichia coli* to highly mannosylated ligands. *ChemBioChem* **2002**, *3*, 836−844.
(28) Appeldoorn, C. C. M.; Joosten, J. A. F.; Maate, F. A.; Dobrindt, U.; Hacker, J.; Liskamp, R. M. J.; Khan, A. S.; Pieters, R. J. Novel multivalent mannose compounds and their inhibition of the adhesion of type 1 fimbriated uropathogenic *E. coli*. *Tetrahedron: Asymmetry* **2005**, *16*, 361−372.
(29) Patel, A.; Lindhorst, T. K. A modular approach for the synthesis of oligosaccharide mimetics. *Carbohydr. Res.* **2006**, *341*, 1657−1668.
(30) Touaibia, M.; Wellens, A.; Shiao, T. C.; Wang, Q.; Sirois, S.; Bouckaert, J.; Roy, R. Mannosylated G(0) dendrimers with nanomolar affinities to *Escherichia coli* FimH. *ChemMedChem* **2007**, *2*, 1190−1201.
(31) Durka, M.; Buffet, K.; Iehl, J.; Holler, M.; Nierengarten, J.-F.; Taganna, J.; Bouckaert, J.; Vincent, S. P. The functional valency of dodecamannosylated fullerenes with *Escherichia coli* FimH—towards novel bacterial antiadhesives. *Chem. Commun.* **2011**, *47*, 1321−1323.
(32) Bouckaert, J.; Li, Z.; Xavier, C.; Almant, M.; Caveliers, V.; Lahoutte, T.; Weeks, S. D.; Kovensky, J.; Gouin, S. G. Heptyl α-D-mannosides grafted on a β-cyclodextrin core to interfere with *Escherichia coli* adhesion: an in vivo multivalent effect. *Chem.—Eur. J.* **2013**, *19*, 7847−7855.
(33) Scharenberg, M.; Schwardt, O.; Rabbani, S.; Ernst, B. Target selectivity of FimH antagonists. *J. Med. Chem.* **2012**, *55*, 9810−9816.
(34) Choudhury, D.; Thompson, A.; Stojanoff, V.; Langermann, S.; Pinkner, J.; Hultgren, S. J.; Knight, S. D. X-ray structure of the FimC-FimH chaperone-adhesin complex from uropathogenic *Escherichia coli*. *Science* **1999**, *285*, 1061−1066.
(35) Hung, C.-S.; Bouckaert, J.; Hung, D.; Pinkner, J.; Widberg, C.; DeFusco, A.; Auguste, C. G.; Strouse, R.; Langermann, S.; Waksman, G.; Hultgren, S. J. Structural basis of tropism of *Eschrichia coli* to the bladder drug in urinary tract infection. *Mol. Microbiol.* **2002**, *44*, 903−915.
(36) Wellens, A.; Garofalo, C.; Nguyen, H.; Van Gerven, N.; Slättegard, R.; Henalsteens, J.-P.; Wyns, L.; Oscarson, S.; De Greve, H.; Hultgren, S. J.; Bouckaert, J. Intervening with urinary tract infections using anti-adhesives based on the crystal structure of the FimH-oligomannose-3 complex. *PLoS One* **2008**, *3*, e2040.
(37) Wellens, A.; Lahmann, M.; Touaibia, M.; Vaucher, J.; Oscarson, S.; Roy, R.; Remaut, H.; Bouckaert, J. The tyrosine gate as a potential entropic lever in the receptor-binding site of the bacterial adhesin FimH. *Biochemistry* **2012**, *51*, 4790−4799.
(38) Totsika, M.; Kostakioti, M.; Hannan, T. J.; Upton, M.; Beatson, S. A.; Janetka, J. W.; Hultgren, S. J.; Schembri, M. A. A FimH inhibitor prevents acute bladder infection and treats chronic cystitis caused by multidrug-resistant uropathogenic *Escherichia coli* ST131. *J. Infect. Dis.* **2013**, *208*, 921−928.
(39) Meanwell, M. A. Synopsis of some recent tactical application of bioisosteres in drug design. *J. Med. Chem.* **2011**, *54*, 2529−2591.
(40) Prieto, M.; Zurita, E.; Rosa, E.; Luñoz, L.; Lloyd-Williams, P.; Giralt, E. Arylboronic acids and arylpinacolboronate esters in Suzuki coupling reactions involving indoles. Partner role swapping and heterocycle protection. *J. Org. Chem.* **2004**, *69*, 6812−6820.
(41) Schulz, M. J.; Coats, S. J.; Hlasta, D. J. Microwave-assisted preparation of aryltetrazoleboronate esters. *Org. Lett.* **2004**, *6*, 3265−3268.
(42) Devos, A.; Remion, J.; Frisque-Hesbain, A. M.; Colens, A.; Ghosez, L. Synthesis of acyl halides under very mild conditions. *J. Chem. Soc., Chem. Commun.* **1979**, 1180−1181.
(43) Rabbani, S.; Jiang, X.; Schwardt, O.; Ernst, B. Expression of the carbohydrate recognition domain of FimH and development of a competitive binding assay. *Anal. Biochem.* **2010**, *407*, 188−195.
(44) Waetherman, R. V.; Kiessling, L. L. Fluorescence anisotropy assay reveals affinities of *C*- and *O*-glycosides for concanavalin A. *J. Org. Chem.* **1996**, *61*, 534−538.
(45) Cer, R. Z.; Mudunuri, U.; Stephens, R.; Lebeda, F. J. IC50-to-Ki: a web-based tool for converting IC50 to Ki values for inhibitors of enzyme activity and ligand binding. *Nucleic Acids Res.* **2009**, *37*, W441−W445.
(46) Lynch, B. A.; Loiacono, K. A.; Tiong, C. L.; Adams, S. E.; MacNeil, I. A. A fluorescence polarization based Src-SH2 binding assay. *Anal. Biochem.* **1997**, *247*, 77−82.
(47) Wu, P.; Brasseur, M.; Schindler, U. A high-throughput STAT binding assay using fluorescence polarization. *Anal. Biochem.* **1997**, *249*, 29−36.
(48) Huang, X. Fluorescence polarization competition assay: the range of resolvable inhibitor potency is limited by the affinity of the fluorescent ligand. *J. Biomol. Screening* **2003**, *8*, 34−38.
(49) Cooper, A. *Biophysical Chemistry*, 2nd ed.; RSC Publishing: Cambridge, U.K., 2011; pp 122−123.
(50) Scharenberg, M.; Jiang, X.; Pang, L.; Navarra, G.; Rabbani, S.; Binder, F.; Schwardt, O.; Ernst, B. Kinetic properties of carbohydrate−lectin interactions: FimH antagonists. *ChemMedChem* **2014**, *9*, 78−83.
(51) Cabani, S.; Gianni, P.; Mollica, V.; Lepori, L. Group contribution to the thermodynamic properties of non-ionic solutes in dilute aqueous solution. *J. Solution Chem.* **1981**, *10*, 563−595.
(52) Hansch, C.; Leo, A.; Taft, R. W. A survey of Hammett substituent constants and resonance and field parameters. *Chem. Rev.* **1991**, *91*, 165−195.
(53) Chen, A.; Wadso, I. Simultaneous determination of delta G, delta H and delta S by an automatic microcalorimetric titration technique: application to protein ligand binding. *J. Biochem Biophys Methods* **1982**, *6*, 307−316.
(54) Freire, E.; Mayorga, O. L.; Straume, M. Isothermal titration calorimetry. *Anal. Chem.* **1990**, *62*, 950A−959A.
(55) Wiseman, T.; Williston, S.; Brandts, J. F.; Lin, L.-N. Rapid measurement of binding constants and heats of binding using a new titration calorimeter. *Anal. Biochem.* **1989**, *179*, 131−137.
(56) Turnbull, W. B.; Daranas, A. H. On the value of c: can low affinity systems be studied by isothermal titration calorimetry? *J. Am. Chem. Soc.* **2003**, *125*, 14859−14866.
(57) Sigurskjold, B. W. Exact analysis of competition ligand binding by displacement isothermal titration calorimetry. *Anal. Biochem.* **2000**, *277*, 260−266.
(58) Velazquez-Campoy, A.; Freire, E. Isothermal titration calorimetry to determine association constants for high-affinity ligands. *Nat. Protoc.* **2006**, *1*, 186−191.
(59) Dearden, J. C.; Bresnen, G. M. The measurement of partition coefficients. *QSAR Comb. Sci.* **1988**, *7*, 133−144.
(60) Kansy, M.; Senner, F.; Gubernator, K. Physicochemical high throughput screening: parallel artificial membrane permeation assay in the description of passive absorption processes. *J. Med. Chem.* **1998**, *41*, 1007−1010.
(61) Hubatsch, I.; Ragnarsson, E. G. E.; Artursson, P. Determination of drug permeability and predicition of drug absorption in Caco-2 monolayers. *Nat. Protoc.* **2007**, *2*, 2111−2119.
(62) Banker, M. J.; Clark, T. H.; Williams, J. A. Development and validation of a 96-well equilibrium dialysis apparatus for measuring plasma protein binding. *J. Pharm. Sci.* **2003**, *92*, 967−974.
(63) Obach, R. S. Prediction of human clearance of twenty-nine drugs from hepatic microsomal intrinsic clearance data: an examination of in vitro half-life approach and nonspecific binding to microsomes. *Drug Metab. Dispos.* **1999**, *27*, 1350−1359.
(64) Chaturvedi, P. R.; Decker, C. J.; Odinecs, A. Prediction of pharmacokinetic properties using experimental approaches during early drug discovery. *Curr. Opin. Chem. Biol.* **2001**, *5*, 452−463.
(65) Di, L.; Kerns, E. H. Profiling drug-like properties in discovery research. *Curr. Opin. Chem. Biol.* **2003**, *7*, 402−408.
(66) Lipinski, C. A. Drug-like properties and the causes of poor solubility and poor permeability. *J. Pharmacol. Toxicol. Methods* **2000**, *44*, 235−249.
(67) Curatolo, W. Physical chemical properties of oral drug candidates in the discovery and exploratory development settings. *Pharm. Sci. Technol. Today* **1998**, *1*, 387−393.
(68) Ishikawa, M.; Hashimoto, Y. Improvement in aqueous solubility in small molecule drug discovery programs by disruption of molecular planarity and symmetry. *J. Med. Chem.* **2011**, *54*, 1539−1554.

DOI: 10.1021/jm501524q
J. Med. Chem. 2015, 58, 2221−2239

(69) Avdeef, A.; Bendels, S.; Di, L.; Faller, B.; Kansy, M.; Sugano, K.; Yamauchi, Y. PAMPA – critical factors for better predictions of absorption. *J. Pharm. Sci.* **2007**, *96*, 2893–2909.
(70) Artursson, P.; Karlsson, J. Correlation between oral drug absorption in humans and apparent drug permeability coefficients in human intestinal epithelial (Caco-2) cells. *Biochem. Biophys. Res. Commun.* **1991**, *175*, 880–885.
(71) Feng, B.; LaPerle, J. L.; Chang, G.; Varma, M. V. S. Renal clearance in drug discovery and development: molecular descriptors, drug transporters and disease state. *Expert Opin. Drug. Metab. Toxicol.* **2010**, *6*, 939–952.
(72) Schmidt, S.; Gonzalez, D.; Derendorf, H. Significance of protein binding in pharmacokinetics and pharmacodynamics. *J. Pharm. Sci.* **2010**, *99*, 1107–1122.
(73) Weisiger, R. A. Dissociation from albumin: A potentially rate-limiting step in the clearance of substances by the liver. *Proc. Natl. Acad. Sci. U.S.A.* **1985**, *82*, 1563–1567.
(74) Smith, D. A.; Jones, B. C.; Walker, D. K. Design of drugs involving the concepts and theories of drug metabolism and pharmacokinetics. *Med. Res. Rev.* **1996**, *16*, 243–266.
(75) Van de Waterbeemd, H.; Smith, D. A.; Beaumont, K.; Walker, D. K. Property-based design: optimization of drug absorption and pharmacokinetics. *J. Med. Chem.* **2001**, *44*, 1313–1333.
(76) Varma, M. V. S.; Feng, B.; Obach, R. S.; Troutman, M. D.; Chupka, J.; Miller, H. R.; El-Kattan, A. Physicochemical determinants of human renal clearance. *J. Med. Chem.* **2009**, *52*, 4844–4852.
(77) Waring, M. J. Lipophilicity in drug discovery. *Expert Opin. Drug Discovery* **2010**, *5*, 235–248.
(78) Zhang, Y.; Huo, M.; Solver, P. K. An add-in program for pharmacokinetic and pharmacodynamic data analysis in Microsoft Excel. *Comput. Methods Programs Biomed.* **2010**, *99*, 306–314.
(79) Scharenberg, M.; Abgottspon, D.; Cicek, E.; Jiang, X.; Schwardt, O.; Rabbani, S.; Ernst, B. Cytometry-based assay for screening FimH antagonists. *Assay Drug Dev. Technol.* **2011**, *9*, 455–464.
(80) Hooton, T. M. Fluoroquinolones and resistance in the treatment of uncomplicated urinary tract infection. *Int. J. Antimicrob. Agents* **2003**, *22*, 65–72.
(81) Jakobsen, L.; Cattoir, V.; Jensen, K. S.; Hammerum, A. M.; Nordmann, P.; Frimodt-Møller, N. Impact of low-level fluoroquinolone resistance genes qnrA1, qnrB19, and qnrS1 on ciprofloxacin treatment of isogenic *Escherichia coli* strains in a murine urinary tract infection model. *J. Antimicrob. Chemother.* **2012**, *67*, 2438–2444.
(82) Mulvey, M. A. Adhesion and entry of uropathogenic *Escherichia coli*. *Cell. Microbiol.* **2002**, *4*, 257–271.
(83) Ballatore, C.; Huryn, D. M.; Smith, A. B. Carboxylic acid (bio)isosteres in drug design. *ChemMedChem* **2013**, *8*, 385–395.
(84) Justice, S. S.; Hung, C.; Theriot, J. A.; Fletcher, D. A.; Anderson, G. G.; Footer, M. J.; Hultgren, S. J. Differentiation and developmental pathways of uropathogenic *Escherichia coli* in urinary tract pathogenesis. *Proc. Natl. Acad. Sci. U.S.A.* **2004**, *101*, 1333–1338.
(85) Mulvey, M. A.; Schilling, J. D.; Hultgren, S. J. Establishment of a persistent *Escherichia coli* reservoir during the acute phase of a bladder infection. *Infect. Immun.* **2001**, *69*, 4572–9.
(86) Houtman, J. C.; Brown, P. C.; Bowden, B.; Yamaguchi, H.; Appella, E.; Samelson, L. E.; Schuck, P. Studying multisite binary and ternary protein interactions by global analysis of isothermal titration calorimetry data in SEDPHAT: application to adaptor protein complexes in cell signaling. *Protein Sci.* **2007**, *16*, 30–42.
(87) *Maestro*, version 9.3; Schrödinger, LLC: New York, NY, 2012.
(88) *MacroModel*, version 9.9; Schrödinger, LLC: New York, NY, 2012.
(89) Hawkins, G. D.; Giesen, D. J.; Lynch, G. C.; Chambers, C. C.; Rossi, I.; Storer, J. W.; Li, J.; Thompson, J. D.; Winget, P.; Lynch, B. J.; Rinaldi, D.; Liotard, D. A.; Cramer, C. J.; Truhlar, D. G. *AMSOL*, version 7.1; University of Minnesota: Minneapolis, MN, 2003; based in part on the following: Liotard, D. A.; Healy, E. F.; Ruiz, J. M.; Dewar, M. J. S. *AMPAC*, version 2.1; Semichem, Inc.: Shawnee, KS.
(90) Chambers, C. C.; Hawkins, G. D.; Cramer, C. J.; Truhlar, D. G. Model for aqueous solvation based on class IV atomic charges and first solvation shell effects. *J. Phys. Chem.* **1996**, *100*, 16385–16398.
(91) Dewar, M. J. S.; Zoebisch, E. G.; Healy, E. F.; Stewart, J. J. P. AM1: a new general purpose quantum mechanical molecular model. *J. Am. Chem. Soc.* **1993**, *115*, 5348–5348 [Erratum to *J. Am. Chem. Soc.* **1985**, *107*, 3902–3909].
(92) Mulvey, M. A.; Schilling, J. D.; Hultgren, S. J. Establishment of a persistent *Escherichia coli* reservoir during the acute phase of a bladder infection. *Infect. Immun.* **2001**, *69*, 4572–4579.
(93) Kabsch, W. Automatic processing of rotation diffraction data from crystals of initially unknown symmetry and cell constants. *J. Appl. Crystallogr.* **1993**, *26*, 795–800.
(94) Leslie, A. G. W. The integration of macromolecular diffraction data. *Acta Crystallogr. D* **2006**, *62*, 48–57.
(95) Winn, M. D.; Ballard, C. C.; Cowtan, K. D.; Dodson, E. J.; Emsley, P.; Evans, P. R.; Keegan, R. M.; Krissinel, E. B.; Leslie, A. G. W.; McCoy, A.; McNicholas, S. J.; Murshudov, G. N.; Pannu, N. S.; Potterton, E. A.; Powell, H. R.; Read, R. J.; Vagin, A.; Wilson, K. S. Overview of the CCP4 suite and current developments. *Acta Crystallogr. D* **2011**, *67*, 235–242.
(96) McCoy, A. J. Solving structures of protein complexes by molecular replacement with Phaser. *Acta Crystallogr. D* **2007**, *63*, 32–41.
(97) Emsley, P.; Cowtan, K. Coot: model-building tools for molecular graphics. *Acta Crystallogr. D* **2004**, *60*, 2126–2132.
(98) Adams, P. D.; Grosse-Kunstleve, R. W.; Hung, L.-W.; Ioerger, T. R.; McCoy, A. J.; Moriarty, N. W.; Read, R. J.; Sacchettini, J. C.; Sauter, N. K.; Terwilliger, T. C. PHENIX: building new software for automated crystallographic structure determination. *Acta Crystallogr., Sect. D: Biol. Crystallogr.* **2002**, *58*, 1948–1954.
(99) van Aalten, D. M. F.; Bywater, R.; Findlay, J. B. C.; Hendlich, M.; Hooft, R. W. W.; Vriend, G. PRODRG, a program for generating molecular topologies and unique molecular descriptors from coordinates of small molecules. *J. Comput.-Aided Mol. Des.* **1996**, *10*, 255–262.
(100) Chen, V. B.; Arendall, W. B.; Headd, J. J.; Keedy, D. A.; Immormino, R. M.; Kapral, G. J.; Murray, L. W.; Richardson, J. S.; Richardson, D. C. MolProbity: all-atom structure validation for macromolecular crystallography. *Acta Crystallogr. D* **2010**, *66*, 12–21.
(101) Bezençon, J.; Wittwer, M. B.; Cutting, B.; Smiesko, M.; Wagner, B.; Kansy, M.; Ernst, B. pK_a determination by ^{1}H NMR spectroscopy—an old methodology revisited. *J. Pharm. Biomed. Anal.* **2014**, *93*, 147–155.
(102) (a) VCCLAB, Virtual Computational Chemistry Laboratory, 2005. http://www.vcclab.org (accessed August 14, 2012). (b) Tetko, I. V.; Gasteiger, J.; Todeschini, R.; Mauri, A.; Livingstone, D.; Ertl, P.; Palyulin, V. A.; Radchenko, E. V.; Zefirov, N. S.; Makarenko, A. S.; Tanchuk, V. Y.; Prokopenko, V. V. Virtual computational chemistry laboratory—design and description. *J. Comput.-Aided Mol. Des.* **2005**, *19*, 453–463.
(103) Diehl, K.-H.; Hull, R. A. Good practice guide to the administration of substances and removal of blood, including routes and volumes. *J. Appl. Toxicol.* **2001**, *21*, 15–23.

DOI: 10.1021/jm501524q
J. Med. Chem. 2015, 58, 2221–2239

5.2. PAPER II

"FimH Antagonists – solubility vs. permeability"

Lijuan Pang,[#] Jacqueline Bezençon[#], Simon Kleeb[#], Said Rabbani, Anja Sigl, Martin Smiesko, Christoph P. Sager, Oliver Schwardt, and Beat Ernst[*]

# equally contributed

Journal of Carbohydrate Chemistry, October 2016

FimH antagonists – solubility *vs.* permeability

Lijuan Pang,† Jacqueline Bezençon,† Simon Kleeb,† Said Rabbani, Anja Sigl, Martin Smiesko, Christoph P. Sager, Deniz Eris, Oliver Schwardt and Beat Ernst*

DOI: 10.1039/9781782626657-00248

Urinary tract infections (UTIs) caused by uropathogenic *Escherichia coli* (UPEC) are among the most prevalent infections worldwide. Since frequent antibiotic treatment favors the emergence of antibiotic resistance, efficient non-antibiotic strategies are urgently needed. The first step of the pathogenesis of UTI is the bacterial adherence to urothelial host cells, a process mediated by the mannose-binding adhesin FimH located at the tip of bacterial pili. In a preliminary study, biphenyl α-D-mannopyranosides with an electron-withdrawing carboxylate on the aglycone were identified as potent FimH antagonists. Although passive permeability could be established by masking the carboxylate as an ester, insufficient solubility and fast hydrolysis did not allow to maintain the therapeutic concentration in the bladder for the requested period of time. By modifying the substitution pattern, molecular planarity and symmetry of the biphenyl aglycone could be disrupted leading to improved solubility. In addition, when heteroatoms were introduced to the aglycone, antagonists with further improved solubility, metabolic stability as well as passive permeability were obtained. The best representative, the pyrrolylphenyl mannoside **42f** exhibited therapeutic urine concentration for up to 6 h and is therefore a promising oral candidate for UTI prevention and/or treatment.

1 Introduction

Urinary tract infections (UTIs) – also known as acute cystitis or bladder infections – are among the most prevalent infectious diseases worldwide. UTIs affect millions of people every year and account for significant morbidity and high medical costs.[1] Since symptomatic UTIs require antibiotic treatment and recurrent antibiotic exposure leads to the ubiquitous problem of antimicrobial resistance, efficient non-antibiotic prevention and treatment strategies are urgently needed.[2] More than 70% of UTIs are caused by uropathogenic *Escherichia coli* (UPEC).[1a,3] In the first step of the infection, UPEC adhere to urothelial cells, which prevents them from being cleared by micturition but also triggers the invasion into host cells.[4] This initial contact is mediated by the bacterial adhesin FimH located at the tip of type 1 pili.[5] FimH consists of an N-terminal lectin domain and a C-terminal pilin domain. The carbohydrate recognition domain (CRD) of the lectin domain specifically recognizes oligmannosides being part of the glycoprotein uroplakin Ia located on the urinary bladder mucosa, whereas the pilin domain regulates the switch between the various affinity states of the CRD.[6] Blocking the FimH-CRD with carbohydrates or mimetics thereof prevents

Institute of Molecular Pharmacy, Pharmacenter, University of Basel, Klingelbergstr. 50, 4056 Basel, Switzerland. E-mail: beat.ernst@unibas.ch
†These authors equally contributed to this work.

the bacterial adhesion as well as the subsequent infection. This approach is therefore regarded as a potential therapy for prevention and/or treatment of UTIs.[7]

Over the last three decades, mannosides and oligomannosides with various aglycones, such as *n*-alkyl,[8d] phenyl,[8e] dioxocyclobutenylaminophenyl,[8f] umbelliferyl,[8e] biphenyl,[8g–k] indol(in)ylphenyl,[8l] triazolyl[8m] or thiazolylamino[8n] have been tested as potential antagonists for preventing type 1 pili-mediated bacterial adhesion.[8] In addition, different multivalent presentations of mannose derivatives have been explored.[9]

In general, when a daily therapy is required, oral administration is the standard care. To achieve oral availability as well as a therapeutic concentration in the bladder over an extended period of time, successful oral absorption (*i.e.* solubility and permeability), metabolic stability, and slow and prolonged renal excretion (*i.e.* renal reabsorption) are required. As previously described,[8h] the carboxylic acid moiety in biphenyl α-D-mannoside **1a** – its electron-withdrawing potential is essential for an enhanced π–π stacking interaction – impairs the membrane permeability and, as a consequence, the potential for oral absorption. Therefore, the polar carboxylate was masked as ester (→**1b**[8h]), exhibiting comparable electron withdrawing properties but improving passive permeability and renal reabsorption by increased lipophilicity. However, since the ester **1b** was characterized by low aqueous solubility (12 $\mu g\,mL^{-1}$) and fast metabolic cleavage ($t_{1/2} = 2.1$ min), the absorptive flux through the intestinal mucosa was limited and the renal excretion accelerated.[10] As a consequence, the therapeutic concentration in the bladder could not be maintained for a sufficient period of time.[8h] Therefore, emanating from antagonist **1b**, these pharmacokinetic drawbacks were addressed by structural modifications of the aglycone (Fig. 1).

2 Results and discussion

To improve relevant pharmacokinetic parameters (*i.e.* oral absorption, metabolism and renal excretion of FimH antagonist **1b**), we focused on three approaches. First, the molecular planarity and symmetry of the biphenyl aglycone was disrupted by modifying the substitution pattern[11] (Fig. 1a). Second, the hydrophobicity was improved by heterocyclic biaryl aglycones (Fig. 1b). Finally, oral availability was improved by replacing the carboxylic acid by the bioisosteric cyano group (Fig. 1c).[8o,11,12]

2.1 Synthesis of FimH antagonists

Biphenyl mannosides (Schemes 1 and 2). Compounds **1a,b**, and **2a,b** (Table 1) were synthesized as previously described.[8h] For the synthesis of **6a** and **6b**, iodide **3**[8l] was reacted with boronic acid **4** in a palladium-catalyzed Suzuki–Miyaura coupling to yield mannoside **5**. Subsequent deprotection afforded the test compounds **6a** and **6b** (Scheme 1).

Lewis acid-promoted glycosylation of phenol **8** with fluoride **7**[13] followed by a Suzuki–Miyaura coupling of bromide **9** with boronic acid **4** gave **10** (Scheme 2). Finally, deprotection yielded biphenyls **11a** and **11b**.

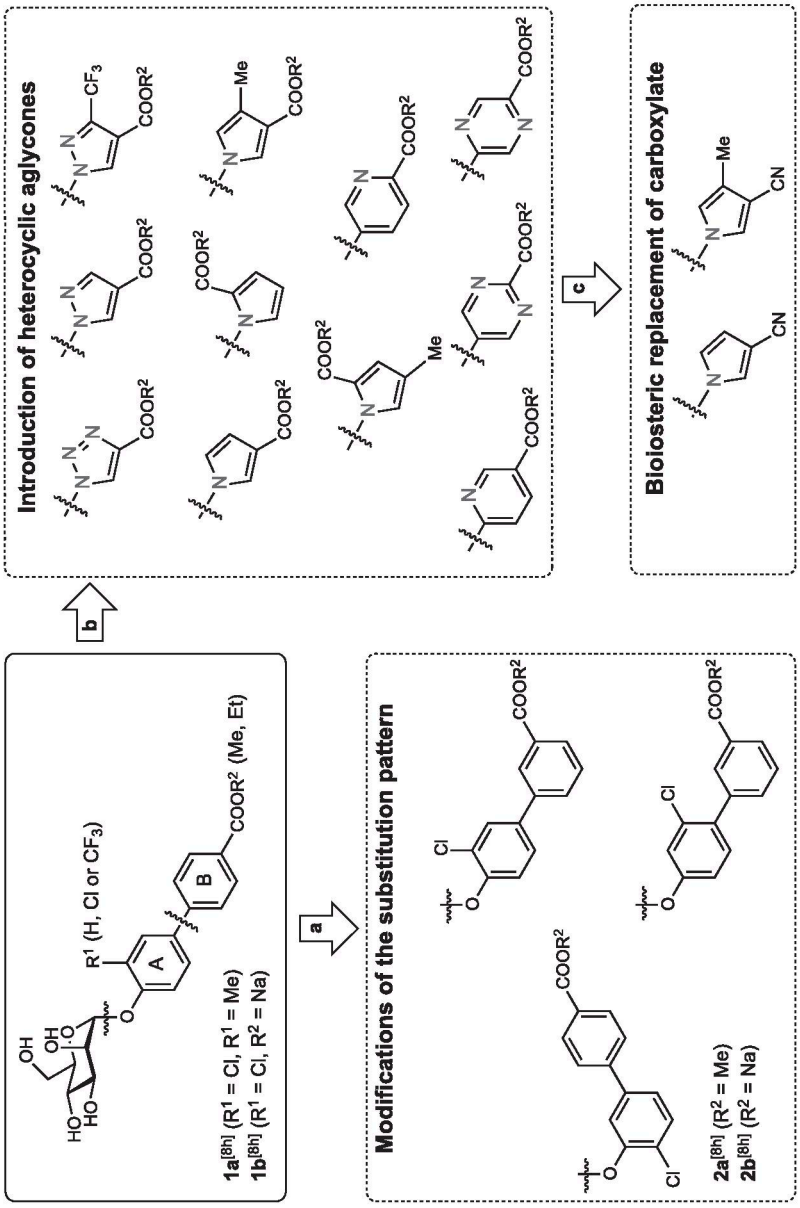

Fig. 1 Variations of the aglycone of FimH antagonists **1a** and **1b** by (a) modifying the substitution pattern, (b) introducing heteroaryl aglycones and (c) replacing the carboxylate moiety with a bioisosteric cyano group. Ring A is adjacent to the anomeric center, whereas ring B is in the terminal position.

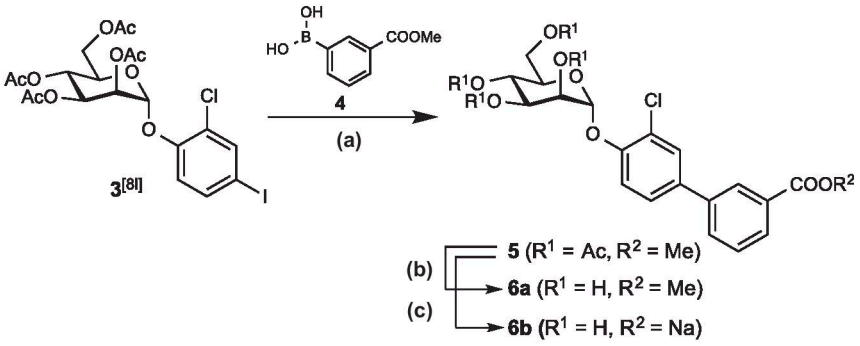

Scheme 1 (a) $Pd(Cl_2)dppf \cdot CH_2Cl_2$, K_3PO_4, DMF, 80 °C, overnight (70%); (b) NaOMe, MeOH, rt, 4 h (quant.); (c) 0.2 N aq. NaOH, MeOH, rt, overnight (50%).

Heteroaromatic building blocks (Scheme 3). Starting with the commercial aminophenols **12a,b**, the azidophenols **13a,b** were obtained *via* a diazotransfer reaction using freshly prepared triflyl azide in pyridine and copper(II) sulfate as catalyst.[14] Because of low stability, **13a,b** were used without purification in a subsequent copper(I)-catalyzed Huisgen cycloaddition[15] with ethyl propiolate, yielding the triazolylphenols **14a,b** (Scheme 3A). By using an Ullmann-type copper-diamine-catalyzed *N*-arylation,[16] 1*H*-pyrazole-4-carboxylate was coupled with 4-iodoanisole (**15**) in *N*-methyl-2-pyrrolidone (NMP) to furnish **16a**. Because of the low reactivity of the ethyl 3-trifluoromethyl-1*H*-pyrazole-4-carboxylate, the coupling reaction was carried out under solvent-free conditions to yield **16b** in quantitative yield. Demethylation of **16** with $AlCl_3$ gave the pyrazolylphenol derivatives **17**. Due to the instability of **17b** under $AlCl_3$/nBu$_4$NI conditions, a solution of $AlCl_3$ in 1-dodecanethiol was used to accelerate the reaction and to suppress byproduct formation (Scheme 3B).[17] The pyrimidinyl derivative **20** was prepared *via* a *n*BuLi-mediated carboxylation with CO_2 followed by esterification (Scheme 3C).[18] To synthesize the cyano-substituted pyrroles **23a,b**, benzotriazol-1-ylmethyl isocyanide (**21**) was treated with the electron-deficient alkenes **22a,b** under basic heterocyclization conditions (Scheme 3D).[19]

Triazolylphenyl and pyrazolylphenyl mannosides (Scheme 4). Mannosylation of the phenols **14a,b** and **17a,b** (see Scheme 3A & B) with mannosyl fluoride **7**[13] and $BF_3 \cdot Et_2O$ as promoter, yielded exclusively the α-mannosides **24a,b** and **27a,b**. Deacetylation (→**25a–c** and **28a,b**) followed by ester hydrolysis gave the test compounds **26a,b** and **29a,b**.

Pyridinylphenyl, pyrazinylphenyl, and pyrimidinylphenyl mannosides (Scheme 5). Mannosyl fluoride **7**[13] was treated with 4-iodophenol or 4-bromo-2-trifluoromethylphenol in the presence of $BF_3 \cdot Et_2O$. The resulting iodide **30**[8k] and bromide **36**[8k] were transformed into the boronic acid pinacol esters **31**[8k] and **37** under Miyaura-borylation conditions. In a palladium-catalyzed Miyaura–Suzuki coupling[20] of the heteroaryl halides **20** (see Scheme 3C) and **32a–c** (commercially available) with boronic acid ester **31**, heteroarylphenyl mannosides **33a–d** were obtained in good to excellent yields. Similarly, mannoside **38** was prepared by coupling of ester **37** and pyridinylchoride **32a**. Deacetylation under Zemplén

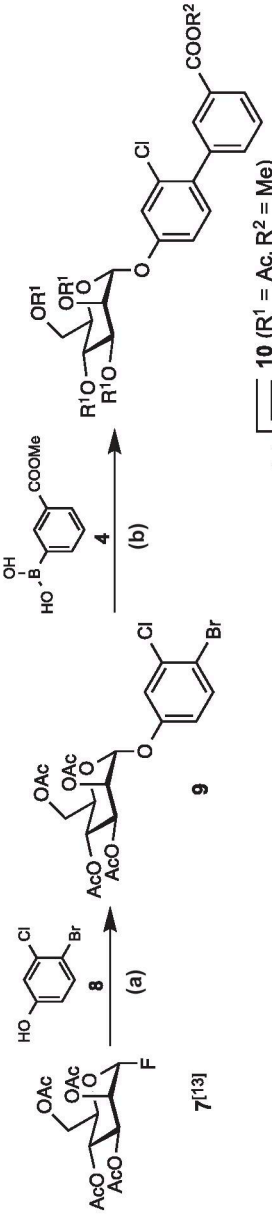

Scheme 2 (a) $BF_3 \cdot Et_2O$, DCM, mol. sieves 4 Å, 0 °C to rt, overnight (90%); (b) $Pd(Cl_2)dppf \cdot CH_2Cl_2$, K_3PO_4, DMF, 80 °C, overnight (76%); (c) NaOMe, MeOH, rt, 4 h (quant.); (d) 0.2 N aq. NaOH, MeOH, rt, overnight (61%).

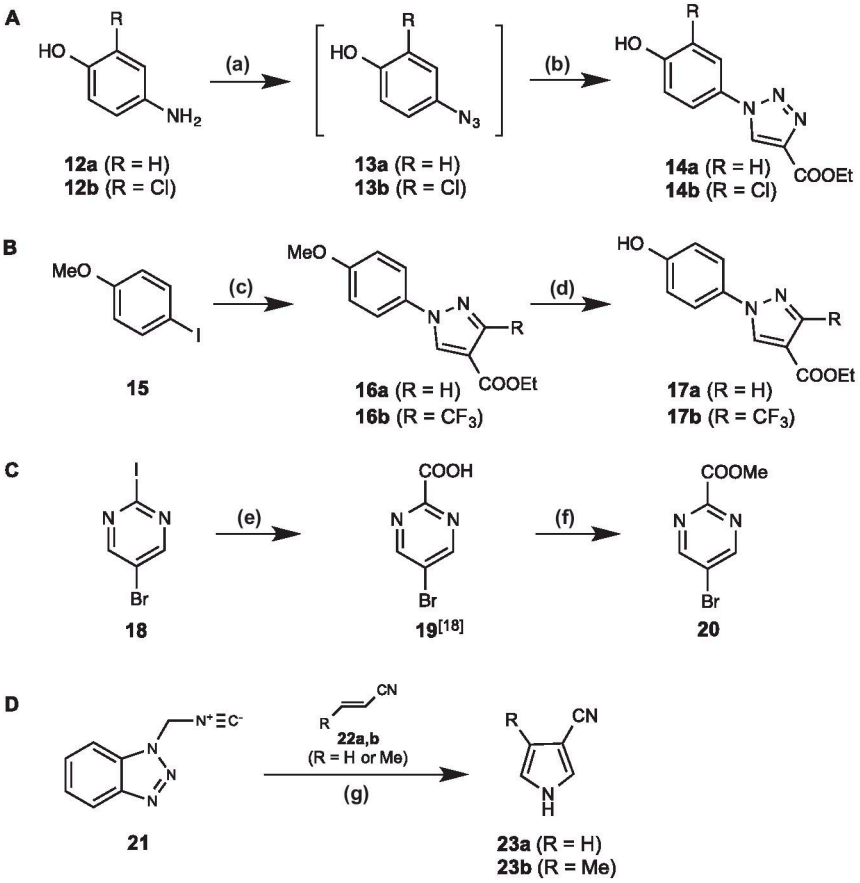

Scheme 3 (a) TfN_3, $CuSO_4$, triethylamine, pyridine, 0 °C to rt, 2 h; (b) ethyl propiolate, $CuSO_4 \cdot 5H_2O$, sodium ascorbate, *t*BuOH/H_2O (1 : 1), rt, 30 min (yield for two steps: 77% for **14a**, 48% for **14b**); (c) ethyl 1*H*-pyrazole-4-carboxylate or ethyl 3-trifluoromethyl-1*H*-pyrazole-4-carboxylate, CuI, *trans*-*N*,*N*′-dimethyl-1,2-cyclohexanediamine, K_2CO_3, NMP as solvent for **16a** and solvent free for **16b**, 110 °C, 24 h (80% for **16a**, quant. for **16b**); (d) $AlCl_3$, cat. nBu_4NI, DCE (for **17a**), or $AlCl_3$ in 1-dodecanethiol (for **17b**), 0 °C to rt (60% for **17a**, 26% for **17b**); (e) i. *n*BuLi, hexane, toluene, –78 °C, 1 h; ii. CO_2 (g), –78 °C to rt, 7 h; (f) conc. H_2SO_4 (0.8 equiv.), MeOH, reflux, overnight (37% for two steps); (g) nitrile **22a,b**, *t*BuOK, THF, 0 °C to reflux, 2 h (60% for **23a**, 54% for **23b**).

conditions (→**34a–d**, **39**) followed by saponification of the methyl ester yielded the sodium salts **35a–d** and **40**.

Pyrrolylphenyl mannosides (Schemes 6 and 7). In a copper catalyzed *N*-arylation, pyrroles **23a,b** (see Scheme 3D) and **23c–f** (commercial) were coupled with mannoside **3**[8l] (*ortho*-Cl) to yield the pyrrolylphenyl mannosides **41a–f** (Scheme 6).[17] Under similar conditions, mannosides **30** (without *ortho*-substituent) and **36** (*ortho*-CF_3) were coupled with pyrrole **23f** to yield **47** and **48** (Scheme 7). Because of partial deacetylation of the sugar moiety during *N*-arylation, the crude products were reacetylated to facilitate purification. Deacetylation of the mannose moiety (→**42a–f**, **49** and **50**) followed by saponification of the alkyl esters gave the test compounds **43–46**, **51** and **52**.

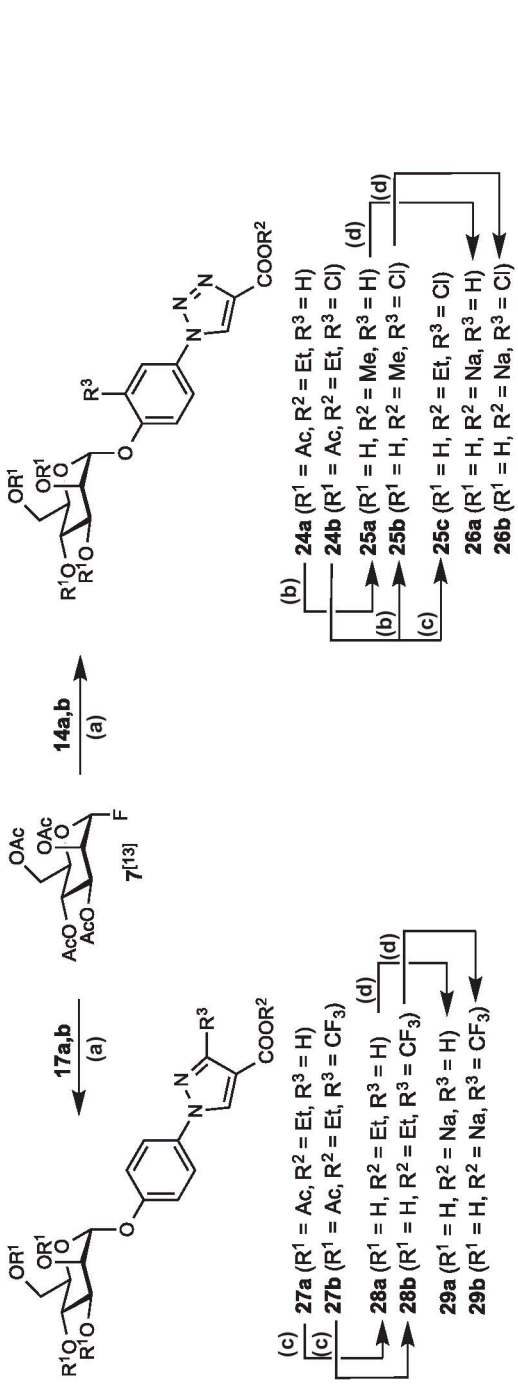

Scheme 4 (a) $BF_3 \cdot Et_2O$, DCM, mol. sieves 4 Å, 0 °C to rt, overnight (79% for **24a**, 76% for **24b**, 98% for **27a**, 64% for **27b**); (b) NaOMe, MeOH, rt, 4 h (74% for **25a**, 80% for **25b**); (c) NaOEt, EtOH, rt, overnight (74% for **25c**, 95% for **28a**, 82% for **28b**); (d) 0.2 N aq. NaOH, MeOH, rt, overnight (30% for **26a**, 90% for **26b**, 70% for **29a**, 79% for **29b**).

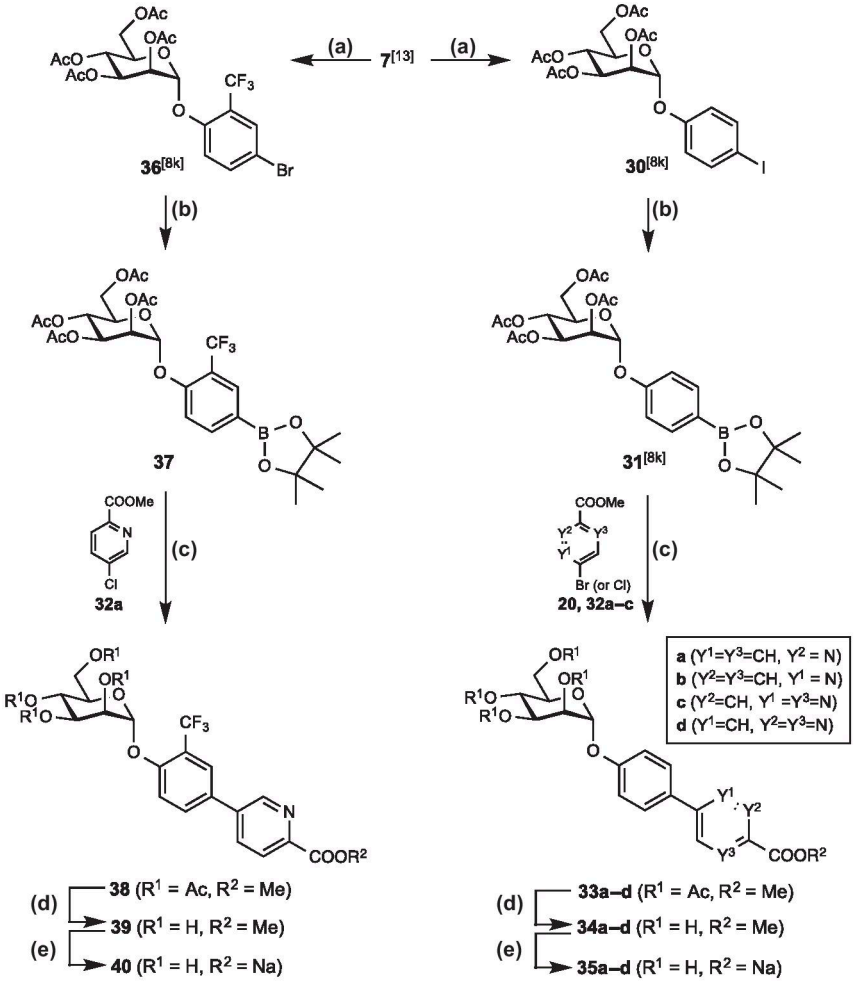

Scheme 5 (a) 4-Iodophenol or 4-bromo-2-trifluoromethylphenol, $BF_3 \cdot Et_2O$, DCM, mol. sieves 4 Å, 0 °C to rt, overnight (70%[8k] for **30**, 80%[8k] for **36**); (b) bis(pinacolato)diborone, $Pd(Cl_2)dppf \cdot CH_2Cl_2$, KOAc, DMF, 85 °C, overnight (80% for **31**, 83% for **37**); (c) $Pd(Cl_2)dppf \cdot CH_2Cl_2$, K_3PO_4, DMF, 85 °C, overnight (60% for **33a**, 80% for **33b**, 68% for **33c**, 40% for **33d**, 57% for **38**); (d) NaOMe, MeOH, rt, 4 h (36% for **34a**, 24% for **34b**, 36% for **34c**, 89% for **34d**, 60% for **39**); (e) 0.2 N aq. NaOH, MeOH, rt, overnight (32% for **35a**, 48% for **35b**, 44% for **35c**, 60% for **35d**, 90% for **40**).

2.2 Physicochemical properties and *in vitro* pharmacokinetics of FimH antagonists

For the assessment of the potential for intestinal absorption, physicochemical properties, *i.e.* lipophilicity ($\log D_{7.4}$), aqueous solubility, and permeability through an artificial membrane (PAMPA, $\log P_e$) as well as a Caco-2 cell monolayer (P_{app}) were determined (Table 1).[21–24] The following permeability thresholds for the effective permeability $\log P_e$ (low permeability is expected for $\log P_e < -6.3$ cm s^{-1}; moderate ≤ -5.7 cm s^{-1}; high > -5.7 cm s^{-1})[25] and for apparent permeability P_{app} (low permeability is expected for $P_{app} < 2 \times 10^{-6}$ cm s^{-1}; moderate $\leq 20 \times 10^{-6}$ cm s^{-1};

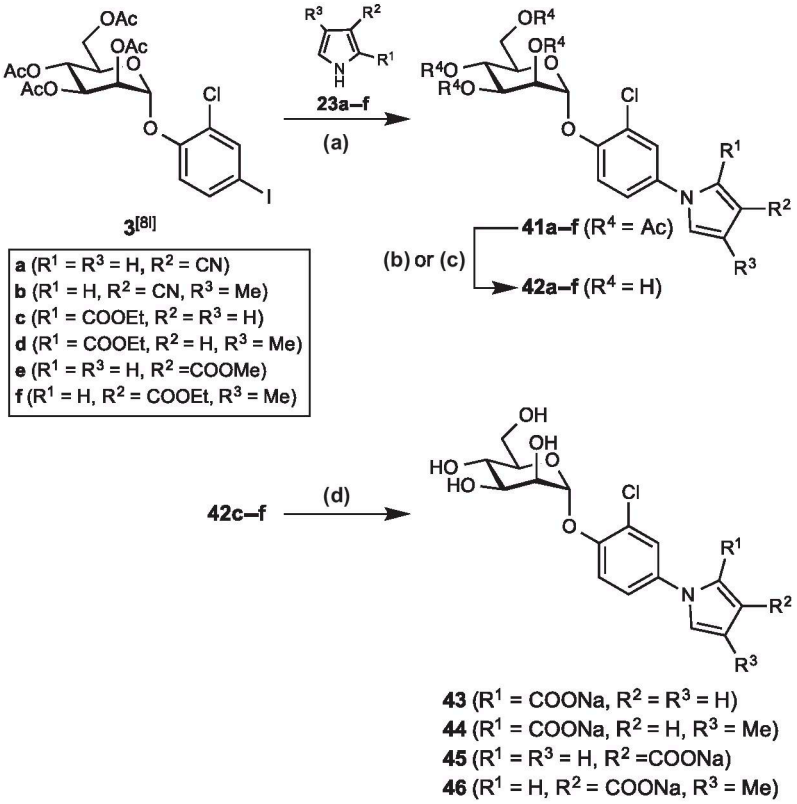

Scheme 6 (a) i. CuI, (±)-*trans*-1,2-diaminocyclohexane, K_3PO_4, 1,4-dioxane, 110 °C, overnight; ii. Ac_2O, DMAP, pyridine, rt, overnight (44% for **41a**, 92% for **41b**, 33% for **41c**, 64% for **41d**, 99% for **41e**, 77% for **41f**); (b) NaOMe, MeOH, rt, 4 h (65% for **42a**, 38% for **42b**, 83% for **42e**); (c) NaOEt, EtOH, rt, overnight (91% for **42c**, 61% for **42d**, 93% for **42f**); (d) NaOH, MeOH/H_2O (1 : 2), rt, 12–48 h (58% for **43**, 40% for **44**, 20% for **45**, 57% for **46**).

high $> 20 \times 10^{-6}$ cm s^{-1})[26] were used to classify the antagonists. As expected, all metabolites, *i.e.* the free carboxylates showed no or low permeability ($\log P_e < -6.3$ cm s^{-1}) and are not further discussed in this section. Furthermore, the esters were incubated with rat liver microsomes (RLM) for estimating their susceptibility to carboxylesterase (CES)-mediated hydrolysis.[27] Table 1 indicates the metabolic half lives ($t_{1/2}$) as determinants of the rate of bioconversion to the respective acid.

Solubility of biphenyl mannosides. As observed in our previous study,[8h] the biphenyl derivatives **1a** and **2a** (Table 1, entries 2 & 4) showed low aqueous solubility (≤24 μg mL^{-1}, Table 1), probably due to the symmetrical *para*-substitution leading to stacking effects. In order to disrupt this symmetry, the carboxylic acid moiety in **1a** was moved from the *para*- to the *meta-position* (→**6a**, entry 6). Since the dihedral angle remained unaffected (Fig. 2; global minima values calculated with MacroModel, version 9.9[30]) only moderately improved aqueous solubility (41 μg mL^{-1}, Table 1) resulted. However, when the chloro substituent on ring A was shifted from the *ortho*- to the *meta-position* (→**11a**, entry 8), the dihedral angle was enlarged from 39.6° in **6a** to 60.3° in **11a** (Fig. 2). The resulting

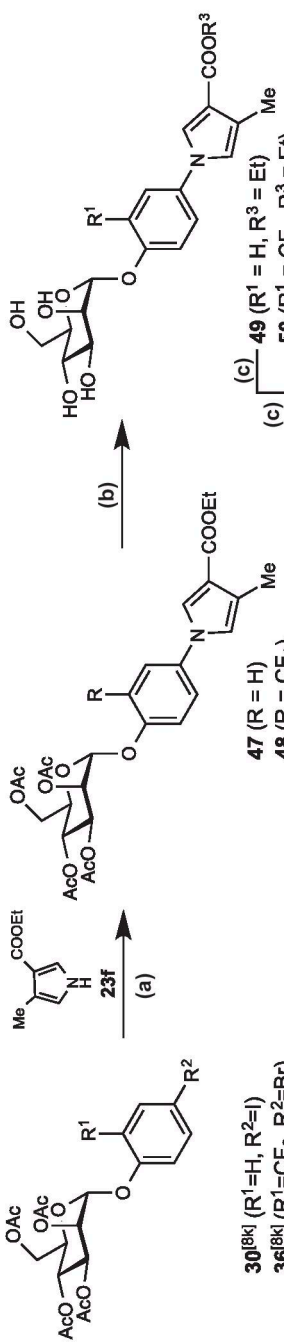

Scheme 7 (a) i. CuI, (±)-*trans*-1,2-diaminocyclohexane, K_3PO_4, 1,4-dioxane, 110 °C, overnight; ii. Ac_2O, DMAP, pyridine, rt, overnight (94% for **47**, 49% for **48**); (b) NaOEt, EtOH, rt, overnight (46% for **49**, 85% for **50**); (c) NaOH, MeOH/H_2O (1 : 2), rt, 48 h (99% for **51**, 35% for **52**).

Table 1 Physicochemical ($\log D_{7.4}$, solubility, PAMPA, and Caco-2), *in vitro* pharmacokinetic (microsomal stability) and pharmacodynamics (IC_{50}) parameters of FimH antagonists; ring A is adjacent to the anomeric center, whereas ring B is in the terminal position.

Entry	Compound		Binding Assay[a]		$\log D_{7.4}$[b]	Solubility[c] [μg mL^{-1}]	PAMPA $\log P_e$[d] [cm s^{-1}]	Caco-2 P_{app}[e] [10^{-6} cm s^{-1}]		Microsomal stability $t_{1/2}$[f] [min]
			IC_{50} [nM]	rIC_{50}				a→b	b→a	
1	**53**[8d]		54.9	1	1.7	>3000[g]	−4.9	7.0 ± 0.6	9.4 ± 0.2	n.d.[h]
2	**1a**[8h] (R^2 = Me)		4.8	0.09	2.3	11.9[g]	−4.6	5.3 ± 0.6	17.5 ± 1.3	2.1
3	**1b**[8h] (R^2 = Na)		6.7	0.12	−0.8	>3000[g]	−10.0 ± 0.0	0.23 ± 0.03	0.38 ± 0.04	n.d.[h]
4	**2a**[8h] (R^2 = Me)		11.8	0.21	1.7 ± 0.1	24.3[g]	−4.7	6.1 ± 1.2	21.1 ± 1.2	22
5	**2b**[8h] (R^2 = Na)		29	0.53	< −1.5	>3000[g]	−10.0 ± 0.0	1.2 ± 0.4	1.2 ± 0.1	n.d.[h]
6	**6a** (R^2 = Me)		16.8	0.31	2.7 ± 0.1	41 ± 3	−4.6 ± 0.2	6.7 ± 0.4	20.7 ± 2.5	72
7	**6b** (R^2 = Na)		12	0.22	n.d.[h]	n.d.[h]	n.d.[h]	n.d.[h]	n.d.[h]	n.d.[h]
8	**11a** (R^2 = Me)		23.3	0.42	2.7 ± 0.1	134 ± 6	−4.5 ± 0.1	4.5 ± 0.3	10.8 ± 0.7	13
9	**11b** (R^2 = Na)		53	0.97	n.d.[h]	n.d.[h]	n.d.[h]	n.d.[h]	n.d.[h]	n.d.[h]

10	**25a** (R^2 = Me)	7.6	0.14	−0.6 ± 0.0	>180	−9.4 ± 0.3	n.d.[h]	n.d.[h]	38
11	**26a** (R^2 = Na)	16	0.29	n.d.[h]	>180	−10.0 ± 0.0	n.d.[h]	n.d.[h]	n.d.[h]
12	**25b** (R^2 = Me)	10.5	0.19	0.0 ± 0.0	>150	−9.1 ± 1.8	n.d.[h]	n.d.[h]	32
13	**25c** (R^2 = Et)	n.d.[h]	—	0.7 ± 0.0	>150	−10	n.d.[h]	n.d.[h]	42
14	**26b** (R^2 = Na)	21	0.38	< −1.5	>150	−6.7 ± 0.1	n.d.[h]	n.d.[h]	n.d.[h]
15	**28a** (R^2 = Et)	32.4	0.59	0.9 ± 0.0	>180	−6.6 ± 0.1	n.d.[h]	n.d.[h]	>120
16	**29a** (R^2 = Na)	111	2.02	n.d.[h]	>180	−10.0 ± 0.0	n.d.[h]	n.d.[h]	n.d.[h]
17	**28b** (R^2 = Et)	31.9	0.58	2.1 ± 0.0	>180	−5.7 ± 0.1	1.3 ± 0.1	12.4 ± 2.4	113
18	**29b** (R^2 = Na)	112	2.04	< −1.5	>180	−10.0 ± 0.0	n.d.[h]	n.d.[h]	n.d.[h]
19	**34a** (R^2 = Me)	n.d.[h]	—	0.2 ± 0.0	>130	−7.5 ± 0.2	0.22 ± 0.05	2.3 ± 0.1	10
20	**35a** (R^2 = Na)	16	0.29	n.d.[h]	>180	−8.6 ± 1.6	n.d.[h]	n.d.[h]	n.d.[h]

Table 1 (*Continued*)

Entry	Compound	R^1	Binding Assay[a] IC_{50} [nM]	Binding Assay[a] rIC_{50}	$\log D_{7.4}$[b]	Solubility[c] [μg mL^{-1}]	PAMPA $\log P_e$[d] [cm s^{-1}]	Caco-2 P_{app}[e] [10^{-6} cm s^{-1}] a→b	Caco-2 P_{app}[e] [10^{-6} cm s^{-1}] b→a	Microsomal stability $t_{1/2}$[f] [min]
21	**34b** (R^2 = Me)		28.6	0.52	1.0 ± 0.0	59 ± 6	−6.3 ± 0.0	0.64 ± 0.06	8.3 ± 0.4	11
22	**35b** (R^2 = Na)		46	0.84	< −1.5	>180	−8.5 ± 1.8	n.d.[h]	n.d.[h]	n.d.[h]
23	**34c** (R^2 = Me)		33.1	0.60	0.1 ± 0.1	>150	−7.6 ± 0.0	0.24 ± 0.01	1.8 ± 0.2	11
24	**35c** (R^2 = Na)		39	0.71	< −1.5	>180	−8.6 ± 1.6	n.d.[h]	n.d.[h]	n.d.[h]
25	**34d** (R^2 = Me)		10.2	0.19	< −1.0	95 ± 6	−8.5 ± 0.1	0.16 ± 0.03	0.22 ± 0.05	24
26	**35d** (R^2 = Na)		35	0.64	n.d.[h]	n.d.[h]	−7.6 ± 1.6	n.d.[h]	n.d.[h]	n.d.[h]
27	**39** (R^2 = Me)		9.3	0.17	1.3 ± 0.1	>180	−8.6 ± 1.7	0.33 ± 0.04	7.2 ± 0.7	8.2
28	**40** (R^2 = Na)		20	0.36	< −1.5	>180	−9.3 ± 1.4	n.d.[h]	n.d.[h]	n.d.[h]
29	**42a**		29	0.53	1.5 ± 0.1	>180	−8.8 ± 2.0	n.d.[h]	n.d.[h]	n.d.[h]

30	**42b**		25	0.46	2.0 ± 0.1	69 ± 20	-6.3 ± 0.1	n.d.[h]	n.d.[h]
31	**42c** ($R^2 = Et$)		60.7	1.11	2.0 ± 0.0	>180	-5.2 ± 0.0	n.d.[h]	>120
32	**43** ($R^2 = Na$)		75	1.37	< -1.5	>180	-10.0 ± 0.0	n.d.[h]	n.d.[h]
33	**42d** ($R^2 = Et$)		42.3	0.77	2.7 ± 0.0	34 ± 4	-4.8 ± 0.1	5.0 ± 0.2	35.6 ± 1.0	84
34	**44** ($R^2 = Na$)		23	0.42	0.7 ± 0.1	>180	-9.2 ± 1.7	n.d.[h]	n.d.[h]	n.d.[h]
35	**42e** ($R^2 = Me$)		18.5	0.34	2.1 ± 0.2	>180	-6.0 ± 0.1	n.d.[h]	n.d.[h]	>120
36	**45** ($R^2 = Na$)		25	0.46	< -1.5	>180	-10.0 ± 0.0	n.d.[h]	n.d.[h]	n.d.[h]
37	**42f** ($R^2 = Et$)		15.2	0.28	2.8 ± 0.1	>180	-4.8 ± 0.1	6.4 ± 0.7	30.0 ± 2.9	>120
38	**46** ($R^2 = Na$)		25	0.46	-0.5 ± 0.1	>180	-10.0 ± 0.0	n.d.[h]	n.d.[h]	n.d.[h]

Table 1 (*Continued*)

Entry	Compound	Binding Assay[a]		$\log D_{7.4}$[b]	Solubility[c] [μg mL^{-1}]	PAMPA $\log P_e$[d] [cm s^{-1}]	Caco-2 P_{app}[e] [10^{-6} cm s^{-1}]		Microsomal stability $t_{1/2}$[f] [min]
		IC_{50} [nM]	rIC_{50}				a→b	b→a	
39	**49** (R^2 = Et)	64.8	1.18	2.3 ± 0.0	>180	−5.1 ± 0.1	1.5 ± 0.5	17.2 ± 0.6	>120
40	**51** (R^2 = Na)	65	1.18	−1.0 ± 0.1	>180	−8.4 ± 1.8	n.d.[h]	n.d.[h]	n.d.[h]
41	**50** (R^2 = Et)	36.9	0.67	3.0 ± 0.1	135 ± 6	−5.0 ± 0.2	5.0 ± 0.3	26.1 ± 1.5	>120
42	**52** (R^2 = Na)	19	0.35	0.1 ± 0.2	>180	−8.6 ± 1.7	n.d.[h]	n.d.[h]	n.d.[h]

[a] The IC_{50} values were determined with a cell-free competitive binding assay.[28] The rIC_{50} values were calculated by dividing the IC_{50} of the compound of interest by the IC_{50} of reference compound **53**. This leads to rIC_{50} values below 1.0 for derivatives with higher affinity than reference **53** and rIC_{50} above 1.0 for compounds with lower affinity than **53**.
[b] Octanol–water distribution coefficients at pH 7.4 ($\log D_{7.4}$) were determined by a miniaturized shake flask procedure. The values are indicated as mean ± SD of sextuplicate determinations.[21]
[c] Kinetic solubility was measured in a 96-well format in triplicate at pH 7.4 using the μSOL Explorer solubility analyzer.[22]
[d] Permeation through an artificial membrane ($\log P_e$, effective permeability) was determined by PAMPA (parallel artificial membrane permeability assay) in quadruplicate at pH 7.4.[23,25]
[e] Permeation through a Caco-2 cell monolayer (P_{app}, apparent permeability) was assessed in the absorptive (a→b) and secretory (b→a) directions in triplicate.[24,29]
[f] Microsomal stability was determined in duplicate with pooled male rat liver microsomes (RLM, 0.125 mg mL^{-1}) at pH 7.4 and 37 °C.[27]
[g] Thermodynamic solubility obtained according to the procedure described in ref. 8*h*.
[h] n.d., not determined.

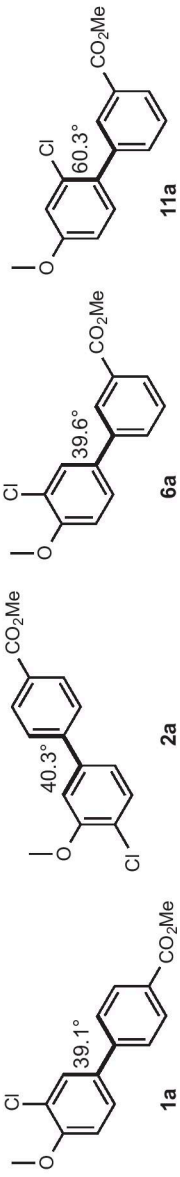

Fig. 2 Dihedral angles between the aromatic rings of biphenyl aglycones of biaryl α-D-mannopyranosides (**1a**, **2a**, **6a**, and **11a**). The global minima values were calculated with MacroModel (version 9.9).[30]

disruption of the molecular planarity enhanced aqueous solubility up to 3-fold (from 41 to 134 $\mu g\,mL^{-1}$).

Permeability of biphenyl mannosides. Due to their high lipophilicity ($\log D_{7.4} \geq 1.7$), all biphenyl mannosides showed high effective ($\log P_e > -5.7$ $cm\,s^{-1}$) and moderate apparent ($P_{app} > 2 \times 10^{-6}\,cm\,s^{-1}$) permeability.

Metabolic stability of biphenyl mannosides. Incubation with rat liver microsomes (RLM) induced a fast degradation of prodrug **1a** ($t_{1/2}$ 2.1 min, Table 1, entry 2). The esters of the biphenyl mannosides **2a** ($t_{1/2}$ 22 min, entry 4), **6a** ($t_{1/2}$ 72 min, entry 6), and **11a** ($t_{1/2}$ 13 min, entry 8) were less susceptible to the carboxylesterase (CES)-mediated metabolic turnover. The differing rates of hydrolysis may result from the change in the molecular geometry and therefore in the accessibility of the ester by the serine hydrolase CES.[31] We therefore attributed the rate differences of the CES-mediated hydrolysis primarily to the differing geometry of the aglycones, which, in case of **1a**, obviously orients the ester bond within the active site in an optimal position.

Overall, despite elevated solubility (134 $\mu g\,mL^{-1}$) and high effective permeability ($\log P_e$ −4.5 $cm\,s^{-1}$) of ester **11a**, fast metabolic ester hydrolysis ($t_{1/2} < 15$ min) reduces its therapeutic potential. Especially, the accelerated renal excretion of the polar metabolite (*i.e.* free carboxylate) impedes the maintenance of the therapeutic concentration in the bladder over an extended period of time.

Solubility of heteroaryl mannosides. In general, heterobiaryl mannosides (Table 1, entries 10–42) exhibited markedly higher aqueous solubility than the reference compound biphenyl α-D-mannoside **1a** (12 $\mu g\,mL^{-1}$). Triazole (→**25a–c**, entries 10, 12 & 13), pyrazole (→**28a**, entry 15), and pyridine derivatives (→**34a–d**, entries 19, 21, 23 & 25) exhibit higher solubility, due to increased polarity ($\log D_{7.4} < 1$). For the pyrazolylphenyl (→**28b**, entry 17), the pyridinylphenyl (→**39**, entry 27), and the pyrrolylphenyl mannosides (entries 29–42) high solubility was determined despite high lipophilicity ($\log D_{7.4} > 1$). As a trade-off, **42d** (entry 33) became the least soluble representative among all assessed heteroaryl mannosides (34 $\mu g\,mL^{-1}$).

Permeability of heteroaryl mannosides. As expected, the increase in polarity and solubility (*e.g.* →**25a**, $\log D_{7.4}$ −0.6, entry 10) leads to a reduced permeability ($\log P_e$ −9.4 $cm\,s^{-1}$), *i.e.* poor oral absorption. Figure 3 illustrates the correlation between lipophilicity ($\log D_{7.4}$) and the effective permeability ($\log P_e$) of the heteroaryl mannoside esters and bioisosteres (entries 10–42). In general, heteroaryl mannosides with lipophilicity $\log D_{7.4} > 1$ have moderate to high effective permeability.

To enhance lipophilicity two strategies were explored: First, an *ortho*-chloro substituent was introduced to ring A of the biaryl aglycone of **25a** (→**25b**, entry 12) and, second, the methyl ester was replaced by an ethyl ester (→**25c**, entry 13). However, both strategies did not or only marginally influence the $\log P_e$ values and therewith the oral absorption potential. For the pyrazolylphenyl derivative **28a** (entry 15), although slightly more lipophilic than the triazolylphenyl **25c** (entry 13), low effective permeability ($\log P_e$ − 6.6 $cm\,s^{-1}$) was observed. By introducing a

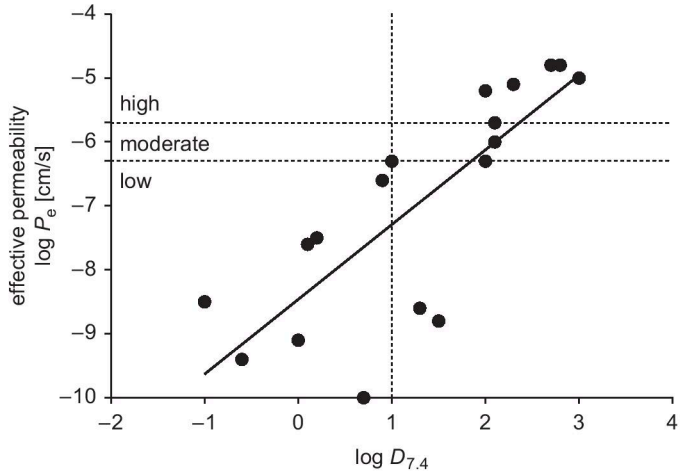

Fig. 3 Plot of $\log D_{7.4}$ *versus* effective permeability $\log P_e$ (cm s^{-1}; pH 7.4) for heteroaryl mannoside esters (entries 10–28, 31–42) and bioisosteres (entries 29 & 30). Data represent the mean only (Goodness of fit, R square = 0.64). Dashed lines on the *y*-axis indicate the thresholds between low, moderate, and high effective permeability (low < -6.3 cm s^{-1}, moderate $\log P_e \leq -5.7$ cm s^{-1} < high).[25] Dashed line on the *x*-axis represent the thresholds for lipophilicity ($\log D_{7.4} > 1$), where moderate effective permeability is reached.

trifluoromethyl substituent on the pyrazole moiety (→ **28b**, entry 17), both lipophilicity (permeability) and solubility were improved, presumably sufficient for a successful intestinal uptake. Whereas introducing an *ortho*-trifluoromethyl substituent to ring A of the biaryl aglycone (→ **39**, entry 27) exhibited despite increased lipophilicity only low effective permeability ($\log P_e$ −8.6 cm s^{-1}). By contrast, the pyrrolylphenyl mannosides **42a–f**, **49** and **50** (Table 1) with $\log D$ values of 1.5 to 3 and the $\log P_e$ values of −6.3 to −4.8 cm s^{-1} suggest modest to high permeability. Starting from antagonist **42c** (entry 31), the introduction of a 4-methyl substituent (→ **42d**, entry 33) increased permeability, however, limited solubility to 34 μg mL^{-1}. In the case of the pyrrolylphenyl derivative **42e** (entry 35), both solubility and permeability could be successively enhanced by introducing a methyl substituent in the 4-position of the pyrrole moiety (→ **49**, entry 39) and by modifying the *ortho*-substituent on ring A of the biaryl aglycone (→ **50**, entry 41 & **42f**, entry 37). Especially, for the antagonists **42f** and **50**, the effective permeability (PAMPA, $\log P_e$ −4.8 cm s^{-1} and −5.0 cm s^{-1}, respectively) suggests a high oral absorption potential. Moreover, the absorptive flux (apical → basal) through the Caco-2 cell monolayer was moderate ($\log P_{app} > 2 \times 10^{-6}$ cm s^{-1}). Although the ratio $P_{app,b\rightarrow a}/P_{app,a\rightarrow b} > 2$ implies efflux–carrier activity,[29] we expected high systemic *in vivo* availability of **42f** and **50**, notably because efflux transporters at human intestines are considered to be easily saturable when compounds are administered at elevated doses (*e.g.* > 100 mg).[32] As expected, the bioisosteric replacement of the carboxylic moiety by a cyano group (→ **42a,b**, entries 29 & 30) increased lipophilicity, but the PAMPA data still indicate

low permeability for both derivatives (log P_e −8.8 cm s^{-1} and −6.3 cm s^{-1}, respectively).

Metabolic stability of heteroaryl mannosides. All five-membered heteroaryl derivatives with ester functions (triazoles → entries 10–14, pyrazoles → entries 15–18, and pyrroles → entries 29–42, Table 1) were found to be less susceptible to CES-mediated bioconversion ($t_{1/2} > 30$ min) than the parent biphenyl mannoside **1a.** Surprisingly, the pyrrolylphenyl esters **42e,f**, **49**, and **50** even proved to be metabolically stable and were only slowly hydrolyzed by carboxylesterases ($t_{1/2} > 120$ min). In contrast, derivatives with six-membered heterocylic moieties (entries 19–28) were cleaved extremely fast ($t_{1/2} < 15$ min) with rates comparable to biphenyl mannoside **1a.**

2.3 *In vitro* binding affinities

Binding affinities were determined in a cell-free competitive binding assay (Table 1).[28] Surprisingly, affinities of the esters (biphenyls and heteroaryl mannosides) were slightly improved compared to the corresponding acids, probably due to reduced desolvation costs.

Biphenyl mannosides. A comparison of antagonist **1b** (entry 3) with its regioisomers **2b**, **6b**, and **11b** (entries 5, 7 & 9) indicates that changing the position of the carboxylic acid on the terminal ring B of the biphenyl aglycone as well as modifying the substitution pattern on ring A substantially reduced affinity. As previously reported, the *ortho*-chloro substituent present in the antagonists **1b** and **6b** provides additional van der Waals contacts leading to binding affinity in the low nanomolar range.[8k]

Heteroaryl mannosides. All heteroaryl mannosides (entries 10–42) were weaker binders than the biphenyl mannoside **1b**, however also showed IC_{50} values in the nanomolar range. *In silico* studies obtained with flexible docking (Glide software package[33]) to the FimH-CRD suggested a similar 'out-docking mode' (Fig. 4) for all heteroaryl mannosides (entries 10–42), establishing π–π-stacking with Tyr48 of the tyrosine gate.[8g]

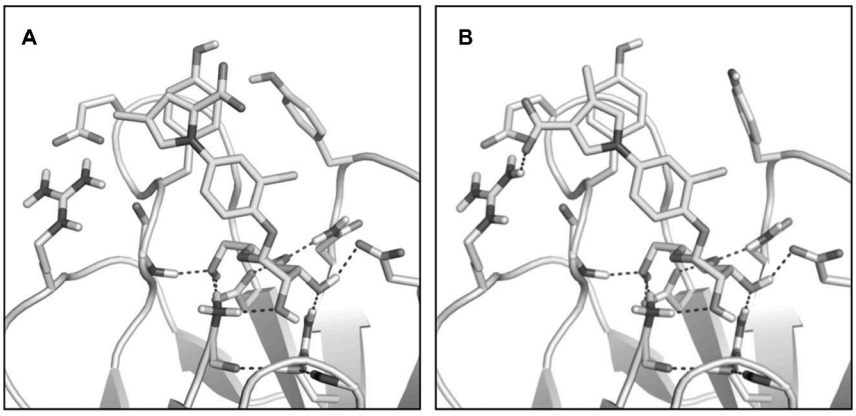

Fig. 4 *In silico* docking studies obtained with flexible docking (Glide software package[33]) to the FimH-CRD (PDB ID: 4XO8); top-scored binding modes of (A) **44** (Table 1, entry 34) and (B) **46** (entry 38).

Therefore, it is quite surprising that the triazolylphenyl mannosides (entries 10–14) and the pyrrolylphenyl mannosides (entries 29–42) showed approximately five-fold higher affinity than the pyrazolylphenyl analogues (entries 15–18). Furthermore, the substitution pattern had also an influence on the binding affinity as observed for the various pyrrolylphenyl mannosides (entries 29–42). In agreement with previous observations,[8i,k] an *ortho*-chloro or an *ortho*-trifluoromethyl substituent on ring A improved affinity approximately 3-fold (**51**, entry 40 *vs.* **46**, entry 38 & **52**, entry 42). Furthermore, the position of the electron-withdrawing carboxylic acid substituent in ring B affected the binding affinity as well. In the 3-position (→**45**, entry 36) a three-fold affinity increase compared to the 2-position (→**43**, entry 32) was observed. With an additional 4-methyl group, affinity was improved by a factor of three (**43**, entry 32 *vs.* **44**, entry 34), presumably due to sterically favored π–π stacking interactions between the heteroaromatic ring B and Tyr48 of the tyrosine gate.

2.4 *In vivo* pharmacokinetic study

Antagonist **42f** (entry 37, Table 1) exhibiting the best *in vitro* PK/PD profile was selected for an *in vivo* pharmacokinetic study. Since its solubility is not sufficient for the planned dose of 10 mg kg^{-1},[10a] 5% DMSO and 1% surfactant Tween 80 were used as solubilizer. The concentration–time profiles in urine and plasma are shown in Fig. 5.

Plasma concentrations of **42f** were low, with a C_{max} of only 0.04 μg mL^{-1} between 40 min and 1.5 h and dropped below the detection limit 3 h post application. In contrast, antagonist **42f** rapidly accumulates in the urine with a C_{max} ranging from 10 to 16 μg mL^{-1} at 1 to 3 h post application. After a stable concentration plateau, which is slightly shifted in time compared to plasma peak levels, **42f** could not be detected in urine 7 h post application.

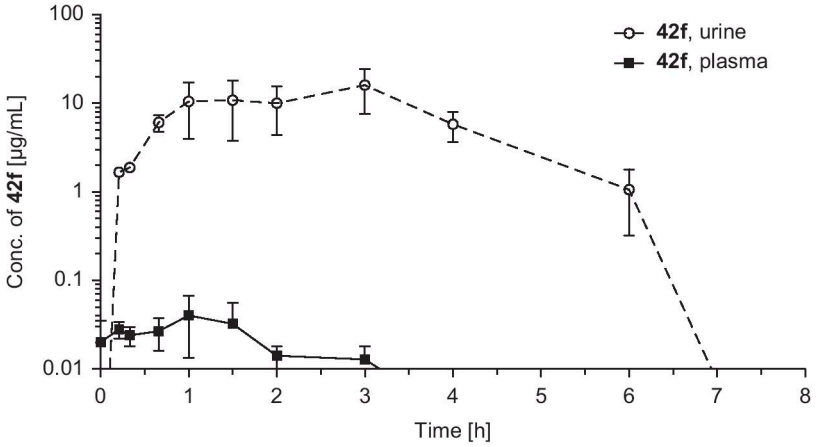

Fig. 5 Urine (dashed line) and plasma (continuous line) concentrations over time of the pyrrolylphenyl mannoside 42f after an application of a dose of 10 mg kg^{-1} (PBS containing 5% DMSO and 1% Tween 80). Shown are mean values with standard error of the mean for groups of three mice (C3H/HeN). The detection limit was at 0.02 μg mL^{-1}.

Accumulation in urine, resulting in a relatively constant plateau concentration over a time-period of about 3 h, can be related to several important interplaying mechanisms. Both, PAMPA[23] and transport through a Caco-2 cell monolayer predicted high (log P_e −4.8 cm s^{-1}) to moderate ($P_{app,a-b}$ 6.4×10^{-6} cm s^{-1}, Table 1) permeability for **42f**.[25,26] Although **42f** is a substrate of efflux transporters (Caco-2 cell experiment; b–a/a–b ratio > 2, Table 1),[29] the efflux transporters (*e.g.* P-gp) can be saturated by the applied high dose of 10 mg kg^{-1}.[32,34] Once in circulation, antagonist **42f** is filtered through the renal glomeruli in the kidneys. Based on its metabolic stability and a log $D_{7.4}$ value of 2.8, reabsorption from the filtrate in the proximal tubuli can be expected, leading to the observed delayed renal excretion.[10b,34,35] In summary, the observed PK profile of **42f** results from a good oral absorption (*i.e.* sufficient solubility and saturation of efflux transporter) with a delayed and prolonged elimination *via* the kidneys due to renal reabsorption.

3 Conclusions

Starting from ester **1a**, the present study aimed to optimize solubility and metabolic stability issues of biaryl mannosides in order to achieve high oral absorption of the ester and slow enzyme-mediated release of the polar metabolites.

First, our strategy to disrupt molecular planarity and symmetry of the biphenyl mannosides by modifying the substitution pattern, proved to be successful for improving solubility. Compared to antagonist **1a**, the ester **11a** showed a ten-fold improved solubility whereas membrane permeability remained high. However, since hepatic esterases rapidly convert ester **11a** to carboxylate **11b**, re-absorption from the tubuli is not possible leading to fast renal excretion. Furthermore, changing the positions of the substituents on the aglycone decreased affinity to the FimH-CRD, overriding the gain in the intestinal uptake potential (entries 4, 6 & 9).

In a second approach, the improvement of solubility and metabolic stability based on heterocyclic aglycones was studied. Thereby, triazole (**25a–c**, entries 10, 12 & 13), pyrazole (**28a,b**, entries 15 & 17), and six-membered heterocyclic moieties (**34a–d**, entries 19, 21, 23 & 25 and **39**, entry 27) proved highly beneficial to the aqueous solubility but in turn reduced lipophilicity and membrane permeability. Overall, only poor oral absorption could be observed. By contrast, the pyrrolylphenyl mannosides – optimized by the introduction of a chloro or trifluoromethyl substituent on ring A and a methyl group on the heterocycle (**42f** and **50**, entries 37 & 41) – exhibited sufficient permeability as well as aqueous solubility. Furthermore, incubations with rat liver microsomes, revealed low propensity to enzyme-mediated hydrolysis ($t_{1/2} > 120$ min), supporting slow elimination due to expected renal re-absorption of the metabolically stable esters.

In summary, our study exemplifies the benefits of two approaches: Rearrangement of the substitution pattern to improve aqueous solubility and introduction of heteroaromatic aglycones to improve aqueous solubility and metabolic stability. For the ester **42f**, an optimal balance of

pharmacodynamic, physicochemical and *in vitro* pharmacokinetic properties was realized. The measured high urine drug levels of **42f** (see Fig. 5) over an extended period of time considerably limit the dosing frequency and makes **42f** a promising candidate to be tested in a UTI disease model.

Abbreviations

Caco-2 cells	colorectal adenocarcinoma cells
CES	carboxylesterase
C_{max}	maximal concentration
CRD	carbohydrate recognition domain
D	octanol–water distribution coefficient
HPLC	high performance liquid chromatography
IC_{50}	half maximal inhibitory concentration
LC-MS	liquid chromatography mass spectrometry
PAMPA	parallel artificial membrane permeability assay
P_{app}	apparent permeability
P_e	effective permeability
RLM	rat liver microsomes
UPEC	uropathogenic *Escherichia coli*
UTI	urinary tract infection

Acknowledgements

The authors thank Prof. Dr med. Radek Skoda, Department of Biomedicine, University Hospital Basel, Switzerland, for giving us access to the animal facility. The financial support by the Swiss National Science Foundation (CS: SNF grant 200020_146202; DE: 31003A_144183; SK: 200020_129935) is gratefully acknowledged.

References

1 (a) T. M. Hooton and W. E. Stamm, Diagnosis and treatment of uncomplicated urinary tract infection, *Infect. Dis. Clin. North Am.*, 1997, **11**, 551–581; (b) T. J. Wiles, R. R. Kulesus and M. A. Mulvey, Origins and virulence mechanisms of uropathogenic *Escherichia coli*, *Exp. Mol. Pathol.*, 2008, **85**, 11–19; (c) S. D. Fihn, Acute uncomplicated urinary tract infection in women, *N. Engl. J. Med.*, 2003, **349**, 259–266.

2 (a) J. D. Schilling and S. J. Hultgren, Recent advances into the pathogenesis of recurrent urinary tract infections: the bladder as a reservoir for uropathogenic *Escherichia coli*, *Int. J. Antimicrob. Agents*, 2002, **19**, 457–460; (b) M. Blango and M. Mulvey, Persistence of uropathogenic *Escherichia coli* in the face of multiple antibiotics, *Antimicrob. Agents Chemother.*, 2010, **54**, 1855–1863.

3 C. Svanborg and G. Godaly, Bacterial virulence in urinary tract infection, *Infect. Dis. Clin. North Am.*, 1997, **11**, 513–529.

4 (a) M. A. Mulvey, Adhesion and entry of uropathogenic *Escherichia coli*, *Cell. Microbiol.*, 2002, **4**, 257–271; (b) D. S. Eto, T. A. Jones, J. L. Sundsbak and M. A. Mulvey, Integrin-mediated host cell invasion by type 1-piliated uropathogenic *Escherichia coli*, *PLoS Pathog.*, 2007, **3**, e100.

5 G. Capitani, O. Eidam, R. Glockshuber and M. G. Grütter, Structural and functional insights into the assembly of type 1 pili from *Escherichia coli*, *Microbes Infect.*, 2006, **8**, 2284–2290.

6 (a) I. Le Trong, P. Aprikian, B. A. Kidd, M. Forero-Shelton, V. Tchesnokova, P. Rajagopal, V. Rodriguez, G. Interlandi, R. Klevit, V. Vogel, R. E. Stenkamp, E. V. Sokurenko and W. E. Thomas, Structural basis for mechanical force regulation of the adhesin FimH via finger trap-like β sheet twisting, *Cell*, 2010, **141**, 645–655; (b) M. M. Sauer, R. P. Jakob, J. Eras, S. Baday, D. Eris, G. Navarra, S. Bernèche, B. Ernst, T. Maier and R. Glockshuber, Catch-bond mechanism of the bacterial adhesin FimH, *Nat. Commun.*, 2016, **7**, 10738.

7 N. Sharon, Carbohydrates as future anti-adhesion drugs for infectious diseases, *Biochim. Biophys. Acta*, 2006, **1760**, 527–537.

8 (a) N. Firon, I. Ofek and N. Sharon, Interaction of mannose-containing oligosaccharides with the fimbrial lectin of *Escherichia coli*, *Biochem. Biophys. Res. Commun.*, 1982, **105**, 1426–1432; (b) N. Firon, I. Ofek and N. Sharon, Carbohydrate specificity of the surface lectins of *Escherichia coli*, *Klebsiella pneumoniae*, and *Salmonella typhimurium*, *Carbohydr. Res.*, 1983, **120**, 235–249; (c) N. Sharon, Bacterial lectins, cell-cell recognition and infectious disease, *FEBS Lett.*, 1987, **217**, 145–157; (d) J. Bouckaert, J. Berglund, M. Schembri, E. De Genst, L. Cools, M. Wuhrer, C.-S. Hung, J. Pinkner, R. Slättegard, A. Zavialov, D. Choudhury, S. Langermann, S. J. Hultgren, L. Wyns, P. Klemm, S. Oscarson, S. D. Knight and H. De Greve, Receptor binding studies disclose a novel class of high-affinity inhibitors of the *Escherichia coli* FimH adhesin, *Mol. Microbiol.*, 2005, **55**, 441–455; (e) N. Firon, S. Ashkenazi, D. Mirelman, I. Ofek and N. Sharon, Aromatic alpha-glycosides of mannose are powerful inhibitors of the adherence of type 1 fimbriated *Escherichia coli* to yeast and intestinal epithelial cells, *Infect. Immun.*, 1987, **55**, 472–476; (f) O. Sperling, A. Fuchs and T. K. Lindhorst, Evaluation of the carbohydrate recognition domain of the bacterial adhesin FimH. Design, synthesis and binding properties of mannoside ligands, *Org. Biomol. Chem.*, 2006, **4**, 3913–3922; (g) Z. Han, J. S. Pinkner, B. Ford, R. Obermann, W. Nolan, S. A. Wildman, D. Hobbs, T. Ellenberger, C. K. Cusumano, S. J. Hultgren and J. W. Janetka, Structure-based drug design and optimization of mannoside bacterial FimH antagonists, *J. Med. Chem.*, 2010, **53**, 4779–4792; (h) T. Klein, D. Abgottspon, M. Wittwer, S. Rabbani, J. Herold, X. Jiang, S. Kleeb, C. Lüthi, M. Scharenberg, J. Bezençon, E. Gubler, L. Pang, M. Smiesko, B. Cutting, O. Schwardt and B. Ernst, FimH antagonists for the oral treatment of urinary tract infections: from design and synthesis to in vitro and in vivo evaluation, *J. Med. Chem.*, 2010, **53**, 8627–8641; (i) C. K. Cusumano, J. S. Pinkner, Z. Han, S. E. Greene, B. A. Ford, J. R. Crowley, J. P. Henderson, J. W. Janetka and S. J. Hultgren, Treatment and prevention of urinary tract infection with orally active FimH inhibitors, *Sci. Transl. Med.*, 2011, **3**, 109–115; (j) Z. Han, J. S. Pinkner, B. Ford, E. Chorell, J. M. Crowley, C. K. Cusumano, S. Campbell, J. P. Henderson, S. J. Hultgren and J. W. Janetka, Lead optimization studies on FimH antagonists: discovery of potent and orally bioavailable *ortho*-substituted biphenyl mannosides, *J. Med. Chem.*, 2012, **55**, 3945–3959; (k) L. Pang, S. Kleeb, K. Lemme, S. Rabbani, M. Scharenberg, A. Zalewski, F. Schädler, O. Schwardt and B. Ernst, FimH antagonists: structure-activity and structure-property relationships for biphenyl α-D-mannopyranosides, *ChemMedChem*, 2012, **7**, 1404–1422; (l) X. Jiang, D. Abgottspon, S. Kleeb, S. Rabbani, M. Scharenberg, M. Wittwer, M. Haug, O. Schwardt and B. Ernst, Anti-adhesion therapy for urinary tract infections – a balanced PK/PD profile

proved to be key for success, *J. Med. Chem.*, 2012, **55**, 4700–4713; (m) O. Schwardt, S. Rabbani, M. Hartmann, D. Abgottspon, M. Wittwer, S. Kleeb, A. Zalewski, M. Smiesko, B. Cutting and B. Ernst, Design, synthesis and biological evaluation of mannosyl triazoles as FimH antagonists, *Bioorg. Med. Chem.*, 2011, **19**, 6454–6473; (n) S. Brument, A. Sivignon, T. I. Dumych, N. Moreau, G. Roos, Y. Guérardel, T. Chalopin, D. Deniaud, R. O. Bilyy, A. Darfeuille-Michaud, J. Bouckaert and S. G. Gouin, Thiazolylamino-mannosides as potent antiadhesives of type 1 piliated *Escherichia coli* isolated from Crohn's disease patients, *J. Med. Chem.*, 2013, **56**, 5395–5406; (o) S. Kleeb, L. Pang, K. Mayer, D. Eris, A. Sigl, R. C. Preston, P. Zihlmann, T. Sharpe, R. P. Jakob, D. Abgottspon, A. S. Hutter, M. Scharenberg, X. Jiang, G. Navarra, S. Rabbani, M. Smiesko, N. Lüdin, J. Bezençon, O. Schwardt, T. Maier and B. Ernst, FimH antagonists: bioisosteres to improve the in vitro and in vivo PK/PD profile, *J. Med. Chem.*, 2015, **58**, 2221–2239.

9 (a) T. K. Lindhorst, C. Kieburg and U. Krallmann-Wenzel, Inhibition of the type 1 fimbriae-mediated adhesion of *Escherichia coli* to erythrocytes by multiantennary D-mannosyl clusters: The effect of multivalency, *Glycoconjugate J.*, 1998, **15**, 605–613; (b) N. Nagahori, R. T. Lee, S.-L. Nishimura, S. Pagé, R. Roy and Y. C. Lee, Inhibition of adhesion of type 1 fimbriated *Escherichia coli* to highly mannosylated ligands, *ChemBioChem*, 2002, **3**, 836–844; (c) C. C. M. Appeldoorn, J. A. F. Joosten, F. A. Maate, U. Dobrindt, J. Hacker, R. M. J. Liskamp, A. S. Khan and R. J. Pieters, Novel multivalent mannose compounds and their inhibition of the adhesion of type 1 fimbriated uropathogenic *E. coli*, *Tetrahedron: Asymmetry*, 2005, **16**, 361–372; (d) A. Patel and T. K. Lindhorst, A modular approach for the synthesis of oligosaccharide mimetics, *Carbohydr. Res.*, 2006, **341**, 1657–1668; (e) M. Touaibia, A. Wellens, T. C. Shiao, Q. Wang, S. Sirois, J. Bouckaert and R. Roy, Mannosylated G(0) dendrimers with nanomolar affinities to *Escherichia coli* FimH, *ChemMedChem*, 2007, **2**, 1190–1201; (f) M. Durka, K. Buffet, J. Iehl, M. Holler, J.-F. Nierengarten, J. Taganna, J. Bouckaert and S. P. Vincent, The functional valency of dodecamannosylated fullerenes with *Escherichia coli* FimH – towards novel bacterial antiadhesives, *Chem. Commun.*, 2011, **47**, 1321–1323; (g) J. Bouckaert, Z. Li, C. Xavier, M. Almant, V. Caveliers, T. Lahoutte, S. D. Weeks, J. Kovensky and S. G. Gouin, Heptyl α-D-mannosides grafted on a β-cyclodextrin core to interfere with *Escherichia coli* adhesion: An *in vivo* multivalent effect, *Chem. – Eur. J.*, 2013, **19**, 7847–7855.

10 (a) C. A. Lipinski, Drug-like properties and the causes of poor solubility and poor permeability, *J. Pharmacol. Toxicol. Methods*, 2000, **44**, 235–249; (b) H. van de Waterbeemd, D. Smith, K. Beaumont and D. Walker, Property-based design: Optimization of drug absorption and pharmacokinetics, *J. Med. Chem.*, 2001, **44**, 1313–1333.

11 (a) M. Ishikawa and Y. Hashimoto, Improvement in aqueous solubility in small molecule drug discovery programs by disruption of molecular planarity and symmetry, *J. Med. Chem.*, 2011, **54**, 1539–1554; (b) A.-E. F. Nassar, A. M. Kamel and C. Clarimont, Improving the decision-making process in the structural modification of drug candidates: enhancing metabolic stability, *Drug Discovery Today*, 2004, **9**, 1020–1028.

12 N. A. Meanwell, Synopsis of some recent tactical application of bioisosteres in drug design, *J. Med. Chem.*, 2011, **54**, 2529–2591.

13 I. L. Scott, R. V. Market, R. J. DeOrazio, H. Meckler and T. P. Kogan, Stereospecific α-D-mannosylation, *Carbohydr. Res.*, 1999, **317**, 210–216.

14 A. Titz, Z. Radic, O. Schwardt and B. Ernst, A safe and convenient method for the preparation of triflyl azide, and its use in diazo transfer reactions to

primary amines, *Tetrahedron Lett.*, 2006, **47**, 2383–2385; R. Yan, F. Yang, Y. Wu, L. Zhang and X. Ye, An efficient and improved procedure for preparation of triflyl azide and application in catalytic diazotransfer reaction, *Tetrahedron Lett.*, 2005, **46**, 8993–8995.

15 V. Rostovtsev, L. Green, V. Fokin and K. Sharpless, A stepwise Huisgen cycloaddition process: Copper(I)-catalyzed regioselective "ligation" of azides and terminal alkynes, *Angew. Chem., Int. Ed.*, 2002, **41**, 2596–2599.

16 J. Antilla, J. Baskin, T. Barder and S. Buchwald, Copper-diamine-catalyzed *N*-arylation of pyrroles, pyrazoles, indazoles, imidazoles, and triazoles, *J. Org. Chem.*, 2004, **69**, 5578–5587.

17 (a) M. Node, K. Nishide, K. Fuji and E. Fujita, Hard acid and soft nucleophile system. 2. Demethylation of methyl esters of alcohol and phenol with an aluminum halide-thiol system, *J. Org. Chem.*, 1980, **45**, 4275–4277; (b) M. Node, K. Kumar, K. Nishide, S. Ohsugi and T. Miyamoto, Odorless substitutes for foul-smelling thiols: Syntheses and applications, *Tetrahedron Lett.*, 2001, **42**, 9207–9210.

18 B. Le Bourdonnec, R. Windh, L. Leister, Q. Zhou, C. Ajello, M. Gu, G. Chu, P. Tuthill, W. Barker, M. Koblish, D. Wiant, T. Graczyk, S. Belanger, J. Cassel, M. Feschenko, B. Brogdon, S. Smith, M. Derelanko, S. Kutz, P. Little, R. DeHaven, D. DeHaven-Hudkins and R. Dolle, Spirocyclic delta opioid receptor agonists for the treatment of pain: Discovery of *N*,*N*-diethyl-3-hydroxy-4-(spiro[chromene-2,4'-piperidine]-4-yl) benzamide (ADL5747), *J. Med. Chem.*, 2009, **52**, 5685–5702.

19 A. Katritzky, D. Cheng and R. Musgrave, Syntheses of imidazoles and pyrroles: BetMIC and TosMIC as complementary reagents, *Heterocycles*, 1997, **44**, 67–70.

20 M. Prieto, E. Zurita, E. Rosa, L. Munoz, P. Lloyd-Williams and E. Giralt, Arylboronic acids and arylpinacolboronate esters in Suzuki coupling reactions involving indoles. Partner role swapping and heterocycle protection, *J. Org. Chem.*, 2004, **69**, 6812–6820.

21 J. C. Dearden and G. M. Bresnen, The measurement of partition coefficients, *Quant. Struct. – Act. Relat.*, 1988, **7**, 133–144.

22 A. Avdeef, High-througput measurements of solubility profiles, in *Pharmacokinetic Optimization in Drug Research; Biological, Physicochemical and Computational Strategies*, ed. B. Testa, H. van de Waterbeemd, G. Folkers and R. Guy, Verlag Helvetica Chimica Acta, Zurich, 2001, pp. 305–326.

23 M. Kansy, F. Senner and K. Gubernator, Physicochemical high throughput screening: Parallel artificial membrane permeation assay in the description of passive absorption processes, *J. Med. Chem.*, 1998, **41**, 1007–1010.

24 P. Artursson and J. Karlsson, Correlation between oral-drug absorption in humans and apparent drug permeability coefficients in human intestinal epithelial (Caco-2) cells, *Biochem. Biophys. Res. Commun.*, 1991, **175**, 880–885.

25 A. Avdeef, S. Bendels, L. Di, B. Faller, M. Kansy, K. Sugano and Y. Yamauchi, PAMPA – critical factors for better predictions of absorption, *J. Pharm. Sci.*, 2007, **96**, 2893–2909.

26 T. Hou, J. Wang, W. Zhang and X. Xu, ADME evaluation in drug discovery. 7. Prediction of oral absorption by correlation and classification, *J. Chem. Inf. Model.*, 2007, **47**, 208–218.

27 M. Taketani, M. Shii, K. Ohura, S. Ninomiya and T. Imai, Carboxylesterase in the liver and small intestine of experimental animals and human, *Life Sci.*, 2007, **81**, 924–932.

28 S. Rabbani, X. H. Jiang, O. Schwardt and B. Ernst, Expression of the carbohydrate recognition domain of FimH and development of a competitive binding assay, *Anal. Biochem.*, 2010, **407**, 188–195.

29 I. Hubatsch, E. G. Ragnarsson and P. Artursson, Determination of drug permeability and prediction of drug absorption in Caco-2 monolayers, *Nat. Protoc.*, 2007, **2**, 2111–2119.
30 MacroModel, version 9.9, Schrödinger, LLC, New York, NY, 2012. Torsion angle measurements are based on the lowest-energy conformers.
31 (a) R. M. Wadkins, C. L. Morton, J. K. Weeks, L. Oliver, M. Wierdl, M. K. Danks and P. M. Potter, Structural constraints affect the metabolism of 7-ethyl-10-[4-(1-piperidino)-1-piperidino]carbonyloxycamptothecin (CPT-11) by carboxylesterases, *Mol. Pharmacol.*, 2001, **60**, 355–362; (b) J. M. Hatfield, M. Wierdl, R. M. Wadkins and P. M. Potter, Modifications of human carboxylesterase for improved prodrug activation, *Expert Opin. Drug Metab. Toxicol.*, 2008, **4**, 1153–1165; (c) G. Vistoli, A. Pedretti, A. Mazzolari and B. Testa, In silico prediction of human carboxylesterase-1 (hCES1) metabolism combining docking analyses and MD simulations, *Bioorg. Med. Chem.*, 2010, **18**, 320–329; T. Satoh and M. Hosokawa, Structure, function and regulation of carboxylesterases, *Chem. Biol. Interact.*, 2006, **162**, 195–211.
32 J. H. Lin, Drug-drug interaction mediated by inhibition and induction of P-glycoprotein, *Adv. Drug Delivery Rev.*, 2003, **21**, 53–81.
33 Glide, version 5.7, Schrödinger, LLC, New York, NY, 2011; 3D representations were made by the PyMOL Molecular Graphics System, Version 1.6 Schrödinger, LLC.
34 D. A. Smith, B. C. Jones and D. K. Walker, Design of drugs involving the concepts and theories of drug metabolism and pharmacokinetics, *Med. Res. Rev.*, 1996, **16**, 243–266.
35 M. V. Varma, B. Feng, R. S. Obach, M. D. Troutman, J. Chupka, H. R. Miller and A. El-Kattan, Physicochemical determinants of human renal clearance, *J. Med. Chem.*, 2009, **52**, 4844–4852.

5.3. PAPER III

"FimH Antagonists: Phosphate Prodrugs Improve Oral Bioavailability"

Simon Kleeb,[#] Xiaohua Jiang,[#] Priska Frei,[#] Anja Sigl, Jacqueline Bezençon, Karen Bamberger, Oliver Schwardt, and Beat Ernst[*]

# equally contributed

Journal of Medicinal Chemistry, March 2016

Journal of Medicinal Chemistry

Article

pubs.acs.org/jmc

FimH Antagonists: Phosphate Prodrugs Improve Oral Bioavailability

Simon Kleeb, Xiaohua Jiang, Priska Frei, Anja Sigl, Jacqueline Bezençon, Karen Bamberger, Oliver Schwardt, and Beat Ernst*

Institute of Molecular Pharmacy, Pharmacenter, University of Basel, Klingelbergstrasse 50, 4056 Basel, Switzerland

Supporting Information

ABSTRACT: The widespread occurrence of urinary tract infections has resulted in frequent antibiotic treatment, contributing to the emergence of antimicrobial resistance. Alternative approaches are therefore required. In the initial step of colonization, FimH, a lectin located at the tip of bacterial type 1 pili, interacts with mannosylated glycoproteins on the urothelial mucosa. This initial pathogen/host interaction is efficiently antagonized by biaryl α-D-mannopyranosides. However, their poor physicochemical properties, primarily resulting from low aqueous solubility, limit their suitability as oral treatment option. Herein, we report the syntheses and pharmacokinetic evaluation of phosphate prodrugs, which show an improved aqueous solubility of up to 140-fold. In a Caco-2 cell model, supersaturated solutions of the active principle were generated through hydrolysis of the phosphate esters by brush border-associated enzymes, leading to a high concentration gradient across the cell monolayer. As a result, the in vivo application of phosphate prodrugs led to a substantially increased C_{max} and prolonged availability of FimH antagonists in urine.

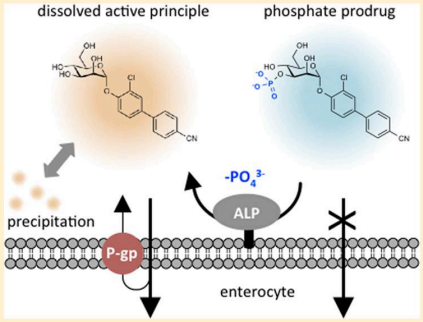

INTRODUCTION

Urinary tract infections (UTIs) are the most frequent cause of bacteriosis in humans, affecting millions of people worldwide.[1] They remain one of the most common indications for prescribing antibiotics to alleviate symptoms (dysuria, frequent and urgent urination, bacteriuria, and pyuria) and to prevent complications (pyelonephritis and urosepsis).[2] However, the frequent and repeated use of antibiotics can induce antimicrobial resistance; therefore, alternative prevention and treatment strategies are urgently needed.[3]

Uropathogenic *Escherichia coli* (UPEC) strains are the causative agent of more than 70% of all UTI episodes.[4,5] The initial step in pathogenesis involves bacterial adherence to the bladder cell surface, preventing UPEC from being cleared by the bulk flow of urine and enabling the bacteria to colonize the urothelial cells.[6] Among the different adhesins expressed on the bacterial surface, mannose-binding type 1 pili are the most prevalent. They consist of a helical rod containing 500−3000 copies of the structural subunit FimA as well as one copy of the FimF, FimG, and FimH subunits.[7] The FimH subunit is expressed at the distal tip of each pilus and exhibits the carbohydrate recognition domain (CRD), which interacts with the mannosylated glycoprotein uroplakin 1a on the mucosal surface of the bladder.[8]

More than three decades ago, Sharon and co-workers described various oligomannosides and aryl α-D-mannosides as potential antagonists of FimH-mediated bacterial adhesion.[9,10] This led to subsequent reports on several monovalent mannose-based FimH antagonists containing various aglycones, such as *n*-alkyl,[11] phenyl,[12] dioxocyclobutenylaminophenyl,[13] umbelliferyl,[12] biphenyl,[14−19] indol(in)ylphenyl,[20] triazolyl,[21] or thiazolylamino.[22] In addition, different multivalent presentations of mannose derivatives have been explored.[23−29] Most importantly, it was recently shown that these α-D-mannopyranosides did not elicit adverse side effects caused by the nonselective binding of FimH antagonists to various mammalian mannose receptors.[30]

In vivo studies in a mouse disease model confirmed the therapeutic potential of biaryl mannosides for an oral treatment of UTI.[15−17,19] However, because only low oral bioavailability could be achieved, basic determinants such as aqueous solubility and membrane permeability should be further optimized.[31] One possible solution is offered by a phosphate prodrug approach, which is applied either when the active principal exhibits high membrane permeability but suffers from low aqueous solubility[32] or when the therapeutic dose exceeds the maximum amount of drug that can be dissolved into intestinal fluids.[33] In a phosphate prodrug approach, the active principle is rapidly released by endogenous phosphatases, such as alkaline phosphatase, an enzyme particularly abundant on the brush border of enterocytes.[34]

The application of this prodrug principle has led to various marketed drugs, such as prednisolone phosphate (**1**),[35] the antiretroviral drug fosamprenavir (**2**),[34,36] or the chemotherapeutic drug fludarabine phosphate (Figure 1).[37]

The goal of the present study was to optimize the physicochemical profile of the biaryl mannosides **3**−**5** by phosphorylation, enhancing aqueous solubility and, consequently, the oral availability.

Received: December 11, 2015
Published: March 9, 2016

DOI: 10.1021/acs.jmedchem.5b01923
J. Med. Chem. 2016, 59, 3163−3182

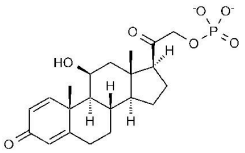
Prednisolone phosphate (1)

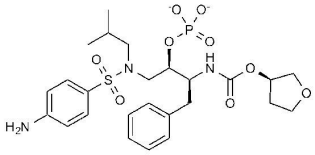
Fosamprenavir (2)

Figure 1. Phosphate prodrugs of marketed drugs.

■ RESULTS AND DISCUSSION

Although exhibiting nanomolar affinity and high permeability, one drawback of FimH antagonists **3**–**5**[14,18−20] is their low aqueous solubility, resulting in limited oral bioavailability. They are therefore perfect candidates for a phosphate prodrug approach. Table 1 summarizes their previously reported binding affinities (IC_{50})[14,18−20] as well as their physicochemical properties (solubility, lipophilicity, and permeability).

For identifying the optimal position of the phosphate promoiety on the mannoside core of FimH antagonists **3**–**5**, a series of phosphate esters was synthesized (Figure 2) and their solubility determined. In the prodrugs **6a**–**d** and **7a**–**d**, the phosphate ester bond was directly linked to the various hydroxyl groups of the mannose moiety. Alternatively, an acetal linker was used in prodrugs **6e** and **8** to increase the distance between the enzymatic cleavage site and thereby enhance accessibility of the phosphate ester and subsequently the dephosphorylation rate. When prodrugs **6e** and **8** are dephosphorylated, the intermediate hemiacetal is expected to collapse, spontaneously releasing the active principle **3** or **5** accompanied by formaldehyde.[45]

Synthesis of Phosphates 6a–d. 2-Phosphate **6a** of biphenyl α-D-mannopyranoside (**3**) was synthesized according to the procedure depicted in Scheme 1. Starting from **3**,[14,18] a benzylidene acetal (→**9**) was formed to protect the 4- and 6-OH of the mannose moiety. The 3-position was subsequently protected by a regioselective dibutyltin oxide-mediated benzylation (→**10**) and then phosphorylation using dibenzyl *N*,*N*-diisopropyl-phosphoramidite in the presence of 1,2,4-triazole, followed by oxidation with *tert*-butylhydroperoxide, afforded the protected intermediate **11**. Global deprotection via catalytic hydrogenation yielded 2-phosphate **6a**.

For the synthesis of 3-phosphate **6b**, the 3-position of **3** was regioselectively benzylated (→**12**), followed by perbenzoylation to give **13** (Scheme 2). Cleavage of the benzyl group by hydrogenation (→**14**) and subsequent phosphorylation afforded an inseparable 3:2-mixture of the protected 3- and 2-phosphates **15** and **16** due to partial migration of the 2-benzoyl moiety. Upon deprotection via catalytic hydrogenation, pure 3-phosphate **6b** could be isolated.

For the synthesis of 4-phosphate **6c**, **9** was benzoylated (→**17**). Reductive opening of the benzylidene acetal with $Me_3N{\cdot}BH_3$ and $AlCl_3$ afforded precursor **18** (Scheme 3). Phosphorylation (→**19**) and subsequent deprotection yielded 4-phosphate **6c**.

For the synthesis of 6-phosphate **6d**, mannoside **3** was tritylated in the 6-position, followed by perbenzoylation (→**20**) and removal of the trityl group (Scheme 4). Then, intermediate **21** was phosphorylated (→**22**) and final global deprotection gave 6-phosphate **6d**.

Synthesis of Phosphates 7a–d. Because of the labile chloro- and cyano-substituents present in biphenyl α-D-mannopyranoside **4**,[19] the 2-phosphate **7a** was obtained via a modified strategy (Scheme 5), omitting a potentially intractable hydrogenation step. Therefore, after protecting the 4- and 6-OH of **4** with a benzylidene acetal (→**23**), the 3-OH of the mannose moiety was selectively benzoylated to afford **24**.[46] Phosphorylation of the 2-OH group with bis[2-(trimethylsilyl)-ethyl] *N*,*N*-diisopropylphosphoramidite in the presence of 1,2,4-triazole, and subsequent oxidation with *tert*-butylhydro-

Table 1. Binding Affinities and Physicochemical Properties of the Biaryl α-D-Mannopyranosides 3–5[f]

Cpd		IC_{50}[a] [nM]	Solubility[b] [μg/mL]	log *P*[c]	PAMPA log P_e[d] [cm/s]	Caco-2 P_{app}[e] [10^{-6} cm/s]	
						a→b	b→a
3[14,18]	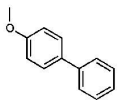	84.9	21	2.1	-4.7	10.0 ± 0.9	19.0 ± 1.2
4[19]	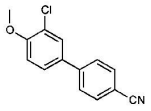	10.1	192	2.1	-5.2	2.2 ± 0.4	22.1 ± 1.5
5[20]	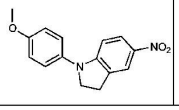	20	24	1.9	-5.5	2.9 ± 0.6	39.3 ± 5.8

[a]IC_{50} values were determined in a cell-free competitive binding assay.[38] [b]Thermodynamic solubility for compounds **5**; kinetic solubility for compound **3** and **4**.[39] [c]Octanol–water partition coefficients (log *P*) were determined by a miniaturized shake-flask procedure.[40] [d]P_e = effective permeability: passive permeation through an artificial membrane was determined by the parallel artificial membrane permeability assay (PAMPA).[41,42] [e]P_{app} = apparent permeability: permeation through a Caco-2 cell monolayer was assessed in the absorptive (a → b) and secretory (b → a) directions in triplicate.[43,44] [f]IC_{50} values, aqueous solubility, log *P*, PAMPA, and Caco-2 cell data were adopted from refs 18–20. The IC_{50} of antagonist **4** and Caco-2 P_{app} values of antagonist **5** were obtained according to the procedure described in ref 18.

DOI: 10.1021/acs.jmedchem.5b01923
J. Med. Chem. 2016, 59, 3163−3182

Journal of Medicinal Chemistry Article

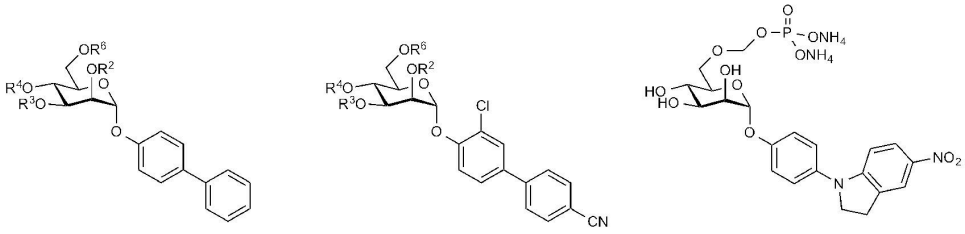

6a: $R^2 = PO_3(NH_4)_2$; R^3, R^4, R^6 = H
6b: $R^3 = PO_3(NH_4)_2$; R^2, R^4, R^6 = H
6c: $R^4 = PO_3(NH_4)_2$; R^2, R^3, R^6 = H
6d: $R^6 = PO_3(NH_4)_2$; R^2, R^3, R^4 = H
6e: $R^2 = CH_2OPO_3(NH_4)_2$; R^2, R^3, R^4 = H

7a: $R^2 = PO_3(NH_4)_2$; R^3, R^4, R^6 = H
7b: $R^3 = PO_3(NH_4)_2$; R^2, R^4, R^6 = H
7c: $R^4 = PO_3(NH_4)_2$; R^2, R^3, R^6 = H
7d: $R^6 = PO_3(NH_4)_2$; R^2, R^3, R^4 = H

8

Figure 2. Phosphate monoesters **6a–e** of biphenyl α-D-mannopyranoside **3**, **7a–d** of substituted biphenyl α-D-mannopyranoside **4** and **8** from indolinylphenyl α-D-mannopyranoside **5**.

Scheme 1[a]

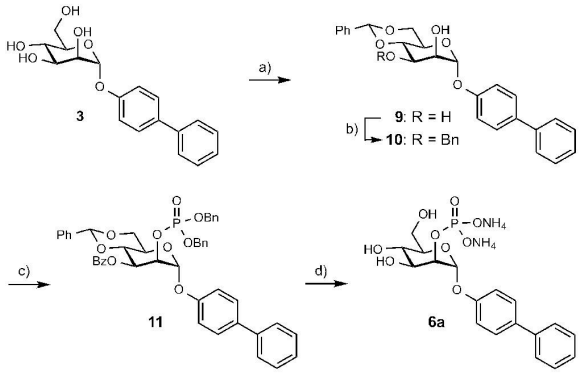

[a](a) $PhCH(OMe)_2$, *p*-TsOH, DMF, 50 °C, overnight (70%); (b) (i) Bu_2SnO, toluene, 135 °C, 3 h, (ii) BnBr, toluene, 115 °C, overnight (80%); (c) dibenzyl *N*,*N*-diisopropylphosphoramidite, 1,2,4-triazole, MeCN, 0 °C to rt, overnight; then 70% aq *tert*-BuOOH, rt, 1 h (62%); (d) (i) H_2 (4 bar), $Pd(OH)_2$/C, EtOAc, cat. HOAc, overnight, (ii) 25% aq NH_3/MeOH (4:1), rt, overnight (45%).

peroxide, yielded intermediate **25**. After cleavage of the (trimethylsilyl)ethyl esters with TFA (→**26**) and subsequent ester hydrolysis upon treatment with NH_3/MeOH, 2-phosphate **7a** was obtained.

Regioselective 3-allylation of **4** (→**27**) followed by benzoylation of the 2-, 4-, and 6-OH gave **28** (Scheme 6). Subsequent cleavage of the allyl group with $PdCl_2$ (→**29**) and phosphorylation afforded intermediate **30** and final deprotection 3-phosphate **7b**.

4-Phosphate **7c** was synthesized in three steps via regioselective dibutyltin oxide-mediated acetylation of **4** in the 2-, 3-, and 6-position[47] (→**31**), phosphorylation of the 4-OH (→**32**), and subsequent cleavage of all protecting groups (Scheme 7).

For the synthesis of 6-phosphate **7d**, a similar protection strategy as for **6d** was used (Scheme 8). The parent compound **4** was tritylated in the 6-position (→**33**), followed by perbenzoylation (→**34**) and removal of the trityl group. Phosphorylation of intermediate **35** (→**36**) and final global deprotection afforded 6-phosphate **7d**.

Synthesis of Acetal-Linked Phosphates 6e and 8. Synthesis of the acetal-linked phosphate **6e** of biphenyl α-D-mannopyranoside (**3**) was achieved by first introducing a 6-*O*-(thiomethyl)methyl group on intermediate **21** with DMSO–acetic anhydride under acidic conditions (→**37**, Scheme 9). Subsequent treatment with phosphoric acid and *N*-iodosuccinimide gave phosphate **38**. Finally, debenzoylation with NH_3/MeOH provided the target compound **6e**.

The acetal-linked phosphate **8** was prepared analogously from indolinylphenyl α-D-mannopyranoside **5**[20] (Scheme 10). Selective TBS-protection of the 6-OH, followed by perbenzoylation (→**39**), and cleavage of the silyl ether yielded precursor **40**. After the introduction of a 6-*O*-(thiomethyl)-methyl group with DMSO–acetic anhydride (→**41**), treatment with phosphoric acid and *N*-iodosuccinimide (→**42**) and debenzoylation, test compound **8** was obtained.

Solubility. The thermodynamic solubility of the phosphate prodrugs was determined in phosphate buffer (50 mM, pH 6.5). The expected improvement of aqueous solubility, which exceeds those of the active principles **3–5** by several orders of magnitude (Table 2), could be confirmed.

ALP-Mediated Hydrolysis. ALP-mediated hydrolysis of the various phosphate esters was studied in Caco-2 cells, which express phosphatase on the apical brush border surface of the confluent cell monolayer.[48] The experimental half-life ($t_{1/2}$) was calculated from the concentration of remaining prodrug vs incubation time (Table 2).

Depending on the position of the promoiety, the prodrugs showed varying propensity to dephosphorylation (Figure 3). The 2- and 3-phosphate esters (**6a**, **6b**, **7a**, and **7b**) were rapidly hydrolyzed ($t_{1/2}$ < 15 min), whereas the 4- and 6-phosphate esters (**6c**, **6d**, **7c**, and **7d**) showed prolonged half-lives ($t_{1/2}$ > 40 min). Improved stability of the latter likely results from reduced access to the ester bonds at C4 and C6 because of steric hindrance.[45,49,50] Therefore, with the introduction of a linker (→**6e**, **8**), accessibility can be improved and the susceptibility to ALP-mediated cleavage was markedly increased ($t_{1/2}$ = 8.7 and 11 min, respectively).

Owing to their high propensity to ALP-mediated hydrolysis, the phosphate esters **6a**, **6b**, **7a**, **7b**, and **8** were almost entirely converted to parent drug within 60 min (Figure 3). For example, Figure 4 depicts the concentration of prodrug **7b** 60 min after application to either the apical or the basolateral side of the Caco-2 system. When applied to the apical chamber, the prodrug was almost quantitatively hydrolyzed. However, when applied to the basal chamber, the prodrug remained the prominent species detected, due to the lack of ALP on the basal

DOI: 10.1021/acs.jmedchem.5b01923
J. Med. Chem. 2016, 59, 3163–3182

Scheme 2[a]

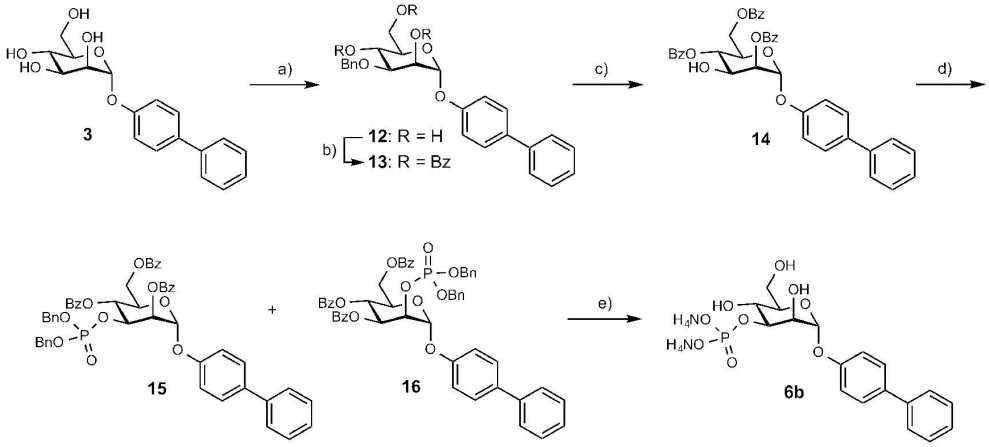

[a](a) (i) Bu_2SnO, MeOH, reflux, 5 h, (ii) BnBr, toluene, 115 °C, overnight (36%); (b) BzCl, cat. DMAP, pyr, rt, overnight (99%); (c) H_2 (4 bar), $Pd(OH)_2/C$, dioxane/EtOAc, cat. AcOH, rt, overnight (73%); (d) dibenzyl *N,N*-diisopropylphosphoramidite (90%), 1,2,4-triazole, MeCN, 0 °C to rt, overnight, then 70% aq *tert*-BuOOH, rt, 1 h (80%, 3:2 mixture of 2-and 3-phosphate derivatives); (e) (i) H_2 (1 bar), $Pd(OH)_2/C$, EtOAc, 5 h, (ii) 25% aq NH_3/MeOH (4:1), rt, overnight (7%).

Scheme 3[a]

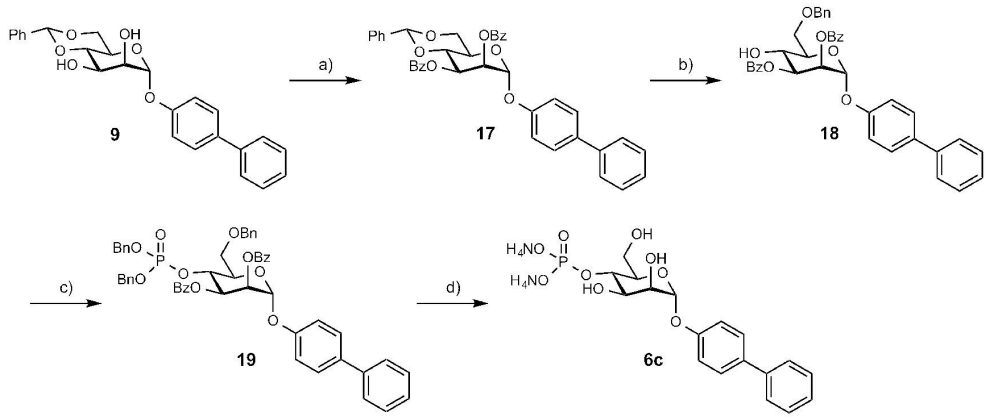

[a](a) BzCl, cat. DMAP, pyr, rt, overnight (60%); (b) $Me_3N{\cdot}BH_3$, $AlCl_3$, THF/H_2O, rt, 1 h (67%); (c) dibenzyl *N,N*-diisopropylphosphoramidite (90%), 1,2,4-triazole, MeCN, 0 °C to rt, overnight, then 70% aq *tert*-BuOOH, 1 h (53%); (d) H_2, $Pd(OH)_2/C$, EtOH/EtOAc, 5 h, quant; (e) 25% aq NH_3/MeOH (4:1), rt, overnight (56%).

Caco-2 cell membrane.[48] In addition, irrespective of dosing on the apical or basal side, the prodrug could not be detected in the receiver compartment, which corroborates the poor membrane permeability of the polar phosphate ester (Figure 4).

Stability in Biorelevant Media. Because chemical stability at various pH conditions and stability for degradation by digestive enzymes (simulated gastric and intestinal fluids,[51,52] for composition, see Table S1 in Supporting Information) turned out to be high (>80% after 2 h; Figure 5), the phosphate prodrugs **7a**, **7c**, and **7d** appear optimally suited to mitigate the solubility problem.

Oral Bioavailability. For oral administration of a phosphate prodrug several absorption rate-limiting factors need to be considered. In addition to unsuitably slow ALP-mediated hydrolysis of the phosphate prodrug, low solubility, poor permeability, and efflux of the active principle can also limit oral absorption.

In Vitro Pharmacokinetic Evaluation. To further examine the benefits associated with improved solubility obtained upon phosphorylation of the active principle, the most labile phosphate prodrugs, **6e**, **7b**, and **8** ($t_{1/2} \leq 12$ min, Table 2), were applied to the apical chambers of the Caco-2 system, and the accumulation of active principles **3**, **4**, and **5** on the basal side of the cell monolayer was monitored (Figure 6a–c). Applying either the active principle or the respective prodrug at equal concentrations (62.5 μM) to the apical chamber resulted in similar basolateral concentrations of the active principle, i.e., the hydrolysis is not the rate limiting step. When higher apical doses of the phosphate prodrugs were applied, the basolateral concentrations were markedly increased (Figure 6a–c).

Once a prodrug has been hydrolyzed in vivo, physicochemical properties of the active principle (i.e., solubility and

DOI: 10.1021/acs.jmedchem.5b01923
J. Med. Chem. 2016, 59, 3163–3182

Scheme 4[a]

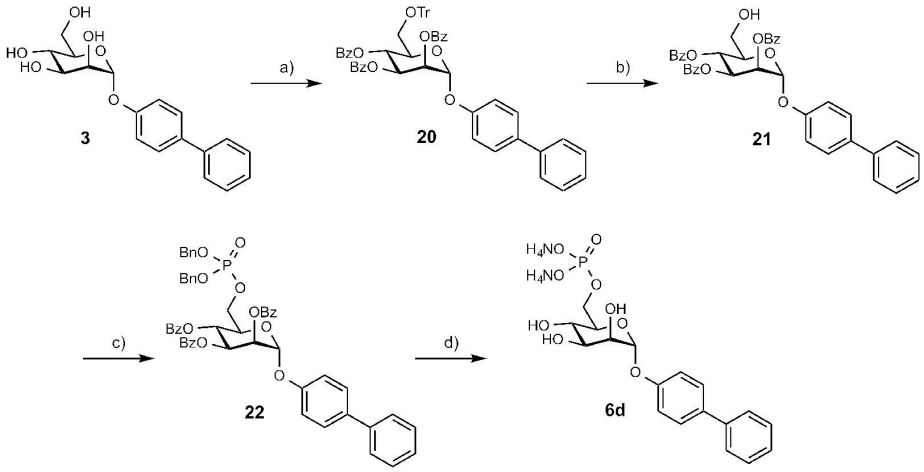

[a](a) (i) TrCl, cat. DMAP, pyr, 80 °C, overnight, (ii) BzCl, 50 °C, overnight (88%); (b) $FeCl_3/H_2O$, DCM, rt, 5 h (62%); (c) dibenzyl *N*,*N*-diisopropylphosphoramidite (90%), 1,2,4-triazole, MeCN, 0 °C to rt, overnight, then 70% aq *tert*-BuOOH, rt, 1 h (66%); (d) (i) H_2, $Pd(OH)_2/C$, EtOH/EtOAc, overnight, (ii) 25% aq NH_3/MeOH (4:1), rt, overnight (55%).

Scheme 5[a]

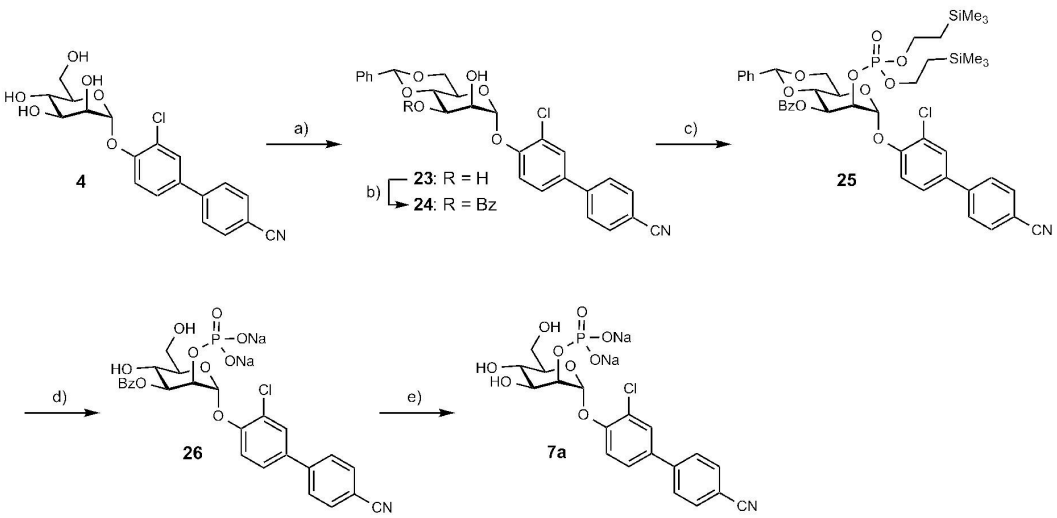

[a](a) $PhCH(OMe)_2$, *p*-TsOH, rt, 17 h (22%); (b) BzCl, DCM/pyr, 0 °C to rt, 3 h (60%); (c) bis[2-(trimethylsilyl)ethyl] *N*,*N*-diisopropylphosphoramidite, 1,2,4-triazole, MeCN, 0 °C to rt, 16 h, then 70% aq *tert*-BuOOH, rt, 1 h (55%); (d) TFA/DCM (1:4), rt, 2 h (61%); (e) 25% aq NH_3/MeOH (4:1), rt, 16 h (71%).

permeability) became the rate-limiting steps for absorption. When after rapid hydrolysis ($t_{1/2}$ < 15 min, Table 2) the active principle precipitated due to low solubility, the available amount for absorption was reduced. Although the active principles **3** and **5** show similar solubilities (Table 1), different basolateral concentrations were observed (Figure 6a,c). In contrast, the basolateral concentrations of compound **3** were similar or higher compared to those of compound **4** (Figure 6a,b) even though compound **4** has an 8-fold higher solubility (Table 1). On the basis of permeability data derived from PAMPA,[39] high passive permeability was predicted for all three antagonists (log P_e < −5.7 cm/s, Table 1).[42] However, for the antagonists **4** and **5**, efflux ratios (b−a/a−b) > 2 (Table 1) in bidirectional Caco-2 experiments were observed, indicating the involvement of an efflux transporter (e.g., P-gp).[44] Because of the high apical concentrations reached from fast ALP-mediated hydrolysis of prodrugs **7b** and **8**, saturation of the transporter mediated efflux occurred, leading to increased basolateral concentrations of **4** and **5** (Figure 6b,c). In contrast, **3** exhibited an efflux ratio <2 (Table 1), i.e., the basolateral concentration rose proportionally to the amount of applied prodrug and did not display saturation kinetics (Figure 6a).[53]

In Vivo Pharmacokinetic Studies. In the mouse PK model, an increased intestinal uptake was anticipated for the prodrug **7c** due to its increased solubility and slower hydrolysis rate. The prodrugs **7b**, **7c**, and **8** were administered per os at a dose of 10 mg/kg but could not be detected in plasma or urine samples. The oral bioavailability of active principle **4** upon administering

DOI: 10.1021/acs.jmedchem.5b01923
J. Med. Chem. 2016, 59, 3163−3182

Scheme 6[a]

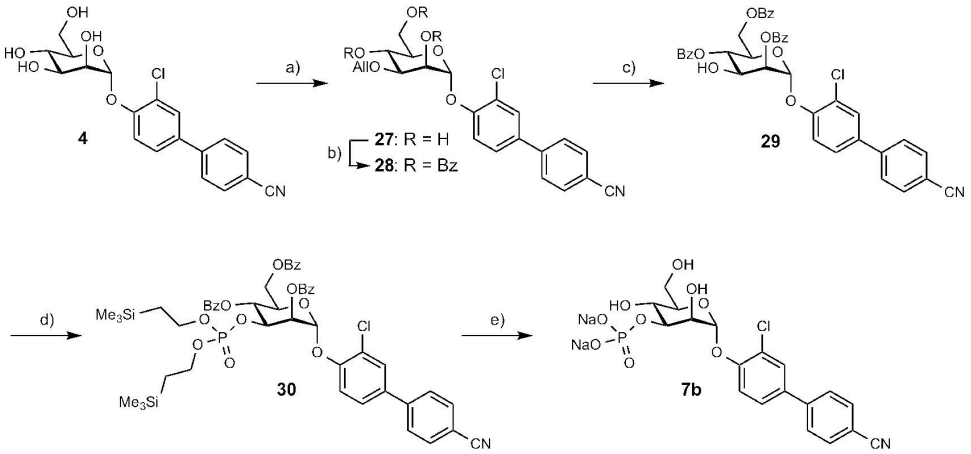

[a](a) (i) Bu_2SnO, toluene, 80 °C, 6 h, (ii) AllBr, Bu_4NI, toluene, 80 °C, 20 h (55%); (b) BzCl, cat. DMAP, pyr, rt, overnight (87%); (c) $PdCl_2$, MeOH, 40 °C, 5 h (84%); (d) (i) bis[2-(trimethylsilyl)ethyl] *N*,*N*-diisopropylphosphoramidite, 1,2,4-triazole, MeCN, 0 °C to rt, 15 h, then 70% aq *tert*-BuOOH, rt, 2 h (32%); (e) (i) TFA/DCM (1:4), rt, 1.5 h, (ii) 25% aq NH_3/MeOH (4:1), rt, overnight (45%).

Scheme 7[a]

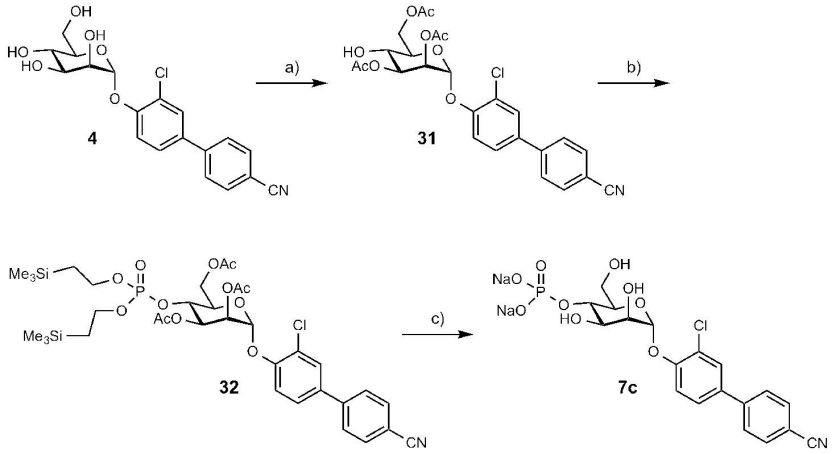

[a](a) (i) Bu_2SnO, MeOH, 70 °C, 2 h, (ii) Ac_2O, MeCN, rt, 16 h (21%); (b) (i) bis-[2-(trimethylsilyl)ethyl] *N*,*N*-diisopropylphosphoramidite, 1,2,4-triazole, MeCN, 0 °C to rt, 15 h, then 70% aq *tert*-BuOOH, rt, 2 h (62%); (c) (i) TFA/DCM (1:4), rt, 2 h; (ii) 25% aq NH_3/MeOH (4:1), rt, 2 h (98%).

prodrug **7b** and **7c** and of active principle **5** upon administration of prodrug **8** are illustrated in Figure 7. Table 3 summarizes the pharmacokinetic parameters (C_{max}, T_{max}, and urine AUC_{0-24}) of the different po applications.

Given the almost identical propensity to ALP-mediated hydrolysis of **7b** and **8**, the different urine profiles must be related to physicochemical properties of their active principles **4** and **5**. Indeed, antagonist **5**, besides having an 8-times lower solubility and therefore a higher propensity to precipitate after release in the small intestines, also permeates biological membranes less easily (shown in the PAMPA results, Table 1). In fact, urine AUC_{0-24} and C_{max} of **5** were similar to the pharmacokinetic parameters of **4** when applied at a dose of 1.25 mg/kg (Table 3).

Because prodrugs **7b** and **8** are rapidly hydrolyzed in vitro, we also assessed the impact of slower ALP-mediated bioactivation and availability of the related active principle in urine. For this purpose, we administered prodrug **7c** (in vitro $t_{1/2}$ of 43 min, Table 2) at a dose of 10 mg/kg (Figure 7). After applying **7c**, compound **4** reached C_{max} (57 μg/mL, Table 3) after only 26 min, as compared to 40.7 μg/mL at 54 min for **7b**; it then remained at elevated levels for the next 3 h. Within the observation period of 3−24 h postadministration, urine levels of the two prodrugs dropped steadily. However, at 6 h, the concentration of active principle **4** originating from prodrug **7c** was approximately three times higher than the one reached with **7b**, resulting in a 2-fold increased urine AUC_{0-24} of **7c**.

The lower concentration of active principle **4** upon po application of **7b** as compared to **7c** can be rationalized by several pharmacokinetic effects. First, the fast dephosphorylation of **7b** leads to a local accumulation of **4** at the brush border in the small intestine. Because of insufficient solubility, the active principle **4** could suffer from precipitation. Because of the slower cleavage of the promoiety in prodrug **7c**, the

DOI: 10.1021/acs.jmedchem.5b01923
J. Med. Chem. 2016, 59, 3163−3182

Scheme 8[a]

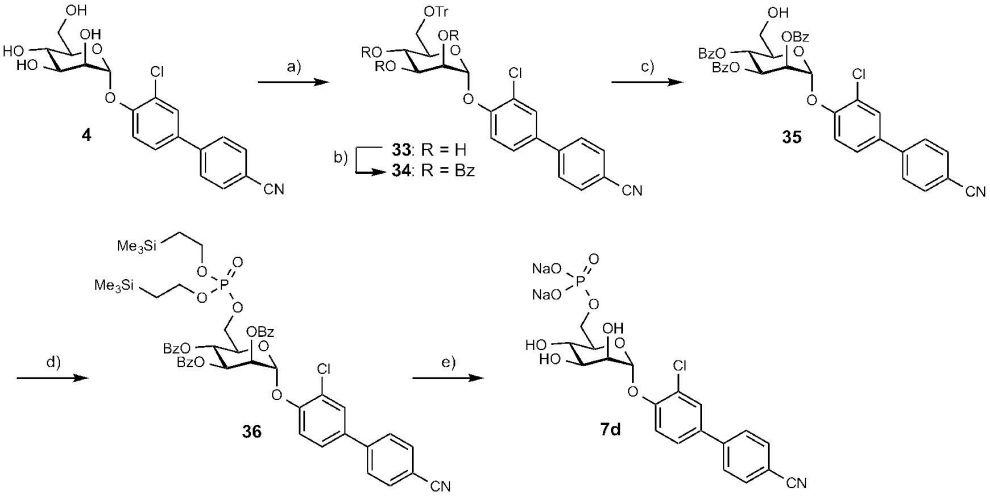

[a](a) TrCl, cat. DMAP, pyr, 80 °C, 16 h (80%); (b) BzCl, cat. DMAP, pyr, rt, 6 h (79%); (c) $FeCl_3$, H_2O, rt, 5 h (85%); (d) (i) bis-[2-(trimethylsilyl)ethyl] *N*,*N*-diisopropylphosphoramidite, 1,2,4-triazole, MeCN, 0 °C to rt, 15 h, then 70% aq *tert*-BuOOH, rt, 1.5h (59%); (e) (i) TFA/DCM (1:4), rt, 2 h, (ii) 25% aq NH_3/MeOH (4:1), rt, overnight (68%).

Scheme 9[a]

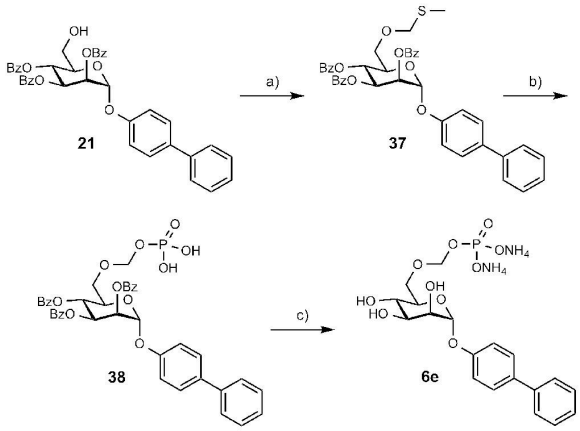

[a](a) DMSO, Ac_2O/AcOH, rt, overnight (35%); (b) H_3PO_4, NIS, THF, 0 °C to rt, 1 h (58%); (c) 25% aq NH_3/MeOH (4:1), rt, overnight (50%).

solubility limit of **4** takes longer to reach, enabling an improved absorption of the active principle. Moreover, although high concentrations of **4** saturate P-gp, its efflux activity still contributes to accumulated concentrations of **4** and consequently to precipitation and intestinal elimination. A slower prodrug hydrolysis apparently optimizes the timely interplay between parent drug uptake and P-gp-mediated efflux, leading to higher net absorption and urine concentrations.

Next, we addressed the question of whether increased solubility indeed leads to higher availability of active principle in the urine. Therefore, urine concentration profiles upon po application of 1.25 mg/kg (based on maximal solubility) or 7.7 mg/kg of **4** (applied as a suspension corresponding to 10 mg/kg of prodrug) were determined (Figure 7).

Oral application of the suspension of **4** resulted in a urine AUC_{0-24} of 106.8 μg × h/mL (C_{max} of 23.6 μg/mL, Table 3) as compared to a urine AUC_{0-24} of 226.4 μg × h/mL (C_{max} of 57 μg/mL, Table 3), achieved with the corresponding prodrug **7c**, demonstrating the beneficial effect of increased solubility on intestinal uptake. In addition, the application of **4** at two doses (1.25 and 7.7 mg/kg; 6.16 times greater) resulted in parallel curves with a similar T_{max} and an approximate difference in urine AUC_{0-24} of a factor of 5 and C_{max} of a factor of 6 (Table 3). This is a useful observation for future dose-finding in patients.

■ SUMMARY AND CONCLUSIONS

For the successful oral application of a phosphate prodrug of an active principle that displays moderate to high membrane permeability but insufficient solubility, several prerequisites need to be fulfilled. Obviously, the solubility of the prodrug should allow dissolving of the required dose (e.g., in our case 10 mg/kg). Second, because phosphate prodrugs are too polar to permeate the enterocyte layer, an efficient release of the active principle is required. Finally, slow enzymatic hydrolysis is preferred to avoid precipitation of the poorly soluble active principle.

We have demonstrated the advantages of the phosphate prodrug approach as applied to FimH antagonists with an insufficient solubility but high passive permeability. An increase in solubility of up to 140-fold could be reached upon phosphorylation of the active principle. Furthermore, either fast or slow hydrolysis was observed, depending on the position of the phosphate promoiety on the mannose ring. When the phosphate ester bond was directly linked at the C2- or C3-position of mannose (→ **6a**, **6b**, **7a**, **7b**) or when an acetal linker at C6- was used (→ **6e** and **8**), enzymatic cleavage was fast ($t_{1/2}$ < 15 min). In contrast, a phosphate at the C4- or C6-position (→ **6c**, **6d**, **7c**, and **7d**) showed an enhanced enzymatic stability ($t_{1/2}$ > 40 min).

Interestingly, even when the rates of hydrolysis were similar, e.g., for prodrugs **7b** and **8**, different physicochemical properties (solubility and permeability) of their active principles influenced the in vivo PK properties. For antagonist **5**, which

DOI: 10.1021/acs.jmedchem.5b01923
J. Med. Chem. 2016, 59, 3163−3182

Scheme 10[a]

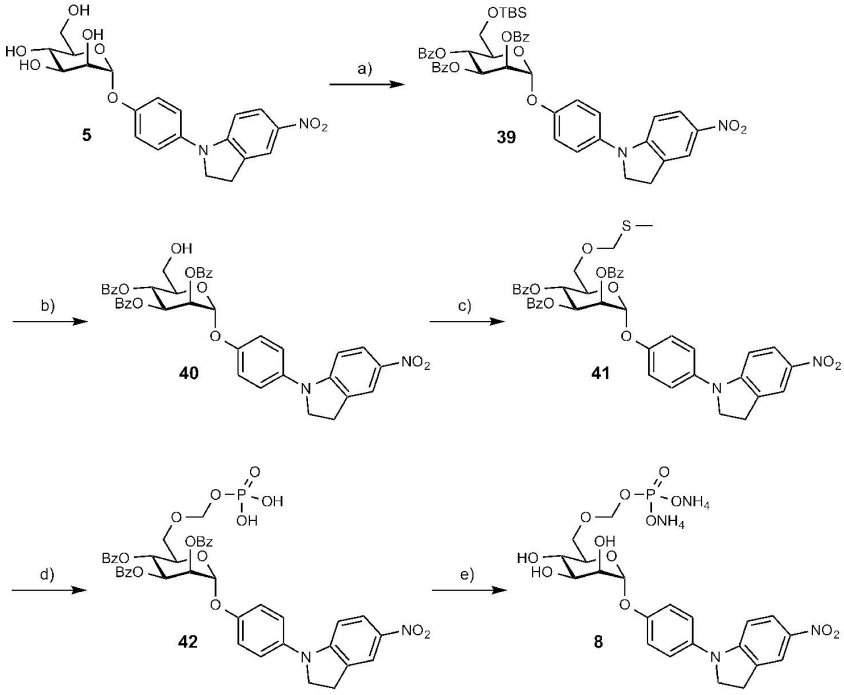

[a](a) (i) TBSCl, cat. DMAP, pyr, rt, overnight, (ii) BzCl, rt, 2 h, (quant); (b) 1 M H_2SO_4/MeOH, rt, 1.5 h (73%); (c) DMSO/Ac_2O/HOAc, rt, overnight (74%); (d) H_3PO_4/NIS/THF, 0 °C to rt, 1 h (67%); (e) 25% aq NH_3/MeOH/DCM, rt, overnight (41%).

Table 2. Aqueous Solubility and Caco-2 Phosphatase-Mediated Hydrolysis ($t_{1/2}$) of Prodrugs 6a–e, 7a–d, 8, and Their Active Principles 3–5, Respectively

compd	solubility [μg/mL]	$t_{1/2}$ [min]
3, active principle[14,18]	21	
6a	>3000	12
6b	>3000	13
6c	2703	>60
6d	>3000	>60
6e	>3000	8.7
4, active principle[19]	192	
7a	>3000	13
7b	>3000	12
7c	>3000	43
7d	>3000	48
5, active principle[20]	24	
8	>3000	11

has an 8-fold lower solubility as compared to **4**, the risk of precipitation from a supersaturated solution in the small intestines needs to be taken into account.

Furthermore, a high concentration gradient across the Caco-2 cell monolayer, as was reached with the more soluble phosphate prodrugs, promotes absorptive flux of the active principles **3**, **4**, and **5** and apparently saturates the efflux carrier activity of **4** and **5**. This observation was confirmed in an in vivo PK study in mice, where urine AUC_{0-24} of the active principle **4** could be doubled when prodrug **7c** was applied instead of active principle **4**. Moreover, in vivo administration of slowly hydrolyzed prodrug **7c** ($t_{1/2}$ < 40 min) exhibited an increase in urine AUC_{0-24} as compared to a phosphate prodrug with fast enzymatic cleavage (**7b**, $t_{1/2}$ < 15 min). Slower conversion to the active principle prolonged intestinal uptake and renal excretion by improving the interplay between solubility, drug uptake, and saturation of P-gp mediated efflux.

■ EXPERIMENTAL SECTION

Synthesis. *General Methods.* NMR spectra were recorded on a Bruker Avance DMX-500 (500.1 MHz) spectrometer. Assignment of ^1H and ^{13}C NMR spectra was achieved using 2D methods (COSY, HSQC). Chemical shifts are expressed in ppm using residual $CHCl_3$ or MeOH as references. Optical rotations were measured with a PerkinElmer polarimeter 341. Electrospray ionization mass spectrometry (ESI-MS) data were obtained on a Waters Micromass ZQ instrument. Microwave-assisted reactions were carried out with a CEM Discover and Explorer. Reactions were monitored by TLC using glass plates coated with silica gel 60 F254 (Merck) and visualized by UV light and/or by charring with a molybdate solution (0.02 M solution of ammonium cerium sulfate dihydrate and ammonium molybdate tetrahydrate in aqueous 10% H_2SO_4). Medium pressure chromatography (MPLC) separations were carried out on a CombiFlash Companion or R_f from Teledyne Isco equipped with RediSep normal-phase or RP-18 reversed-phase flash columns. Commercially available reagents were purchased from Fluka, Aldrich, or Alfa Aesar (Germany). Solvents were purchased from Sigma-Aldrich (Buchs, Switzerland) or Acros Organics (Geel, Belgium) and were dried prior to use where indicated. MeOH was dried by reflux with sodium methoxide and distilled and stored under argon atmosphere. Dichloromethane (DCM) and acetonitrile (MeCN) were dried by filtration over Al_2O_3 (Fluka, type 5016 A basic) and stored over molecular sieves under argon. Molecular sieves (4 Å) were activated in vacuo at 300 °C for 0.5 h before use.

Compound Purity. Each test compound was purified by chromatography on silica (DCM/MeOH) or reversed-phase chromatography (RP-18, H_2O/MeOH) prior to HPLC, HRMS, NMR, and

DOI: 10.1021/acs.jmedchem.5b01923
J. Med. Chem. 2016, 59, 3163–3182

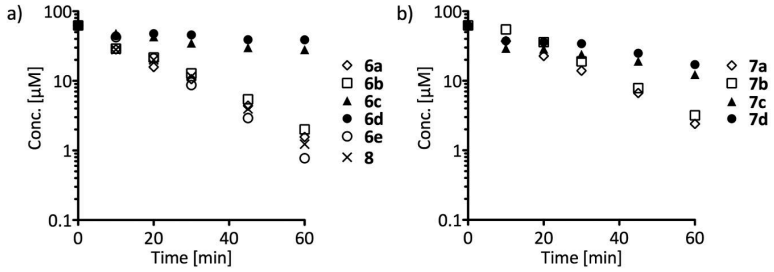

Figure 3. Decomposition of phosphomonoester prodrugs **6a–d** and **7a–d** and phosphonooxymethyl ether prodrugs **6e** and **8** in the apical compartment of the Caco-2 cell assay: (a) **6a–e**, **8**; (b) **7a–d**. Prodrugs dissolved in Dulbecco's Modified Eagle's Medium (62.5 μM) were applied to the apical chamber and the concentrations of unchanged prodrug were monitored by LC-MS.

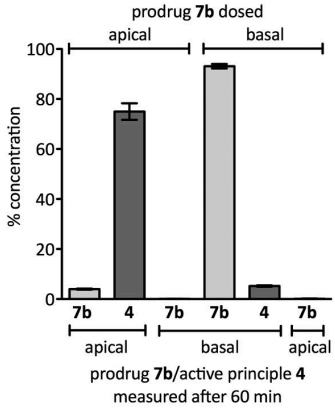

Figure 4. Conversion of prodrug **7b** to the active principle **4** in a Caco-2 cell monolayer model after 60 min of incubation. A prodrug solution (62.5 μM) was applied either into the apical or basal chamber. Columns represent the percentage concentrations of prodrug and active principle 60 min after initiation of the experiment. Concentration of prodrug **7b** determined at time point t = 0 min is defined as 100%.

activity testing. The purity of all test compounds was determined by NMR and HPLC [method A: Beckman Coulter Gold, consisting of pump 126, DAD 168 (190–410 nm) and autosampler 508; column, Waters Atlantis T3, 3 μm, 2.1 mm × 100 mm; A, H_2O + 0.1% TFA; B, MeCN + 0.1% TFA; gradient, 5% B for 0.5 min, 5% B → 70% B over 19.5 min; flow rate, 0.5 mL/min. Method B: Agilent 1100/1200 with UV detection (190–410 nm); column, Waters Atlantis T3, 3 μm, 2.1 mm × 100 mm; A, H_2O + 0.01% TFA; B, MeCN + 0.01% TFA; gradient, 5% B for 1 min, 5% B → 95% B over 19 min; flow rate, 0.5 mL/min. Detection: 254 nm.] to be ≥95% (for ^{1}H NMR spectra and HPLC traces, see Supporting Information).

General Procedure for Phosphorylation. To an ice-cooled solution (0 °C) of protected mannoside (1 equiv) and 1,2,4-triazole (4 equiv) in dry MeCN was added dibenzyl *N,N*-diisopropylphosphoramidite or bis[2-(trimethylsilyl)ethyl] *N,N*-diisopropylphosphoramidite (2 equiv), and the mixture was stirred for 30 min at 0 °C and then overnight at rt. Then, 70% aq *tert*-butylhydroperoxide (4 equiv) was added and the solution was stirred for 1 h. The reaction was quenched with 1 M aq $Na_2S_2O_3$ and 1 M aq $NaHCO_3$, and the mixture was extracted twice with DCM. The combined organic layers were dried over Na_2SO_4, filtered, and the solvents removed in vacuo. The residue was purified by MPLC on silica gel (petroleum ether/EtOAc) to yield the phosphorylated compounds.

*Biphenyl 2-O-Phosphoryl-α-D-mannopyranoside Diammonium Salt (**6a**).* Hydrogenolysis of compound **11** (100 mg, 0.129 mmol) was conducted in a Parr shaker with 10% $Pd(OH)_2/C$ (12 mg) and a catalytic amount of HOAc in EtOAc (6.0 mL) under hydrogen (4 bar) at rt overnight. Then, the reaction suspension was filtered through Celite and the filtrate was concentrated in vacuo. The residue was stirred in 25% aq NH_3 (4 mL) and MeOH (1 mL) overnight. Then, the solvents were removed under reduced pressure, and the residue was purified by MPLC on silica (DCM/MeOH/H_2O, 6:4:0.6) to give **6a** (26.0 mg, 45%) as a white solid; $[\alpha]_D^{20}$ + 66.7 (c 0.12, H_2O). ^{1}H NMR (D_2O, 500 MHz): δ = 3.77–3.82 (m, 3H, H-5, H-6), 3.87 (t, J = 10.0 Hz, 1H, H-4), 4.14 (ddd, J = 2.0, 3.0, 10.0 Hz, 1H, H-3), 4.62 (ddd, J = 2.0, 3.0, 8.5 Hz, 1H, H-2), 5.89 (d, J = 1.5 Hz, 1H, H-1), 7.31

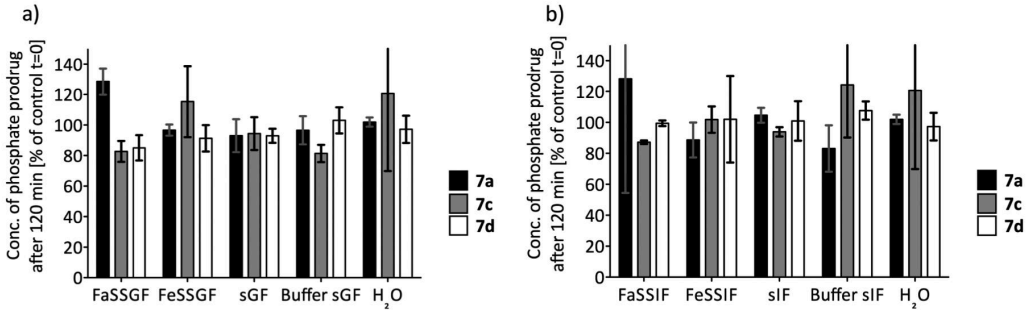

Figure 5. Stability of the phosphate prodrugs **7a** (black column), **7c** (gray column), and **7d** (white column) in biorelevant media. Percentage of the remaining compound concentration relative to the initial concentration (t = 0 min) after 120 min of incubation in (a) simulated gastric fluids (FaSSGF, fasted-state simulated gastric fluid; FeSSGF, fed-state simulated gastric fluid; sGF, simulated gastric fluid; buffer sGF, prepared equally to sGF but without pepsin) and (b) simulated intestinal fluids (FaSSIF, fasted-state simulated intestinal fluid; FeSSIF, fed-state simulated intestinal fluid; sIF, simulated intestinal fluid; buffer sIF, prepared equally to sIF but without pancreatin) are shown. For composition see Table S1 in Supporting Information. H_2O was used as a reference media. Data represent the mean (triplicates) with its corresponding standard deviation.

DOI: 10.1021/acs.jmedchem.5b01923
J. Med. Chem. 2016, 59, 3163–3182

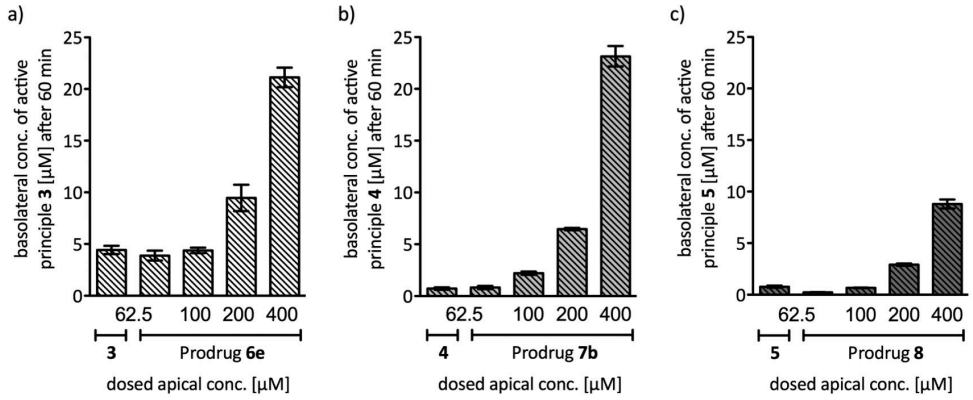

Figure 6. Accumulation of active principle (a) **3**, (b) **4**, and (c) **5** in the basal receiver chamber of a Caco-2 cell system 60 min after applying (a) active principle **3** or prodrug **6e**, (b) active principle **4** or prodrug **7b**, and (c) active principle **5** or prodrug **8** into the apical chamber. The active principles were dosed at a concentration of 62.5 μM, which corresponds to approximately the aqueous solubilities of **3** and **5**. The phosphate prodrugs were dosed at four different concentrations (62.5, 100, 200, and 400 μM).

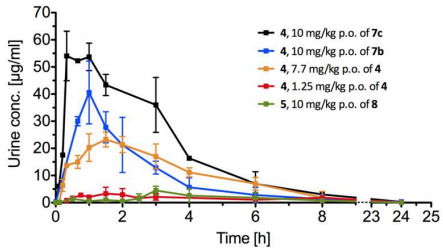

Figure 7. Urine concentrations of active principle **4** in C3H/HeN mice upon po administration of **4** (1.25 and 7.7 mg/kg po) or the related phosphate prodrugs **7b**, **7c** (10 mg/kg po) and the urine concentration of the active principle **5** upon po administration of phosphate prodrug **8** (10 mg/kg po). Shown are mean values with standard deviations for groups of three (**4**, 1.25 mg/kg, **7b**, **7c**, and **8**) or five (**4**, 7.7 mg/kg) mice.

(m, 2H, Ar-H), 7.44 (m, 1H, Ar-H), 7.55 (t, J = 7.5 Hz, 2H, Ar-H), 7.71 (m, 4H, Ar-H). ^{13}C NMR (D_2O, 126 MHz): δ = 60.5 (C-6), 66.6 (C-4), 70.1 (d, J = 5 Hz, C-3), 73.5 (C-5), 73.6 (d, J = 5 Hz, C-2), 97.0 (d, J = 3 Hz, C-1), 117.2, 117.6, 126.7, 127.4, 128.0, 128.2, 129.1, 135.3, 140.0, 155.0 (12C, Ar-C). ESI-MS: m/z: calcd for $C_{18}H_{20}O_9P$ $[M - 2NH_4 + H]^-$, 411.08; found, 411.06.

*Biphenyl 3-O-Phosphoryl-α-D-mannopyranoside Diammonium Salt (**6b**).* Hydrogenolysis of a 3:2-mixture of **15** and **16** (130 mg, 0.144 mmol) in EtOAc (6 mL) was conducted in the presence of 10% $Pd(OH)_2/C$ (15 mg) with a hydrogen balloon at rt for 5 h. Then, the reaction suspension was filtered through Celite and the filtrate was concentrated in vacuo. The residue was stirred in 25% aq NH_3 (4 mL) and MeOH (1 mL) at rt overnight. The solvents were removed under reduced pressure, and the residue was purified by MPLC on silica gel (DCM/MeOH/H_2O, 6:4:0.6) to provide **6b** (4.5 mg, 7%, still containing some of the 2-phosphate impurity) as white solid; $[\alpha]_D^{20}$ + 91.7 (c 0.12, D_2O). ^{1}H NMR (D_2O, 500 MHz): δ = 3.75−3.83 (m, 3H, H-5, H-6), 3.92 (t, J = 9.5 Hz, 1H, H-4), 4.39 (m, 1H, H-2), 4.55 (dt, J = 3.0, 9.0 Hz, 1H, H-3), 5.72 (s, 1H, H-1), 7.32 (m, 2H, Ar-H), 7.45 (m, 1H, Ar-H), 7.54 (t, J = 7.5 Hz, 2H, Ar-H), 7.71 (m, 4H, Ar-H). ^{13}C NMR (D_2O, 126 MHz): δ = 61.4 (C-6), 66.9 (d, J = 3 Hz, C-4), 70.0 (d, J = 3 Hz, C-2), 74.0 (C-5), 75.0 (d, J = 5 Hz, C-3), 98.5 (C-1), 118.1, 118.3, 127.31, 127.34, 128.0, 128.8, 129.8, 135.8, 140.6, 155.7 (12C, Ar-C). ESI-MS: m/z: calcd for $C_{18}H_{20}O_9P$ $[M - 2NH_4 + H]^-$, 411.08; found, 411.12.

*Biphenyl 4-O-Phosphoryl-α-D-mannopyranoside Diammonium Salt (**6c**).* Hydrogenolysis of **19** (80 mg, 90 μmol) was done in EtOAc (4 mL) in the presence of 10% $Pd(OH)_2/C$ (12 mg) with hydrogen balloon at rt overnight. Then the reaction suspension was filtered through Celite, and the filtrate was concentrated in vacuo to provide the debenzylated intermediate. The crude intermediate (52 mg) was stirred in MeOH (1 mL) and 25% aq NH_3 (4 mL) overnight. The solvent was removed under reduced pressure, and the residue was purified by MPLC on silica (DCM/MeOH/H_2O, 4:1:0.1) to yield **6c** (18 mg, 56%) as a white solid; $[\alpha]_D^{20}$ + 104.8 (c 0.20, H_2O). ^{1}H NMR (D_2O, 500 MHz): δ = 3.75−3.87 (m, 3H, H-5, H-6), 4.24 (m, 3H, H-2, H-3, H-4), 5.70 (s, 1H, H-1), 7.30 (d, J = 8.5 Hz, 2H, Ar-H), 7.43 (t, J = 7.5 Hz, 1H, Ar-H), 7.54 (t, J = 8.0 Hz, 2H, Ar-H), 7.70 (d, J = 8.0 Hz, 4H, Ar-H). ^{13}C NMR (D_2O, 126 MHz): δ = 60.6 (C-6), 69.6 (C-2), 69.7 (d, J = 5 Hz, C-4), 70.7 (C-3), 72.6 (d, J = 7 Hz, C-5), 97.9 (C-1), 117.6, 126.7, 127.4, 128.2, 129.1, 135.3, 140.0, 155.1 (12C, Ar-C). ESI-MS: m/z: calcd for $C_{18}H_{20}O_9P$ $[M - 2NH_4 + H]^-$, 411.08; found, 411.11.

*Biphenyl 6-O-Phosphoryl-α-D-mannopyranoside Diammonium Salt (**6d**).* Hydrogenolysis of **22** (64.0 mg, 70.0 μmol) was done in EtOAc/EtOH (5 mL, 3:2) in the presence of 10% $Pd(OH)_2/C$ (7.5 mg) with hydrogen balloon at rt overnight. The reaction suspension

Table 3. Pharmacokinetic Parameters (C_{max}, T_{max}, and Urine AUC_{0-24}) Determined after a Single po Application of Compounds 4, 7b, 7c, and 8, in Female C3H/HeN mice.[a]

parameter	4	4	7b (prodrug of 4)	7c (prodrug of 4)	8 (prodrug of 5)
dose (mg/kg) po	1.25	7.7	10	10	10
C_{max} (μg/mL)	3.9 ± 1.9	23.6 ± 3.1	40.7 ± 11.4	57.0 ± 4.2	4.5 ± 1.6
T_{max} (h)	1.4 ± 0.6	1.4 ± 0.2	0.9 ± 0.2	0.44 ± 0.2	3.0 ± 0.0
urine AUC_{0-24} (μg × h/mL)	21.5 ± 5.2	106.8 ± 18.0	103.9 ± 7.7	226.4* ± 42.8	24.6 ± 10.7

[a]Values were calculated using PKsolver and are shown as mean with standard deviation.[54] C_{max}, maximal concentration; T_{max}, time were C_{max} is reached; AUC, area under the curve. *Statistical differences at p < 0.001 (Two-Way ANOVA, Prism; GraphPad Software, version 5.0f), compared to all other po applications.

DOI: 10.1021/acs.jmedchem.5b01923
J. Med. Chem. 2016, 59, 3163−3182

was filtered through Celite, and the filtrate was concentrated in vacuo. The crude intermediate was stirred in MeOH (1 mL) and 25% aq NH_3 (4 mL) overnight. The solvents were removed under reduced pressure, and the residue was purified by MPLC on silica (DCM/MeOH/H_2O, 4:1:0.1) to yield **6d** (16.0 mg, 55%) as a white solid; $[\alpha]_D^{20}$ + 74.1 (*c* 0.16, H_2O). ^1H NMR (D_2O, 500 MHz): δ = 3.83 (m, 1H, H-5), 3.89 (ddd, *J* = 1.9, 4.9, 12.0 Hz, 1H, H-6a), 4.01 (t, *J* = 9.9 Hz, 1H, H-4), 4.08 (m, 1H, H-6b), 4.11 (dd, *J* = 3.5, 10.0 Hz, 1H, H-3), 4.21 (dd, *J* = 1.8, 3.4 Hz, 1H, H-2), 5.69 (d, *J* = 1.4 Hz, 1H, H-1), 7.28 (m, 2H, Ar-H), 7.49 (t, *J* = 7.4 Hz, 1H, Ar-H), 7.54 (t, *J* = 7.7 Hz, 2H, Ar-H), 7.70 (d, *J* = 8.7 Hz, 4H, Ar-H). ^{13}C NMR (D_2O, 126 MHz): δ = 62.6 (*J* = 4 Hz, C-6), 65.8 (C-4), 70.0, 70.1 (C-2, C-3), 72.9 (d, *J* = 8 Hz, C-5), 98.4 (C-1), 117.5, 127.4, 126.7, 128.3, 129.1, 135.3, 140.0, 155.1 (12C, Ar-C). ESI-MS: *m*/*z*: calcd for $C_{18}H_{20}O_9P$ $[M - 2NH_4 + H]^-$, 411.08; found, 411.09.

*Biphenyl 6-O-(Phosphonooxymethyl)-α-D-mannopyranoside Diammonium Salt (**6e**).* Compound **38** (110 mg, 0.146 mmol) was stirred in MeOH (1 mL) and 25% aq NH_3 (4 mL) overnight. The solvents were removed under reduced pressure, and the residue was purified by MPLC on RP-18 (H_2O/MeOH) to yield **6e** (32.3 mg, 50%) as a white solid; $[\alpha]_D^{20}$ + 75.5 (*c* 0.32, H_2O). ^1H NMR (D_2O, 500 MHz): δ = 3.85 (dd, *J* = 2.0, 11.5 Hz, 1H, H-6a), 3.88 (m, 1H, H-5), 3.93 (t, *J* = 9.5 Hz, 1H, H-4), 4.10 (dd, *J* = 3.5, 9.5 Hz, 1H, H-3), 3.97 (dd, *J* = 4.0, 11.5 Hz, 1H, H-6b), 4.22 (dd, *J* = 2.0, 3.5 Hz, 1H, H-2), 4.94 (A of ABX, *J* = 5.5, 11.0 Hz, 1H, CH_2), 5.04 (B of ABX, *J* = 5.5, 8.5 Hz, 1H, CH_2), 5.69 (d, 1.5 Hz, 1H, H-1), 7.28 (m, 2H, Ar-H), 7.44 (m, 1H, Ar-H), 7.54 (m, 2H, Ar-H), 7.69–7.72 (m, 4H, Ar-H) ^{13}C NMR (D_2O, 126 MHz): δ = 66.1 (C-4), 66.6 (C-6), 69.9 (C-2), 70.3 (C-3), 72.2 (C-5), 90.4 (d, *J* = 4 Hz, CH_2), 98.3 (C-1), 117.5, 126.7, 127.4, 128.3, 128.8, 129.1, 132.5, 135.4, 140.0, 155.0 (12C, Ar-C). ESI-MS: *m*/*z*: calcd for $C_{19}H_{22}O_{10}P$ $[M - 2NH_4 + H]^-$, 441.10; found, 440.92.

*3′-Chloro-4′-(2-O-phosphoryl-α-D-mannopyranosyloxy)-biphenyl-4-carbonitrile Disodium Salt (**7a**).* Compound **26** (34.7 mg, 56.0 μmol) was dissolved in MeOH (0.25 mL) and 25% aq NH_3 (1 mL). The mixture was stirred for 16 h at rt. The solvents were removed in vacuo, and the residue was dissolved in H_2O (0.5 mL) containing a drop of 1 M aq NaOH and purified by MPLC on RP-18 (H_2O/MeOH) to yield pure 2-phosphate **7a** (20.4 mg, 71%) as the sodium salt; $[\alpha]_D^{20}$ + 17.9 (*c* 0.78, H_2O). ^1H NMR (500 MHz, D_2O): δ = 3.70–3.82 (m, 3H, H-5, H-6), 3.92 (t, *J* = 9.8 Hz, 1H, H-4), 4.13 (dd, *J* = 3.0, 9.7 Hz, 1H, H-3), 4.66 (dt, *J* = 2.4, 8.3 Hz, 1H, H-2), 5.97 (d, *J* = 1.2 Hz, 1H, H-1), 7.40 (d, *J* = 8.7 Hz, 1H, Ar-H), 7.45–7.53 (m, 4H, Ar-H), 7.66 (d, *J* = 8.4 Hz, 2H, Ar-H). ^{13}C NMR (126 MHz, D_2O): δ = 62.0 (C-6), 68.6 (C-4), 72.3 (d, *J* = 3 Hz, C-3), 73.8 (d, *J* = 4 Hz, C-2), 99.2 (d, *J* = 5 Hz, C-1), 111.0, 118.9, 121.2, 125.5, 128.2, 128.4, 130.1, 134.4, 135.4, 144.7, 152.5 (13C, 12 Ar-C, CN). IR (KBr): ν = 3436 (vs, OH), 2230 (w, CN) cm^{-1}. ESI-MS: *m*/*z*: calcd for $C_{19}H_{18}ClNO_9P$ $[M - 2Na + H]^-$, 470.04; found, 469.96.

*3′-Chloro-4′-(3-O-phosphoryl-α-D-mannopyranosyloxy)-biphenyl-4-carbonitrile Disodium Salt (**7b**).* A solution of **30** (89.1 mg, 90 μmol) in dry DCM (2 mL) was treated with TFA (500 μL) for 1.5 h at rt under argon. Then, the mixture was evaporated to dryness in vacuo to yield the benzoylated intermediate, which was dissolved in MeOH (1 mL) and 25% aq NH_3 (4 mL). The mixture was stirred at rt overnight. The solvents were removed in vacuo, and the residue was dissolved in H_2O (1 mL) containing two drops of 1 M aq NaOH and purified by MPLC on RP-18 (H_2O/MeOH, 95:5–4:1) to yield **7b** (20.7 mg, 45%); $[\alpha]_D^{20}$ + 42.5 (*c* 0.82, H_2O). ^1H NMR (500 MHz, D_2O): δ = 3.74 (dd, *J* = 5.8, 12.4 Hz, 1H, H-6a), 3.77–3.83 (m, 2H, H-6b, H-5), 3.91 (t, *J* = 9.6 Hz, 1H, H-4), 4.43 (dd, *J* = 1.8, 3.4 Hz, 1H, H-2), 4.55 (dt, *J* = 3.4, 8.8 Hz, 1H, H-3), 5.76 (d, *J* = 1.5 Hz, 1H, H-1), 7.42 (d, *J* = 8.7 Hz, 1H, Ar-H), 7.58 (dd, *J* = 2.3, 8.7 Hz, 1H, Ar-H), 7.71 (d, *J* = 8.5 Hz, 2H, Ar-H), 7.75 (d, *J* = 2.3 Hz, 1H, Ar-H), 7.80 (d, *J* = 8.5 Hz, 2H, Ar-H). ^{13}C NMR (126 MHz, D_2O): δ = 62.2 (C-6), 68.3 (d, *J* = 3 Hz, C-4), 70.9 (d, *J* = 4 Hz, C-2), 74.9 (d, *J* = 5 Hz, C-3), 75.3 (C-5), 99.8 (C-1), 111.1, 121.2, 125.7, 128.2, 128.6, 130.3, 134.4, 135.9, 144.9, 152.5 (13C, 12 Ar-C, CN). IR (KBr): ν = 3436 (vs, OH), 2230 (w, CN) cm^{-1}. ESI-MS: *m*/*z*: calcd for $C_{19}H_{18}ClNO_9P$ $[M - 2NH_4+H]^-$, 470.04; found, 470.12.

*3′-Chloro-4′-(2,3,4-O-benzoyl-4-O-phosphoryl-α-D-mannopyranosyloxy)-biphenyl-4-carbonitrile Disodium Salt (**7c**).* Prepared according to the procedure described for **7b**. Compound **32** (37.3 mg, 27 μmol) was subsequently treated with TFA (300 μL) in DCM (1.2 mL) for 2 h, and then with MeOH (0.5 mL) and 25% aq NH_3 (2 mL) for 2 h. Purification by MPLC on RP-18 (H_2O/MeOH, 95:5–4:1) yielded **7c** (23.6 mg, 98%); $[\alpha]_D^{20}$ + 70.0 (*c* 0.81, H_2O). ^1H NMR (500 MHz, D_2O): δ = 3.64–3.71 (m, 2H, H-6a, H-5), 3.85 (dd, *J* = 4.1, 12.5 Hz, 1H, H-6b), 4.17–4.28 (m, 3H, H-3, H-2, H-4), 5.56 (s, 1H, H-1), 7.11 (d, *J* = 1.9 Hz, 1H, Ar-H), 7.16 (d, *J* = 8.7 Hz, 1H, Ar-H), 7.19 (m, 3H, Ar-H), 7.41 (d, *J* = 8.3 Hz, 2H, Ar-H). ^{13}C NMR (126 MHz, D_2O): δ = 60.7 (C-6), 69.2 (d, *J* = 5 Hz, C-4), 69.6, 70.9 (C-2, C-3), 73.3 (d, *J* = 7 Hz, C-5), 98.6 (C-1), 109.5, 117.5, 119.5, 124.1, 126.6, 128.2, 132.8, 134.0, 142.7, 151.4 (13C, 12 Ar-C, CN). IR (KBr): ν = 3433 (vs, OH), 2227 (w, CN) cm^{-1}. ESI-MS: *m*/*z*: calcd for $C_{19}H_{18}ClNO_9P$ $[M - 2Na + H]^-$, 470.04; found, 470.07.

*3′-Chloro-4′-(6-O-phosphoryl-α-D-mannopyranosyloxy)-biphenyl-4-carbonitrile Disodium Salt (**7d**).* Prepared according to the procedure described for **7b**. Compound **36** (50.8 mg, 90 μmol) was subsequently treated with TFA (400 μL) in DCM (1.6 mL) for 2 h and then with MeOH (0.5 mL) and 25% aq NH_3 (2 mL) overnight. Purification by MPLC on RP-18 (H_2O/MeOH, 95:5–4:1) yielded **7d** (18.1 mg, 68%); $[\alpha]_D^{20}$ + 40.3 (*c* 0.58, H_2O). ^1H NMR (500 MHz, D_2O): δ = 3.75 (d, *J* = 9.6 Hz, 1H, H-5), 3.81 (m, 1H, H-6a), 4.04–4.13 (m, 2H, H-4, H-6b), 4.15 (dd, *J* = 3.4, 10.1 Hz, 1H, H-3), 4.25 (dd, *J* = 1.8, 3.3 Hz, 1H, H-2), 5.66 (d, *J* = 1.4 Hz, 1H, H-1), 7.23 (d, *J* = 8.7 Hz, 1H, Ar-H), 7.33 (d, *J* = 2.3 Hz, 1H, Ar-H), 7.35–7.41 (m, 3H, Ar-H), 7.55 (d, *J* = 8.4 Hz, 2H, Ar-H). ^{13}C NMR (126 MHz, D_2O): δ = 62.8 (d, *J* = 4 Hz, C-6), 66.2 (C-4), 70.5, 70.6 (C-2, C-3), 74.2 (d, *J* = 7 Hz, C-5), 99.3 (C-1), 110.0, 118.0, 120.3, 124.6, 127.3, 129.1, 133.4, 134.5, 143.6, 152.0 (13C, 12 Ar-C, CN). IR (KBr): ν = 3436 (vs, OH), 2225 (w, CN) cm^{-1}. ESI-MS: *m*/*z*: calcd for $C_{19}H_{18}ClNO_9P$ $[M - 2Na + H]^-$, 470.04; found, 470.02.

*4-(5-Nitroindolin-1-yl)phenyl 6-O-(phosphonooxy)-methyl α-D-Mannopyranoside Diammonium Salt (**8**).* Compound **42** (278 mg, 0.337 mmol) was stirred in a mixture of MeOH (5 mL), DCM (4 mL). and 25% aq NH_3 (8 mL) overnight. The solvent was removed under reduced pressure, and the residue was purified by MPLC on RP-18 (H_2O/MeOH) to give **8** (78 mg, 41%). ^1H NMR (D_2O, 500 MHz): δ = 3.21 (t, *J* = 8.4 Hz, 2H, CH_2), 3.81 (dd, *J* = 1.8, 11.3 Hz, 1H, H-6a), 3.86 (m, 1H, H-5), 3.91 (t, *J* = 9.7 Hz, 2H, NCH_2), 3.96 (dd, *J* = 4.2, 11.3 Hz, 1H, H-6b), 4.04 (dd, *J* = 3.5, 9.6 Hz, 1H, H-3), 4.14 (t, *J* = 8.8 Hz, 2H, CH_2), 4.16 (dd, *J* = 1.8, 3.4 Hz, 1H, H-2), 4.89 (A of ABX, *J* = 5.6, 10.8 Hz, 1H, CH_2), 5.00 (B of ABX, *J* = 5.6, 8.1 Hz, 1H, CH_2), 5.60 (s, 1H, H-1), 6.86 (d, *J* = 8.9 Hz, 1H, Ar-H), 7.22 (d, *J* = 8.9 Hz, 2H, Ar-H), 7.39 (d, *J* = 8.8 Hz, 2H, Ar-H), 8.01 (s, 1H, Ar-H), 8.05 (d, *J* = 9.3 Hz, 1H, Ar-H). ^{13}C NMR (D_2O, 126 MHz): δ = 26.3 (CH_2), 53.6 (NCH_2), 66.1, 66.3 (C-4, C-6), 69.9 (C-2), 70.2 (C-3), 72.3 (C-5), 90.1 (d, *J* = 4 Hz, CH_2), 98.7 (C-1), 105.6, 118.1, 121.2, 121.9, 122.0, 127.0, 132.5, 136.6, 137.5, 151.9, 154.6 (12C, 12 Ar-C). ESI-MS: *m*/*z*: calcd for $C_{21}H_{24}N_2O_{12}P$ $[M - 2NH_4 + H]^-$, 527.11; found, 527.18.

*Biphenyl 4,6-O-Benzylidene-α-D-mannopyranoside (**9**).* To a mixture of biphenyl α-D-mannopyranoside (**1**)[14,18] (1.16 g, 3.51 mmol) and benzaldehyde dimethyl acetal (1.58 mL, 10.5 mmol) in dry MeCN/DMF (10 mL/1 mL) was added *p*-toluenesulfonic acid (40 mg). The reaction mixture was stirred at 80 °C overnight and then neutralized with satd aq $NaHCO_3$. Then the mixture was diluted with DCM (20 mL) and washed with water (2 × 10 mL) and brine (10 mL). The organic layer was dried over Na_2SO_4 and concentrated. The residue was purified by MPLC on silica (DCM/MeOH, 20:1–9:1) to afford **9** (1.03 g, 70%) as a white solid; $[\alpha]_D^{20}$ + 163.1 (*c* 1.09, $CHCl_3$/MeOH, 1:1). ^1H NMR ($CDCl_3$, 500 MHz): δ = 3.83 (t, *J* = 10.0 Hz, 1H, H-6a), 3.99 (td, *J* = 4.5, 9.5 Hz, 1H, H-5), 4.04 (t, *J* = 9.5 Hz, 1H, H-4), 4.22 (dd, *J* = 5.0, 10.0 Hz, 1H, H-6b), 4.28 (m, 1H, H-2), 4.33 (dd, *J* = 3.5, 9.5 Hz, 1H, H-3), 5.60 (s, 1H, PhC*H*), 5.66 (s, 1H, H-1), 7.13 (m, 2H, Ar-H), 7.31–7.50 (m, 8H, Ar-H), 7.55 (m, 4H, Ar-H). ^{13}C NMR ($CDCl_3$, 126 MHz): δ = 63.8 (C-5), 68.6 (C-3), 68.7 (C-6), 70.9 (C-2), 78.7 (C-4), 98.1 (C-1), 102.3 (PhCH), 116.6, 126.3, 126.8, 127.0, 128.3, 128.4, 128.8, 129.0, 129.3, 129.7, 134.5, 135.7, 137.1,

DOI: 10.1021/acs.jmedchem.5b01923
J. Med. Chem. 2016, 59, 3163–3182

140.5, 155.4 (18C, Ar-C). ESI-MS: *m/z*: calcd for $C_{25}H_{24}NaO_6$ [M + Na]$^+$, 443.15; found, 443.12.

Biphenyl 3-O-Benzyl-4,6-O-benzylidene-α-D-mannopyranoside (10). A suspension of **9** (380 mg, 0.900 mmol) and dibutyltin oxide (247 mg, 0.990 mmol) in dry toluene (6 mL) was refluxed at 135 °C for 3 h. The mixture was concentrated to dryness, and tetrabutylammonium bromide (320 mg, 0.990 mmol) and benzyl bromide (0.13 mL, 1.08 mmol) in dry toluene (6 mL) were added. The reaction mixture was stirred at 115 °C overnight, the solvent was removed under reduced pressure, and the residue was purified by MPLC on silica (petroleum ether/EtOAc, 6:1−4:1) to give **10** (370 mg, 80%) as a white solid; $[\alpha]_D^{20}$ + 139.6 (*c* 2.66, $CHCl_3$). ^{1}H NMR ($CDCl_3$, 500 MHz): δ = 3.87 (t, *J* = 10.5 Hz, 1H, H-6a), 4.01 (td, *J* = 5.0, 10.0 Hz, 1H, H-5), 4.17 (dd, *J* = 3.0, 9.5 Hz, 1H, H-3), 4.20−4.26 (m, 2H, H-6b, H-4), 4.31 (dd, *J* = 1.5, 3.0 Hz, 1H, H-2), 4.82 (d, *J* = 12.0 Hz, 1H, OC*H*$_2$Ph), 4.97 (d, *J* = 12.0 Hz, 1H, OC*H*$_2$Ph), 5.66 (s, 1H, PhC*H*), 5.69 (d, *J* = 1.0 Hz, 1H, H-1), 7.13 (m, 2H, Ar-H), 7.37−7.46 (m, 10H, Ar-H), 7.51−7.58 (m, 7H, Ar-H). ^{13}C NMR ($CDCl_3$, 126 MHz): δ = 64.0 (C-5), 68.7 (C-6), 70.0 (C-2), 73.3 (OCH_2Ph), 75.4 (C-3), 78.7 (C-4), 97.9 (C-1), 101.7 (PhCH), 116.7, 126.1, 126.8, 127.8, 127.0, 127.8, 128.0, 128.2, 128.3, 128.5, 128.7, 128.8, 128.9, 129.0, 129.7, 134.5, 135.7, 137.4, 137.9, 140.5, 155.3 (24C, Ar-C). ESI-MS: *m/z*: calcd for $C_{32}H_{30}NaO_6$ [M + Na]$^+$, 533.19; found, 533.17.

Biphenyl 2-O-Dibenzylphosphoryl-3-O-benzyl-4,6-O-benzylidene-α-D-mannopyranoside (11). According to the general procedure, compound **10** (194 mg, 0.250 mmol) was reacted with 1,2,4-triazole (69.5 mg, 1.00 mmol) and dibenzyl *N*,*N*-diisopropylphosphoramidite (90%, 187 μL, 0.500 mmol) in MeCN (3.0 mL), followed by treatment with 70% aq *tert*-butylhydroperoxide (150 μL) to yield **11** (120 mg, 62%) as a white solid; $[\alpha]_D^{20}$ + 55.3 (*c* 0.38, DCM). ^{1}H NMR ($CDCl_3$, 500 MHz): δ = 3.81 (t, *J* = 10.5 Hz, 1H, H-6a), 3.99 (td, *J* = 5.0, 10.0 Hz, 1H, H-5), 4.11 (t, *J* = 10.0 Hz, 1H, H-4), 4.22 (m, 2H, H-3, H-6b), 4.85 (m, 2H, OCH_2Ph), 5.30 (m, 1H, H-2), 5.08−5.12 (m, 4H, OCH_2Ph), 5.62 (m, 2H, H-1, PhC*H*), 7.03 (m, 2H, Ar-H), 7.26−7.58 (m, 27H, Ar-H). ^{13}C NMR ($CDCl_3$, 126 MHz): δ = 64.6 (C-5), 68.5 (C-6), 69.5 (d, *J* = 6 Hz, OCH_2Ph), 69.6 (d, *J* = 6 Hz, OCH_2Ph), 72.8 (OCH_2Ph), 73.9 (d, *J* = 5 Hz, C-3), 74.6 (d, *J* = 6 Hz, C-2), 78.2 (C-4), 97.2 (d, *J* = 3 Hz, C-1), 101.6 (PhCH), 116.8, 126.0, 126.8, 126.9, 127.0, 127.6, 127.7, 127.74, 127.85, 127.92, 128.19, 128.22, 128.3, 128.45, 128.52, 128.6, 128.7, 128.9, 135.66, 135.71, 135.76, 135.8, 135.9, 137.4, 137.5, 138.0, 140.5, 155.0 (36C, Ar-C). ESI-MS: *m/z*: calcd for $C_{46}H_{44}O_9P$ [M + H]$^+$, 771.27; found, 771.37.

Biphenyl 3-O-Benzyl-α-D-mannopyranoside (12). Biphenyl α-D-mannopyranoside (**3**, 665 mg, 2.00 mmol) and dibutyltin oxide (548 mg, 2.20 mmol) were dissolved in dry MeOH (10 mL). The mixture was refluxed for 5 h and then concentrated to dryness under reduced pressure. To a solution of the residue in dry toluene (10 mL) were added tetrabutylammonium bromide (709 mg, 2.20 mmol) and benzyl bromide (285 μL, 2.40 mmol). The mixture was stirred at 115 °C overnight and then concentrated to dryness in vacuo. The residue was purified by chromatography on silica (petroleum ether/EtOAc, 4:1−1:3) to yield **12** (306 mg, 36%) as a white solid; $[\alpha]_D^{20}$ + 99.8 (*c* 1.38, $CHCl_3$). ^{1}H NMR ($CDCl_3$, 500 MHz): δ = 3.00 (s, 3H, 2,4,6-OH), 3.71 (m, 2H, H-5, H-6a), 3.81 (m, 1H, H-6b), 3.96 (dd, *J* = 3.0, 9.5 Hz, 1H, H-3), 4.17 (m, 2H, H-2, H-4), 4.70 (d, *J* = 11.5 Hz, 1H, OCH_2Ph), 4.79 (d, *J* = 11.5 Hz, 1H, OCH_2Ph), 5.65 (d, *J* = 1.5 Hz, 1H, H-1), 7.10 (m, 2H, Ar-H), 7.31−7.44 (m, 8H, Ar-H), 7.50−7.52 (m, 4H, Ar-H). ^{13}C NMR ($CDCl_3$, 126 MHz): δ = 61.5 (C-6), 65.5 (C-4), 67.9 (C-2), 72.3 (OCH_2Ph), 72.8 (C-5), 79.4 (C-3), 97.7 (C-1), 116.6, 126.8, 126.9, 128.26, 128.29, 128.3, 128.7, 128.8, 135.6, 137.4, 140.5, 155.4 (18C, Ar-C). ESI-MS: *m/z*: calcd for $C_{25}H_{26}NaO_6$ [M + Na]$^+$, 445.16; found, 445.14.

Biphenyl 2,4,6-Tri-O-benzoyl-3-O-benzyl-α-D-mannopyranoside (13). To a solution of **12** (306 mg, 0.724 mmol) in pyridine (5 mL) were added benzoyl chloride (400 μL, 3.43 mmol) and DMAP (5 mg). The reaction mixture was stirred at rt overnight then quenched with MeOH (0.5 mL) and concentrated under reduced pressure. The residue was purified by MPLC on silica (petroleum ether/EtOAc, 4:1−3:1) to yield **13** (499 mg, 99%) as a white solid; $[\alpha]_D^{20}$ + 7.1 (*c* 1.52, $CHCl_3$). ^{1}H NMR ($CDCl_3$, 500 MHz): δ = 4.40−4.46 (m, 3H, H-6a, H-3, H-5), 4.62−4.65 (m, 2H, OCH_2Ph, H-6b), 4.79 (d, *J* = 12.4 Hz, 1H, OCH_2Ph), 5.80 (d, *J* = 2.0 Hz, 1H, H-1), 5.91 (dd, *J* = 2.0, 3.0 Hz, 1H, H-2), 5.97 (t, *J* = 9.7 Hz, 1H, H-4), 7.12−7.23 (m, 7H, Ar-H), 7.34 (m, 3H, Ar-H), 7.42−7.54 (m, 11H, Ar-H), 7.61 (m, 2H, Ar-H), 8.03 (m, 4H, Ar-H), 8.16 (m, 2H, Ar-H).^{13}C NMR ($CDCl_3$, 126 MHz): δ = 63.0 (C-6), 68.0 (C-4), 68.5 (C-5), 69.6 (C-2), 71.3 (OCH_2Ph), 74.1 (C-3), 96.3 (C-1), 116.9, 126.8, 127.0, 127.7, 127.9, 128.2, 128.26, 128.28, 128.4, 128.5, 128.7, 129.3, 129.4, 129.7, 129.8, 129.9, 130.0, 132.9, 133.3, 133.4, 135.9, 137.3, 140.3, 155.2 (36C, Ar-C), 165.4, 165.7, 166.1 (3 CO). ESI-MS: *m/z*: calcd for $C_{46}H_{38}NaO_9$ [M + Na]$^+$, 757.24; found, 757.29.

Biphenyl 2,4,6-Tri-O-benzoyl-α-D-mannopyranoside (14). Hydrogenolysis of **13** (499 mg, 0.679 mmol) was conducted in dioxane/EtOAc (6 mL, 5:1) in the presence of 10% Pd(OH)$_2$/C (50 mg) and a catalytic amount of AcOH in a Parr shaker under hydrogen (4 bar) at rt overnight. The reaction suspension was filtered through Celite, and the filtrate was concentrated in vacuo. The residue was purified by MPLC on silica (petroleum ether/EtOAc, 9:1−4:1) to give **14** (314 mg, 73%) as colorless syrup; $[\alpha]_D^{20}$ + 56.5 (*c* 1.02, $CHCl_3$). ^{1}H NMR ($CDCl_3$, 500 MHz): δ = 2.58 (d, *J* = 8.0 Hz, 1H, 3-OH), 4.48 (m, 2H, H-5, H-6a), 4.64 (m, 2H, H-3, H-6b), 5.66 (dd, *J* = 2.0, 3.5 Hz, 1H, H-2), 5.77 (t, *J* = 9.5 Hz, 1H, H-4), 5.82 (d, *J* = 2.0 Hz, 1H, H-1), 7.31−7.35 (m, 3H, Ar-H), 7.22 (m, 2H-Ar-H), 7.42−7.53 (m, 11H, Ar-H), 7.61 (m, 2H, Ar-H), 7.97 (dd, *J* = 1.0, 8.0 Hz, 2H, Ar-H), 8.10 (m, 4H, Ar-H). ^{13}C NMR ($CDCl_3$, 126 MHz): δ = 63.0 (C-6), 69.0, 69.2 (C-5, C-3), 72.6 (C-2), 70.2 (C-4), 95.7 (C-1), 116.8, 126.8, 127.0, 128.3, 128.4, 128.6, 128.8, 129.1, 129.0, 129.7, 129.9, 130.0, 133.1, 133.69, 133.73, 136.0, 140.4, 155.2 (30C, Ar-C), 165.9, 166.1, 166.8 (3 CO). ESI-MS: *m/z*: calcd for $C_{39}H_{32}NaO_9$ [M + Na]$^+$, 667.19; found, 667.29.

Biphenyl 2,4,6-Tri-O-benzoyl-3-dibenzylphosphoryl-α-D-mannopyranoside (15). According to the general procedure, compound **14** (211 mg, 0.335 mmol) was reacted with 1,2,4-triazole (92.5 mg, 1.34 mmol) and dibenzyl *N*,*N*-diisopropylphosphoramidite (90%, 250 μL, 0.670 mmol) in MeCN (5 mL), followed by treatment with 70% aq *tert*-butylhydroperoxide (190 μL, 1.34 mmol) to yield **15** and the 2-phosphoryl derivative **16** (245 mg, 80%) as an inseparable 3:2 mixture.

Analytical data for **15**: ^{1}H NMR ($CDCl_3$, 500 MHz): δ = 4.62 (m, 2H, H-5, H-6a), 4.76 (dd, *J* = 7.5, 12.0 Hz, 1H, H-6b), 4.85−5.11 (m, 4H, OCH_2Ph), 5.55 (td, *J* = 3.5, 9.0 Hz, 1H, H-3), 5.81 (d, *J* = 1.5 Hz, 1H, H-1), 5.87 (dd, *J* = 1.9, 3.4 Hz, 1H, H-2), 6.04 (m, 1H, H-4), 6.92−8.11 (m, 34H, Ar-H). ^{13}C NMR ($CDCl_3$, 126 MHz): δ = 62.8 (C-5), 67.6 (d, *J* = 6 Hz, C-4), 69.5 (C-6), 69.8 (d, *J* = 5.6 Hz, *C*H$_2$Ph), 71.0 (d, *J* = 2 Hz, C-2), 69.8 (d, *J* = 6 Hz, *C*H$_2$Ph), 73.7 (d, *J* = 5 Hz, C-3), 95.7 (C-1), 116.8, 126.8, 127.6, 127.7, 127.9, 128.0, 128.20, 128.23, 128.27, 128.32, 128.4, 128.50, 128.54, 128.57, 128.62, 129.7, 129.9, 130.0, 133.0, 133.5, 133.6, 136.1, 140.3, 155.1 (42C, Ar-C), 165.3, 165.5, 166.0 (3 CO). ESI-MS: *m/z*: calcd for $C_{53}H_{45}NaO_{12}P$ [M + Na]$^+$, 927.25; found, 927.23.

Analytical data for **16**: ^{1}H NMR ($CDCl_3$, 500 MHz): δ = 4.62 (m, 1H, H-6a), 4.51 (m, 1H, H-5), 4.42 (m, 1H, H-6b), 4.85−5.11 (m, 4H, OCH_2Ph), 5.20 (m, 1H, H-2), 5.66 (d, *J* = 1.5 Hz, 1H, H-1), 5.95 (td, *J* = 2.7, 10.0 Hz, 1H, H-3), 6.04 (m, 1H, H-4), 6.92−8.11 (m, 34H, Ar-H). ESI-MS: *m/z*: calcd for $C_{53}H_{45}NaO_{12}P$ [M + Na]$^+$, 927.25; found, 927.23.

Biphenyl 2,3-Di-O-benzoyl-4,6-O-benzylidene-α-D-mannopyranoside (17). To a solution of compound **9** in pyridine (5 mL) were added benzoyl chloride (0.33 mL, 2.84 mmol) and DMAP (5 mg). The mixture was stirred at rt overnight and then concentrated under reduced pressure. The residue was purified by MPLC on silica (petroleum ether/EtOAc, 6:1−4:1) to provide **17** (270 mg, 60%) as a white solid; $[\alpha]_D^{20}$ + 21.8 (*c* 1.08, $CHCl_3$). ^{1}H NMR ($CDCl_3$, 500 MHz): δ = 4.00 (t, *J* = 9.5 Hz, 1H, H-6a), 4.32−4.38 (m, 2H, H-6b, H-5), 4.48 (t, *J* = 9.5 Hz, 1H, H-4), 5.73 (s, 1H, PhC*H*), 5.82 (d, *J* = 1.5 Hz, 1H, H-1), 5.97 (dd, *J* = 1.5, 3.5 Hz, 1H, H-2), 6.10 (dd, *J* = 3.5, 10.5 Hz, 1H, H-3), 7.25 (m, 2H, Ar-H), 7.35−7.39 (m, 6H, Ar-H), 7.45−7.61 (m, 11H, Ar-H), 7.68 (t, *J* = 7.5 Hz, 1H, Ar-H), 7.99 (m, 2H, Ar-H), 8.17 (m, 2H, Ar-H). ^{13}C NMR ($CDCl_3$, 126 MHz): δ = 64.6 (C-5), 68.7 (C-6), 68.8 (C-3), 70.8 (C-2), 76.6 (C-4), 96.7 (C-1), 102.0 (PhCH), 116.8, 126.1, 126.9, 127.0, 128.2, 128.25, 128.3, 128.4,

DOI: 10.1021/acs.jmedchem.5b01923
J. Med. Chem. 2016, 59, 3163−3182

128.6, 128.7, 129.0, 129.3, 129.6, 129.8, 129.9, 130.1, 133.1, 133.6, 136.0, 136.9, 140.5, 155.1 (30C, Ar-C), 165.36, 165.45 (2 CO). ESI-MS: m/z: calcd for $C_{39}H_{32}NaO_8$ $[M + Na]^+$, 651.20; found, 651.17.

*Biphenyl 2,3-Di-O-benzoyl-6-O-benzyl-α-D-mannopyranoside (**18**).* To a solution of **17** (270 mg, 0.429 mmol) in dry THF (4 mL) were added $Me_3N{\cdot}BH_3$ (125 mg, 1.72 mmol) and $AlCl_3$ (341 mg, 2.56 mmol). After 15 min, H_2O (15.5 μL) was added and the reaction mixture was stirred at rt for 45 min. The reaction was quenched with 1 M aq HCl, diluted with DCM (20 mL), and washed with water (10 mL) and brine (10 mL). The combined organic layers were dried over Na_2SO_4. The solvent was removed under reduced pressure and the residue purified by MPLC on silica (petroleum ether/EtOAc, 6:1−3:1) to afford **18** (178 mg, 67%) as a white solid; $[\alpha]_D^{20}$ + 10.8 (*c* 1.21, $CHCl_3$). ^{1}H NMR ($CDCl_3$, 500 MHz): δ = 3.85 (dd, *J* = 4.0, 11.0 Hz, 1H, H-6a), 3.97 (dd, *J* = 4.5, 11.0 Hz, 1H, H-6b), 4.14 (m, 1H, H-5), 4.53 (t, *J* = 10.0 Hz, 1H, H-4), 4.59 (d, *J* = 12.0 Hz, 1H, OCH_2Ph), 4.70 (d, *J* = 12.0 Hz, 1H, OCH_2Ph), 5.79 (d, *J* = 1.5 Hz, 1H, H-1), 5.81 (dd, *J* = 1.5, 3.0 Hz, 1H, H-2), 5.85 (dd, *J* = 3.5, 9.5 Hz, 1H, H-3), 7.24 (m, 2H, Ar-H), 7.33−7.39 (m, 7H, Ar-H), 7.42−7.48 (m, 5H, Ar-H), 7.54−7.57 (m, 5H, Ar-H), 7.62 (t, *J* = 7.5 Hz, 1H, Ar-H), 7.98 (m, 2H, Ar-H), 8.10 (m, 2H, Ar-H). ^{13}C NMR ($CDCl_3$, 126 MHz): δ = 67.4 (C-4), 69.8 (C-6), 70.3 (C-2), 72.0 (C-5), 72.6 (C-3), 73.7 (OCH_2Ph), 96.0 (C-1), 116.8, 126.9, 127.0, 127.6, 127.7, 128.3, 128.4, 128.6, 128.7, 129.88, 129.92, 133.4, 133.5, 135.9, 137.9, 140.5, 155.4 (30C, Ar-C), 165.5, 166.7 (2 CO). ESI-MS: m/z: calcd for $C_{39}H_{34}NaO_8$ $[M + Na]^+$, 653.22; found, 653.25.

*Biphenyl 4-O-Dibenzylphosphoryl-2,3-di-O-benzoyl-6-O-benzyl-α-D-mannopyranoside (**19**).* According to the general procedure, compound **18** (160 mg, 0.253 mmol) was reacted with 1,2,4-triazole (70.0 mg, 1.01 mmol) and dibenzyl *N*,*N*-diisopropylphosphoramidite (90%, 190 μL, 0.510 mmol) in MeCN (2 mL), followed by treatment with 70% aq *tert*-butylhydroperoxide (200 μL) to yield **19** (120 mg, 53%) as a glassy solid; $[\alpha]_D^{20}$ + 29.2 (*c* 1.18, $CHCl_3$). ^{1}H NMR ($CDCl_3$, 500 MHz): δ = 3.85 (dd, *J* = 1.5, 11.0 Hz, 1H, H-6a), 3.94 (dd, *J* = 4.0, 11.5 Hz, 1H, H-6b), 4.24 (m, 1H, H-5), 4.56 (s, 2H, OCH_2Ph), 4.63 (dd, *J* = 8.5, 12.0 Hz, 1H, OCH_2Ph), 4.74 (dd, *J* = 7.0, 12.0 Hz, 1H, OCH_2Ph), 4.81 (dd, *J* = 8.5, 12.0 Hz, 1H, OCH_2Ph), 4.88 (dd, *J* = 7.5, 12.0 Hz, 1H, OCH_2Ph), 5.43 (q, *J* = 9.5 Hz, 1H, H-4), 5.79 (d, *J* = 2.0 Hz, 1H, H-1), 5.85 (dd, *J* = 2.0, 3.0 Hz, 1H, H-2), 6.04 (dd, *J* = 3.5, 10.0 Hz, 1H, H-3), 6.92 (m, 2H, Ar-H), 7.11−7.61 (m, 28H, Ar-H), 7.99 (dd, *J* = 1.0, 8.5 Hz, 2H, Ar-H), 8.04 (dd, *J* = 1.0, 8.0 Hz, 2H, Ar-H). ^{13}C NMR ($CDCl_3$, 126 MHz): δ = 68.4 (C-6), 69.2 (d, *J* = 5 Hz, OCH_2Ph), 69.3 (d, *J* = 6 Hz, OCH_2Ph), 70.3 (C-2), 70.5 (d, *J* = 2 Hz, C-3), 71.4 (d, *J* = 6 Hz, C-5), 71.6 (d, *J* = 6 Hz, C-4), 73.4 (OCH_2Ph), 95.8 (C-1), 116.9, 126.9, 127.0, 127.39, 127.43, 127.45, 127.5, 127.7, 127.9, 128.2, 128.27, 128.32, 128.36, 128.40, 128.5, 128.6, 128.7, 129.4, 130.0, 133.2, 133.5, 135.3, 135.4, 135.5, 135.6, 136.0, 138.3, 140.5, 155.4 (42C, Ar-C), 165.4, 165.5 (2 CO). ESI-MS: m/z: calcd for $C_{53}H_{47}NaO_{11}P$ $[M + Na]^+$, 913.28; found, 913.31.

*Biphenyl 2,3,4-Tri-O-benzoyl-6-O-trityl-α-D-mannopyranoside (**20**).* To a solution of **3** (414 mg, 1.24 mmol) in pyridine were added trityl chloride (417 mg, 1.49 mmol) and DMAP (10 mg). The mixture was stirred at 80 °C overnight and then cooled to rt. Then, benzoyl chloride (50 μL, 4.92 mmol) was added and the mixture was stirred at 50 °C overnight. The mixture was diluted with DCM (50 mL) and washed with 0.1 M aq HCl (20 mL) and satd aq $NaHCO_3$ (20 mL). The organic layer was dried over Na_2SO_4, filtered, and the solvent removed in vacuo. The residue was purified by MPLC on silica (petroleum ether/EtOAc, 6:1−4:1) to give **20** (1.35 g, 88%), which contained some perbenzoylated substance as impurity but was used in the next step without a second purification.

*Biphenyl 2,3,4-Tri-O-benzoyl-α-D-mannopyranoside (**21**).* To a solution of **20** (1.35 g, 1.52 mmol) in dry DCM were added anhydrous $FeCl_3$ (493 mg, 3.04 mmol) and distilled water (3.28 mL, 18.2 mmol). The mixture was stirred at rt for 5 h. Then, the mixture was diluted with DCM (50 mL) and washed with water (30 mL). The organic layer was dried over Na_2SO_4, filtered, and the solvent removed in vacuo. The residue was purified by MPLC on silica (petroleum ether/EtOAc) to yield **21** (608 mg, 62%); $[\alpha]_D^{20}$ −1.8 (*c* 0.75, DCM). ^{1}H NMR ($CDCl_3$, 500 MHz): δ = 2.70 (dd, *J* = 6.0, 8.4 Hz, 1H, 6-OH), 3.76 (ddd, *J* = 3.3, 5.9, 13.0 Hz, 1H, H-6a), 3.85 (ddd, *J* = 2.0, 8.5, 12.8 Hz, 1H, H-6a), 4.21 (dt, *J* = 2.6, 10.1 Hz, 1H, H-5), 5.90 (d, *J* = 1.7 Hz, 1H, H-1), 5.91 (dd, *J* = 1.9, 3.3 Hz, 1H, H-2), 5.98 (t, *J* = 10.1 Hz, 1H, H-4), 6.25 (dd, *J* = 3.4, 10.1 Hz, 1H, H-3), 7.26−7.35 (m, 5H, Ar-H), 7.39−7.48 (m, 5H, Ar-H), 7.51−7.59 (m, 7H, Ar-H), 7.65 (m, 1H, Ar-H), 7.88 (m, 2H, Ar-H), 8.01 (m, 2H, Ar-H), 8.15 (m, 2H, Ar-H). ^{13}C NMR ($CDCl_3$, 126 MHz): δ = 61.2 (C-6), 67.1 (C-4), 69.5 (C-3), 70.5 (C-2), 71.8 (C-5), 96.1 (C-1), 116.8, 127.0, 127.1, 128.4, 128.5, 128.6, 128.8, 128.9, 129.1, 129.2, 129.8, 130.0, 130.1, 133.4, 133.8, 133.9, 136.2, 140.5, 155.4 (30C, Ar-C), 165.6, 165.7, 166.7 (3 CO). ESI-MS: m/z: calcd for $C_{39}H_{32}NaO_9$ $[M + Na]^+$, 667.19; found, 667.22.

*Biphenyl 6-O-Dibenzylphosphoryl-2,3,4-tri-O-benzoyl-α-D-mannopyranoside (**22**).* According to the general procedure, compound **21** (107 mg, 0.158 mmol) was reacted with 1,2,4-triazole (44.0 mg, 0.632 mmol) and dibenzyl *N*,*N*-diisopropylphosphoramidite (90%, 120 μL, 0.316 mmol) in MeCN (2 mL), followed by treatment with 70% aq *tert*-butylhydroperoxide (86 μL, 0.632 mmol) to yield **22** (94.4 mg, 66%) as a glassy solid; $[\alpha]_D^{20}$ −0.7 (*c* 0.28, DCM). ^{1}H NMR ($CDCl_3$, 500 MHz): δ = 4.27 (m, 2H, H-6), 4.46 (m, 1H, H-5), 4.93−5.02 (m, 4H, OCH_2Ph), 5.80 (d, *J* = 1.7 Hz 1H, H-1), 5.90 (dd, *J* = 2.0, 3.1 Hz, 1H, H-2), 6.07 (t, *J* = 10.0 Hz, 1H, H-4), 6.13 (dd, *J* = 3.3, 10.0 Hz, 1H, H-3), 7.19−7.63 (m, 18H, Ar-H), 7.89 (m, 2H, Ar-H), 7.98 (m, 2H, Ar-H), 8.15 (m, 2H, Ar-H). ^{13}C NMR ($CDCl_3$, 126 MHz): δ = 65.8 (d, *J* = 5 Hz, C-6), 66.4 (C-4), 69.4 (d, *J* = 4 Hz, OCH_2Ph), 69.5 (d, *J* = 4 Hz, OCH_2Ph), 69.9 (C-3), 70.3 (d, *J* = 8 Hz, C-5), 70.4 (C-2), 96.1 (C-1), 117.0, 127.0, 127.1, 127.8, 128.0, 128.4, 128.45, 128.46, 128.5, 128.6, 133.4, 133.7, 135.7, 135.8, 136.3, 140.4, 155.5 (42C, Ar-C), 165.4, 165.5, 165.6 (3 CO). ESI-MS: m/z: calcd for $C_{53}H_{45}NaO_{12}P$ $[M + Na]^+$, 927.25; found, 927.23.

*4′-(4,6-O-Benzylidene-α-D-mannopyranosyloxy)-3′-chloro-biphenyl-4-carbonitrile (**23**).* To a solution of **4**[19] (500 mg, 1.28 mmol) in anhydrous DMF (20 mL) were added benzaldehyde dimethyl acetal (575 μL, 3.83 mmol) and *p*-toluenesulfonic acid (20 mg). The mixture was stirred at 50 °C overnight. Then, the reaction mixture was neutralized with satd aq $NaHCO_3$ (10 mL), diluted with DCM (30 mL), and washed with water (3 × 10 mL) and brine (10 mL). The organic layer was dried over Na_2SO_4, filtered, and the solvents removed in vacuo. The residue was purified by MPLC on silica (DCM/MeOH, 1:0−5:1, + 0.5% NEt_3) to yield **23** (132 mg, 22%); $[\alpha]_D^{20}$ + 62.3 (*c* 0.59, $CHCl_3$/MeOH, 1:1). ^{1}H NMR (500 MHz, $CDCl_3$): δ = 3.76 (t, *J* = 10.2 Hz, 1H, H-6a), 3.91 (td, *J* = 4.8, 9.8 Hz, 1H, H-5), 3.99 (t, *J* = 9.4 Hz, 1H, H-4), 4.14 (dd, *J* = 4.8, 10.3 Hz, 1H, H-6a), 4.28−4.33 (m, 2H, H-2, H-3), 5.53 (s, 1H, PhC*H*), 5.62 (s, 1H, H-1), 7.19 (m, 1H, Ar-H), 7.29−7.31 (m, 3H, Ar-H), 7.38 (m, 1H, Ar-H), 7.40−7.44 (m, 2H, Ar-H), 7.54−7.58 (m, 3H, Ar-H), 7.63−7.67 (m, 2H, Ar-H). ^{13}C NMR (126 MHz, $CDCl_3$): δ = 64.2 (C-5), 68.5, 70.6 (3C, C-2, C-3, C-6), 78.4 (C-4), 98.7 (C-1), 102.4 (PhCH), 111.2, 116.8, 118.7, 124.6, 126.2, 126.6, 127.4, 128.4, 132.5, 143.7, 151.8 (19 C, 18 Ar-C, CN). ESI-MS: m/z: calcd for $C_{33}H_{26}ClNNaO_7$ $[M + Na]^+$, 502.90; found, 502.04.

*4′-(3-O-Benzoyl-4,6-O-benzylidene-α-D-mannopyranosyloxy)-3′-chloro-biphenyl-4-carbonitrile (**24**).* To a solution of **23** (131 mg, 0.275 μmol) in DCM/pyridine (6 mL, 5:1) was added dropwise over 30 min a 0.1 M benzoyl chloride solution in dry DCM (2.8 mL, 0.280 mmol) at 0 °C under argon. The mixture was stirred another 30 min at 0 °C, then the ice-bath was removed and stirring continued for 2 h at rt. Then, the mixture was diluted with DCM (10 mL) and washed with 0.1 M aq HCl (5 mL) and satd aq $NaHCO_3$ (10 mL). The organic layer was dried with Na_2SO_4, filtered, and concentrated. The residue was purified by MPLC on silica (petroleum ether/EtOAc, + 0.5% NEt_3) to yield **24** (96.8 mg, 60%); $[\alpha]_D^{20}$ + 113.8 (*c* 1.02, DCM). ^{1}H NMR (500 MHz, $CDCl_3$): δ = 3.91 (t, *J* = 10.2 Hz, 1H, H-6a), 4.17 (td, *J* = 4.9, 9.7 Hz, 1H, H-5), 4.24 (dd, *J* = 4.8, 10.2 Hz, 1H, H-6b), 4.45 (t, *J* = 9.9 Hz, 1H, H-4), 4.65 (dd, *J* = 1.6, 3.2 Hz, 1H, H-2), 5.64 (s, 1H, PhC*H*), 5.70 (d, *J* = 1.2 Hz, 1H, H-1), 7.25−7.34 (m, 4H, Ar-H), 7.37−7.47 (m, 5H, Ar-H), 7.51−7.60 (m, 4H, Ar-H), 7.51−7.60 (m, 2H, Ar-H), 8.06−8.11 (m, 2H, Ar-H). ^{13}C NMR (126 MHz, $CDCl_3$): δ = 65.1 (C-5), 68.4 (C-6), 69.1 (C-2), 71.2 (C-3), 75.6 (C-

DOI: 10.1021/acs.jmedchem.5b01923
J. Med. Chem. 2016, 59, 3163−3182

4), 99.1 (C-1), 101.8 (PhCH), 110.8, 116.9, 118.6, 124.8, 126.0, 126.3, 127.2, 128.1, 128.3, 132.6, 133.2, 136.9, 143.5, 151.6 (25C, 24 Ar-C, CN), 165.7 (CO). IR (KBr): ν = 3437 (vs, OH), 2227 (m, CN), 1721 (vs, C═O) cm^{-1}. ESI-MS: m/z: calcd for $C_{33}H_{26}ClNNaO_7$ $[M + Na]^+$, 606.13; found, 606.11.

*4′-(3-O-Benzoyl-4,6-O-benzylidene-2-O-bis[2-(trimethylsilyl)-ethoxy]phosphoryl-α-D-mannopyranosyloxy)-3′-chloro-biphenyl-4-carbonitrile (**25**).* According to the general procedure, compound **24** (96.8 mg, 0.166 mmol) was reacted with 1,2,4-triazole (45.8 mg, 0.663 mmol) and bis[2-(trimethylsilyl)ethyl] *N,N*-diisopropylphosphoramidite (136 μL, 0.331 mmol) in MeCN (3.0 mL), followed by treatment with 70% aq *tert*-butylhydroperoxide (91 μL, 0.663 mmol) to yield **25** (79.6 mg, 55%) as a 4:1-mixture of 2- and 3-phosphorylated isomers. ^1H NMR (500 MHz, $CDCl_3$): δ = −0.09, −0.02 (2s, 18H, 2 $Si(CH_3)_3$), 0.92−01.06 (m, 4H, 2 $SiCH_2$), 3.87 (td, J = 4.5, 10.1 Hz, 1H, H-6a), 4.12 (m, 6H, H-5, H-6b, 2 OCH_2), 4.36 (t, J = 9.9 Hz, 1H, H-4), 5.17 (ddd, J = 1.7, 3.1, 9.1 Hz, 1H, H-2), 5.63 (s, 1H, PhC*H*), 5.81 (m, 1H, H-3), 5.84 (d, J = 1.5 Hz, 1H, H-1), 7.22−7.33 (m, 4H, Ar-H), 7.37−7.45 (m, 4H, Ar-H), 7.46−7.56 (m, 2H, Ar-H), 7.57−7.64 (m, 3H, Ar-H), 7.66−7.71 (m, 2H, Ar-H), 8.08−8.14 (m, 2H, Ar-H). ^{13}C NMR (126 MHz, $CDCl_3$): δ = −1.7, −1.6 (6C, $Si(CH_3)_3$), 19.4 (d, J = 5 Hz, 2C, 2 $SiCH_2$), 65.2 (C-5), 66.9 (t, J = 6 Hz, 2C, 2 OCH_2), 68.4 (C-6), 69.1 (d, J = 5 Hz, C-3), 73.2 (d, J = 5 Hz, C-2), 75.4 (C-4), 97.8 (d, J = 2 Hz, C-1), 101.9 (PhCH), 111.1, 117.1, 118.6, 125.0, 126.2, 126.4, 127.3, 128.2, 128.3, 128.6, 129.0, 129.7, 129.9, 130.0, 132.6, 133.2, 134.9, 136.8, 143.5, 151.5 (25C, 24 Ar-C, CN), 165.6 (CO). ESI-MS: m/z: calcd for $C_{49}H_{67}ClN_2O_{10}PSi_2$ $[M + NEt_3 + H]^+$, 965.38; found, 965.53.

*4′-(3-O-Benzoyl-2-O-phosphoryl-α-D-mannopyranosyloxy)-3′-chloro-biphenyl-4-carbonitrile Disodium Salt (**26**).* A solution of **25** (79.6 mg, 0.275 mmol) in dry DCM (1.5 mL) was treated with TFA (150 μL) for 1 h at rt under argon. Then, a drop of water was added and stirring continued for 30 min. The solvents were removed in vacuo, and the residue was dissolved in H_2O (1 mL) containing a drop of 1 M aq NaOH and purified by MPLC on RP-18 (H_2O/MeOH, 95:5−4:1) to yield **26** (34.7 mg, 61%) as a 4:1-mixture of 2- and 3-phosphate. ^1H NMR (500 MHz, CD_3OD): δ = 3.78−3.90 (m, 3H, H-5, H-6), 4.20 (t, J = 9.9 Hz, 1H, H-4), 5.01 (ddd, J = 2.0, 3.1, 9.4 Hz, 1H, H-2), 5.60−5.65 (td, J = 2.6, 10.1 Hz, 1H, H-3), 5.91 (d, J = 1.6 Hz, 1H, H-1), 7.45−7.53 (m, 3H, Ar-H), 7.57−7.65 (m, 2H, Ar-H), 7.75−7.81 (m, 5H, Ar-H), 8.15−8.18 (m, 2H, Ar-H). ^{13}C NMR (126 MHz, CD_3OD): δ = 62.2 (C-6), 65.3 (C-4), 73.9 (dd, J = 5.8 Hz, 2C, C-2, C-3), 76.3 (C-5), 98.8 (d, J = 2 Hz, C-1), 112.0, 118.8, 119.7, 125.8, 127.9, 131.0, 133.9, 136.0, 145.0, 153.2 (19C, 18 Ar-C, CN), 167.8 (CO). ESI-MS: m/z: calcd for $C_{26}H_{22}ClNO_{10}P$ $[M - 2Na + H]^-$, 574.07; found, 574.21.

*4′-(3-O-Allyl-α-D-mannopyranosyloxy)-3′-chloro-biphenyl-4-carbonitrile (**27**).* A suspension of **4** (90.1 mg, 0.230 mmol) and dibutyltin oxide (62.7 mg, 0.252 mmol) in toluene (4 mL) was stirred for 6 h at 80 °C under argon. Then, tetrabutylammonium iodide (78.1 mg, 0.242 mmol) and allyl bromide (23 μL, 0.277 mmol) were added to the still turbid mixture and stirring was continued for another 20 h at 80 °C. Afterward, the solvent was removed in vacuo, and the residue was purified by MPLC on RP-18 (H_2O/MeOH) to yield **27** (54.7 mg, 55%) as a colorless solid. ^1H NMR (500 MHz, CD_3OD): δ = 3.65 (d, J = 6.3 Hz, 1H, H-5), 3.72 (dd, J = 5.3, 12.0 Hz, 1H, H-6a), 3.78 (dd, J = 2.5, 12.0 Hz, 1H, H-6b) 3.83−3.90 (m, 2H, H-3, H-4), 4.20−4.32 (m, 3H, H-2, allyl-H1a, allyl-H1b), 5.22 (dd, J = 1.7, 10.4 Hz, 1H, allyl-H3a), 5.39 (dd, J = 1.7, 17.3 Hz, 1H, allyl-H3b), 5.64 (d, J = 1.8 Hz, 1H, H-1), 6.04 (ddt, J = 5.9, 10.4, 16.3 Hz, 1H, allyl-H2), 7.48 (d, J = 8.7 Hz, 1H, Ar-H), 7.60 (dd, J = 2.3, 8.6 Hz, 1H, Ar-H), 7.75 (d, J = 2.3 Hz, 1H, Ar-H), 7.76−7.80 (m, 4H, Ar-H). ^{13}C NMR (126 MHz, CD_3OD): δ = 62.6 (C-6), 67.1 (C-4), 68.6 (C-2), 72.1 (allyl-C1), 76.1 (C-5), 79.6 (C-3), 100.5 (C-1), 111.8, 117.9 118.6, 119.8, 125.5, 127.9, 128.5, 129.8, 133.9, 135.5, 136.4, 145.1, 153.6 (15C, 12 Ar-C, CN, allyl-C2, allyl-C3). ESI-MS: m/z: calcd for $C_{22}H_{22}ClNNaO_6$ $[M + Na]^+$, 454.10; found, 453.89.

*4′-(3-O-Allyl-2,4,6-tri-O-benzoyl-α-D-mannopyranosyloxy)-3′-chloro-biphenyl-4-carbonitrile (**28**).* To a solution of **27** (194 mg, 0.449 mmol) and DMAP (10 mg) in pyridine (5 mL) was added benzoyl chloride (261 μL, 2.25 mmol) under argon. The mixture was stirred at rt overnight. MeOH (1 mL) was added, and the mixture was stirred for 10 min. Then, the solvents were removed under reduced pressure and the residue was dissolved in DCM (20 mL) and washed with 1 M aq HCl (10 mL) and satd aq $NaHCO_3$ (10 mL). The organic phase was dried (Na_2SO_4) and concentrated. The residue was purified by MPLC on silica (petroleum ether/EtOAc) to yield **28** (292 mg, 87%) as a foam; $[\alpha]_D^{20}$ + 44.1 (c 1.46, $CHCl_3$). ^1H NMR (500 MHz, $CDCl_3$): δ = 4.13 (m, 1H, allyl-H1a), 4.24 (dd, J = 5.4, 13.0 Hz, 1H, allyl-H1b), 4.42−4.49 (m, 2H, H-5, H-6a), 4.52 (dd, J = 3.3, 9.8 Hz, 1H, H-3), 5.16 (dd, J = 1.1, 10.3 Hz, 1H, allyl-H3a), 5.29 (dd, J = 1.5, 17.2 Hz, 1H, allyl-H3b), 5.79 (ddt, J = 5.9, 10.4, 16.7 Hz, 1H, allyl-H2), 5.87 (d, J = 1.8 Hz, 1H, H-1), 5.91 (m, 1H, H-2), 5.98 (t, J = 9.8 Hz, 1H, H-4), 7.30−7.39 (m, 4H, Ar-H), 7.41−7.45 (m, 2H, Ar-H), 7.46−7.53 (m, 2H, Ar-H), 7.57−7.63 (m, 3H, Ar-H), 7.68 (m, 1H, Ar-H), 7.70−7.74 (m 2H, Ar-H), 8.00−8.05 (m, 2H, Ar-H), 8.10−8.17 (m, 4H, Ar-H). ^{13}C NMR (126 MHz, $CDCl_3$): δ = 62.8 (C-6), 67.8 (C-4), 68.8 (C-2), 70.2 (C-5), 71.1 (allyl-C1), 73.9 (C-3), 96.5 (C-1), 111.1, 116.9, 118.2, 118.6, 124.4, 127.2, 128.4, 129.9, 132.6, 132.9, 133.3, 133.8, 143.3, 151.6 (33C, 30 Ar-C, CN, allyl-C2, allyl-C3), 165.4, 165.7, 166.0 (3 CO). ESI-MS: m/z: calcd for $C_{43}H_{34}ClNNaO_9$ $[M + Na]^+$, 766.18; found, 768.12.

*4′-(2,4,6-Tri-O-benzoyl-α-D-mannopyranosyloxy)-3′-chloro-biphenyl-4-carbonitrile (**29**).* A flask was charged with **28** (292 mg, 0.391 mmol), anhydrous $PdCl_2$ (10.8 mg, 0.118 mmol), and a magnetic stirring bar. The flask was evacuated and flushed with argon. The procedure was repeated twice. Then, dry MeOH (4 mL) was added and the mixture was stirred at 40 °C for 5 h. The mixture was filtered and the filtrate concentrated in vacuo. The residue was purified by MPLC on silica (petroleum ether/EtOAc) to yield **29** (231 mg, 84%); $[\alpha]_D^{20}$ + 55.0 (c 1.01, $CHCl_3$). ^1H NMR (500 MHz, $CDCl_3$): δ = 4.35−4.41 (m, 2H, H-5, H-6a), 4.57 (m, 1H, H-6b), 4.66 (dd, J = 3.4, 9.9 Hz, 1H, H-3), 5.65 (dd, J = 1.8, 3.4 Hz, 1H, H-2), 5.73 (t, J = 9.8 Hz, 1H, H-4), 5.81 (d, J = 1.7 Hz, 1H, H-1), 7.18−7.27 (m, 4H, Ar-H), 7.34−7.45 (m, 5H, Ar-H), 7.49−7.59 (m, 5H, Ar-H), 7.62−7.67 (m, 2H, Ar-H), 7.87−7.92 (m, 2H, Ar-H), 8.00−8.05 (m, 4H, Ar-H). ^{13}C NMR (126 MHz, $CDCl_3$): δ = 62.7 (C-6), 68.8 (C-3), 69.8 (C-5), 69.9 (C-4), 72.3 (C-2), 96.1 (C-1), 111.2, 116.9, 118.7, 124.6, 127.3, 128.6, 128.9, 129.7, 132.7, 133.1, 133.8, 134.5, 151.5 (31C, 30 Ar-C, CN), 165.8, 165.9, 166.8 (3 CO). IR (KBr): ν = 3446 (m, OH), 2228 (m, CN), 1725 (vs, C═O) cm^{-1}. ESI-MS: m/z: calcd for $C_{40}H_{30}ClNNaO_9$ $[M + Na]^+$, 726.15; found, 726.49.

*4′-(2,4,6-Tri-O-benzoyl-3-O-bis[2-(trimethylsilyl)ethoxy]-phosphoryl-α-D-mannopyranosyloxy)-3′-chloro-biphenyl-4-carbonitrile (**30**).* According to the general procedure, compound **29** (198 mg, 0.281 mmol) was reacted with 1,2,4-triazole (77.8 mg, 1.13 mmol) and bis[2-(trimethylsilyl)ethyl] *N,N*-diisopropylphosphoramidite (232 μL, 0.563 mmol) in MeCN (3 mL), followed by treatment with 70% aq *tert*-butylhydroperoxide (154 μL, 1.13 mmol) to yield **30** (89.1 mg, 32%); $[\alpha]_D^{20}$ + 35.9 (c 0.99, $CHCl_3$). ^1H NMR (500 MHz, $CDCl_3$): δ = −0.10, 0.00 (2s, 18H, 2 $Si(CH_3)_3$), 0.69−0.85 (m, 2H, $SiCH_2$), 1.01−1.09 (m, 2H, $SiCH_2$), 3.83−3.98 (m, 2H, OCH_2), 4.09−4.21 (m, 2H, OCH_2), 4.49−4.57 (m, 2H, H-5, H-6a), 4.67 (d, J = 10.1 Hz, 1H, H-6b), 5.55 (ddt, J = 3.4, 9.5 Hz, 1H, H-3), 5.92 (d, J = 1.6 Hz, 1H, H-1), 5.99 (dd, J = 1.9, 3.3 Hz, 1H, H-2), 6.12 (t, J = 9.8 Hz, 1H, H-4), 7.34−7.40 (m, 4H, Ar-H), 7.48−7.58 (m, 5H, Ar-H), 7.63−7.73 (m, 5H, Ar-H), 7.76−7.80 (m, 2H, Ar-H), 8.03−8.06 (m, 2H, Ar-H), 8.17−8.20 (m, 2H, Ar-H), 8.21−8.25 (m, 2H, Ar-H). ^{13}C NMR (126 MHz, $CDCl_3$): δ = −1.9, −1.8 (6C, 2 $Si(CH_3)_3$), 19.0 (d, J = 6 Hz, $SiCH_2$), 19.3 (d, J = 6 Hz, $SiCH_2$), 62.5 (C-6), 66.5 (d, J = 1 Hz, OCH_2), 66.6 (d, J = 1 Hz, OCH_2), 67.3 (d, J = 5 Hz, C-4), 70.0 (C-5), 70.8 (d, J = 2 Hz, C-2), 72.6 (d, J = 5 Hz, C-3), 96.4 (C-1), 111.2, 117.4, 118.6, 124.9, 128.2, 129.1, 129.1, 129.6, 130.1, 132.6, 132.9, 133.5, 133.7, 135.0 (31C, 30 Ar-C, CN), 165.32, 165.34, 165.8 (3 CO). ESI-MS: m/z: calcd for $C_{50}H_{55}ClNNaO_{12}PSi_2$ $[M + Na]^+$, 1006.26; found, 1006.44.

*4′-(2,3,6-Tri-O-acetyl-α-D-mannopyranosyloxy)-3′-chloro-biphenyl-4-carbonitrile (**31**).* According to a described procedure,[47] a solution of **4** (100 mg, 0.255 mmol) and dibutyltin oxide (340 mg, 0.562 mmol) in dry MeOH (5 mL) was stirred under reflux for 2 h at

DOI: 10.1021/acs.jmedchem.5b01923
J. Med. Chem. 2016, 59, 3163−3182

70 °C. Afterward, the solvent was removed in vacuo and the residue was dissolved in dry MeCN (5 mL) and cooled to 0 °C. Then, a solution of Ac_2O (80 μL, 0.842 mmol) in dry MeCN (1 mL) was added dropwise at 0 °C. The mixture was stirred at rt for 16 h. The reaction was quenched with MeOH (1 mL), the solvents were removed in vacuo, and the residue was purified by MPLC on silica (petroleum ether/EtOAc) to yield **31** (27.0 mg, 21%); $[\alpha]_D^{20}$ + 63.6 (*c* 0.98, $CHCl_3$). ^{1}H NMR (500 MHz, $CDCl_3$): δ = 2.06, 2.11, 2.16 (3s, 9H, 3 $COCH_3$), 3.94 (t, *J* = 9.8 Hz, 1H, H-4), 2.02 (ddd, *J* = 2.1, 4.6, 9.9 Hz, 1H, H-5), 4.27 (dd, *J* = 2.1, 12.3 Hz, 1H, H-6a), 4.50 (dd, *J* = 4.7, 12.3 Hz, 1H, H-6b), 5.47 (dd, *J* = 3.5, 9.7 Hz, 1H, H-3), 5.50 (dd, *J* = 1.8, 3.4 Hz, 1H, H-2), 5.58 (d, *J* = 1.6 Hz, 1H, H-1), 7.26 (m, 1H, Ar-H), 7.41 (dd, *J* = 2.3, 8.6 Hz, 1H, Ar-H), 7.59−7.62 (m, 3H, Ar-H), 7.68−7.72 (m, 2H, Ar-H). ^{13}C NMR (126 MHz, $CDCl_3$): δ = 20.7, 20.8, 20.8 (3 $COCH_3$), 62.8 (C-6), 65.5 (C-4), 69.4 (C-2), 71.1 (C-3), 72.2 (C-5), 96.7 (C-1), 111.2, 117.2, 118.7, 125.0, 126.4, 127.4, 129.2, 132.7, 134.9, 143.5, 151.6 (13C, 12 Ar-C, CN), 169.9, 170.8, 171.3 (3 CO). IR (KBr): ν = 3436 (vs, OH), 2229 (m, CN), 1756 (vs, C═O) cm^{-1}. ESI-MS: *m*/*z*: calcd for $C_{25}H_{24}ClNNaO_9$ $[M + Na]^+$, 540.10; found, 540.08.

*4′-(2,3,6-Tri-O-acetyl-4-O-bis[2-(trimethylsilyl)ethoxy]-phosphoryl-α-D-mannopyranosyloxy)-3′-chloro-biphenyl-4-carbonitrile (**32**).* According to the general procedure, compound **31** (39.3 mg, 76 μmol) was reacted with 1,2,4-triazole (21.0 mg, 0.304 mmol) and bis[2-(trimethylsilyl)ethyl] *N*,*N*-diisopropylphosphoramidite (63 μL, 0.152 mmol) in MeCN (1 mL), followed by treatment with 70% aq *tert*-butylhydroperoxide (42 μL, 0.304 mmol) to yield **32** (37.3 mg, 62%); $[\alpha]_D^{20}$ + 65.0 (*c* 1.07, $CHCl_3$). ^{1}H NMR (500 MHz, $CDCl_3$): δ = 0.04, 0.05 (2s, 18H, 2 $Si(CH_3)_3$), 1.04−1.14 (m, 4H, 2 $SiCH_2$), 2.04, 2.13, 2.20 (3s, 9H, 3 $COCH_3$), 4.08−4.19 (m, 5H, H-5, 2 OCH_2), 4.33 (dd, *J* = 5.2, 12.3 Hz, 1H, H-6a), 4.42 (dd, *J* = 2.0, 12.3 Hz, 1H, H-6b), 4.79 (q, *J* = 9.6 Hz, 1H, H-4), 5.51 (dd, *J* = 1.8, 3.5 Hz, 1H, H-2), 5.59 (d, *J* = 1.7 Hz, 1H, H-1), 5.68 (dd, *J* = 3.6, 9.7 Hz, 1H, H-3) 7.27 (m, 1H, Ar-H), 7.43 (dd, *J* = 2.3, 8.6 Hz, 1H, Ar-H), 7.60−7.65 (m, 3H, Ar-H), 7.70−7.74 (m, 2H, Ar-H). ^{13}C NMR (126 MHz, $CDCl_3$): δ = −1.6, −1.5 (6C, 2 $Si(CH_3)_3$), 19.5, 19.6 (2 $SiCH_2$), 20.7, 20.8, 20.9 (3 $COCH_3$), 62.2 (C-6), 66.7 (d, *J* = 2 Hz, OCH_2), 66.8 (d, *J* = 1 Hz, OCH_2), 68.8 (d, *J* = 2 Hz, C-3), 69.5 (C-2), 70.4 (d, *J* = 6 Hz) and 70.5 (d, *J* = 5 Hz) (C-4, C-5), 96.4 (C-1), 111.3, 117.3, 118.6, 125.0, 126.4, 127.4, 129.2, 132.7, 135.1, 143.5, 151.6 (13C, 12 Ar-C, CN), 169.7, 169.9, 170.3 (3 CO). IR (KBr): ν = 2229 (m, CN), 1753 (vs, C═O) cm^{-1}. ESI-MS: *m*/*z*: calcd for $C_{35}H_{49}ClNNaO_{12}PSi_2$ $[M + Na]^+$, 820.21; found, 820.14.

*3′-Chloro-4′-(6-O-trityl-α-D-mannopyranosyloxy)-biphenyl-4-carbonitrile (**33**).* To a solution of **4** (150 mg, 0.383 mmol) in pyridine were added trityl chloride (128 mg, 0.459 mmol) and DMAP (5 mg). The mixture was stirred at 80 °C for 16 h. Then, the solvent was removed in vacuo and the residue was purified by MPLC on silica (petroleum ether/EtOAc, + 0.5% NEt_3) to yield **33** (189 mg, 80%). ^{1}H NMR (500 MHz, CD_3OD): δ = 3.30 (dd, *J* = 7.5, 16.1 Hz, 1H, H-6a), 3.46 (d, *J* = 9.3 Hz, 1H, H-6b), 3.63 (t, *J* = 9.7 Hz, 1H, H-4), 3.88 (t, *J* = 9.0 Hz, 1H, H-5), 4.02 (dd, *J* = 3.3, 9.4 Hz, 1H, H-3), 4.20 (m, 1H, H-2), 5.75 (s, 1H, H-1), 7.03−7.16 (m, 10H, Ar-H), 7.26−7.35 (m, 6H, Ar-H), 7.55 (d, *J* = 8.3 Hz, 2H, Ar-H), 7.58−7.64 (m, 3H, Ar-H), 7.70 (d, *J* = 2.0 Hz, 2H, Ar-H). ^{13}C NMR (126 MHz, CD_3OD): δ = 65.0 (C-6), 68.7 (C-4), 71.5 (C-2), 72.6 (C-3), 75.0 (C-5), 87.54 (CPh_3), 99.9 (C-1), 111.7, 118.7, 119.7, 127.7, 127.8, 128.3, 129.7, 133.7, 134.9, 144.7, 145.3, 153.3 (31C, 30 Ar-C, CN). ESI-MS: *m*/*z*: calcd for $C_{59}H_{44}ClNNaO_9$ $[M + Na]^+$, 656.18; found, 656.15.

*4′-(2,3,4-Tri-O-benzoyl-6-O-trityl-α-D-mannopyranosyloxy)-3′-chloro-biphenyl-4-carbonitrile (**34**).* Prepared according to the procedure described for **28** from **33** (189 mg, 0.299 mmol), benzoyl chloride (173 μL, 1.21 mmol), and DMAP (10 mg) to yield **34** (223 mg, 79%); $[\alpha]_D^{20}$ + 8.1 (*c* 1.10, $CHCl_3$). ^{1}H NMR (500 MHz, $CDCl_3$): δ = 3.42−3.50 (m, 2H, H-6), 4.39 (m, 1H, H-5), 6.05 (d, *J* = 1.5 Hz, 1H, H-1), 6.10 (dd, *J* = 1.9, 3.2 Hz, 1H, H-2), 6.15 (dd, *J* = 3.3, 10.1 Hz, 1H, H-3), 6.23 (t, *J* = 10.1 Hz, 1H, H-4), 7.10−7.19 (m, 9H, Ar-H), 7.28−7.39 (m, 4H, Ar-H), 7.41−7.60 (m, 12H, Ar-H), 7.63−7.71 (m, 3H, Ar-H), 7.81−7.85 (m, 2H, Ar-H), 7.93−7.98 (m, 2H, Ar-H), 8.23−8.28 (m, 2H, Ar-H). ^{13}C NMR (126 MHz, $CDCl_3$): δ = 62.0 (C-6), 66.7 (C-4), 70.0 (C-3), 70.3 (C-2), 71.6 (C-5), 86.6 (CPh_3), 96.4 (C-1), 111.0, 118.6, 124.8, 126.5, 126.8, 127.2, 127.6, 128.1, 128.2, 128.4, 128.6, 128.9, 128.97, 129.02, 129.55, 129.61, 129.8, 132.5, 133.1, 133.6, 134.6, 143.4, 143.5, 151.6 (49C, 48 Ar-C, CN), 165.0, 165.3, 165.4 (3 CO). IR (KBr): ν = 2227 (m, CN), 1731 (vs, C═O) cm^{-1}. ESI-MS: *m*/*z*: calcd for $C_{59}H_{44}ClNNaO_9$ $[M + Na]^+$, 968.26; found, 968.47.

*4′-(2,3,4-Tri-O-benzoyl-α-D-mannopyranosyloxy)-3′-chloro-biphenyl-4-carbonitrile (**35**).* Prepared according to the procedure described for **21** by reacting **34** (122 mg, 0.129 mmol) with $FeCl_3$ (41.8 mg, 0.258 mmol) and water (27.9 μL, 1.55 mmol) in DCM (10 mL) for 5 h to yield **35** (77.4 mg, 85%); $[\alpha]_D^{20}$ + 6.2 (*c* 1.02, $CHCl_3$). ^{1}H NMR (500 MHz, $CDCl_3$): δ = 3.80 (qd, *J* = 2.7, 13.1 Hz, 2H, H-6) 4.25 (d, *J* = 10.0 Hz, 1H, H-5), 5.95 (s, 1H, H-1), 5.96−6.03 (m, 2H, H-2, H-4), 6.29 (dd, *J* = 3.4, 10.2 Hz, 1H, H-3), 7.25−7.32 (m, 2H, Ar-H), 7.38−7.56 (m, 8H, Ar-H), 7.61−7.73 (m, 6H, Ar-H), 7.88 (d, *J* = 7.3 Hz, 2H, Ar-H), 8.01 (d, *J* = 7.3 Hz, 2H, Ar-H), 8.14 (d, *J* = 7.2 Hz, 2H, Ar-H). ^{13}C NMR (125 MHz, $CDCl_3$): δ = 60.9 (C-6), 66.8 (C-4), 69.2 (C-3), 70.2 (C-2), 72.3 (C-5), 96.6 (C-1), 111.2, 117.0, 118.6, 124.9, 126.5, 127.3, 128.3, 128.4, 128.5, 128.7, 128.9, 129.2, 129.6, 129.90, 129.91, 132.7, 133.3, 133.7, 133.8, 134.9, 143.5, 151.6 (31C, 30 Ar-C, CN), 165.37, 165.43, 166.6 (3 CO). IR (KBr): ν = 3436 (vs, OH), 2228 (m, CN), 1731 (vs, C═O) cm^{-1}. ESI-MS: *m*/*z*: calcd for $C_{40}H_{30}ClNNaO_9$ $[M + Na]^+$, 726.15; found, 726.24.

*4′-(2,3,4-Tri-O-benzoyl-6-O-bis[2-(trimethylsilyl)ethoxy]-phosphoryl-α-D-mannopyranosyloxy)-3′-chloro-biphenyl-4-carbonitrile (**36**).* According to the general procedure, compound **35** (61.3 mg, 87 μmol) was reacted with 1,2,4-triazole (24.1 mg, 0.348 mmol) and bis[2-(trimethylsilyl)ethyl] *N*,*N*-diisopropylphosphoramidite (72 μL, 0.174 mmol) in MeCN (2 mL), followed by treatment with 70% aq *tert*-butylhydroperoxide (48 μL, 0.348 mmol) to yield **36** (50.8 mg, 59%). ^{1}H NMR (500 MHz, $CDCl_3$): δ = −0.07, −0.04 (2 s, 18H, 2 $Si(CH_3)_3$) 0.94−1.03 (m, 4H, 2 $SiCH_2$), 4.03−4.15 (m, 4H, 2 OCH_2), 4.26 (dd, *J* = 3.8, 5.6 Hz, 2H, H-6), 4.52 (m, 1H, H-5), 5.86 (d, *J* = 1.7 Hz, 1H, H-1), 5.97 (dd, *J* = 2.0, 3.2 Hz, 1H, H-2), 6.07 (t, *J* = 10.1 Hz, 1H, H-4), 6.15 (dd, *J* = 3.3, 10.1 Hz, 1H, H-3), 7.27−7.33 (m, 2H, Ar-H), 7.37−7.54 (m, 8H, Ar-H), 7.61−7.76 (m, 6H, Ar-H), 7.85−7.89 (m, 2H, Ar-H), 7.95−8.00 (m, 2H, Ar-H), 8.11−8.15 (m, 2H, Ar-H).^{13}C NMR (126 MHz, $CDCl_3$): δ = −1.65, −1.64 (6C, 2 $Si(CH_3)_3$), 19.4 (d, *J* = 6 Hz, $SiCH_2$), 19.5 (d, *J* = 6 Hz, $SiCH_2$), 65.3 (d, *J* = 5 Hz, C-6), 66.1 (C-4), 66.4 (d, *J* = 6 Hz, 2C, 2 OCH_2), 69.5 (C-3), 70.1 (C-2), 70.8 (d, *J* = 8 Hz, C-5), 96.9 (C-1), 111.3, 117.7, 118.6, 125.1, 126.7, 127.4, 128.3, 128.4, 128.7, 128.8, 128.9, 129.0, 129.2, 129.7, 129.8, 130.0, 132.7. 133.3, 133.5, 133.7, 135.2, 143.5, 151.9 (31C, 30 Ar-C, CN), 165.2, 165.35, 165.39 (3 CO). ESI-MS: *m*/*z*: calcd for $C_{50}H_{55}ClNNaO_{12}PSi_2$ $[M + Na]^+$, 1006.26; found, 1006.52.

*Biphenyl 2,3,4-Tri-O-benzoyl-6-O-(methylthiomethyl)-α-D-mannopyranoside (**37**).* To a solution of compound **21** (469 mg, 0.726 mmol) in Ac_2O (2.5 mL) and AcOH (0.25 mL) was added DMSO (2.5 mL). The mixture was stirred at rt for 24 h, then diluted with EtOAc (50 mL) and washed with satd aq $NaHCO_3$ (2 × 20 mL) and H_2O (2 × 20 mL) and brine (20 mL). The organic layer was dried over Na_2SO_4 and the solvents removed under diminished pressure. The residue was purified by MPLC on silica (petroleum ether/EtOAc, 9:1−6:1) to yield **37** (171 mg, 35%), which contained some impurities but was used in the next step without further purification.

*Biphenyl 2,3,4-Tri-O-benzoyl-6-O-(phosphonooxy)-methyl-α-D-mannopyranoside (**38**).* Compound **37** (170 mg, 0.250 mmol) was dissolved in a premixture of H_3PO_4 (147 mg, 1.50 mmol) in THF (1.5 mL). Then, *N*-iodosuccinimide (84.0 mg, 0.375 mmol) was added and the mixture was stirred for 15 min at 0 °C and for 1 h at rt. The reaction was then quenched with 1 M aq $Na_2S_2O_3$, diluted with DCM/MeOH (20 mL, 4:1), and washed with satd aq $NaHCO_3$ (10 mL). The organic layer was dried over Na_2SO_4, and the solvents were removed in vacuo at <20 °C. The residue was purified by MPLC on silica (DCM/MeOH, 1:0−3.5:1) to yield **38** (110 mg, 58%). ^{1}H NMR (CD_3OD, 500 MHz): δ = 3.90 (dd, *J* = 4.5, 11.6 Hz, 1H, H-6a), 4.01 (d, *J* = 10.2 Hz, 1H, H-6b), 4.47 (m, 1H, H-5), 5.06 (A of ABX, *J* = 5.5, 9.5 Hz, 1H, CH_2), 5.16 (B of ABX, *J* = 5.5, 9.1 Hz, 1H, CH_2), 5.89

DOI: 10.1021/acs.jmedchem.5b01923
J. Med. Chem. 2016, 59, 3163−3182

(s, 1H, H-1), 5.92 (s, 1H, H-2), 6.05 (m, 2H, H-4, H-3), 7.26−7.68 (m, 18 H, Ar-H), 7.79 (d, J = 7.6 Hz, 2H, Ar-H), 7.96 (d, J = 7.6 Hz, 2H, Ar-H), 8.13 (d, J = 7.5 Hz, 2H, Ar-H). ^{13}C NMR (CD_3OD, 126 MHz): δ = 68.2 (C-4), 68.7 (C-6), 71.5 (C-2), 71.86 (C-5), 71.9 (C-3), 92.8 (d, J = 4 Hz, CH_2), 97.6 (C-1), 118.4, 127.7, 128.0, 129.3, 129.4, 129.6, 129.8, 129.9, 130.3, 130.4, 130.5, 130.6, 130.7, 130.9, 134.5, 134.6, 134.9, 137.4, 141.8, 156.8 (30C, Ar-C), 166.8, 167.0 (3C, 3 CO). ESI-MS: m/z: calcd for $C_{40}H_{35}NaO_{13}P$ $[M + Na]^+$, 777.17; found, 777.13.

*4-(5-Nitroindolin-1-yl)phenyl-2,3,4-tri-O-benzoyl-6-O-(tert-butylsilyldimethyl)-α-D-mannopyranoside (**39**).* To a solution of **5**[20] (709 mg, 1.69 mmol) in pyridine were added *tert*-butyldimethylsilyl chloride (319 mg, 2.12 mmol) and DMAP (20.6 mg), and the mixture was stirred at rt overnight. Then, a solution of benzoyl chloride (0.98 mL, 8.45 mmol) in pyridine (2.0 mL) was added and the mixture was stirred at rt for 2 h. The mixture was diluted with DCM (30 mL) and subsequently washed with 0.1 M aq HCl (10 mL) and satd aq $NaHCO_3$ (10 mL). The organic layer was dried over Na_2SO_4, filtered, and the solvent removed in vacuo. The residue was purified by MPLC on silica (petroleum ether/EtOAc, 9:1−7:3) to yield crude **39** (1.43 g, quant) as a yellow solid, which was used in the next step without further purification. ^{1}H NMR ($CDCl_3$, 500 MHz): δ = −0.01 (s, 3H, $Si(CH_3)_2$), 0.00 (s, 3H, $Si(CH_3)_2$), 0.87 (s, 9H, $C(CH_3)_3$), 3.22 (t, J = 8.5 Hz, 2H, CH_2), 3.83 (dd, J = 2.3, 11.5 Hz, 1H, H-6a), 3.88 (dd, J = 4.7, 11.5 Hz, 1H, H-6b), 4.10 (t, J = 8.7 Hz, 2H, NCH_2), 4.43 (m, 1H, H-5), 5.77 (d, J = 1.8 Hz, 1H, H-1), 5.87 (m, 1H, H-2), 6.03−6.15 (m, 2H, H-3, H-4), 6.77 (d, J = 8.9 Hz, 1H, Ar-H), 7.22−7.31 (m, 6H, Ar-H), 7.38 (t, J = 7.8 Hz, 2H, Ar-H), 7.41−7.55 (m, 5H, Ar-H), 7.60−7.67 (m, 1H, Ar-H), 7.88 (dd, J = 1.2, 8.3 Hz, 2H, Ar-H), 7.94−8.01 (m, 3H, Ar-H), 8.03 (dd, J = 2.3, 8.9 Hz, 1H, Ar-H), 8.14 (dd, J = 1.2, 8.3 Hz, 1H, Ar-H). ^{13}C NMR ($CDCl_3$, 126 MHz): δ = −5.51, −5.50 ($Si(CH_3)_2$), 25.8 (3C, $C(CH_3)_3$), 27.1 (CH_2), 53.7 (NCH_2), 62.1 (C-6), 66.6 (C-3), 70.3, 70.4 (C-2, C-4), 72.3 (C-5), 96.4 (C-1), 105.3, 118.0, 121.1, 122.0, 126.1, 128.3, 128.4, 128.43, 128.6, 129.1, 129.2, 129.3, 129.7, 129.8, 130.0, 131.0, 133.2, 133.3, 133.6, 136.8, 139.1, 152.8, 153.8 (30C, Ar-C), 165.3, 165.6, 165.7 (3 CO). ESI-MS: m/z: calcd for $C_{47}H_{48}N_2NaO_{11}Si$ $[M + Na]^+$, 867.29; found, 867.25.

*4-(5-Nitroindolin-1-yl)phenyl-2,3,4-tri-O-benzoyl-α-D-mannopyranoside (**40**).* A solution of **39** (1.43 g, 1.69 mmol) in DCM/MeOH (16 mL, 1:1) was treated with 1 M H_2SO_4 in MeOH (1.6 mL) for 1.5 h at rt. The reaction mixture was neutralized with NEt_3, and the solvents were removed in vacuo. The residue was purified by MPLC on silica (petroleum ether/EtOAc, 3:1−3:2) to yield **40** (900 mg, 73%). ^{1}H NMR ($CDCl_3$, 500 MHz): δ = 3.22 (t, J = 8.6 Hz, 2H, CH_2), 3.77 (dd, J = 3.3, 13.0 Hz, 1H, H-6a), 3.84 (dd, J = 1.8, 13.0 Hz, 1H, H-6b), 4.11 (t, J = 9.4 Hz, 2H, NCH_2), 4.20 (m, 1H, H-5), 5.83 (d, J = 1.6 Hz, 1H, H-1), 5.88 (dd, J = 1.9, 3.3 Hz, 1H, H-2), 5.96 (t, J = 10.1 Hz, 1H, H-4), 6.22 (dd, J = 3.4, 10.2 Hz, 1H, H-3), 6.78 (d, J = 8.9 Hz, 1H, Ar-H), 7.21−7.34 (m, 6H, Ar-H), 7.37−7.43 (m, 3H, Ar-H), 7.45 (t, J = 7.4 Hz, 1H, Ar-H), 7.50−7.57 (m, 3H, Ar-H), 7.65 (t, J = 7.5 Hz, 1H, Ar-H), 7.84−7.89 (m, 2H, Ar-H), 7.97−8.02 (m, 3H, Ar-H), 8.04 (dd, J = 2.3, 8.9 Hz, 1H, Ar-H), 8.12−8.16 (m, 2H, Ar-H). ^{13}C NMR ($CDCl_3$, 126 MHz): δ = 27.1 (CH_2), 53.7 (NCH_2), 61.1 (C-6), 67.0 (C-4), 69.3 (C-3), 70.4 (C-2), 71.8 (C-5), 96.4 (C-1), 105.4, 117.6, 121.1, 122.0, 126.1, 127.0, 128.3, 128.4, 128.5, 128.6, 128.7, 129.0, 129.03, 129.5, 129.7, 129.9, 130.0, 131.1, 133.4, 133.77, 133.8, 137.0, 139.2, 152.5, 153.6 (30C, Ar-C), 165.5, 165.6, 166.6 (3 CO). ESI-MS: m/z: calcd for $C_{41}H_{34}N_2NaO_{11}$ $[M + Na]^+$, 753.21; found, 753.33.

*4-(5-Nitroindolin-1-yl)phenyl-2,3,4-tri-O-benzoyl-6-O-(methylthio)methyl α-D-mannopyranoside (**41**).* Degassed DMSO (2.5 mL) was added to a degassed mixture of **40** (200 mg, 0.273 mmol) in Ac_2O (1.65 mL) and HOAc (0.5 mL). The mixture was stirred at rt overnight, then diluted with EtOAc (20 mL) and subsequently washed with satd aq $NaHCO_3$ (2 × 10 mL), H_2O (2 × 10 mL), and brine (10 mL). The organic layer was dried over Na_2SO_4 and concentrated. The residue was purified by MPLC on silica (petroleum ether/EtOAc, 3:1−7:3) to yield **41** (160 mg, 74%). ^{1}H NMR ($CDCl_3$, 500 MHz): δ = 2.08 (s, 3H, CH_3), 3.23 (t, J = 8.6 Hz, 2H, CH_2), 3.72 (dd, J = 2.4, 11.1 Hz, 1H, H-6a), 3.89 (dd, J = 4.5, 11.2 Hz, 1H, H-6b), 4.12 (m, 2H, NCH_2), 4.43 (m, 1H, H-5), 4.61, 4.72 (A, B of ABX, J = 11.6 Hz, 2H, CH_2), 5.79 (d, J = 1.6 Hz, 1H, H-1), 5.86 (m, 1H, H-2), 6.03−6.11 (m, 2H, H-3, H-4), 6.78 (d, J = 8.9 Hz, 1H, Ar-H), 7.22−7.33 (m, 7H, Ar-H), 7.36−7.42 (m, 2H, Ar-H), 7.46 (t, J = 7.4 Hz, 1H, Ar-H), 7.48−7.56 (m, 3H, Ar-H), 7.64 (t, J = 7.5 Hz, 1H, Ar-H), 7.85−7.91 (m, 2H, Ar-H), 7.96−8.01 (m, 3H, Ar-H), 8.04 (dd, J = 2.2, 8.8 Hz, 1H, Ar-H), 8.10−8.17 (m, 2H, Ar-H). ^{13}C NMR ($CDCl_3$, 126 MHz): δ = 13.9 (CH_3), 27.1 (CH_2), 53.7 (NCH_2), 66.3 (C-6), 67.8 (C-4), 70.1 (C-3), 70.4 (C-2), 71.7 (C-5), 75.9 (CH_2), 96.5 (C-1), 105.4, 117.9, 121.1, 122.0, 126.1, 128.4, 128.5, 128.7, 129.0, 129.2, 129.7, 129.8, 131.0, 131.1, 133.3, 133.4, 133.7, 137.0, 139.2, 152.7, 153.7 (30C, Ar-C), 165.5, 165.60, 165.62 (3 CO). ESI-MS: m/z: calcd for $C_{43}H_{38}N_2NaO_{11}S$ $[M + Na]^+$, 813.21; found, 813.32.

*4-(5-Nitroindolin-1-yl)phenyl 2,3,4-tri-O-benzoyl-6-O-(phosphonooxy)-methyl α-D-manno-pyranoside (**42**).* Compound **41** (400 mg, 0.500 mmol) was dissolved in a mixture of H_3PO_4 (366 mg, 3.73 mmol) in THF (5 mL). Then, *N*-iodosuccinimide (225 mg, 1.00 mmol) was added and the mixture was stirred for 15 min at 0 °C and for 1 h at rt. The reaction was quenched with 1 M aq $Na_2S_2O_3$ and 28% aq ammonia (2 mL), then the volatiles were removed in vacuo at <30 °C. The residue was purified by MPLC on silica (DCM/[MeOH/H_2O 10:1], 1:0−3.5:1) to yield slightly impure **42** (278 mg, 67%), which was used in the next step without further purification.

Physicochemical and Pharmacokinetic Characterization. *Materials.* Dimethyl sulfoxide (DMSO), hydrochloric acid ≥37% (HCl), pepsin (from porcine gastric mucosa, ≥ 250 units/mg solid), pancreatin (from porcine pancreas, 4× USP specifications), acetic acid, sodium taurocholate hydrate, lecithin, sodium acetate trihydrate, maleic acid, glyceryl monooleate, sodium oleate, Dulbecco's Modified Eagle's Medium (DMEM)-high glucose, L-glutamine solution, penicillin−streptomycin solution, Dulbecco's Phosphate Buffered Saline (DPBS), and trypsin-EDTA solution were purchased from Sigma-Aldrich (St. Louis, MO, USA). MEM nonessential amino acid (MEM-NEAA) solution, fetal bovine serum (FBS), and DMEM without sodium pyruvate and phenol red were bought from Invitrogen (Carlsbad, CA, USA). Methanol (MeOH), acetonitrile (MeCN), and dichloromethane (DCM) were obtained from Acros Organics (Geel, Belgium). Monopotassium phosphate (KH_2PO_4) and sodium hydroxide (NaOH) were bought from Merck (Merck KGaA, Darmstadt, Germany). Sodium chloride (NaCl) was purchased from Hänseler (Hänseler AG, AR, Switzerland). Long-life, heat-treated and homogenized milk (UHTmilk) containing 3.5% fat was bought from Coop (Coop Qualité & Prix, Switzerland). The Caco-2 cells were kindly provided by Prof. G. Imanidis, FHNW, Muttenz, and originated from the American Type Culture Collection (Rockville, MD, USA).

Aqueous Solubility. Microanalysis tubes (LaboTech J. Stofer LTS AG, Muttenz, Switzerland) were charged with 500 μg of solid substance and 100 μL of phosphate buffer (50 mM, pH 6.5). The tubes were briefly shaken by hand, sonicated for 15 min, and vigorously shaken (600 rpm, 25 °C, 2 h) on an Eppendorf Thermomixer Comfort (Eppendorf, Hamburg, Germany). Afterward, they were left undisturbed for 24 h. Then, the compound solutions were filtered (MultiScreen HTS 96-well filtration system, Millipore, Billerica, MA) by centrifugation (1500 rpm, 25 °C, 3 min). The filtrates were further diluted with buffer (1:1000 and 1:10000), and the concentrations were determined by LC-MS (see below).

Colorectal Adenocarcinoma (Caco-2) Cell Permeation Assay and Hydrolysis Studies. Caco-2 cells were cultivated in tissue culture flasks (BD Biosciences, Franklin Lakes, NJ, USA) with DMEM high glucose medium, containing L-glutamine (2 mM), nonessential amino acids (0.1 mM), penicillin (100 U/mL), streptomycin (100 μg/mL), and fetal bovine serum (10%). The cells were kept at 37 °C in humidified air containing 5% CO_2, and the medium was changed every second day. When approximately 90% confluence was reached, the cells were split in a 1:10 ratio and distributed to new tissue culture flasks. At passage numbers between 60 and 65, they were seeded at a density of 5.3 × 10^5 cells per well to Transwell six-well plates (Corning Inc., Corning, NY, USA) with 2.5 mL of culture medium in the basolateral and 2.0 mL in the apical compartment. The medium was renewed on

DOI: 10.1021/acs.jmedchem.5b01923
J. Med. Chem. 2016, 59, 3163−3182

alternate days. Enzymatic hydrolysis and permeation experiments were performed between days 19 and 21 post seeding. Prior to the experiment, the integrity of the Caco-2 monolayers was evaluated by measuring the transepithelial electrical resistance (TEER) with an Endohm tissue resistance instrument (World Precision Instruments Inc., Sarasota, FL, USA). Only wells with TEER values higher than 250 Ω cm^2 were used. After the experiment, TEER values were assessed again for each well, and results from wells with values below 250 Ω cm^2 were discarded.

Permeation experiments with the compounds **3**−**5** were performed in the apical-to-basolateral and basolateral-to-apical directions in triplicates. Transport medium (DMEM without sodium pyruvate and phenol red) was withdrawn from the donor compartments of three wells and replaced by the same volume of compound stock solution (10 mM in DMSO) to reach an initial sample concentration of 62.5 μM. The Transwell plate was shaken (600 rpm, 37 °C) on a Heidolph Titramax 1000 plate-shaker (Heidolph Instruments GmbH & Co. KG, Schwabach, Germany). Samples (40 μL) were withdrawn from the donor and acceptor compartments 30 min after initiation of the experiment, and the compound concentrations were determined by LC-MS. Apparent permeability (P_{app}) was calculated according to eq 1:

$$P_{app} = \frac{dQ}{dt} \times \frac{1}{A \times c_0} \quad (1)$$

where dQ/dt is the compound flux (mol s^{-1}), A the surface area of the monolayer (cm^2), and c_0 the initial concentration in the donor compartment (mol cm^{-3}).[19]

Hydrolysis studies with the compounds **6a**−**e**, **7a**−**d**, and **8** were performed in triplicates. Transport medium was withdrawn from the apical compartments of three wells and replaced by the same volume of compound stock solution (10 mM in H_2O) to reach an initial sample concentration of 62.5 μM. The Transwell plate was shaken (600 rpm, 37 °C) on a Heidolph Titramax 1000 plate-shaker. Samples (40 μL) were withdrawn from the apical compartment 10, 20, 30, 45, and 60 min after the initiation of the experiment and the concentrations of prodrug were determined by LC-MS. Metabolic half-life ($t_{1/2}$) was calculated from the slope of the linear regression from the natural log remaining compound concentration versus incubation time relationship.

Studies of hydrolysis and subsequent permeation in the apical-to-basolateral and basolateral-to-apical directions were performed with compound **7b** in triplicate. Transport medium was withdrawn from the apical or basal donor compartments of three wells and replaced by the same volume of compound stock solution (10 mM in H_2O) to reach an initial sample concentration of 62.5 μM. The Transwell plate was shaken (600 rpm, 37 °C) on a Heidolph Titramax 1000 plate-shaker. Samples (40 μL) were withdrawn form the apical and basal compartments 60 min after the initiation of the experiment, and the concentrations of prodrug **7b** and active principle **4** were determined by LC-MS.

Studies of hydrolysis and subsequent permeation in the apical-to-basolateral direction were performed with the compounds **6e**, **7b**, and **8** at different concentrations (100, 200, or 400 μM) in duplicate. Transport medium was withdrawn from the apical compartments of two wells and replaced by the same volume of compound stock solution (16, 32, or 64 mM in H_2O) to reach initial sample concentrations of 100, 200, or 400 μM. The Transwell plate was shaken (600 rpm, 37 °C) on a Heidolph Titramax 1000 plate-shaker. Samples (40 μL) were withdrawn from the basal compartments 60 min after the initiation of the experiment and the concentrations of prodrug **6e**, **7b**, and **8** as well as active principle **3**−**5**, respectively, were determined by LC-MS.

Stability Studies in Biorelevant Media. Biorelevant media were prepared according to United States Pharmacopea (USP) specifications and Dressman et al.[51,52] as described below and are considered to be stable at ambient storage conditions for at least 72 h.[55] Table S1 (see Supporting Information) shows the composition of these biorelevant media used to mimic gastric and intestinal conditions.[51,52,55]

Simulated Gastric Fluid (sGF) and Simulated Intestinal Fluid (sIF). sGF and sIF were prepared according to the United States Pharmacopeia (USP 28).[51] For the preparation of sGF, sodium chloride, and pepsin were mixed in bidistilled water and then the pH was adjusted to 1.2 by adding 37% aq HCl. For sIF, monopotassium phosphate and pancreatin were mixed in bidistilled water and then the pH was adjusted to 6.8 by adding 0.2 M NaOH. In parallel, two buffer solutions were prepared equally to sGF and sIF, without pepsin (buffer sGF) and pancreatin (buffer sIF), respectively.

Fasted State Simulated Gastric Fluid (FaSSGF). First, a NaCl solution was prepared and its pH was adjusted to 1.6 with 37% aq HCl. The solution was then transferred into a round-bottom flask, and sodium taurocholate hydrate was dissolved by continuous stirring. Then, a freshly prepared solution of lecithin in dichloromethane (DCM) (100 mg/mL) was added. The resulting emulsion was turbid. The DCM was then evaporated at 40 °C. For the first 15 min, the pressure was kept at 650 mbar. It was then decreased stepwise to a final pressure of 100 mbar and maintained for another 15 min. The product was a clear solution, having no perceptible smell of DCM. Next, pepsin was added under continuous stirring and, as a last step, the pH (1.6) and the volume of the solution were adjusted.

Fed State Simulated Gastric Fluid (FeSSGF). Sodium acetate trihydrate and NaCl were dissolved in bidistilled water. Acetic acid was added followed by a pH adjustment to 5.0 with 0.2 M NaOH. The resulting solution was mixed 1:1 with ultrahigh temperature milk.

Fasted State Simulated Intestinal Fluid (FaSSIF). Blank buffer was prepared using appropriate amounts of NaCl, sodium hydroxide, and maleic acid in bidistilled water, and the pH was then adjusted to 6.5 with 0.2 M NaOH. The solution was then transferred into a round-bottom flask and sodium taurocholate hydrate was added under continuous stirring. Afterward, a freshly prepared solution of lecithin in DCM (100 mg/mL) was added. The resulting emulsion was turbid. The DCM was then evaporated at 40 °C (same procedure as for the FaSSGF). As a last step, the volume and pH (6.5) of the solution were adjusted again.

Fed State Simulated Intestinal Fluid (FeSSIF). Blank buffer was prepared using appropriate amounts of NaCl, sodium hydroxide, and maleic acid in bidistilled water, and the pH was then adjusted to 5.8 with 0.2 M NaOH. The solution was transferred into a round-bottom flask, and sodium taurocholate hydrate was added under continuous stirring. Afterward, a freshly prepared solution of lecithin in dichloromethane (DCM) (100 mg/mL) was added. The resulting emulsion was turbid. The DCM was then evaporated at 40 °C (same procedure as for the FaSSGF). A freshly prepared solution of glyceryl monooleate in DCM (50 mg/mL) was added, and a second evaporation step was performed. Next, appropriate amounts of sodium oleate and pancreatin were added slowly under continuous stirring and, as a last step, the volume and pH (5.8) of the solution were adjusted again.

Stability Assay. All fluids were preheated at 37 °C. The compounds (**7a**, **7c**, and **7d**) were then added to yield 20 μM solutions (t = 0 min). Incubations were performed on a Heidolph 1000 incubator (500 rpm, 37 °C). After an incubation time of 0, 10, 20, 30, 60, and 120 min, samples (30 μL) were withdrawn, precipitated with ice-cooled methanol (120 μL), put into the freezer (−20 °C, 10 min), and then centrifuged (13200 rpm, 3 min). The supernatant was transferred into a 96-well plate. The concentration of analyte in the supernatant was analyzed by LC-MS.

LC-MS Measurement. Analyses were performed using an 1100/1200 series HPLC system coupled to a 6410 triple quadrupole mass detector (Agilent Technologies, Inc., Santa Clara, CA, USA) equipped with electrospray ionization. The system was controlled with the Agilent MassHunter workstation data acquisition software (version B.01.04). The column used was an Atlantis T3 C18 column (2.1 mm × 50 mm) with a 3 μm particle size (Waters Corp., Milford, MA, USA). The mobile phase consisted of two eluents: eluent A (H_2O, containing 0.1% formic acid, v/v for compounds **5**, **6a**−**e**, **7c**, **7d**, and **8**; ammonium acetate buffer, 10 mM, pH 5 for compounds **3** and **4**;

DOI: 10.1021/acs.jmedchem.5b01923
J. Med. Chem. 2016, 59, 3163−3182

formiate buffer, 10 mM, pH 3 for compounds **7a** and **7b**) and eluent B (MeCN, containing 0.1% formic acid, v/v), delivered at 0.6 mL/min. The gradient was ramped from 95% A/5% B to 5% A/95% B over 1 min and then held at 5% A/95% B for 0.1 min. The system was then brought back to 95% A/5% B, resulting in a total duration of 4 min. MS parameters such as fragmentor voltage, collision energy, polarity were optimized individually for each analyte, and the molecular ion was followed for each compound in the multiple reaction monitoring mode. The concentrations of the analytes were quantified by the Agilent Mass Hunter quantitative analysis software (version B.01.04).

In Vivo Pharmacokinetics. For the PK studies, eight-week-old female C3H/HeN mice (21–27 g) from Harlan (Venray, The Netherlands) were purchased. The mice were housed in groups of three to five per cage and kept under specific pathogen-free conditions in the Animal House of the Department of Biomedicine, University Hospital of Basel. For experimentation, all guidelines according to the Swiss veterinary law were followed. The animals were kept in a 12 h/12 h light/dark cycle and had chow and water ad libitum. After 1 week of acclimatization, the mice were used in groups of three (five for **4**, 7.7 mg/kg) for the pharmacokinetic studies. Compounds were diluted in PBS and applied using an oral gavage (1.25 and 7.7 mg/kg for **4**, and 10 mg/kg for **8** and **7b**, **7c**). Prodrug solutions consisted of prodrug (min. 94%) and active principle (max 6%). Blood and urine samples (10 μL) were taken before the experiment (0 min) and at 6, 13, 20, 40 min, 1, 1.5, 2, 3, 4, 6, 8, and 24 h after administration. Directly after sampling, the samples were diluted in methanol (1:5) to precipitate proteins. After centrifugation (11 min, 13000 rpm), the supernatant was transferred to a 96-well plate and analyzed by LC-MS as described before. The samples at 0 min were used to define the detection limit in plasma and urine. Sampling and administration was performed following the guidelines in ref 56.

■ ASSOCIATED CONTENT

Supporting Information

The Supporting Information is available free of charge on the ACS Publications website at DOI: 10.1021/acs.jmedchem.5b01923.

Composition of biorelevant media, HPLC data, and chromatograms for target compounds, ^{1}H NMR spectra for target compounds (PDF)

■ AUTHOR INFORMATION

Corresponding Author

*Phone: +41 61 267 15 51. Fax: +41 61 267 15 52. E-mail: beat.ernst@unibas.ch.

Author Contributions

S.K., X.J., and P.F. contributed equally to the project

Notes

The authors declare no competing financial interest.

■ ACKNOWLEDGMENTS

We thank Prof. Dr. med. Radek Skoda, Department of Biomedicine, University Hospital Basel, Switzerland, for giving us access to the animal facility and Rachel Hevey for critical reading of the manuscript.

■ ABBREVIATIONS USED

ALP, alkaline phosphatase; C_{max}, maximum concentration; Caco-2 cells, colorectal adenocarcinoma cells; compd, compound; CRD, carbohydrate recognition domain; EtOAc, ethyl acetate; FimH, fimbrial adhesive protein H; FaSSGF, fasted state simulated gastric fluid; FeSSGF, fed state simulated gastric fluid; LC-MS, liquid chromatography–mass spectrometry; MeCN, acetonitrile; MPLC, medium pressure liquid chromatography; NIS, *N*-iodosuccinimide; *P*, octanol–water partition coefficient; P_{app}, apparent permeability; P_e, effective permeability; PAMPA, parallel artificial membrane permeability assay; PK, pharmacokinetic; $t_{1/2}$, half-life; T_{max}, time when maximum concentration is observed; UPEC, uropathogenic *Escherichia coli*; UTI, urinary tract infection

■ REFERENCES

(1) Fihn, S. D. Clinical practice. Acute uncomplicated urinary tract infection in women. *N. Engl. J. Med.* **2003**, *349*, 259–266.

(2) Wiles, T. J.; Kulesus, R. R.; Mulvey, M. A. Origins and virulence mechanisms of uropathogenic Escherichia coli. *Exp. Mol. Pathol.* **2008**, *85*, 11–19.

(3) Sanchez, G. V.; Master, R. N.; Karlowsky, J. A.; Bordon, J. M. In vitro antimicrobial resistance of urinary Escherichia coli isolates among U.S. outpatients from 2000 to 2010. *Antimicrob. Agents Chemother.* **2012**, *56*, 2181–2183.

(4) Hooton, T. M.; Stamm, W. E. Diagnosis and treatment of uncomplicated urinary tract infection. *Infect. Dis. Clin. North Am.* **1997**, *11*, 551–581.

(5) Svanborg, C.; Godaly, G. Bacterial virulence in urinary tract infection. *Infect. Dis. Clin. North Am.* **1997**, *11*, 513–529.

(6) Schilling, J. D.; Mulvey, M. A.; Hultgren, S. J. Structure and function of Escherichia coli type 1 pili: new insight into the pathogenesis of urinary tract infections. *J. Infect. Dis.* **2001**, *183*, S36–S40.

(7) Capitani, G.; Eidam, O.; Glockshuber, R.; Grütter, M. G. Structural and functional insights into the assembly of type 1 pili from Escherichia coli. *Microbes Infect.* **2006**, *8*, 2284–2290.

(8) Sharon, N. Carbohydrates as future anti-adhesion drugs for infectious diseases. *Biochim. Biophys. Acta, Gen. Subj.* **2006**, *1760*, 527–537.

(9) Firon, N.; Ofek, I.; Sharon, N. Interaction of mannose-containing oligosaccharides with the fimbrial lectin of *Escherichia coli*. *Biochem. Biophys. Res. Commun.* **1982**, *105*, 1426–1432.

(10) Firon, N.; Ofek, I.; Sharon, N. Carbohydrate specificity of the surface lectins of *Escherichia coli*, *Klebsiella pneumoniae*, and *Salmonella typhimurium*. *Carbohydr. Res.* **1983**, *120*, 235–249.

(11) Bouckaert, J.; Berglund, J.; Schembri, M.; De Genst, E.; Cools, L.; Wuhrer, M.; Hung, C.-S.; Pinkner, J.; Slättegard, R.; Zavialov, A.; Choudhury, D.; Langermann, S.; Hultgren, S. J.; Wyns, L.; Klemm, P.; Oscarson, S.; Knight, S. D.; De Greve, H. Receptor binding studies disclose a novel class of high-affinity inhibitors of the *Escherichia coli* FimH adhesin. *Mol. Microbiol.* **2005**, *55*, 441–455.

(12) Firon, N.; Ashkenazi, S.; Mirelman, D.; Ofek, I.; Sharon, N. Aromatic alpha-glycosides of mannose are powerful inhibitors of the adherence of type 1 fimbriated *Escherichia coli* to yeast and intestinal epithelial cells. *Infect. Immun.* **1987**, *55*, 472–476.

(13) Sperling, O.; Fuchs, A.; Lindhorst, T. K. Evaluation of the carbohydrate recognition domain of the bacterial adhesin FimH. Design, synthesis and binding properties of mannoside ligands. *Org. Biomol. Chem.* **2006**, *4*, 3913–3922.

(14) Han, Z.; Pinkner, J. S.; Ford, B.; Obermann, R.; Nolan, W.; Wildman, S. A.; Hobbs, D.; Ellenberger, T.; Cusumano, C. K.; Hultgren, S. J.; Janetka, J. W. Structure-based drug design and optimization of mannoside bacterial FimH antagonists. *J. Med. Chem.* **2010**, *53*, 4779–4792.

(15) Klein, T.; Abgottspon, D.; Wittwer, M.; Rabbani, S.; Herold, J.; Jiang, X.; Kleeb, S.; Lüthi, C.; Scharenberg, M.; Bezençon, J.; Gubler, E.; Pang, L.; Smiesko, M.; Cutting, B.; Schwardt, O.; Ernst, B. FimH antagonists for the oral treatment of urinary tract infections: from design and synthesis to in vitro and in vivo evaluation. *J. Med. Chem.* **2010**, *53*, 8627–8641.

(16) Cusumano, C. K.; Pinkner, J. S.; Han, Z.; Greene, S. E.; Ford, B. A.; Crowley, J. R.; Henderson, J. P.; Janetka, J. W.; Hultgren, S. J. Treatment and prevention of urinary tract infection with orally active FimH inhibitors. *Sci. Transl. Med.* **2011**, *3*, 109ra115.

(17) Han, Z.; Pinkner, J. S.; Ford, B.; Chorell, E.; Crowley, J. M.; Cusumano, C. K.; Campbell, S.; Henderson, J. P.; Hultgren, S. J.;

DOI: 10.1021/acs.jmedchem.5b01923
J. Med. Chem. 2016, 59, 3163–3182

Janetka, J. W. Lead optimization studies on FimH antagonists: discovery of potent and orally bioavailable *ortho*-substituted biphenyl mannosides. *J. Med. Chem.* **2012**, *55*, 3945−3959.
(18) Pang, L.; Kleeb, S.; Lemme, K.; Rabbani, S.; Scharenberg, M.; Zalewski, A.; Schädler, F.; Schwardt, O.; Ernst, B. FimH antagonists: structure-activity and structure-property relationships for biphenyl α-D-mannopyranosides. *ChemMedChem* **2012**, *7*, 1404−1422.
(19) Kleeb, S.; Pang, L.; Mayer, K.; Eris, D.; Sigl, A.; Preston, R. C.; Zihlmann, P.; Abgottspon, D.; Hutter, A.; Scharenberg, M.; Jiang, X.; Navarra, G.; Rabbani, S.; Smiesko, M.; Lüdin, N.; Jakob, R. P.; Bezençon, J.; Schwardt, O.; Maier, T.; Sharpe, T.; Ernst, B. FimH antagonists: bioisosteres to improve the in vitro and in vivo PK/PD profile. *J. Med. Chem.* **2015**, *58*, 2221−2239.
(20) Jiang, X.; Abgottspon, D.; Kleeb, S.; Rabbani, S.; Scharenberg, M.; Wittwer, M.; Haug, M.; Schwardt, O.; Ernst, B. Anti-adhesion therapy for urinary tract infections − a balanced PK/PD profile proved to be key for success. *J. Med. Chem.* **2012**, *55*, 4700−4713.
(21) Schwardt, O.; Rabbani, S.; Hartmann, M.; Abgottspon, D.; Wittwer, M.; Kleeb, S.; Zalewski, A.; Smiesko, M.; Cutting, B.; Ernst, B. Design, synthesis and biological evaluation of mannosyl triazoles as FimH antagonists. *Bioorg. Med. Chem.* **2011**, *19*, 6454−6473.
(22) Brument, S.; Sivignon, A.; Dumych, T. I.; Moreau, N.; Roos, G.; Guérardel, Y.; Chalopin, T.; Deniaud, D.; Bilyy, R. O.; Darfeuille-Michaud, A.; Bouckaert, J.; Gouin, S. G. Thiazolylaminomannosides as potent antiadhesives of type 1 piliated *Escherichia coli* isolated from Crohn's disease patients. *J. Med. Chem.* **2013**, *56*, 5395−5406.
(23) Lindhorst, T. K.; Kieburg, C.; Krallmann-Wenzel, U. Inhibition of the type 1 fimbriae-mediated adhesion of *Escherichia coli* to erythrocytes by multiantennary D-mannosyl clusters: The effect of multivalency. *Glycoconjugate J.* **1998**, *15*, 605−613.
(24) Nagahori, N.; Lee, R. T.; Nishimura, S.-L.; Pagé, S.; Roy, R.; Lee, Y. C. Inhibition of adhesion of type 1 fimbriated *Escherichia coli* to highly mannosylated ligands. *ChemBioChem* **2002**, *3*, 836−844.
(25) Appeldoorn, C. C. M.; Joosten, J. A. F.; Ait el Maate, F. A.; Dobrindt, U.; Hacker, J.; Liskamp, R. M. J.; Khan, A. S.; Pieters, R. J. Novel multivalent mannose compounds and their inhibition of the adhesion of type 1 fimbriated uropathogenic *E. coli*. *Tetrahedron: Asymmetry* **2005**, *16*, 361−372.
(26) Patel, A.; Lindhorst, T. K. A modular approach for the synthesis of oligosaccharide mimetics. *Carbohydr. Res.* **2006**, *341*, 1657−1668.
(27) Touaibia, M.; Wellens, A.; Shiao, T. C.; Wang, Q.; Sirois, S.; Bouckaert, J.; Roy, R. Mannosylated M(0) dendrimers with nanomolar affinities to *Escherichia coli* FimH. *ChemMedChem* **2007**, *2*, 1190−1201.
(28) Durka, M.; Buffet, K.; Iehl, J.; Holler, M.; Nierengarten, J.-F.; Taganna, J.; Bouckaert, J.; Vincent, S. P. The functional valency of dodecamannosylated fullerenes with *Escherichia coli* FimH - towards novel bacterial antiadhesives. *Chem. Commun.* **2011**, *47*, 1321−1323.
(29) Bouckaert, J.; Li, Z.; Xavier, C.; Almant, M.; Caveliers, V.; Lahoutte, T.; Weeks, S. D.; Kovensky, J.; Gouin, S. G. Heptyl α-D-mannosides grafted on a β-cyclodextrin core to interfere with *Escherichia coli* adhesion: An in vivo multivalent effect. *Chem. - Eur. J.* **2013**, *19*, 7847−7855.
(30) Scharenberg, M.; Schwardt, O.; Rabbani, S.; Ernst, B. Target selectivity of FimH antagonists. *J. Med. Chem.* **2012**, *55*, 9810−9816.
(31) Van de Waterbeemd, H.; Smith, D. A.; Beaumont, K.; Walker, D. K. Property-based design: Optimization of drug absorption and pharmacokinetics. *J. Med. Chem.* **2001**, *44*, 1313−1333.
(32) Amidon, G. L.; Lennernäs, H.; Shah, V. P.; Crison, J. R. A theoretical basis for a biopharmaceutic drug classification: the correlation of in vitro drug product dissolution and in vivo bioavailability. *Pharm. Res.* **1995**, *12*, 413−420.
(33) Heimbach, T.; Oh, D.-M.; Li, L. Y.; Forsberg, M.; Savolainen, J.; Leppänen, J.; Matsunaga, Y.; Flynn, G.; Fleisher, D. Absorption rate limit considerations for oral phosphate prodrugs. *Pharm. Res.* **2003**, *20*, 848−856.
(34) Stella, V. J.; Nti-Addae, K. W. Prodrug strategies to overcome poor water solubility. *Adv. Drug Delivery Rev.* **2007**, *59*, 677−694.
(35) Stewart, B. H.; Amidon, G. L.; Brabec, R. K. Uptake of prodrugs by rat intestinal mucosal cells: mechanism and pharmaceutical implications. *J. Pharm. Sci.* **1986**, *75*, 940−945.
(36) Wire, M. B.; Shelton, M. J.; Studenberg, S. Fosamprenavir: clinical pharmacokinetics and drug interactions of the amprenavir prodrug. *Clin. Pharmacokinet.* **2006**, *45*, 137−168.
(37) Hersh, M. R.; Kuhn, J. G.; Phillips, J. L.; Clark, G.; Ludden, T. M.; Von Hoff, D. D. Pharmacokinetic study of fludarabine phosphate (NSC 312887). *Cancer Chemother. Pharmacol.* **1986**, *17*, 277−280.
(38) Rabbani, S.; Jiang, X. H.; Schwardt, O.; Ernst, B. Expression of the carbohydrate recognition domain of FimH and development of a competitive binding assay. *Anal. Biochem.* **2010**, *407*, 188−195.
(39) Alsenz, J.; Kansy, M. High throughput solubility measurement in drug discovery and development. *Adv. Drug Delivery Rev.* **2007**, *59*, 546−567.
(40) Waring, M. J. Lipophilicity in drug discovery. *Expert Opin. Drug Discovery* **2010**, *5*, 235−248.
(41) Kansy, M.; Senner, F.; Gubernator, K. Physicochemical high throughput screening: Parallel artificial membrane permeation assay in the description of passive absorption processes. *J. Med. Chem.* **1998**, *41*, 1007−1010.
(42) Avdeef, A.; Bendels, S.; Di, L.; Faller, B.; Kansy, M.; Sugano, K.; Yamauchi, Y. PAMPA - Critical factors for better predictions of absorption. *J. Pharm. Sci.* **2007**, *96*, 2893−2909.
(43) Artursson, P.; Karlsson, J. Correlation between oral drug absorption in humans and apparent drug permeability coefficients in human intestinal epithelial (Caco-2) cells. *Biochem. Biophys. Res. Commun.* **1991**, *175*, 880−885.
(44) Hubatsch, I.; Ragnarsson, E. G. E.; Artursson, P. Determination of drug permeability and prediction of drug absorption in Caco-2 monolayers. *Nat. Protoc.* **2007**, *2*, 2111−2119.
(45) DeGoey, D. A.; Grampovnik, D. J.; Flosi, W. J.; Marsh, K. C.; Wang, X. C.; Klein, L. L.; McDaniel, K. F.; Liu, Y.; Long, M. A.; Kati, W. M.; Molla, A.; Kempf, D. J. Water-soluble prodrugs of the human immunodeficiency virus protease inhibitors lopinavir and ritonavir. *J. Med. Chem.* **2009**, *52*, 2964−2970.
(46) Ma, Z.; Zhang, J.; Kong, F. Facile synthesis of arabinomannose penta- and decasaccharide fragments of the lipoarabinomannan of the equine pathogen, Rhodococcus equi. *Carbohydr. Res.* **2004**, *339*, 1761−1771.
(47) Dong, H.; Pei, Z.; Byström, S.; Ramström, O. Reagent-Dependent Regioselective Control in Multiple Carbohydrate Esterifications. *J. Org. Chem.* **2007**, *72*, 1499−1502.
(48) Yuan, H.; Li, N.; Lai, Y. Evaluation of in vitro models for screening phosphatase-mediated bioconversion of phosphate ester prodrugs. *Drug Metab. Dispos.* **2009**, *37*, 1443−1447.
(49) Kearny, A. S.; Stella, V. J. The in vitro enzymic labilities of chemically distinct phosphomonoester prodrugs. *Pharm. Res.* **1992**, *9*, 497−503.
(50) Dhareshwar, S. S.; Stella, V. J. A novel prodrug strategy for beta-dicarbonyl carbon acids: syntheses and evaluation of the physicochemical characteristics of C-phosphoryloxymethyl (POM) and phosphoryloxymethyloxymethyl (POMOM) prodrug derivatives. *J. Pharm. Sci.* **2010**, *99*, 2711−2723.
(51) *The United States Pharmacopeia (USP 28)*; U. S. Pharmacopeia: Rockville, MD, 2004.
(52) Dressman, J. B.; Thelen, K.; Jantratid, E. Towards quantitative prediction of oral drug absorption. *Clin. Pharmacokinet.* **2008**, *47*, 655−667.
(53) Stephens, R. H.; O'Neill, C. A.; Warhurst, A.; Carlson, G. L.; Rowland, M.; Warhurst, G. Kinetic profiling of P-glycoprotein-mediated drug efflux in rat and human intestinal epithelia. *J. Pharmacol. Exp. Ther.* **2001**, *296*, 584−591.
(54) Zhang, Y.; Huo, M.; Zhou, J.; Xie, S. PKSolver: An add-in program for pharmacokinetic and pharmacodynamic data analysis in Microsoft Excel. *Comput. Methods Programs Biomed.* **2010**, *99*, 306−314.

DOI: 10.1021/acs.jmedchem.5b01923
J. Med. Chem. 2016, 59, 3163−3182

(55) Jantratid, E.; Janssen, N.; Reppas, C.; Dressman, J. B. Dissolution media simulating conditions in the proximal human gastrointestinal tract: an update. *Pharm. Res.* **2008**, *25*, 1663−1676.
(56) Diehl, K.-H.; Hull, R.; Morton, D.; Pfister, R.; Rabemampianina, Y.; Smith, D.; Vidal, J.-M.; Van de Vorstenbosch, C. A good practice guide to the administration of substances and removal of blood, including routes and volumes. *J. Appl. Toxicol.* **2001**, *21*, 15−23.

DOI: 10.1021/acs.jmedchem.5b01923
J. Med. Chem. 2016, 59, 3163−3182

5.4. MANUSCRIPT I

"Treatment regimens of FimH antagonists against urinary tract infection – PK/PD of an anti-adhesive therapy"

Anja Sigl, Priska Frei, Katharina Mayer, and Beat Ernst

Shall be submitted to *Antimicrobial Agents and Chemotherapy*

Treatment regimens of FimH antagonists against urinary tract infection – PK/PD of an anti-adhesive therapy

Anja Sigl, Priska Frei, Katharina Mayer, and Beat Ernst#

Institute of Molecular Pharmacy, University of Basel, Switzerland

Running Head: FimH antagonists against urinary tract infections

#Address correspondence to Beat Ernst, beat.ernst@unibas.ch

ABSTRACT

Anti-adhesion therapies, a new therapeutic approach to treat infectious diseases, avoids killing of the pathogens, reduces selective pressure and therefore the development of resistances. In urinary tract infections (UTIs), uropathogenic *E. coli* (UPEC) use FimH-adhesins located at the tip of type 1 pili for the attachment and invation to and into urothelial cells of the host. This adhesion process is a prerequisite for invasion, colonization, and biofilm formation. FimH antagonists provide a novel strategy for preventing UTI by impeding the interaction of FimH with the urothelial ligand. In this study, the previously published 3′-chloro-4′-(α-D-mannopyranosyloxy)biphenyl-4-carbonitrile (Kleeb, S. *et al. J. Med. Chem.* **58,** 2221–2239, 2015) was applied to study the potential for a therapeutic application within the UTI infection cycle. This includes a long-term preventive study (24 h), different treatment regimens, and combination therapies with ciprofloxacin (CIP). Thereby, an effective therapeutic outcome was governed by a specific concentration-MAC_{90} (minimal anti-adhesive concentration) ratio, which was most effective before the intracellular growth phase and after bacterial egress from infected cells. A single preventive dose was effective up to 12 hours after infection and resulted in a 2.2 Log_{10} CFU/ml decrease of bacterial colonies in the bladder. Also, the antagonist was very effective in a combination therapy with CIP, clearing the bladder from almost all bacteria compared to CIP alone. Overall, the 3-chloro-4'-cyanobiphenyl α-D-mannopyranoside proofed effective in different treatment set-ups, where the effect was governed by an effective concentration/MAC_{90} magnitude and the duration within the infection.

INTRODUCTION

With increasing antimicrobial resistance rates worldwide, anti-adhesive therapies could provide a new strategy to combat bacterial infections. However, this new mode of action poses new challenges for optimal treatment regimens, as the relationship of drug concentration and efficacy is not yet established. Nevertheless, the anti-adhesive approach was successfully applied in humans and prevented urinary tract infection (UTI). It was shown that prophylaxis with high doses of D-mannose reduced the recurrence rate of UTI to the same extent as prophylaxis with nitrofurantoin (1).

UTI is a highly prevalent infection, affecting 50% of women at least once in their lifetime. Moreover, a recurrence rate of 25% within 6 months is challenging any UTI treatment and can rapidly lead to resistances (2–4). Up to 90% of the community acquired UTIs are caused by uropathogenic *E. coli* (UPEC) (3, 5). UPEC possesses several virulence factors, which enhance the urologic infection potential. One of the most important virulence factors are type 1 pili. With the lectin FimH, located at the tip of the type 1 pili, the bacteria bind to the highly mannosylated glycoprotein uroplakin 1a on the luminal bladder cell surface and initiate the infection cascade (6–8). Infections with strains unable to express type 1 fimbriae show a 100-1000 fold reduced bacterial load in the bladder (9).

The pathogenic cycle was divided into three stages according to the formation of intracellular bacterial communities (IBCs), which are termed as early, middle, and late IBCs (10). The initial attachment and invasion process (up to 3 h post infection, early IBC) is followed by an intracellular replication in a biofilm like structure (4-8 h post infection, middle IBC) and ultimately results in new bacterial egress (starting at 12h post infection, late IBC) (10–13). Back in the bladder lumen, bacteria can initiate a new infection round or infect underlying immature cells, leading to the establishment of a quiescent intracellular reservoir (QIR) (14, 10, 12, 15). An average middle IBC is built up of approximately 10^3-10^5 colony forming units (CFU) (10, 12, 15). Bacteria that are able to invade, but do not form IBCs, are rapidly cleared from the urinary tract (16). Also, genes important for the establishment of an IBC were shown to be positively selected in uropathogenic strains (16, 17). Thus, IBCs are important for bacterial persistence and are most challenging to treat. Within an IBC, bacteria are protected from urine flow, from immune reactions, and also from most antibiotic treatments. IBC formation was described in humans, different mouse strains, and also in cultured bladder cells (18, 19). Therefore, mice offer a good model to study the pathogenesis of UTI. It was shown that the experimentally induced bladder infection in C3H/HeN mice, which were mainly used for UTI studies, is most active within the first 24 hours post infection (hpi). After 48 hours, up to 40% of infected mice developed a persistent bacteriuria and chronic cystitis, whereas the remaining animals cleared the infection (20).

FimH antagonists mimic the physiological ligand and target the initial adhesion by binding to the FimH lectin, preventing the attachment to the bladder epithelial surface. This results in the clearance of the bacteria with urine flow. Compared to D-mannose, antagonists with improved pharmacokinetic (PK) and pharmacodynamic (PD) properties were synthesized and effectively depleted bacterial loads in the bladder of mice up to 3 Log_{10} units (21–25). The anti-adhesive mechanism of action offers the possibility for preventive applications. Yet, FimH antagonists could also impede bacteria emerging from infected cells from starting a new infection cycle. Accordingly, Totsika *et al.* showed a beneficial effect of FimH antagonists in treating recurrent cystitis (26). However, FimH antagonists were so far not characterized for their PK/PD characteristics. In other words, it is not clear, how FimH antagonists have to be applied to be most effective in the context of the UTI infection cycle.

In our study, the potent *para*-cyano biphenyl α-D-mannopyranoside (**10j** in (25)) was used to study the effect of a preventive application in a 24-hour infection. The results were used to create different treatment regimens, taking into account the infection cycle stages. Also, urine concentrations of the antagonist were studied in detail, both in uninfected and infected mice. Furthermore, the antagonist was used in a combination therapy with ciprofloxacin (CIP). The results presented here should assist optimal treatment regimens for future applications of anti-adhesive therapies for prevention and/or treatment of UTI in patients.

MATERIALS AND METHODS

Bacterial cultivation. Cystitis isolate UTI89 was kindly provided from the group of Prof. Urs Jenal, Biozentrum, University of Basel. For experiments, the strain was cultivated overnight at 37°C in 10 ml Luria-Bertani broth (LB, Becton, Dickinson and Company, France). For harvesting bacteria, the liquid broth was centrifuged (1857 g, 10 min) and bacterial pellets were washed three times in Dulbecco's phosphate buffered saline (PBS, Sigma-Aldrich, Switzerland). Bacterial concentrations for infection were determined via optical density (OD_{600}) measurements and plating on BBL Levine Eosin Methylene Blue (EMB) agar plates (Becton Dickinson, France) in serial dilutions to determine the exact bacterial concentration in CFU per ml (CFU/ml).

Animal studies. For all animal studies, female C3H/HeN (Envigo (former Harlan), Netherlands) were used. They were housed two to six animals per cage in a 12h/12h light/dark cycle, in specific-pathogen free conditions in the Animal Facility of the Department of Biomedicine at the University Hospital of Basel. After one week of acclimatization, nine to ten week old mice were used for the experiments. Before and during experiments, animals had free access to chow and water at any time. For administration volumes and sampling the good practice guidelines were followed (27). Numbers of animals used were estimated *a priori*, depending on the type of study, using the G*3Power program (28). All experiments were performed according to the regulations of the Swiss veterinary law for animal experimentation.

Pharmacokinetic study. The antagonist was diluted in DMSO (5% of final volume, Sigma-Aldrich, Switzerland) and in 1% Tween 80 (Sigma-Aldrich, Switzerland) in PBS. For oral application, a gavage (Fine Science Tools, Germany) with syringes (Soft-Ject, 1 ml syringes, Henke Sass Wolf, Germany) was used.
The application was followed by urine sampling at several time points for 24 hours. For the PK study in infection, mice were additionally infected 40 min post application. Urine samples were directly diluted after sampling with methanol (99%, Acros Organics, Chemie Brunschwig, Switzerland) and centrifuged for 11 min at 15700 g. The supernatants were transferred to a 96-well plate and the analyte concentrations were determined by LC-MS. For the analysis, a 1100/1200 Series HPLC System coupled to a 6410 Triple Quadrupole mass detector (Agilent Technologies, Inc., USA) with electrospray ionization was used. An Atlantis T3 C18 column (2.1 mm × 50 mm) with 3 µm particle size (Waters Corp., USA) was used. The mobile phase consisted of solvent A (10 mM ammonium acetate, pH 5.0 in 95:5, H_2O/MeCN) and solvent B (MeCN containing 0.1% formic acid v/v) both delivered at a flow rate of 0.6 mL/min. Within a total duration of 4 min, the gradient was changed from 95% A/5% B to 5% A/95% B during 1 min and held at 5% A/95% B for 0.1 min before returning to 95% A/5% B for the remaining 2.9 min. MS parameters such as fragmentor voltage, collision energy, and polarity were optimized previously. Data was quantified using Agilent Mass Hunter Quantitative Analysis software (version B.01.04) and was analyzed using Prism Software (GraphPad Prism).

General procedures for all infection studies. For all infection studies, the drinking water of the mice was supplemented with 5% glucose (monohydrate, AppliChem, BioChemica, Switzerland) three days before the start of the experiment.

The antagonist was applied orally, 40 minutes before infection with UTI89 to assure sufficient concentration in the bladder. CIP was applied subcutaneously (s.c.) either preventively 10 min before infection or as a treatment to the indicated time points at a dose of 8 mg/kg, corresponding to a human dose of 500 mg (29). Before infection, remaining urine in the bladder was expelled or collected by gentle pressure on the abdomen. Mice were anaesthetized in 2.5 vol% isoflurane/oxygen mixture (Attane, Minrad Inc, USA) and placed on their back. Infection was performed transurethrally using a polyethylene catheter (Intramedic polyethylene tubing, inner diameter 0.28 mm, outer diameter 0.61 mm, Beckton Dickinson, Switzerland), on a syringe (Hamilton Gastight Syringe 50 µl, removable 30G needle, BGB Analytik AG, Boeckten, Switzerland). After gentle insertion of the catheter into the bladder, 50 µl of bacterial suspension of UTI89 ($5.5x10^9$-$2.25x10^{10}$ CFU/ml) was slowly injected. This corresponded to approximately 10^7-10^8 CFU per mouse. For the low inoculum, mice were infected with 10^5-10^6 CFU per mouse. Urine was collected at different time points depending on the experiment. Mice were killed by CO_2 and bladder and kidneys were aseptically removed. Organs were homogenized in phosphate buffered saline (PBS) using a tissue lyser (Retsch, Haan, Germany). Serial dilutions of urine, bladder, and kidneys were plated on EMB agar plates and CFU were counted after overnight incubation at 37°C.

Remaining urine was used for determination of antagonist concentrations, analyzed by LC-MS. Therefore, urine samples were immediately diluted with methanol (99%) and centrifuged for 11 min at 15700 g. The supernatants were transferred to a 96-well plate for LC-MS analysis as described above.

Generally, data was analyzed using Prism Software (GraphPad Prism).

Long-term prevention study. The *para*-cyano biphenyl α-D-mannopyranoside (**10j** in 6) was applied orally 40 minutes before infection and mice were killed with CO_2 at 3, 6, 12, and 24 hours post infection (hpi). A control group of four mice per time-point was used, which received no treatment. Organs were processed as described before.

Regimen 1. Antagonist (10 mg/kg) was applied orally 40 minutes before infection, 3, and 6 hpi. CIP (8 mg/kg) was given similarly, 10 minutes prior to infection s.c., and 3, and 6 hpi for comparison of the treatment efficacy. Mice were killed with CO_2 9 hpi. The control group received no treatment. During infection, urine was collected and urine levels of the antagonist were analyzed by LC-MS. Organs were crushed and analyzed as described before.

Regimen 2. The phosphate prodrug (30) was added to the 5% glucose containing drinking water at a concentration of 100 µg/ml 24 hours before infection. With an average intake of circa 250 µl per hour for a 25 g mouse (internal surveillance), the dose would correspond to 1 mg/kg per mouse and hour. Antagonist concentration in the drinking water remained stable throughout the whole experiment (data not shown). During infection, urine was collected and antagonist levels were analyzed by LC-MS. Organs were crushed and analyzed as described before.

Regimen 3 and 4. The antagonist (10 mg/kg) was applied at different time points relative to infection in combination with CIP (8 mg/kg). The schedules are displayed in Figure 3.

RESULTS

A single preventive application of FimH antagonist reduces the bacterial load in the bladder for 12 hours. The *para*-cyano biphenyl α D-mannopyranoside (**10j** from (25), Figure 1B) proofed effective in reducing bacterial counts in a 3 h infection with UTI89 by approximately 1000-fold (25). However, this time span only allows to study the initial event of an infection cycle, namely attachment and invasion. Also, it does not indicate whether the therapeutic outcome is dependent on a time-dependent ($T>MAC_{90}$) or a concentration-dependent (C_{max}/MAC_{90}) effect, respectively. Therefore, the duration of the effect of a single 10 mg/kg application of the FimH antagonist was studied in a 24 h experiment. Since urine concentrations, as determined in a pharmacokinetic (PK) study, remained over the minimal anti-adhesive concentration (MAC_{90}, 0.09 µg/ml, (25)) for 24 hours, the effect of the antagonist could theoretically last 24 hours (Figure 1A). The MAC_{90} was determined using an *in vitro* cell infection assay, which was previously published (31, 32). It represents the minimal concentration needed for a therapeutic effect.

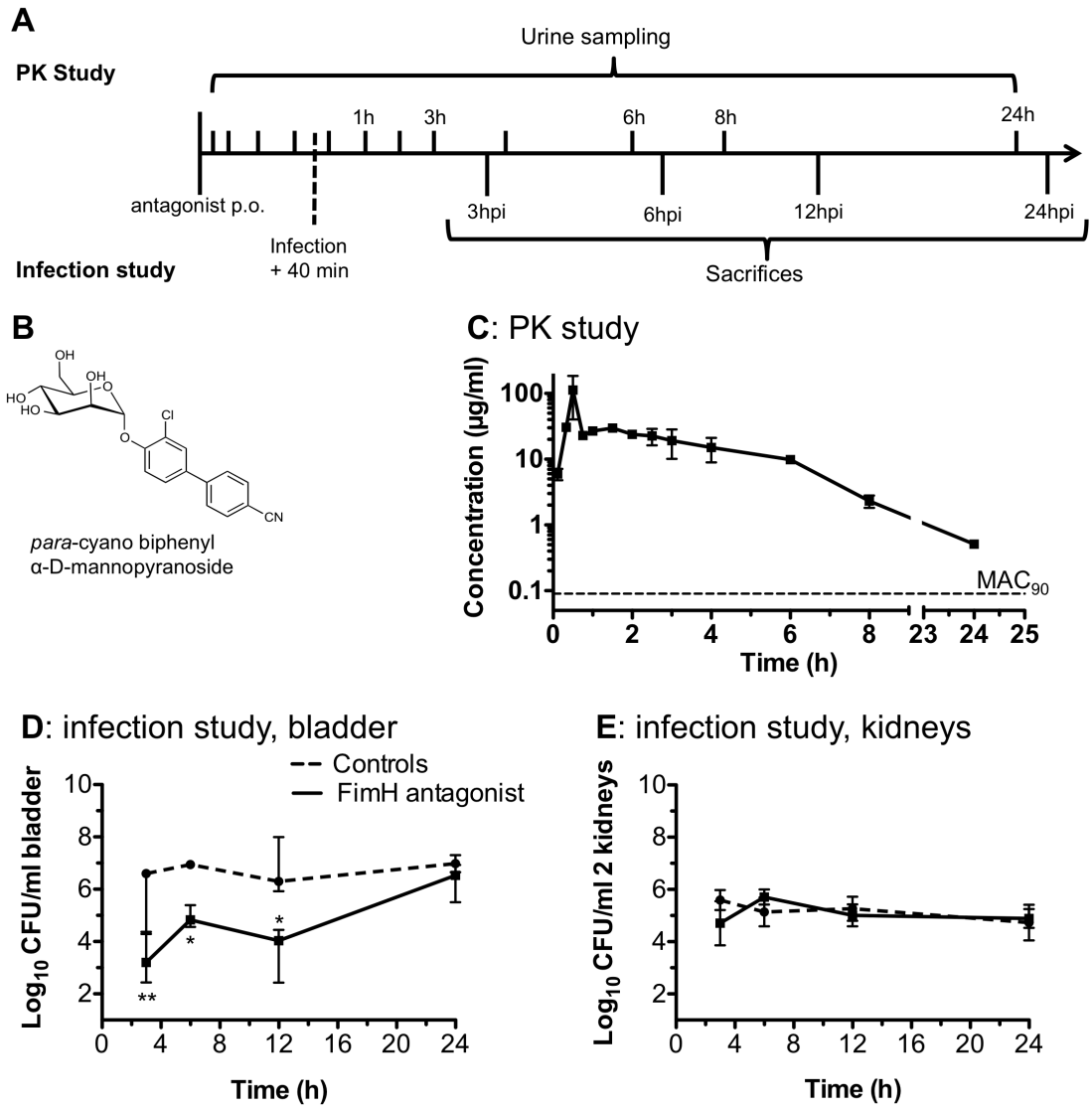

Figure 1. The antagonist exerts a preventive effect up to 12 hours post infection. The *para*-cyano biphenyl α D-mannopyranoside (**10j** in (25), B) was orally applied (10 mg/kg) for the PK and the infection study (A). Urine concentrations of the antagonist were sampled at several time points and plotted over time (C). The MAC_{90} is indicated as dashed line. Concentrations stay over the MAC_{90} value for 24 hours. The development of the infection over 24 h with (continuous line) and without (dashed line) preventive treatment with 10 mg/kg in bladder (D) and kidneys (E) showed a significant reduction of bacterial counts in the bladder for 12 hours (Mann-Whitney U test, **, $p<0.01$, *, $p<0.05$) Shown are median values with the interquartile range. PK: pharmacokinetic, MAC_{90}: minimal anti-adhesive concentration.

The antagonist reached a C_{max} of 112.6 µg/ml at 0.5 h after application and showed a slow and steady decrease over time (Figure 1C). The high concentrations were beneficial for the therapeutic effect. The single preventive application resulted in a CFU reduction for up to 12 hpi, yet, only in the bladder and not in the kidneys.

Interestingly, the increase in CFU counts between 3 hpi (3.6 Log_{10} CFU/ml) and 6 hpi (4.8 Log_{10} CFU/ml) in the intervention group and also slightly in the control group (from 6.6 to 6.9 Log_{10} CFU/ml) could indicate a phase of intracellular bacterial replication. Bacterial counts of the intervention groups matched control levels after 24 hours (Figure 1D&E). Likely, this is due to the high bacterial challenge after fluxing together with decreasing antagonist concentrations over time, although concentrations still remain over the MAC_{90} (Figure 1C).

Overall, the preventive effect upon a single application of the antagonist was measurable for up to 12 hpi. At this time point, bacterial regrowth overwhelmed the antagonist effect. Yet, the simple $T>MAC_{90}$ is not representative for a positive treatment outcome.

The antagonist reduces bacterial loads independent of the inoculum. Since $T>MAC_{90}$ is not representative for the therapeutic time-span, the effect might be concentration-dependent. Assuming that a positive therapeutic outcome depends on the duration of a certain therapeutically relevant concentration-MAC_{90} ratio, it would be interesting to influence either the concentration of antagonist in the urine or the MAC_{90} to change a specific ratio. Therefore, the preventive effect of the antagonist was studied using a lower inoculum, which results in a lower number of type 1 pili and thus, a lower MAC_{90} threshold. Mice were preventively treated with 10 mg/kg before infection with 10^5-10^6 CFU per mouse, which is roughly 100-times less than the inoculum for the previous study (10^7-10^8 CFU per mouse) (Figure 2). The control groups received no treatment and bacterial load in the bladder reached 5.7 Log_{10} CFU/ml at 24 hpi (data not shown), which was slightly lower than with the high inoculum (7 Log_{10} CFU/ml).

Bladder counts of the treated group were reduced from 5 Log_{10} CFU/ml (controls) to 2.1 Log_{10} CFU/ml at 3 hpi (Figure 2A). This is the same 1000-fold reduction at 3 hpi as it was achieved with the higher inoculum. At 6 hpi, the difference between controls and treated group was only approximately 1.5 Log_{10} CFU/ml, mainly due to the low infection of control groups. Bacterial reduction was also observed in the kidneys at 3 hpi (Figure 2B).

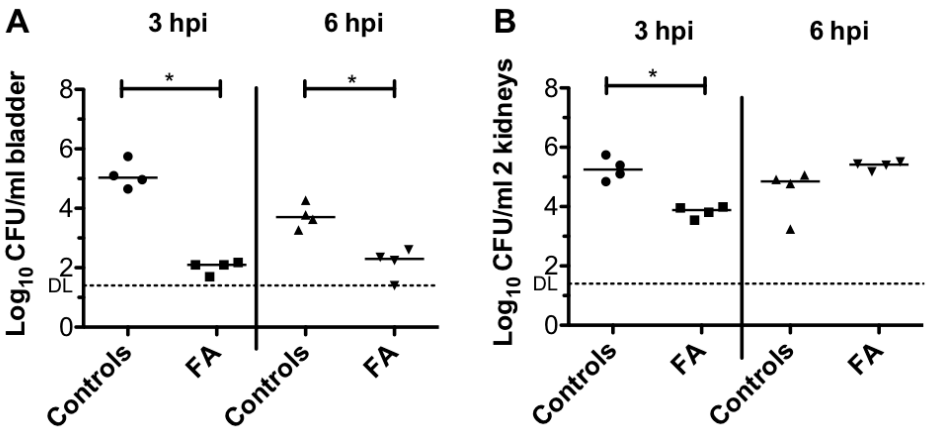

Figure 2. The therapeutic effect is independent of the inoculum. Preventive oral application of FimH antagonist (FA, 10 mg/kg p.o.) and infection with an inoculum of 10^5-10^6 CFU per mouse. (A) Bladder and (B) kidney CFU counts at 3 hpi and 6 hpi. A line in each group indicates the median. (Mann-Whitney U test, *, $p<0.05$). DL: detection limit (dashed line).

Likely, reaching a certain excess of antagonist compared to the MAC_{90} is predictive for a therapeutic outcome. However, exceeding this effective ratio will not proportionally increase the effect.

Different treatment regimens indicate the importance of the concentration related to the MAC_{90} and the possibility for combination therapies. To increase antagonist concentrations in urine and therefore prolonging the effective concentration/MAC_{90} ratio, both, a frequent dosing (Regimen 1) and a drinking-water prevention (Regimen 2) were studied (Figure 3). In Regimen 1, following a single preventive dose (10 mg/kg), two further applications at 3 hpi and 6 hpi were added. In Regimen 2, the continuous supply of FimH antagonist via the drinking water could increase urine levels even higher and reach a constant level. Furthermore, a combination therapy with antibiotics could offer another possibility to apply FimH antagonists in UTI treatment. Therefore, ciprofloxacin (CIP), an antibiotic often used against UTI (2, 33–36), was studied in two set-ups. Regimen 3 studied the additional preventive application to a CIP treatment. In Regimen 4, the antagonist was added therapeutically to a CIP treatment of an established infection (Figure 3).

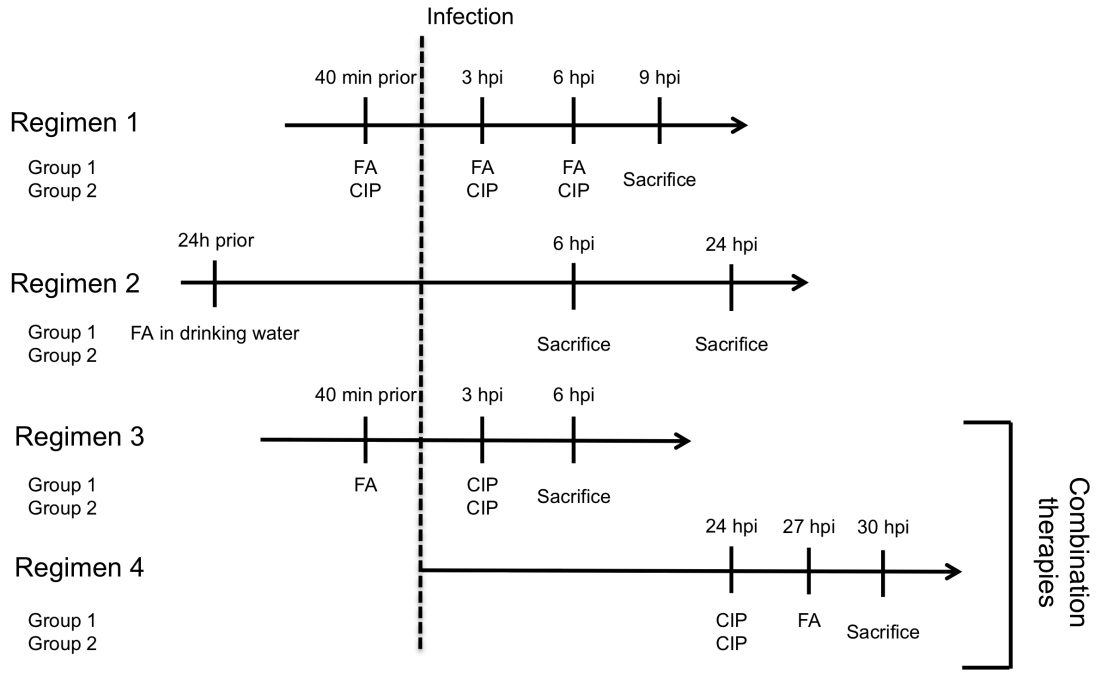

Figure3. Treatment set-ups studied using the *para*-cyano biphenyl α D-mannopyranoside. Regimen 1 combines the preventive dose with further therapeutic doses. Regimen 2 is a drinking-water prevention and Regimens 3 and 4 are combination therapies with ciprofloxacin (CIP, 8 mg/kg, s.c.). hpi: hours post infection, FA: antagonist, 10 mg/kg, p.o.

The accumulation of antagonist in urine significantly reduces the bacterial counts in the bladder (Regimen 1). The frequent application of antagonist was compared to the same treatment with CIP. The results are presented in Figure 4.

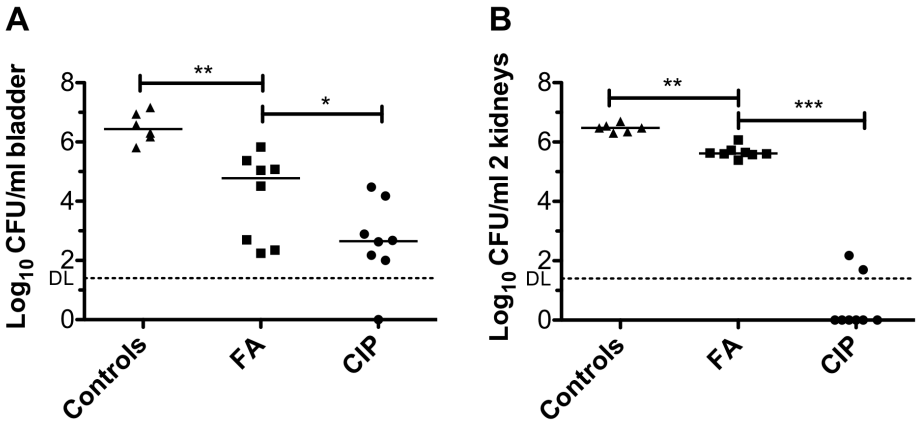

Figure 4. Frequent antagonist applications lowers bacterial burden in infection. Bacterial counts in Log_{10} CFU/ml in bladder (A) and kidneys (B) after several dosages of 10 mg/kg of antagonist (named FA) or 8 mg/kg CIP. In each group, a line indicates the median. Significance testing was

performed with Mann-Whitney U test (*, p<0.05, **, p<0.01, ***, p<0.001). DL: detection limit (dashed line).

The antagonist treatment resulted in a clear reduction of bladder and kidney colony counts compared to the controls. The median reduction in the bladder compared to controls was 1.7 Log_{10} CFU/ml with antagonist and 3.8 Log_{10} CFU/ml with CIP. Still, the reduction in the kidneys was only 0.9 Log_{10} CFU/ml with antagonist. Also, despite the high activity of CIP in both organs, not all bacteria were completely eliminated from the bladder.

Urine levels of antagonist were monitored during the infection (Fig. S1). The urine levels reached C_{max} after the 2nd dosing at 6.6 hpi, with 153 µg/ml (Supplementary Figure 1). Therefore, the increased dosing frequency resulted in an accumulation of antagonist in the urine, exceeding the C_{max} of a single application (112.6 µg/ml) and remained constant after the third application at levels above 100 µg/ml.

Overall, the increase in dosing frequency resulted in a significant CFU reduction in the bladder. Nevertheless, compared to the long-term effect of a preventive application (Figure 1D&E), there was no benefit of additional dosing. Thus, the reduction effect was mainly dependent on the initial preventive dose. The long-term prevention study showed a 2.2 Log_{10} CFU/ml reduction at 12 hpi, which is higher than the reduction observed here after 9 hours of infection (1.7 Log_{10} units).

The uptake of antagonist via the drinking water was only effective for a short time (Regimen 2). The phosphate prodrug of the *para*-cyano biphenyl α D-mannopyranoside (30) was added to the drinking water at 100 µg/ml. The uptake (average dosing of 1 mg/kg per mouse per hour) led to concentrations between 7.8 and 23.2 µg/ml of the antagonist in the urine of the mice, after 24 hours of addition, at the time of infection. However, there were high individual differences. After infection, concentrations decreased rapidly to 2-7.2 µg/ml at 48 hours (24 hpi) (Supplementary Figure 2). Regimen 2 resulted in decreased bladder counts at 6 hpi, but not at 24 hpi, probably due to the decreased antagonist concentration at this time-point. The antagonist showed no effect upon kidney bacterial load (Figure 5).

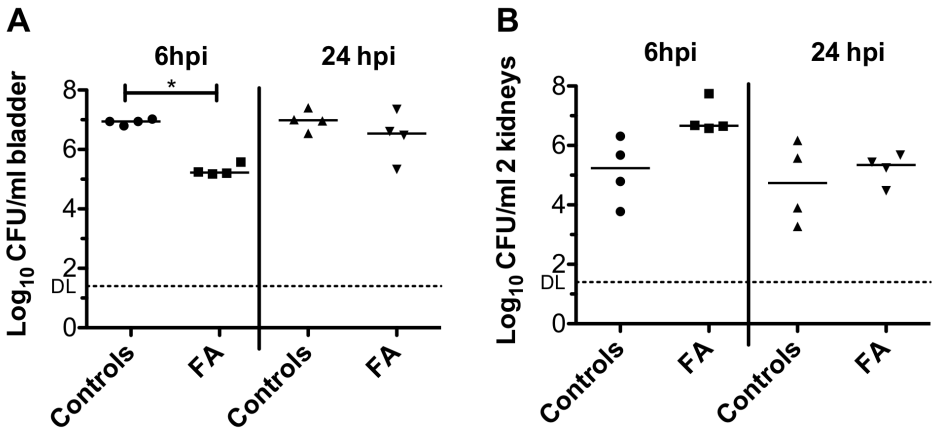

Figure 5. Drinking water prevention reduces colony counts in bladder at 6 hpi, but not at 24 hpi. Bacterial counts after a 24 hours preventive application of antagonist (FA) via the drinking water at a concentration of 100 µg/ml, corresponding to an approximate average dose of 1 mg/kg per mouse per hour. In each group, the median is indicated by a line. Significance testing with Mann-Whitney U test, *, $p<0.5$. DL: detection limit (dashed line).

Bladder colony counts were significantly and uniformly reduced by a factor of approximately 100 at 6 hpi, whereas the bacterial load in the kidneys was not affected by the treatment. At 24 hpi, bacterial counts of the intervention and treatment groups equalized between 6.5-7 Log_{10} CFU/ml in the bladder and around Log_{10} 5 CFU/ml in the kidneys.

Urine levels of antagonist after oral application accumulate up to 8 hours. The urine levels of the mice in Regimen 2 decreased rapidly after infection, probably due to bacterial binding and excretion in a high extent. Urine concentrations of the antagonist determined in a PK study do not account for this effect and might therefore not correctly reflect the concentrations in an infection. Therefore, urine concentrations of the antagonist during infection were analyzed (Figure 6). Surprisingly, the analyzed urine levels showed an accumulation between 3 and 8 hours after oral application, resulting in urine levels of 35 µg/ml at 8 hours. This accumulation was not observed in uninfected mice (Figure 6, dotted line).

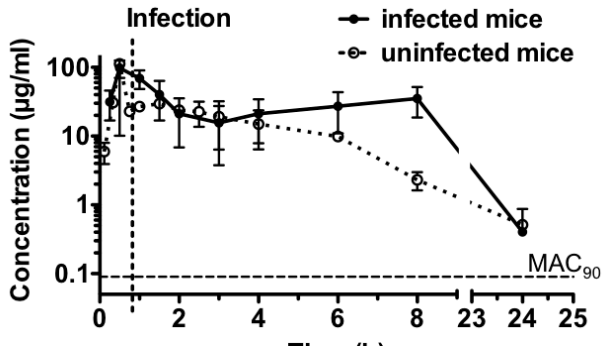

Figure 6. Antagonist concentrations in infected mice accumulate between 3 to 8 hours after application. Urine concentration levels over time of infected mice (bold line) compared to non-infected mice (dotted line, see Figure 1C). Urine levels are similar up to 3 hours, but differ between 3 and 8 hours after application. In infected mice, levels reach 35 µg/ml at 8 hours compared to 2.3 µg/ml in uninfected mice. MAC_{90} (minimal anti-adhesive concentration) is indicated with a dashed line.

FimH antagonists potentiate the effect of CIP in the bladder and the kidneys (Regimens 3 and 4). A further application possibility of FimH antagonists would be a combination therapy with antibiotics, thereby limiting the antibiotic dose and use.
Two combination therapy set-ups with FimH antagonist and CIP were studied (Figure 3, Regimen 3 and 4). Regimen 3 combines a preventive dose of antagonist, followed by a CIP application 3 h after infection. Regimen 4 was used to test the possibility of treating an established infection, where the FimH antagonist was applied three hours after the CIP dose.

Generally, in both regimens, CFU counts were low in all treated groups, with medians between zero and 3 Log_{10} CFU/ml for bladder and kidneys. Control values in the bladder reached 7 Log_{10} CFU/ml in both regimens, indicating a stable infection over the total time range of the experiment. Thus, the bacterial counts were reduced by more than half in Regimens 3 and 4. The preventive addition of antagonist (Regimen 3) completely depleted bacterial counts from the bladder and nearly eradicated bacteria from the kidneys as well. Thereby, group 1 (receiving a preventive dose of antagonist) had a 100-fold lower bacterial load than group 2 and the same is true for the kidneys (Figure 6).

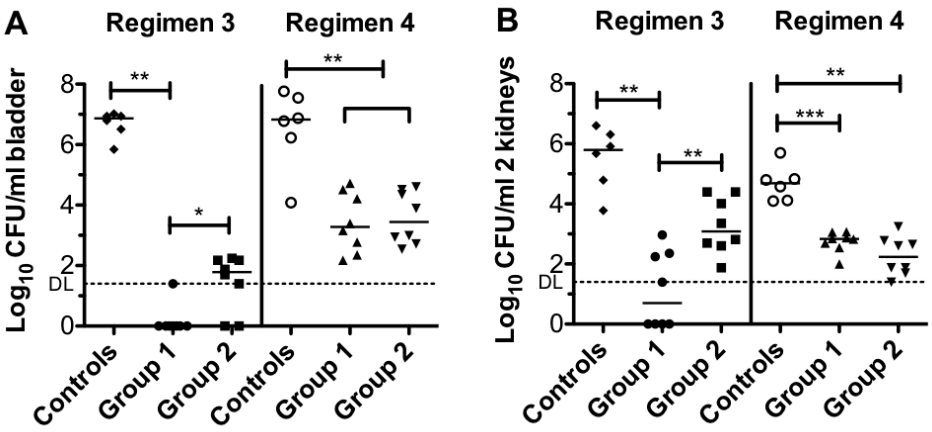

Figure 7. Combining a preventive application of antagonist with CIP eradicates nearly all bacteria from the bladder. Bacterial colony counts in Log_{10} CFU/ml in bladder (A) and kidneys (B) resulting of the two different combination regimens 3 and 4 (Figure 3). A line in each group indicates the median. For significance, the Mann-Whitney U test was used (**, $p<0.01$, ***, $p<0.001$). DL: detection limit (dashed line).

However, there was no beneficial effect (Figure 7, Regimen 4) upon addition of antagonist in combination to CIP as a therapeutic measure. Although CIP depleted bacterial counts in the treated groups compared to controls by half, there was no additional reduction of colony counts in bladder, nor kidneys with the antagonist. These results confirm the finding that FimH antagonists are most potent upon preventive dosing and can strongly enhance antibiotic potency in the bladder and the kidneys.

DISCUSSION

To elucidate possible treatment possibilities of FimH antagonists as an anti-adhesive therapy for the treatment of UTI, a potent FimH antagonist [*para*-cyano biphenyl α D-mannopyranoside, **10j** in (25)] was studied in different treatment regimens using the well established UTI mouse model (37–39). The antagonist was previously shown to reduce bacterial loads in the bladder upon a single preventive oral dose by 1000-fold after the first 3h of infection and exceeded the effect of CIP (25). The first three hours of an infection are dictated by attachment and invasion of bacteria to and into bladder cells (10–13). To expand the previous studies, the preventive effect of the antagonist was studied within a 24 hours infection period. The concentration of the

antagonist in the urine stayed above the MAC_{90} for 24 hours, implying a therapeutic effect for this time span (Figure 1C). The resulting bacterial counts in the bladder revealed an increase of CFU between 3 hpi and 6 hpi in both, the intervention and also slightly in the control group (Figure 1D). This could indicate a phase of intracellular replication starting after the initial attachment, which is in agreement with literature, where a rapid intracellular growth phase of bacteria up to 8 hours after infection is reported (10–13). Between 6 hpi and 12 hpi, bacterial loads in the bladder of the treated group dropped again, reaching levels similar to 3 hpi, possibly because of the fluxing of bacteria from infected cells and re-exposure to FimH antagonists. This bacterial egress would be slightly earlier as expected from literature reports (approx. 12 hpi (10–13)). This study proofed a response to a preventive FimH antagonist treatment up to 12 hpi. Despite the fact that the decrease of bacterial CFU in the first 12 hours of an infection is related to the active immune response, i.e., cell shedding and the activity of neutrophils, the bacterial burden in the control group remained high (11).

Furthermore, this study also indicates that type 1 pili are re-expressed after invasion and fluxing of bacteria, which is consistent with the findings in the *in vitro* bladder infection model by Andersen *et al*. (15).

Finally, 24 hpi bacterial counts of the intervention group matched the control counts. Thus, $T>MAC_{90}$ as determined from the PK study, is not the predictive index for a positive treatment outcome.

To investigate if the therapeutic outcome depends on the antagonist concentration in relation to the MAC_{90}, both parameters, the antagonist concentration and the MAC_{90} were varied. First, to lower the MAC_{90}, mice were infected with a lower bacterial inoculum, resulting in a lower number of type 1 pili, which have to be blocked to prevent the infection. The antagonist proofed to be effective in depleting bladder colony counts independent of the inoculum used. The bacterial reduction at 3 hpi with a high inoculum (Figure 1 D&E) and the reduction using a low inoculum (Figure 2) was approximately 1000-fold. Therefore, against expectations, the antagonist did not result in a higher bacterial reduction, despite the higher magnitude of the concentration/MAC_{90} ratio. This suggests that if an effective concentration-MAC_{90} magnitude is reached, no further proportional increase in bacterial reduction can be achieved.

Regimen 1 aimed at an accumulation of antagonist concentration in urine to proof the concentration-dependent effect. Although antagonist accumulation was successful (Figure S1), the resulting bacterial reduction at 9 hpi (1.7 Log_{10} CFU/ml, Figure 4) was lower than at 12 hpi (2.2 Log_{10} CFU/ml) in the preventive study with a single application. However, this goes in hand with the proposed steps of the infection cycle. Likely, at 9 hpi the intracellular bacterial replication is ongoing and CFU counts mainly result from IBCs, which are not accessible for FimH antagonists. Therefore, one should aim at accumulating antagonist concentrations in urine at the time of bacterial egress, which would be after 12 hpi, at least in an experimental infection, as studied here.

The superior effect of CIP in regimen 1 might also be attributed to the frequent dosing (every 3 hours). CIP is a fluoroquinolone and the effect is governed by the area under the curve above the minimal inhibitory concentration (AUC/MIC) (40, 41). Frequent dosing increases AUC/MIC and results in high bacterial reductions. Although this treatment was rather beneficial for the reduction of bacterial burden, it might not be optimal in terms of resistance development or side effects.

Supplying the drinking water with antagonist was assumed to result in a constant uptake and expand the time span of the effective concentration/MAC_{90} ratio. Furthermore, this would guarantee the antagonist supply at the critical time-point of 12 hpi, where bacteria egress from the first intracellular infection round. Yet, the reduction was only effective for a short time-span (6 hpi) and did not result in decreased colony counts at 24 hpi. The PK urine curves (Figure S2) together with the decreasing bacterial loads in the bladder immediately after infection (Figure 5) indicate that the antagonist rapidly binds to the bacteria and is consequently excreted in high concentrations. Conceivably, the uptake of antagonist via drinking water is too low to deal with rapidly increasing bacterial counts, explaining the missing effect at 24 hpi. In other words, the effective concentration/MAC_{90} ratio is not reached after bacterial addition due to a decreasing antagonist concentration. Furthermore, concurrently, especially during the phase of intracellular replication, bacterial numbers rise rapidly, which increases the required MAC_{90} levels in urine after bacterial fluxing. Thus, decreasing antagonist concentrations with a simultaneously increasing MAC_{90} due to increasing bacterial numbers, lead to an

inefficient antagonist concentration. Since MAC_{90} values determined *in vitro* miss the dynamic nature within the infection cycle, the MAC_{90} represents only the first infection events lasting up to 3 hpi, but is not representative for later stages.
Overall, this strongly indicates that the positive therapeutic effect is dependent on the duration of a specific concentration-MAC_{90} ratio, where both parameters, the antagonist concentration and the MAC_{90}, are dynamic within the infection cycle.

Contrarily to the assumption that in infected mice antagonist concentrations decrease more rapidly due to bacterial binding and elimination, urine concentrations in infected mice showed an accumulation of antagonist between 3 and 8 hours. Yet, again, this goes in hand with the described intracellular replication phase of bacteria, which starts at approximately 3 hours post infection (10–13). Therefore, after initial binding and elimination of bacteria, the antagonist accumulates in the urine during the phase of intracellular bacterial growth. Hypothetically, this effect might be increased by reduced water uptake of infected mice together with decreased urination frequency, which would have to be studied specifically. The high concentrations determined here at 8 hours could also be representative for the levels at 12-13 hours, where bacterial egress starts. This would explain the therapeutic effect up to 12 hpi registered in the long-term prevention study (Figure 1D). This supports the previous statement that treatment should focus on a preventive dose with subsequent doses every 12 hours to accumulate antagonist concentrations at the time, when bacteria are most accessible: when they are in the bladder lumen.

Within the combination therapies, the antagonist showed a high potential in improving the therapeutic effect of CIP, but only when applied preventively (Figure 6). However, compared to the CIP treatment in Regimen 1 (Figure 4), the addition of antagonist cleared the bladder from bacteria, which was not achieved with CIP only, even with frequent dosing. Additionally, kidney counts decreased markedly within the group treated with antagonist and CIP compared to CIP only (Regimen 3, group 1 compared to Regimen 1, CIP treated group). This confirms the additional effect of a FimH antagonist to antibiotic treatment, which was previously reported by Cusumano *et al*. (22). Important for the synergism is the preventive decline of the initial bacterial number invading bladder cells and establishing the infection. Normally, high urine concentrations of antibiotics are necessary for treating UTI, but the infection can only

be completely resolved when high tissue concentrations are reached in the bladder and kidneys as well (41). CIP was shown to effectively act on intracellular bacteria (42). Therefore, the combination of a FimH antagonist preventing bacterial attachment in the urine together with the intracellular and interstitial action of an adequate antibiotic therapy is most promising for a fast clearance of UTI.

Generally, it remains questionable, how these results translate from mice to humans. Regarding antibiotic research, the PK/PD indices found in animal models normally translate to applications in humans (43, 44). However, a classical PK/PD evaluation with an indicative PK/PD index ($T>MAC_{90}$, AUC/MAC_{90}, or C_{max}/MAC_{90}) for an optimal treatment could not be established in this case. Here, the preventive effect of FimH antagonists can best be described by the duration of a specific concentration-MAC_{90} ratio. Yet, the MAC_{90} determined *in vitro*, is only indicative within the first 3 to 6 hpi, but not throughout infection because of increasing bacterial counts.
Furthermore, the correlation of treatment regimens to human applications might be different for anti-adhesive compared to antibiotic treatment, as murine models work with high inocula and the experimental infection is a rather acute event. Because the MAC_{90} depends on inoculum size, it would be interesting to test a more natural course of infection, where only few ascending bacteria initiate the infection. It might be that the antagonists bear an even higher potency in prevention and could possibly also diminish the infection in the kidneys. Also, frequent dosing combined with repeated urination could help to eliminate bacteria more effectively and keep antagonist levels high, which, however, is difficult to test in the mouse model. Nevertheless, establishing an optimal treatment regimen for anti-adhesive therapies is crucial and might decide over failure or success of the therapy, as it was the case in clinical studies by Kranjčec *et al.* or Ukkonen *et al.* (1, 45).

In summary, an anti-adhesive therapy with FimH antagonists in UTI relies on the initial preventive dose, which must be above the defined MAC_{90} value and the achievement of a therapeutic effective concentration-MAC_{90} ratio and its duration. Possibly, bacteria rapidly bind to the FimH antagonist in urine and are eliminated by urinal voiding. However, some will be able to invade bladder cells and form IBCs, a source for bacterial persistence. In some cases, the immune system is capable of eliminating intracellular reservoirs and clearing the infection. Otherwise additional

antibiotic therapy might be needed. Therefore, a highly dosed preventive application of FimH antagonist might work for a person facing immediate risk for UTI (e.g., catheterized patients), whereas a drinking water prevention might help patients suffering from recurrent UTIs, where the exact time of recurrence is not clear and low bacterial numbers start a new infection. In any case, the preventive application of FimH antagonists also offers the possibility for a combination with an antibiotic treatment at later stages and could help to diminish antibiotic use in prophylaxis, minimizing side effects, and reduce resistance development.

FINANCIAL CONTRIBUTION

The financial support by the Swiss National Science Foundation (SNF Grant 31003A-144183) is gratefully acknowledged. The funding agency had no part in any way in experimental design, data collection, or reporting.

ACKNOWLEDGEMENTS

We thank Prof. Dr. med. Radek Skoda, Department of Biomedicine, University Hospital Basel, Switzerland, for the access to the animal facility.

REFERENCES

1. **Kranjčec B**, **Papeš D**, **Altarac S**. 2014. D-mannose powder for prophylaxis of recurrent urinary tract infections in women: a randomized clinical trial. World J Urol **32**:79–84.
2. **Hooton TM**, **Stamm WE**. 1997. Diagnosis and treatment of uncomplicated urinary tract infection. Infect Dis Clin North Am **11**:551–581.
3. **Foxman B**. 2002. Epidemiology of urinary tract infections: incidence, morbidity, and economic costs. Am J Med **113**:5–13.
4. **Ronald A**. 2002. The etiology of urinary tract infection: traditional and emerging pathogens. Am J Med **113**:14–19.
5. **Fihn SD**. 2003. Acute Uncomplicated Urinary Tract Infection in Women. N Engl J Med **349**:259–266.

6. **Krogfelt KA**, **Bergmans H**, **Klemm P**. 1990. Direct evidence that the FimH protein is the mannose-specific adhesin of Escherichia coli type 1 fimbriae. Infect Immun **58**:1995–1998.
7. **Mulvey MA**, **Schilling JD**, **Martinez JJ**, **Hultgren SJ**. 2000. Bad bugs and beleaguered bladders: Interplay between uropathogenic Escherichia coli and innate host defenses. Proc Natl Acad Sci **97**:8829–8835.
8. **Ofek I**, **Hasty DL**, **Abraham SN**, **Sharon N**. 2000. Role of bacterial lectins in urinary tract infections. Molecular mechanisms for diversification of bacterial surface lectins. Adv Exp Med Biol **485**:183–192.
9. **Iwahi T**, **Abe Y**, **Nakao M**, **Imada A**, **Tsuchiya K**. 1983. Role of type 1 fimbriae in the pathogenesis of ascending urinary tract infection induced by escherichia coli in mice. Infect Immun **39**:1307–1315.
10. **Justice SS**, **Hung C**, **Theriot JA**, **Fletcher DA**, **Anderson GG**, **Footer MJ**, **Hultgren SJ**. 2004. Differentiation and developmental pathways of uropathogenic Escherichia coli in urinary tract pathogenesis. Proc Natl Acad Sci U S A **101**:1333–1338.
11. **Mulvey MA**, **Schilling JD**, **Hultgren SJ**. 2001. Establishment of a Persistent Escherichia coli Reservoir during the Acute Phase of a Bladder Infection. Infect Immun **69**:4572–4579.
12. **Schwartz DJ**, **Chen SL**, **Hultgren SJ**, **Seed PC**. 2011. Population Dynamics and Niche Distribution of Uropathogenic Escherichia coli during Acute and Chronic Urinary Tract Infection. Infect Immun **79**:4250–4259.
13. **Hannan TJ**, **Totsika M**, **Mansfield KJ**, **Moore KH**, **Schembri MA**, **Hultgren SJ**. 2012. Host–pathogen checkpoints and population bottlenecks in persistent and intracellular uropathogenic Escherichia coli bladder infection. FEMS Microbiol Rev **36**:616–648.
14. **Anderson GG**, **Palermo JJ**, **Schilling JD**, **Roth R**, **Heuser J**, **Hultgren SJ**. 2003. Intracellular Bacterial Biofilm-Like Pods in Urinary Tract Infections. Science **301**:105–107.
15. **Andersen TE**, **Khandige S**, **Madelung M**, **Brewer J**, **Kolmos HJ**, **Møller-Jensen J**. 2012. Escherichia coli Uropathogenesis In Vitro: Invasion, Cellular Escape, and Secondary Infection Analyzed in a Human Bladder Cell Infection Model. Infect Immun **80**:1858–1867.

16. **Chen SL**, **Hung CS**, **Pinkner JS**, **Walker JN**, **Cusumano CK**, **Li Z**, **Bouckaert J**, **Gordon JI**, **Hultgren SJ**. 2009. Positive selection identifies an in vivo role for FimH during urinary tract infection in addition to mannose binding. Proc Natl Acad Sci **106**:22439–22444.
17. **Chen SL**, **Hung C-S**, **Xu J**, **Reigstad CS**, **Magrini V**, **Sabo A**, **Blasiar D**, **Bieri T**, **Meyer RR**, **Ozersky P**, **Armstrong JR**, **Fulton RS**, **Latreille JP**, **Spieth J**, **Hooton TM**, **Mardis ER**, **Hultgren SJ**, **Gordon JI**. 2006. Identification of genes subject to positive selection in uropathogenic strains of Escherichia coli: A comparative genomics approach. Proc Natl Acad Sci **103**:5977–5982.
18. **Garofalo CK**, **Hooton TM**, **Martin SM**, **Stamm WE**, **Palermo JJ**, **Gordon JI**, **Hultgren SJ**. 2007. Escherichia coli from Urine of Female Patients with Urinary Tract Infections Is Competent for Intracellular Bacterial Community Formation. Infect Immun **75**:52–60.
19. **Rosen DA**, **Hooton TM**, **Stamm WE**, **Humphrey PA**, **Hultgren SJ**. 2007. Detection of Intracellular Bacterial Communities in Human Urinary Tract Infection. PLoS Med **4**:e329.
20. **Hannan TJ**, **Mysorekar IU**, **Hung CS**, **Isaacson-Schmid ML**, **Hultgren SJ**. 2010. Early Severe Inflammatory Responses to Uropathogenic E. coli Predispose to Chronic and Recurrent Urinary Tract Infection. PLoS Pathog **6**:e1001042.
21. **Klein T**, **Abgottspon D**, **Wittwer M**, **Rabbani S**, **Herold J**, **Jiang X**, **Kleeb S**, **Lüthi C**, **Scharenberg M**, **Bezençon J**, **Gubler E**, **Pang L**, **Smiesko M**, **Cutting B**, **Schwardt O**, **Ernst B**. 2010. FimH Antagonists for the Oral Treatment of Urinary Tract Infections: From Design and Synthesis to in Vitro and in Vivo Evaluation. J Med Chem **53**:8627–8641.
22. **Cusumano CK**, **Pinkner JS**, **Han Z**, **Greene SE**, **Ford BA**, **Crowley JR**, **Henderson JP**, **Janetka JW**, **Hultgren SJ**. 2011. Treatment and Prevention of Urinary Tract Infection with Orally Active FimH Inhibitors. Sci Transl Med **3**:109ra115–109ra115.
23. **Abgottspon D**, **Ernst B**. 2012. In vivo evaluation of FimH antagonists - a novel class of antimicrobials for the treatment of urinary tract infection. Chimia **66**:166–169.

24. **Han Z**, **Pinkner JS**, **Ford B**, **Chorell E**, **Crowley JM**, **Cusumano CK**, **Campbell S**, **Henderson JP**, **Hultgren SJ**, **Janetka JW**. 2012. Lead Optimization Studies on FimH Antagonists: Discovery of Potent and Orally Bioavailable Ortho-substituted Biphenyl Mannosides. J Med Chem **55**:3945–3959.
25. **Kleeb S**, **Pang L**, **Mayer K**, **Eris D**, **Sigl A**, **Preston RC**, **Zihlmann P**, **Sharpe T**, **Jakob RP**, **Abgottspon D**, **Hutter AS**, **Scharenberg M**, **Jiang X**, **Navarra G**, **Rabbani S**, **Smiesko M**, **Lüdin N**, **Bezençon J**, **Schwardt O**, **Maier T**, **Ernst B**. 2015. FimH Antagonists: Bioisosteres To Improve the in Vitro and in Vivo PK/PD Profile. J Med Chem **58**:2221–2239.
26. **Totsika M**, **Kostakioti M**, **Hannan TJ**, **Upton M**, **Beatson SA**, **Janetka JW**, **Hultgren SJ**, **Schembri MA**. 2013. A FimH Inhibitor Prevents Acute Bladder Infection and Treats Chronic Cystitis Caused by Multidrug-Resistant Uropathogenic Escherichia coli ST131. J Infect Dis **208**:921–928.
27. **Diehl K-H**, **Hull R**, **Morton D**, **Pfister R**, **Rabemampianina Y**, **Smith D**, **Vidal J-M**, **Vorstenbosch CVD**. 2001. A good practice guide to the administration of substances and removal of blood, including routes and volumes. J Appl Toxicol **21**:15–23.
28. **Faul F**, **Erdfelder E**, **Buchner A**, **Lang A-G**. 2009. Statistical power analyses using G*Power 3.1: Tests for correlation and regression analyses. Behav Res Methods **41**:1149–1160.
29. **Jakobsen L**, **Cattoir V**, **Jensen KS**, **Hammerum AM**, **Nordmann P**, **Frimodt-Møller N**. 2012. Impact of low-level fluoroquinolone resistance genes qnrA1, qnrB19 and qnrS1 on ciprofloxacin treatment of isogenic Escherichia coli strains in a murine urinary tract infection model. J Antimicrob Chemother dks224.
30. **Kleeb S**, **Jiang X**, **Frei P**, **Sigl A**, **Bezençon J**, **Bamberger K**, **Schwardt O**, **Ernst B**. FimH Antagonists - Phosphate Prodrugs Improve Oral Bioavailability.
31. **Jiang X**, **Abgottspon D**, **Kleeb S**, **Rabbani S**, **Scharenberg M**, **Wittwer M**, **Haug M**, **Schwardt O**, **Ernst B**. 2012. Antiadhesion therapy for urinary tract infections--a balanced PK/PD profile proved to be key for success. J Med Chem **55**:4700–4713.

32. **Scharenberg M**, **Abgottspon D**, **Cicek E**, **Jiang X**, **Schwardt O**, **Rabbani S**, **Ernst B**. 2011. A Flow Cytometry-Based Assay for Screening FimH Antagonists. ASSAY Drug Dev Technol **9**:455–464.
33. **Naber KG**, **Bergman B**, **Bishop MC**, **Bjerklund-Johansen TE**, **Botto H**, **Lobel B**, **Jinenez Cruz F**, **Selvaggi FP**, **Urinary Tract Infection (UTI) Working Group of the Health Care Office (HCO) of the European Association of Urology (EAU)**. 2001. EAU guidelines for the management of urinary and male genital tract infections. Urinary Tract Infection (UTI) Working Group of the Health Care Office (HCO) of the European Association of Urology (EAU). Eur Urol **40**:576–588.
34. **Hooton TM**. 2003. Fluoroquinolones and resistance in the treatment of uncomplicated urinary tract infection. Int J Antimicrob Agents **22, Supplement 2**:65–72.
35. **Taur Y**, **Smith MA**. 2007. Adherence to the Infectious Diseases Society of America Guidelines in the Treatment of Uncomplicated Urinary Tract Infection. Clin Infect Dis **44**:769–774.
36. **Grabe M**, **Bjerklung-Johansen TE**, **Botto H**, **Cek M**, **Naber KG**, **Pickard RS**, **Tenke P**, **Wagenlehner F**, **Wullt B**. Guidelines on Urological Infections.
37. **Hagberg L**, **Engberg I**, **Freter R**, **Lam J**, **Olling S**, **Svanborg Eden C**. 1983. Ascending, unobstructed urinary tract infection in mice caused by pyelonephritogenic Escherichia coli of human origin. Infect Immun **40**:273–283.
38. **Hvidberg H**, **Struve C**, **Krogfelt KA**, **Christensen N**, **Rasmussen SN**, **Frimodt-Møller N**. 2000. Development of a Long-Term Ascending Urinary Tract Infection Mouse Model for Antibiotic Treatment Studies. Antimicrob Agents Chemother **44**:156–163.
39. **Hung C-S**, **Dodson KW**, **Hultgren SJ**. 2009. A murine model of urinary tract infection. Nat Protoc **4**:1230–1243.
40. **Andes D**, **Craig WA**. 2002. Animal model pharmacokinetics and pharmacodynamics: a critical review. Int J Antimicrob Agents **19**:261–268.
41. **Frimodt-Møller N**. 2002. Correlation between pharmacokinetic/pharmacodynamic parameters and efficacy for antibiotics in the treatment of urinary tract infection. Int J Antimicrob Agents **19**:546–553.

42. **Craig W**, **Dalhoff A**. 1998. Pharmacodynamics of Fluoroquinolones in Experimental Animals, p. 207–232. *In* Kuhlmann, PDJ, Dalhoff, PDA, Zeiler, DH-J (eds.), Quinolone Antibacterials. Springer Berlin Heidelberg.

43. **Ambrose PG**, **Bhavnani SM**, **Rubino CM**, **Louie A**, **Gumbo T**, **Forrest A**, **Drusano GL**. 2007. Pharmacokinetics-Pharmacodynamics of Antimicrobial Therapy: It's Not Just for Mice Anymore. Clin Infect Dis **44**:79–86.

44. **Craig WA**. 1998. Pharmacokinetic/Pharmacodynamic Parameters: Rationale for Antibacterial Dosing of Mice and Men. Clin Infect Dis **26**:1–12.

45. **Ukkonen P**, **Varis K**, **Jernfors M**, **Herva E**, **Jokinen J**, **Ruokokoski E**, **Zopf D**, **Kilpi T**. 2000. Treatment of acute otitis media with an antiadhesive oligosaccharide: a randomised, double-blind, placebo-controlled trial. Lancet **356**:1398–1402.

5.5. MANUSCRIPT II

"The preventive effect of FimH antagonists on biofilms formed on a catheter surface"

Anja Sigl, Justyna Nowakowska*, Oliver Schwardt, Lijuan Pang, Priska Frei, Nina Khanna*, and Beat Ernst

Infection Biology Laboratory, Department of Biomedicine, University and University Hospital of Basel, Switzerland

Shall be submitted to *Antimicrobial Agents and Chemotherapy*

FimH Antagonists Prevent Biofilm Formation on Catheter Surfaces

Anja Sigl[a], Justyna Nowakowska[b], Nina Khanna[b,c], and Beat Ernst[a]#

Institute of Molecular Pharmacy, University of Basel, Switzerland[a]; Infection Biology Laboratory, Department of Biomedicine, University and University Hospital of Basel, Switzerland[b]; Division of Infectious Diseases and Hospital Epidemiology, Department of Biomedicine and Clinical Research University Hospital of Basel, Switzerland[c]

Running Head: FimH antagonists in biofilm prevention

#Address correspondence to Beat Ernst, beat.ernst@unibas.ch

ABSTRACT

Catheter-associated urinary tract infections (CAUTI) are frequent complications in hospitals and health-care institutions. About 30% of CAUTI are caused by uropathogenic *Escherichia coli* (UPEC), which express type 1 fimbriae on their surface, mediating the adhesion to the catheter surface and initiate biofilm formation. As a result, this provides a persistent bacterial source for urinary tract infection (UTI). The molecular basis of the bacterial adhesion is the lectin FimH located at the tip of type 1 fimbriae. FimH antagonists block the FimH-mediated adhesion and consequently impede biofilm formation. At low concentrations, FimH antagonists successfully prevented biofilm formation of different UPEC strains. However, already established biofilms could not be eliminated. In a novel catheter-associated biofilm model, the most potent FimH antagonist (*para*-cyano biphenyl α-D-mannopyranoside at concentrations of 6.25 µg/ml) reduced the type 1 pili-mediated biofilm mass of UTI89 by 50%, yet, without affecting bacterial viability. Co-application of the FimH antagonist and ciprofloxacin provided access to the bacteria within the biofilm for ciprofloxacin and resulted in an almost 3 Log_{10} CFU reduction of viable bacteria. In conclusion, FimH antagonists could provide a valuable preventive measure for decreasing CAUTIs and potentiating the activity of antibiotics.

INTRODUCTION

Urethral catheterization is a major risk factor for the development of urinary tract infections (UTIs), one of the most common bacterial infections worldwide (1, 2). Approximately 15-20% of patients in hospitals and health-care institutions require catheterization and 80% of all hospital-acquired UTIs are related to catheters (3, 4). Already a short catheterization of 2 to 10 days leads to a symptomatic catheter-associated UTI (CAUTI) in one out of four patients (5). Moreover, in more than one million annual cases in the United States, CAUTI is responsible for an increase in morbidity, for the generation of high treatment costs, and for the development of asymptomatic bacteriuria (ABU) (1). In 30% of all CAUTIs, the infection is caused by uropathogenic *Escherichia coli* (UPEC) (6–9).

A key factor of bacterial colonization of the urinary tract is the ability to form biofilms (10). Biofilm is a form of complex grouped bacterial growth within an extracellular matrix, where the individual cells adhere to each other and/or to surfaces (11). Biofilms on urinary catheters provide a survival advantage to the associated bacteria resulting in increased tolerance for antibiotics by more than 1000-fold compared to planktonic cells and also renders bacteria unsusceptible to biocides (12–15). Therefore, bacteria causing CAUTI are resistant towards antibiotics used for UTI treatment (16, 17). Several virulence factors are important for biofilm formation and urovirulence (18–20). Flagella and type 1 fimbriae are involved in the initiation of biofilm formation, allowing for movement along a surface and initial attachment (21, 22). Thereby, type 1 pili can mediate adhesion to many biotic and abiotic surfaces, such as catheters (23, 24). Other adhesins, for example curli, but also the production of an exopolysaccharide (EPS) matrix, are essential for maturation and integrity of the biofilm structure (21, 22, 25–28).

Type 1 pili are not only a major contributor to the establishment of a UPEC biofilm, but also for biofilm maintenance in general and on urinary catheters (21, 22, 29, 30). An analysis of urine from catheterized patients and from colonized catheters revealed that almost 90% of the bacteria expressed type 1 fimbriae in contrast to only 4% in non-catheterized cystitis patients (31, 32). Since deletion of bacteria in biofilms is difficult, a preventive approach is requested. Yet, when urinary catheters

were conditioned with antimicrobial agents before insertion, contradictory results were obtained (33, 34). Nevertheless, a preventive approach towards CAUTI could reduce incidence rates and the burden of patients.

FimH antagonists are mannose derivatives, able to prevent biofilm formation by blocking the lectin FimH at the tip of bacterial type 1 pili, which mediates binding to mannosylated surfaces (21, 22). In addition, it was postulated that the ability for high-affinity mannose-binding of UPEC selects for strong biofilm formers, which promotes a FimH antagonist based treatment (21). As shown in a murine mouse model, FimH antagonists offer a valuable option to prevent bacterial persistence on the catheter surface (30).

For effective testing of FimH antagonists to prevent CAUTI, a rapid and reliable high-throughput testing is required. The murine catheter model, as mentioned above, is critical to perform, since mice tend to remove the inserted catheters (internal communication). In addition to ethical considerations, difficulties also arise from the availability of catheter material in the appropriate size. Therefore, to effectively test various bacterial strains, representatives of different FimH antagonist families, and diverse catheter materials, a high-throughput format for rapid screening is needed. Although an *in vitro* catheter-model has been published previously, it is highly laborious, requires large amounts of assay media and test compounds (35).

Here, the systematic analysis of FimH antagonists to inhibit UPEC biofilms was studied in an adapted crystal violet (CV) assay in LB medium with several UPEC strains. The most potent antagonist was chosen for biofilm prevention studies on a catheter surface in pooled human urine. Therefore, a novel *in vitro* catheter model was developed, where biofilm formation was effectively inhibited with low antagonist concentrations. Furthermore, the antagonist potentiated the activity of ciprofloxacin (CIP). Therefore, FimH antagonists present a valuable option for a preventive therapy or in a combination therapy with antibiotics against CAUTI.

MATERIALS AND METHODS

Bacterial strains. UTI89 and *Δfim*UTI89 were kindly provided by Prof. Urs Jenal, (Biocenter, University of Basel, Switzerland), J96 by Prof. James R Johnson, (University of Minnesota Medical School, Minnesota, USA (36)), and the strain C175-94 (37) by Dr. Carsten Struve and Prof. Karen Krogfelt, (Statens Serum Institute, Copenhagen, Denmark).

Bacterial cultivation. Bacteria were incubated at static conditions overnight at 37° in 10 ml Luria-Bertani broth (LB, Becton and Dickinson, Allschwil, Switzerland). The next day, the bacteria were subcultured for additional 4 hours to reach the logarithmic phase. Prior to the assays, the optical density (OD_{600}) of the culture was measured and bacteria were diluted in assay medium to obtain the desired inoculum as indicated in the figure legends.

Collection of human urine. Urine was collected from over 20 healthy male and female donors. The collected urine from all donors was pooled, centrifuged (1'857*g*, 5 min), sterile filtered (0.2 µm), and stored at -20°C in aliquots. Aliquots were defrosted in the amounts that were used for the assay the same day. Before using for the assays, aliquots were tested for a normal composition of the urine, using the Combur 10 Test® (Roche, Rotkreuz, Switzerland). According to this test, the urine used for the assays had the following compositions: specific gravity (1.005-1.015), pH (6), leucocyte count (neg.), nitrite (neg.), proteins (neg.), glucose (< 1000 mg/dl), ketone (neg.), urobilinogen (normal), bilirubin (neg.), and erythrocytes/hemoglobin (neg.). Where indicated, 0.5% casamino acids (CAA) and 0.4% glycerol (both from Sigma-Aldrich, Buchs, Switzerland) were added to the urine samples before assays.

96-well plate crystal violet (CV) staining assay. The assay was performed as previously described by O'Toole *et al.*, with some modifications (38). In brief, flat-bottom polystyrene 96-well plates (Falcon, Becton and Dickinson, Allschwil Switzerland) were coated with the collected human urine (200 µL) overnight at 4°C. The next day, urine was discarded and the bacterial solution (100 µL) was inoculated into the wells, either in the absence (controls) or presence of FimH antagonist at the

indicated concentrations (100 µl, diluted in PBS, Sigma-Aldrich, Buchs, Switzerland). Background levels were determined from urine-coated wells, which contained assay medium and PBS and were equally processed. The plates were incubated at 25°C for the assigned time. Then, bacteria were discarded and the wells were washed twice with PBS. The remaining biofilm was fixed either at 60°C (CV assay in LB) or with 200 µl ice-cold methanol (Acros Organics, Chemie Brunschwig, Basel, Switzerland) for 10 min and air-drying for additional 15 min (for assays using human urine). The biofilm was stained with 0.5% CV (Sigma-Aldrich, Buchs, Switzerland) for 20 min at room temperature. After removal of the dye, the wells were washed with sterile water to remove final traces of the dye. To solubilize the absorbed CV, 200 µl of 30% acetic acid (Sigma Aldrich, Buchs, Switzerland) were added to each well followed by the transfer of 100 µl into a second 96-well plate. The absorption was quantified at 590 nm using a HT synergy reader from BioTek, Lucerne, Switzerland. Background absorptions were subtracted from the sample values. Resulting negative values were set to zero. The statistical analysis was performed with Prism (GraphPad Prism, 5.0) and one-way ANOVA with Dunnett's post test (CI 95%) to compare treated wells to control biofilm.

Microscopy. GFP transformed UTI89 and *Δfim*UTI89 (39) were used. The biofilm was cultivated in µ-slides 8-well (ibidi, Munich, Germany) in pooled human urine containing 0.5% CAA and 0.4% glycerol and kept in a tilted position as described by Merritt *et al.* (40). The slide was incubated at 25°C for 48 hours. Then, the liquid was discarded and wells were washed with PBS. Samples were fixed with ice-cold methanol for 10 min, followed by drying at room temperature for 15 min. After the addition of the mounting medium Vectashield H1000 (VectorLabs, Burlingame, CA, USA), the slide was sealed and observed with a 100X magnification on a Delta Vision Core microscope and processed with SoftWorx 4.1.2 and Imarisx64 (Imaging Core Facility, University of Basel).

Catheter-associated biofilm model. The assay set-up was inspired by the Calgary biofilm device (41) and was performed in the same way as the 96-well CV assay, described above. Silicone-catheters for children (Uromed AG, Muri AG, Switzerland) were cut into consistent pieces of 7 mm or 20 mm (for deep-well assays) using a cutting device designed for this purpose, sterilized for 1 hour in 70% EtOH and

carefully dried before use. The pieces were fixed to the lid of the flat-bottom polystyrene 96-well plates (Falcon, Becton and Dickinson, Allschwil, Switzerland) or deep-well plates (Eppendorf, Basel, Switzerland) using nail polish (essence, color and go, cosnova, Germany, made in France) as gluing agent (frequently used in microscopy, (42, 43)), in such a way that they entered the wells, but did not touch the bottom or walls of the wells. A schematic representation of a single well with a catheter piece is shown in Figure 1. The numbers represent distances for the short and long catheter pieces in millimeters and filling volumes of 200 µl for normal (A) and 500 µl for deep-well plates (B), respectively.

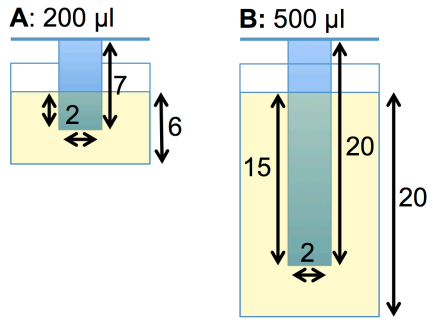

Figure 15. 96-well assay format with silicone catheter pieces. Catheter pieces (blue) protruding into wells filled with urine (yellow). Distances in mm for the normal 96-well plates (A) and the deep-well plates (B), where a larger urine volume could be used, are indicated.

After incubation, the lid with the catheter pieces was washed and transferred to a new plate for staining followed by a washing step to ensure that only the adherent bacteria on the catheter surface are quantified and not those on the walls of the wells.

For CV staining of catheter pieces incubated in deep-well plates, they were detached and transferred to 1.5 ml tubes for further processing. For fixation (methanol), staining (0.5% CV) and de-staining (30% acetic acid) solutions of 200 and 500 µl were used for the catheter pieces of 7 and 20 mm, respectively. For absorption read-out of CV, 100 µl of de-staining solution from each well were transferred to a new 96-well plate.

Background absorptions were subtracted from the sample values. Statistical analysis was performed with Prism (GraphPad Prism, 5.0) and one-way ANOVA with Dunnett's post test was used (CI 95%) to compare treated wells to the control biofilm.

For the determination of the colony forming units (CFU), catheter pieces were detached with sterile forceps and transferred into separate tubes for extensive washing with PBS. The pieces were washed on the outside and inside by up-and-down pipetting. This step was repeated twice before the catheter pieces were transferred to new tubes containing 1.5 ml sterile PBS. The tubes with catheter pieces were sonicated for 5 min (UltraSonic 460/H, Roth, Karlsruhe, Germany) and vortexed (Vortex Genie 2, Scientific Industries, New York, USA) at medium speed for another minute. Serial dilutions were plated on Eosin methylene blue (EMB) containing agar plates (Becton and Dickinson, Allschwil, Switzerland) and incubated at 37°C overnight for the evaluation of bacterial counts (per cm of catheter inserted into urine and available for colonization) the next day.

RESULTS

Prevention of UPEC biofilm formation by FimH antagonists in a concentration-dependent manner. Initially, the ability of UPEC to form biofilm was tested using the 96-well plate CV staining assay (see Methods). A previously established standard protocol (38) was adapted to optimise the conditions allowing maximal biofilm growth for the strains of interest (data not shown). Strains used for the assays were UTI89, J96, and C175-94. The FimH knockout strain *Δfim*UTI89 served as a negative control. In general, UTI89 formed the most abundant biofilm of all tested strains when cultured at 25°C in urine pre-coated wells with Luria-Bertani (LB) broth containing 0.5% casamino acids (CAA) and 0.4% glycerol. The pre-coating with urine turned out to be essential.

In a next step, five FimH antagonists from different compound classes were tested for their inhibitory activity of UPEC biofilm formation (Figure 2). *n*-Heptyl-α-D-mannopyranoside (**1**) was used as a reference compound (44). The FimH antagonist

2 with a squarate aglycone (45), **3** with a heterocyclic aglycone (46), **4** (47) and **5** (48) with a biphenyl aglycone were used as test compounds.

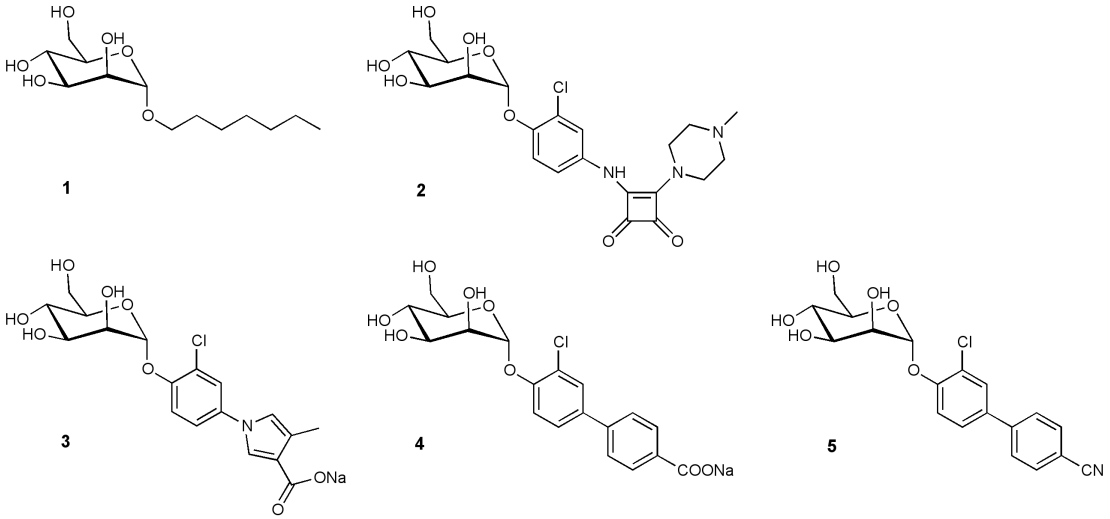

Figure 16. Structures of FimH antagonists tested for their activity to inhibit UPEC biofilm formation. FimH antagonists from four different chemical classes were studied; *n*-heptyl αD-mannopyranoside (**1**) (reference compound) (44), 2-Chloro-4-[(4-methylpiperazin-1-yl-3,4-dioxocyclo-but-1-en-1-yl)amino]phenyl αD-mannopyranoside (**2**) (45), 1-[3-chloro-4-(α-D-mannopyranosyl) phenyl]-4-methyl-1*H*-pyrrole-3-carboxylate (**3**) (46), 3′-chloro-4′-(αD-mannopyranosyloxy)biphenyl-4-carboxylate (**4**) (47), and 3′-chloro-4′-(αD-mannopyranosyloxy)biphenyl-4-carbonitrile (**5**) (48).

First, the prophylactic and therapeutic potential of the FimH antagonists **1**, **2**, and **4** to inhibit biofilm formation was assessed using the optimized CV staining assay. The biofilm of UTI89 was either grown in presence of a FimH antagonist for 24 and 48 hours, respectively (preventive application) or the antagonist was added to a 24-hours pre-formed biofilm for additional 24 hours of incubation (therapeutic application). In both approaches, a concentration-dependent activity could be observed. When therapeutically applied, FimH antagonists stopped further biofilm formation of the *E. coli* strain UTI89 at the level of their addition (Figure 3).

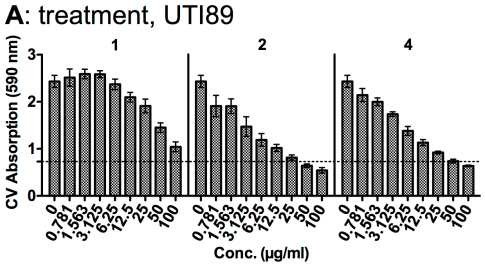

Figure 17. Influence of FimH antagonists on UTI89 biofilm formation upon therapeutic application. FimH antagonists **1**, **2**, and **4** were added to pre-formed 24 h biofilm (inoculum $1x10^3$ CFU/well) and incubated for further 24 hours before analysis by CV staining. Dotted line represents the 24 h biofilm values. Bars represent means with standard deviations (SDs) from one experiment. CV: crystal violet.

In contrast, when FimH antagonist and inoculum were applied simultaneously (preventive application), the biofilm mass was clearly reduced compared to the control at 24 and 48 hours (Figure 4A and 4B). Notably, *Δfim*UTI89 did not produce biofilm to a significant extent, suggesting the importance of functional type 1 pili for biofilm formation (Figure S1, Supplementary Information). Based on these results, the effect of antagonists **1**-**5** on biofilm formation was tested with additional UPEC strains, *i.e.*, J96 and C174-95. Since these strains formed less abundant biofilm compared to UTI89, the initial inoculum was increased from $1x10^3$ to $1x10^4$ CFU/ml. In order to allow a direct strain comparison, UTI89 and *Δfim*UTI89 were re-analyzed under these conditions (Figure 4C-4E and Figure S2, Supplementary Information).

Similarly to the effect on UTI89, biofilm formation of J96 was prevented in a concentration-dependent manner. For C174-95, a similar effect was detected with antagonist **1** (Figure 4E). However, compound **2**, **3**, **4**, and **5** inhibited biofilm of C174-95 independent of the concentrations used.

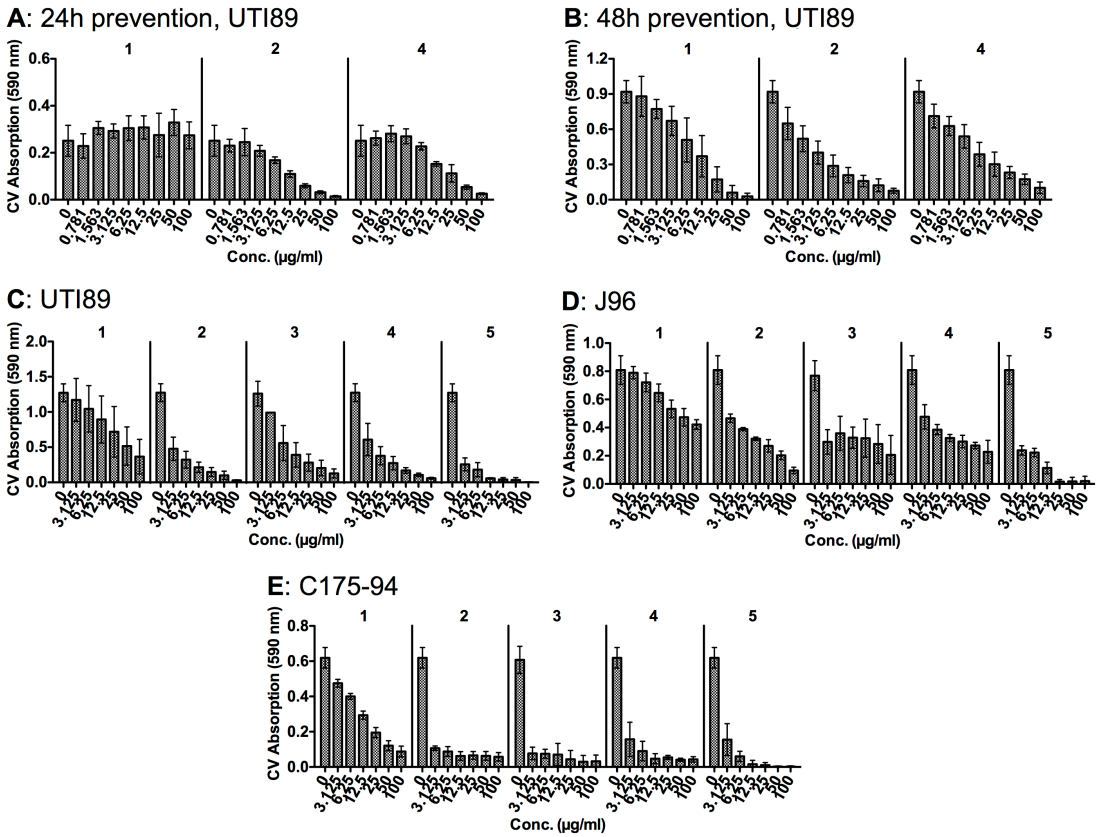

Figure 18. Prevention of UPEC biofilm formation by FimH inhibitors. (A and B) To test the preventive application, FimH antagonists **1**, **2**, and **4** were transferred to the wells of a 96-well plate together with the inoculum ($1x10^3$ CFU/well) and incubated for 24 hours or 48 hours before CV staining. Bars represent means with standard deviations (SDs) from one experiment (A) and from at least two independent experiments prepared in triplicates (B). (C-D) FimH inhibitors **1**-**5** were transferred to the wells of 96-well plates together with the inoculum ($1x10^4$ CFU/well) of different strains (C: UTI89, D: J96, E: C175-94) and incubated for 48 hours before CV staining. Bars represent means with standard deviations (SDs) from two (compound **3**) or three independent experiments prepared in triplicates. CV: crystal violet.

In conclusion, none of the tested FimH antagonists was able to clear an established bacterial biofilm when applied therapeutically. However, **2**, **3**, **4**, and **5** showed a high potency in preventing biofilm formation of different UPEC strains. For all strains, the reference compound **1** was characterized by the lowest activity.

Type 1 pili-dependent biofilm formation in human urine. To test the effect of FimH antagonists on biofilm formation under realistic conditions, the influence of human urine was evaluated in 96-well plate CV staining assay (see Methods). All bacterial strains grew well in pooled human urine collected from over 20 healthy,

female and male donors (data not shown). The quantitative amount of biofilm mass produced by UTI89 and *Δfim*UTI89 in urine and in urine supplemented with 0.5% CAA and 0.4% glycerol, as used in the previous assay in LB medium, is displayed in Figure 5A.

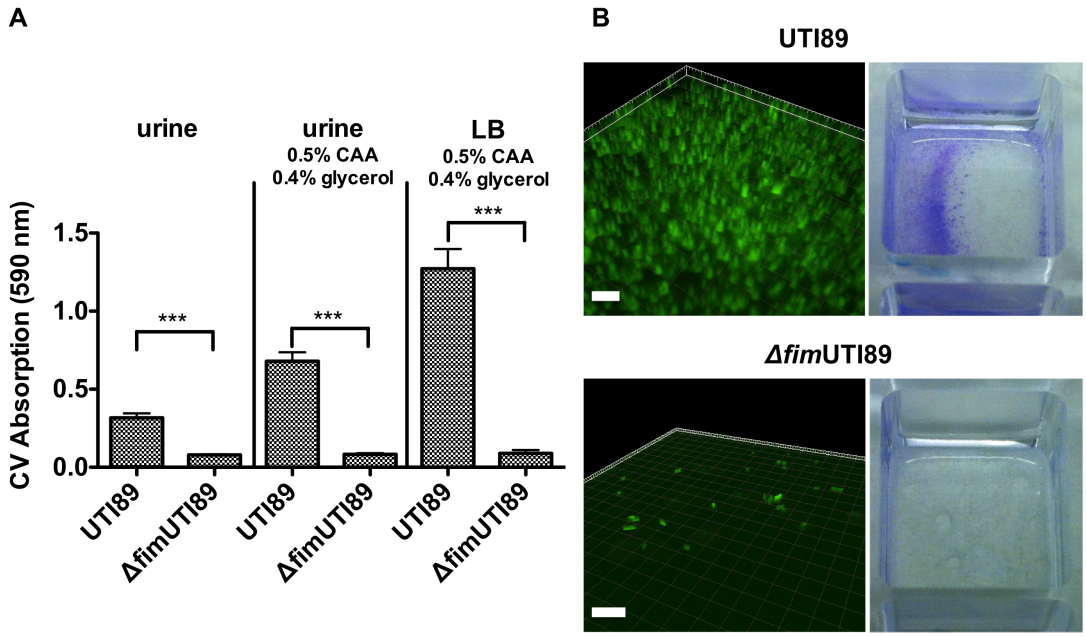

Figure 19. Biofilm formation in human urine required bacteria with type 1 pili and was enhanced when 0.5% CAA and 0.4% glycerol was supplemented. (A) CV staining of UTI89 and *Δfim*UTI89 biofilm grown for 48 hours in urine only, urine supplemented with 0.5% CAA and 0.4% glycerol compared to LB with 0.5% CAA and 0.4% glycerol (inoculum $1x10^4$ CFU/well). Statistical significance was determined with two-tailed t-test (***, p >0.0001). (B) GFP-expressing UTI89 and *Δfim*UTI89 (39) biofilm formation after 48 hours observed by fluorescence microscopy at 100X magnification (bar represent 5 µm for UTI89 and 10 µm for *Δfim*UTI89) and respective CV stained biofilms images in the wells that were incubated in a tilted position. CV: crystal violet.

Interestingly, in case of UTI89, the CV signal was reduced in urine compared to LB. Yet, the absorption values for *Δfim*UTI89 were similar in urine only (CV absorption 0.08) and in urine with supplements (CV absorption 0.08) to the cultivation in LB (CV absorption 0.09) indicating a stable background signal (Figure 5A vs. Figure S1, Supplementary Information). Although the biofilm growth by UTI89 (positive control) and *Δfim*UTI89 (negative control) in urine without supplements could clearly be distinguished (Figure 5A), an even more pronounced difference was obtained when the urine was supplemented with 0.5% CAA and 0.4% glycerol. Thus, for further experiments, urine was supplemented with CAA and glycerol. To counter-check

these results, biofilms of GFP-expressing UTI89 and *Δfim*UTI89 (39) were analyzed by fluorescence microscopy (Figure 5B). UTI89 formed a well-structured three-dimensional biofilm, when incubated for 48 hours at 25°C, whereas the knockout strain did not form a biofilm under these conditions. The biofilm of UTI89 was also seen by eye in the corresponding wells, when stained with CV.

In summary, UTI89 was able to form a mature biofilm in pooled human urine, which was further enhanced by supplementation with CAA and glycerol. Furthermore, the dependency of biofilm formation on type 1 pili could be confirmed.

Prevention of UPEC biofilm formation in urine. Next, the most potent FimH antagonist, the biphenyl mannoside **5** (Figure 2), was tested for the capacity to prevent biofilm formation of UPEC strains in urine supplemented with 0.5% CAA and 0.4% glycerol in the 96-well plate CV staining assay. Antagonist **5** was selected based on its excellent effect in an *in vivo* UTI disease model (48), but also because it exhibited the best effect in the prevention assay performed in LB (Figure 4). The activity was compared to reference **1** (Figure 6).

In agreement with the findings in LB medium, UTI89 and J96 turned out to be the strongest biofilm formers in urine, whereas biofilm formation by C175-94 was much less pronounced. When FimH antagonist **5** was applied, UTI89 and J96 biofilms could be reduced by approximately 60% at a concentration of only 6.25 µg/ml (Figure 6A and B, respectively). At this concentration, reference compound **1** did only marginally reduce the biofilm and background levels could not be reached even at the highest concentrations of 100 µg/ml. The reduction of C175-94 biofilm with antagonist **5,** was concentration-independent, whereas a concentration-dependent effect could be observed for reference compound **1**. Finally, *Δfim*UTI89 did not form biofilm, indicated by absorption on the background level (data not shown).

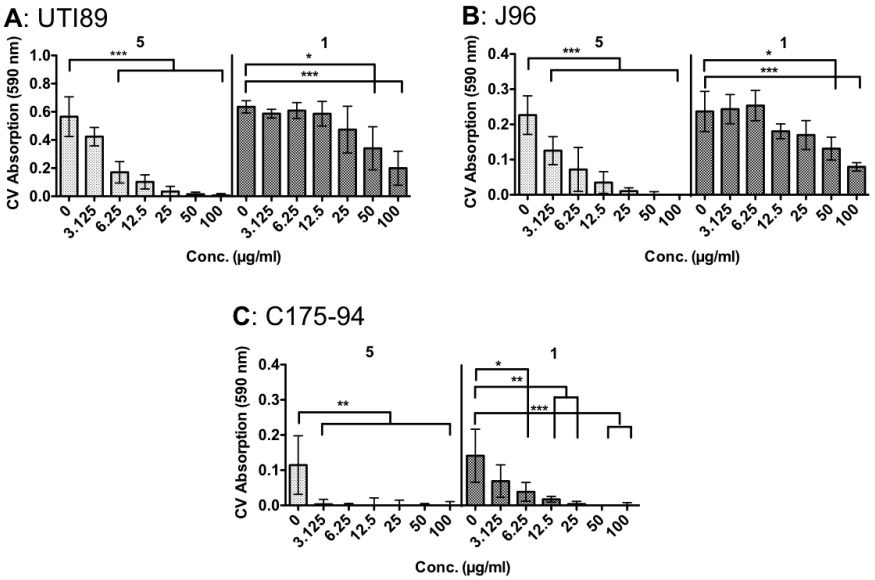

Figure 20. Biofilm prevention in human urine. (A-C) Biofilm prevention of **1** (reference compound) and **5** against different UPEC strains (A: UTI89, B: J96, and C: C175-94) grown in urine containing 0.5% CAA and 0.4% glycerol (inoculum $1x10^4$ CFU/well). Similar to the results in LB, the values show a concentration-dependent inhibition of biofilm formation. Bars represent means with standard deviations (SDs) from three independent experiments prepared in duplicates to quadruplicates. One-way ANOVA with Dunnett's post test was used to determine the statistical significance (p) of biofilm reduction compared to untreated controls (*, $p < 0.05$; **, $p<0.01$, ***, $p<0.001$). CV: crystal violet.

Prevention of UPEC biofilm formation on catheter surfaces. For simulating the *in vivo* conditions of the bacterial colonization on catheters, a novel *in vitro* catheter-associated biofilm model was developed. Catheter pieces were uniformly cut into 7-mm pieces and attached to the lid of 96-well plate, similar to the Calgary biofilm device described by Ceri *et al*. (41). Catheter pieces protrude into urine-containing wells by 2 mm, which allows their bacterial colonization (Figure 7A). Thereafter, the biofilm formation on the surface of catheter pieces was evaluated by CV staining.

In this model, both antagonists **1** and **5** were able to prevent the biofilm formation of UTI89 in a concentration-dependent fashion (Figure 7B and C, respectively). However, compound **5** turned out to be much more potent. At concentrations as low as 6.25 µg/ml it reduced the biofilm mass by more than 50% compared to the untreated sample (Figure 7B).

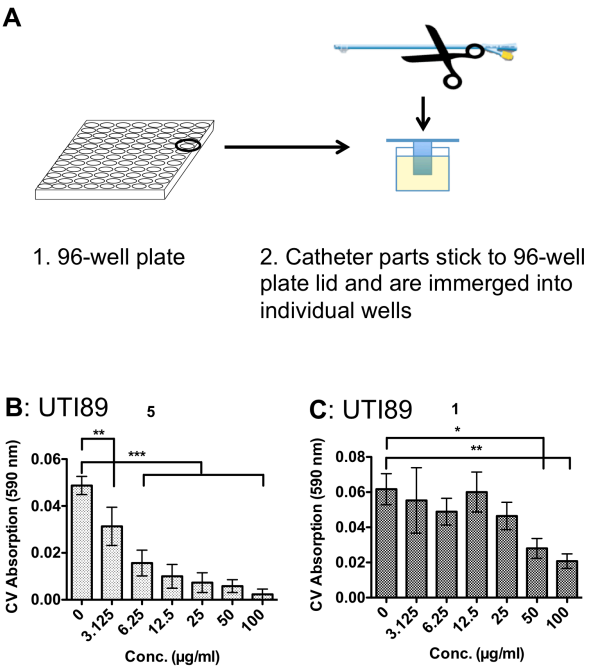

Figure 21. Prevention of biofilm formation on catheter surfaces. (A) Schematic representation of the catheter-associated biofilm model. Catheter pieces were cut into 7mm pieces and attached to the 96-well plate lid, directly entering single wells. As determined by CV staining of catheter pieces, both, **5** (B) and **1** (C) were able to prevent biofilm formation (48 h, 25°C, inoculum $1x10^4$ CFU/well). Bars represent means with standard deviations (SDs) from three independent experiments prepared in duplicates. One-way ANOVA with Dunnett's post test was used to determine the statistical significance (p) of biofilm reduction compared to untreated control (*, $p < 0.05$; **, $p < 0.01$). CV: crystal violet.

Overall, the CV absorption was low (maximum absorption value reached around 0.06) due to the small catheter surface exposed to the urine (catheter pieces only immerged by 2 mm into 200 µl liquid volume). Thus, the surface available for bacterial colonization is approximately two times 13 mm^2 (internal and external surface), neglecting capillary forces, which increases the internal surface available for colonization to a small extent. To expand this surface and assess the validity of these experiments, longer (2 cm) catheter pieces were cut and inserted into deep-well 96-well plates, leading to an approximately six-fold increase in catheter surface, namely to 0.94 cm^2 (internal and external, neglecting capillary forces). With this modified model, the biofilm inhibition potential of FimH antagonist **5** was evaluated by CV staining as well as enumeration of CFU/cm, indicating the number of bacteria per cm of catheter surface entering into the liquid (Figure 8).

Despite the increased surface available for bacterial colonization, the maximal CV signal was only three times higher, because biofilm formation was mainly observed at the air-liquid contact surface of the catheter piece. *E. coli* is known to form oxygen-dependent biofilms, because oxygen supports type 1 pili expression (49, 50).

In summary, CV staining showed the same concentration-dependent inhibition of biofilm mass by **5**, with a reduction of biofilm by over 50% at a concentration of 12.5 µg/ml (Figure 8A). Yet, although biofilm mass substantially decreased, bacteria remained viable (Figure 8B). Even at the highest concentration of **5** (100 µg/ml), the biofilm consisted of over 10^6 CFU/cm.

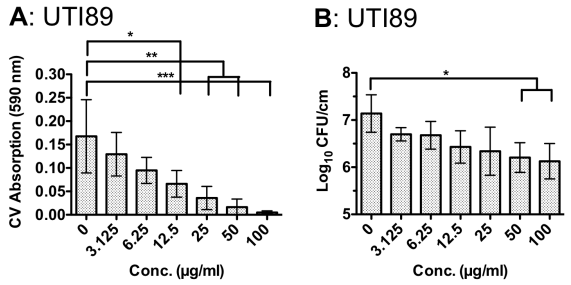

Figure 22. Prevention of biofilm formation in a modified catheter-associated biofilm model. (A) The effect of **5** on UTI89 biofilm formed on catheter pieces with a length of 2 cm was measured with CV staining. (B) Viable bacteria on the catheter surfaces (CFU/cm) were enumerated within the same assay. Experiments were performed for 48 hours at 25°C with an inoculum of $1x10^4$ CFU/well. Bars represent means with standard deviations (SDs) (of Log_{10} transformed values in B) from three independent experiments prepared in duplicates. One-way ANOVA with Dunnett's post test was used to determine the statistical significance (p) compared to untreated control (*, $p < 0.05$).

In conclusion, **5** showed a high efficacy to prevent biofilm formation of UTI89 on a catheter surface, however caused only a small reduction of viable bacteria (Figure 8). This suggests an influence of FimH antagonists on the structural integrity of the extracellular polymeric substances (EPS) or on the bacterial ability to produce EPS. However, when EPS is damaged or reduced by FimH antagonists, accessibility of bacteria for antibiotic treatment may be improved.

Enhanced effect on biofilm formation by combination therapy. To test this hypothesis, a combination therapy with FimH antagonists and antibiotics commonly used in UTI was studied in the catheter-associated biofilm model. Therefore,

antagonist **5** (indicated as FA) was tested in combination with ciprofloxacin (CIP) and trimethoprim-sulfamethoxazole (TMP/SMZ), two antibiotics recommended for UTI treatment (51–56). After 24 hours of biofilm formation by UTI89 in the presence of **5** (preventive application) under the previously used conditions, CIP or TMP/SMZ were added at high concentrations of 100 µg/ml or 50 µg/ml, respectively, leading to a significantly reduced biofilm mass (Figure 9A).

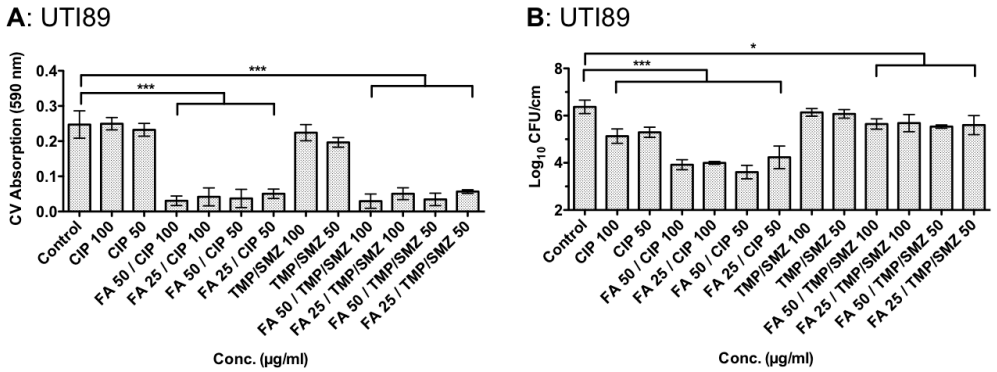

Figure 23. FimH antagonist 5 in combination with antibiotics. CV staining (A) and CFU/cm (B) of catheter treated with CIP or TMP/SMZ alone or in combination with **5** (indicated as FA) and CIP or TMP/SMZ. Concentrations (in µg/ml) are indicated besides the corresponding therapeutics on the x-axis. Experiments were performed for 48h at 25°C with an inoculum of $1x10^4$ CFU/well, antibiotics were added after 24h. Shown are mean with SDs (of Log_{10} transformed values for CFU per cm of the catheter length inserted into urine, 1.5 cm). Values derived from three independent experiments prepared in duplicates. One-way ANOVA with Dunnett's post test was used for statistical analysis (*, $p < 0.05$; **, $p<0.01$, ***, $p<0.001$).

Importantly, antibiotic treatment with CIP and TMP/SMZ alone was not able to reduce the biofilm of UTI89 on the catheter surface, suggesting a protective effect of the EPS. Furthermore, despite antibiotic treatment, evaluation of CFU/cm (per cm of catheter length inserted into urine and available for colonization) revealed a high proportion of surviving bacteria (Figure 9B). However, the combination therapy with **5** and CIP reduced bacterial counts by almost 3 Log_{10}. In contrast, with TMP/SMZ and **5** the bacterial counts could not be reduced, although the biofilm mass was substantially lowered. Moreover, the effect on biofilm mass and bacterial viability was not concentration-dependent, suggesting that even low concentrations of FimH antagonist and antibiotic in combination are sufficient for decreasing the biofilm.

DISCUSSION

In this report we could demonstrate that FimH antagonists are able to successfully prevent the formation of UPEC biofilm on various surfaces, importantly, on a catheter surface, which is of importance for prevention of CAUTI. FimH antagonists do not act on pre-formed biofilms, but inhibit further biofilm growth. This suggests that type 1 pili are not only important for the initial adhesion to the urothelial surface, but also for cell-to-cell contacts and/or the integrity of EPS as proposed by Rodrigues and Elimelech (57), who suggested that type 1 pili are important for the coherence of the mannose-rich EPS matrix. However, it also indicates that FimH antagonists are not able to permeate a functional biofilm matrix to act on previously formed connections between bacteria.

Interestingly, biofilm formation of UPEC is much lower at the conditions present in the human body, i.e., in physiological human urine and at 37°C. This suggests an anti-biofilm environment in humans, since the biofilm mass in urine was reduced by approximately 70% compared to LB. This is in agreement with other reports on poor biofilm formation in urine (58).

All tested FimH antagonists were able to reduce biofilm mass of different UPEC strains in human urine, tested with the CV staining assay. Nevertheless, the extent of biofilm formation was different for each strain. Both, in LB and in urine, UTI89 was the best biofilm former opposed to C175-94, which showed low biofilm forming ability. Hung *et al.* correlated the mannose affinity of UPEC with their ability to form biofilms (21). Indeed, UTI89 is a strong mannose-binder, whereas C175-94 shows a low mannose-binding potential (data not shown). These finding obviously support the previous hypothesis on the importance of type 1 pili for the integrity of the EPS.

Whereas antagonist **5** effectively reduced biofilm mass of all tested UPEC strains and was able to lower biofilm formation on a catheter surface, its effect on viable bacteria within the biofilm was minor. However, combining a preventive application of the FimH antagonist **5** with a therapeutic application of CIP after the first 24 hours, significantly reduced both, the biofilm mass and numbers of viable bacteria. A possible reason for this potent effect might be the disruption of the EPS matrix. By

blocking type 1 pili, not only the attachment of cells to a surface is blocked, but also the first inter-cellular contacts necessary to establish a biofilm. Besides type 1 pili, Ag43, and curli mediate autoaggregation and thus the ability for the formation of microcolonies, the starting point for biofilms (26, 59–63). However, since type 1 pili are longer organelles than Ag43 or curli, they can and prevent their intercellular contact (63). When they are blocked, the smaller adhesive organelles might not be able to interconnect to the same extent. Therefore, the decreasing biofilm mass indicates a disruption of the integrity of biofilm matrix, leaving the bacteria susceptible to antibiotic treatment, as it was demonstrated in this study.

The concept of an anti-adhesive therapy to prevent or reduce biofilms was already reported over one decade ago. Pratt and Kolter showed that methyl α-D-mannoside is a potent biofilm inhibitor of *E. coli* (22). In addition, Hultgren et al. reported that FimH antagonists inhibit CAUTI caused by UPEC in mice (30). However, since UPEC are not the only bacterial strains causing CAUTI and numerous additional species might be involved, such as *Klebsiella pneumonia* or *Pseudomonas aeruginosa* (64), the anti-adhesive concept has a much broader applicability. For example, type 1 pili are encoded by many Enterobacteriacea, offering targets that might be related to other bacterial infections (65). In a similar manner, biofilms related to *P. aeruginosa* were inhibited and dispersed with fucosides, blocking the fucose-specific lectin LecB (66). Thus, a future anti-adhesive therapy for CAUTI patients could include a cocktail of several anti-adhesives to successfully prevent the adhesion of multiple species and strains. Likely, this combination of several anti-adhesive drugs could be a valuable option for preventing CAUTIs and would lead to decreased antibiotic use and resistance.

In summary, FimH antagonists could provide a novel preventive approach for CAUTI. They inhibited biofilm formation on several surfaces and in different media, but most important, on the surface of conventionally used silicone catheters in the presence of human urine. Furthermore, they potentiated antibiotic effects, even when those were added after biofilm formation. Since they are derivatives of the naturally occurring D-mannose and rapidly cleared through urine, we estimate the possibility of adverse effects in humans to be small.

FUNDING INFORMATION

The financial support of the Swiss National Science Foundation (SNCF interdisciplinary grant K-32K1-120904) is gratefully acknowledged. There were no requirements for the design, data collection, or interpretation from SNCF.

ACKNOWLEDGEMENTS

We thank Uromed Switzerland for providing us with free catheters for our research and the Imaging Core Facility of the University of Basel for their scientific advices. Also, we are grateful for the bacterial strains provided by Prof. Jenal, Biocenter, University of Basel, Switzerland, Prof. Johnson, University of Minnesota Medical School, Minneapolis/MN, USA, and Dr. Carsten Struve and Prof. Karen Krogfelt, Statens Serum Institut, Copenhagen, Denmark. The cutting device was assembled by Raymond Strittmatter, mechanical workshop of the Biocenter, University of Basel, Switzerland.

REFERENCES

1. **Tambyah PA**, **Maki DG**. 2000. Catheter-associated urinary tract infection is rarely symptomatic: a prospective study of 1,497 catheterized patients. Arch Intern Med **160**:678–682.
2. **Foxman B**. 2002. Epidemiology of urinary tract infections: incidence, morbidity, and economic costs. Am J Med **113**:5–13.
3. **Warren JW**. 2001. Catheter-associated urinary tract infections. Int J Antimicrob Agents **17**:299–303.
4. **Hartstein AI**, **Garber SB**, **Ward TT**, **Jones SR**, **Morthland VH**. 1981. Nosocomial Urinary Tract Infection: A Prospective Evaluation of 108 Catheterized Patients. Infect Control **2**:380–386.
5. **Saint S**. 2000. Clinical and economic consequences of nosocomial catheter-related bacteriuria. Am J Infect Control **28**:68–75.
6. **Nicolle DLE**. 2005. Catheter-Related Urinary Tract Infection. Drugs Aging **22**:627–639.

7. **Macleod SM**, **Stickler DJ**. 2007. Species interactions in mixed-community crystalline biofilms on urinary catheters. J Med Microbiol **56**:1549–1557.
8. **Ma KL**, **Wang CX**. 2013. Analysis of the spectrum and antibiotic resistance of uropathogens in vitro: Results based on a retrospective study from a tertiary hospital. Am J Infect Control **41**:601–606.
9. **Mohajer MA**, **Darouiche RO**. 2013. Prevention and Treatment of Urinary Catheter-Associated Infections. Curr Infect Dis Rep **15**:116–123.
10. **Soto SM**, **Smithson A**, **Horcajada JP**, **Martinez JA**, **Mensa JP**, **Vila J**. 2006. Implication of biofilm formation in the persistence of urinary tract infection caused by uropathogenic Escherichia coli. Clin Microbiol Infect **12**:1034–1036.
11. **Costerton JW**, **Lewandowski Z**, **Caldwell DE**, **Korber DR**, **Lappin-Scott HM**. 1995. Microbial Biofilms. Annu Rev Microbiol **49**:711–745.
12. **Nickel JC**, **Ruseska I**, **Wright JB**, **Costerton JW**. 1985. Tobramycin resistance of Pseudomonas aeruginosa cells growing as a biofilm on urinary catheter material. Antimicrob Agents Chemother **27**:619–624.
13. **Costerton JW**, **Stewart PS**, **Greenberg EP**. 1999. Bacterial Biofilms: A Common Cause of Persistent Infections. Science **284**:1318–1322.
14. **Davies D**. 2003. Understanding biofilm resistance to antibacterial agents. Nat Rev Drug Discov **2**:114–122.
15. **Vickery K**, **Deva A**, **Jacombs A**, **Allan J**, **Valente P**, **Gosbell IB**. 2012. Presence of biofilm containing viable multiresistant organisms despite terminal cleaning on clinical surfaces in an intensive care unit. J Hosp Infect **80**:52–55.
16. **Kurtaran B**, **Candevir A**, **Tasova Y**, **Kibar F**, **Inal AS**, **Komur S**, **Aksu HSZ**. 2010. Antibiotic resistance in community-acquired urinary tract infections: prevalence and risk factors. Med Sci Monit Int Med J Exp Clin Res **16**:CR246–251.
17. **Hossain MD**, **Ahsan S**, **Kabir MS**. 2014. Antibiotic resistance patterns of uropathogens isolated from catheterized and noncatheterized patients in Dhaka, Bangladesh. Tzu Chi Med J **26**:127–131.
18. **Jacobsen SM**, **Stickler DJ**, **Mobley HLT**, **Shirtliff ME**. 2008. Complicated Catheter-Associated Urinary Tract Infections Due to Escherichia coli and Proteus mirabilis. Clin Microbiol Rev **21**:26–59.

19. **Spurbeck RR**, **Stapleton AE**, **Johnson JR**, **Walk ST**, **Hooton TM**, **Mobley HLT**. 2011. Fimbrial Profiles Predict Virulence of Uropathogenic Escherichia coli Strains: Contribution of Ygi and Yad Fimbriae. Infect Immun **79**:4753–4763.
20. **Wurpel DJ**, **Beatson SA**, **Totsika M**, **Petty NK**, **Schembri MA**. 2013. Chaperone-Usher Fimbriae of Escherichia coli. PLoS ONE **8**:e52835.
21. **Hung C**, **Zhou Y**, **Pinkner JS**, **Dodson KW**, **Crowley JR**, **Heuser J**, **Chapman MR**, **Hadjifrangiskou M**, **Henderson JP**, **Hultgren SJ**. 2013. Escherichia coli Biofilms Have an Organized and Complex Extracellular Matrix Structure. mBio **4**:e00645–13.
22. **Pratt LA**, **Kolter R**. 1998. Genetic analysis of Escherichia coli biofilm formation: roles of flagella, motility, chemotaxis and type I pili. Mol Microbiol **30**:285–293.
23. **Harber MJ**, **Mackenzie R**, **Asscher AW**. 1983. A Rapid Bioluminescence Method for Quantifying Bacterial Adhesion to Polystyrene. J Gen Microbiol **129**:621–632.
24. **Cookson AL**, **Cooley WA**, **Woodward MJ**. 2002. The role of type 1 and curli fimbriae of Shiga toxin-producing Escherichia coli in adherence to abiotic surfaces. Int J Med Microbiol **292**:195–205.
25. **Kikuchi T**, **Mizunoe Y**, **Takade A**, **Naito S**, **Yoshida S**. 2005. Curli fibers are required for development of biofilm architecture in Escherichia coli K-12 and enhance bacterial adherence to human uroepithelial cells. Microbiol Immunol **49**:875–884.
26. **Vidal O**, **Longin R**, **Prigent-Combaret C**, **Dorel C**, **Hooreman M**, **Lejeune P**. 1998. Isolation of an Escherichia coli K-12 Mutant Strain Able To Form Biofilms on Inert Surfaces: Involvement of a New ompR Allele That Increases Curli Expression. J Bacteriol **180**:2442–2449.
27. **Cegelski L**, **Pinkner JS**, **Hammer ND**, **Cusumano CK**, **Hung CS**, **Chorell E**, **Åberg V**, **Walker JN**, **Seed PC**, **Almqvist F**, **Chapman MR**, **Hultgren SJ**. 2009. Small-molecule inhibitors target Escherichia coli amyloid biogenesis and biofilm formation. Nat Chem Biol **5**:913–919.
28. **McCrate OA**, **Zhou X**, **Reichhardt C**, **Cegelski L**. 2013. Sum of the Parts: Composition and Architecture of the Bacterial Extracellular Matrix. J Mol Biol **425**:4286–4294.

29. **Hadjifrangiskou M**, **Gu AP**, **Pinkner JS**, **Kostakioti M**, **Zhang EW**, **Greene SE**, **Hultgren SJ**. 2012. Transposon Mutagenesis Identifies Uropathogenic Escherichia coli Biofilm Factors. J Bacteriol **194**:6195–6205.
30. **Guiton PS**, **Cusumano CK**, **Kline KA**, **Dodson KW**, **Han Z**, **Janetka JW**, **Henderson JP**, **Caparon MG**, **Hultgren SJ**. 2012. Combinatorial Small-Molecule Therapy Prevents Uropathogenic Escherichia coli Catheter-Associated Urinary Tract Infections in Mice. Antimicrob Agents Chemother **56**:4738–4745.
31. **Lim JK**, **Gunther NW**, **Zhao H**, **Johnson DE**, **Keay SK**, **Mobley HLT**. 1998. In Vivo Phase Variation of Escherichia coli Type 1 Fimbrial Genes in Women with Urinary Tract Infection. Infect Immun **66**:3303–3310.
32. **Reisner A**, **Maierl M**, **Jörger M**, **Krause R**, **Berger D**, **Haid A**, **Tesic D**, **Zechner EL**. 2014. Type 1 Fimbriae Contribute to Catheter-Associated Urinary Tract Infections Caused by Escherichia coli. J Bacteriol **196**:931–939.
33. **Johnson JR**, **Kuskowski MA**, **Wilt TJ**. 2006. Systematic review: antimicrobial urinary catheters to prevent catheter-associated urinary tract infection in hospitalized patients. Ann Intern Med **144**:116–126.
34. **Pickard R**, **Lam T**, **MacLennan G**, **Starr K**, **Kilonzo M**, **McPherson G**, **Gillies K**, **McDonald A**, **Walton K**, **Buckley B**, **Glazener C**, **Boachie C**, **Burr J**, **Norrie J**, **Vale L**, **Grant A**, **N'Dow J**. 2012. Antimicrobial catheters for reduction of symptomatic urinary tract infection in adults requiring short-term catheterisation in hospital: a multicentre randomised controlled trial. The Lancet **380**:1927–1935.
35. **Stahlhut SG**, **Struve C**, **Krogfelt KA**, **Reisner A**. 2012. Biofilm formation of Klebsiella pneumoniae on urethral catheters requires either type 1 or type 3 fimbriae. Fems Immunol Med Microbiol **65**:350–359.
36. **Hull RA**, **Gill RE**, **Hsu P**, **Minshew BH**, **Falkow S**. 1981. Construction and expression of recombinant plasmids encoding type 1 or D-mannose-resistant pili from a urinary tract infection Escherichia coli isolate. Infect Immun **33**:933–938.
37. **Struve C**, **Krogfelt KA**. 1999. In vivo detection of Escherichia coli type 1 fimbrial expression and phase variation during experimental urinary tract infection. Microbiol Read Engl **145 (Pt 10)**:2683–2690.

38. **O'Toole GA**, **Pratt LA**, **Watnick PI**, **Newman DK**, **Weaver VB**, **Kolter R**. 1999. [6] Genetic approaches to study of biofilms, p. 91–109. *In* Doyle, RJ (ed.), Methods in Enzymology. Academic Press.
39. **Scharenberg M**, **Abgottspon D**, **Cicek E**, **Jiang X**, **Schwardt O**, **Rabbani S**, **Ernst B**. 2011. A Flow Cytometry-Based Assay for Screening FimH Antagonists. ASSAY Drug Dev Technol **9**:455–464.
40. **Merritt JH**, **Kadouri DE**, **O'Toole GA**. 2005. Growing and Analyzing Static BiofilmsCurrent Protocols in Microbiology. John Wiley & Sons, Inc.
41. **Ceri H**, **Olson ME**, **Stremick C**, **Read RR**, **Morck D**, **Buret A**. 1999. The Calgary Biofilm Device: New Technology for Rapid Determination of Antibiotic Susceptibilities of Bacterial Biofilms. J Clin Microbiol **37**:1771–1776.
42. **Kliot A**, **Kontsedalov S**, **Lebedev G**, **Brumin M**, **Cathrin PB**, **Marubayashi JM**, **Skaljac M**, **Belausov E**, **Czosnek H**, **Ghanim M**. 2014. Fluorescence in situ Hybridizations (FISH) for the Localization of Viruses and Endosymbiotic Bacteria in Plant and Insect Tissues. J Vis Exp.
43. **Fu L**, **Sztul E**. 2015. Characterization of Intracellular Aggresomes by Fluorescent Microscopy, p. 307–317. *In* García-Fruitós, E (ed.), Insoluble Proteins. Springer New York.
44. **Ratliff TL**. 2005. Receptor Binding Studies Disclose a Novel Class of High-Affinity Inhibitors of the Escherichia Coli FimH Adhesin. J Urol **174**:1150.
45. **Scharenberg M**, **Schwardt O**, **Rabbani S**, **Ernst B**. 2012. Target Selectivity of FimH Antagonists. J Med Chem **55**:9810–9816.
46. **Pang L**, **Bezençon J, Kleeb S**, **Rabbani S**, **Sigl A**, **Smieško M**, **Sager CP**, **Eris D, Schwardt O**, **Ernst B**. 2017. FimH Antagonists - solubility vs. permeability. Carbohydr. Chem., **42**:248–273
47. **Klein T**, **Abgottspon D**, **Wittwer M**, **Rabbani S**, **Herold J**, **Jiang X**, **Kleeb S**, **Lüthi C**, **Scharenberg M**, **Bezençon J**, **Gubler E**, **Pang L**, **Smiesko M**, **Cutting B**, **Schwardt O**, **Ernst B**. 2010. FimH Antagonists for the Oral Treatment of Urinary Tract Infections: From Design and Synthesis to in Vitro and in Vivo Evaluation. J Med Chem **53**:8627–8641.
48. **Kleeb S**, **Pang L**, **Mayer K**, **Eris D**, **Sigl A**, **Preston RC**, **Zihlmann P**, **Sharpe T**, **Jakob RP**, **Abgottspon D**, **Hutter AS**, **Scharenberg M**, **Jiang X**, **Navarra G**, **Rabbani S**, **Smiesko M**, **Lüdin N**, **Bezençon J**, **Schwardt O**, **Maier T**,

Ernst B. 2015. FimH Antagonists: Bioisosteres To Improve the in Vitro and in Vivo PK/PD Profile. J Med Chem **58**:2221–2239.

49. **Colón-González M**, **Méndez-Ortiz MM**, **Membrillo-Hernández J**. 2004. Anaerobic growth does not support biofilm formation in Escherichia coli K-12. Res Microbiol **155**:514–521.
50. **Floyd KA**, **Moore JL**, **Eberly AR**, **Good JAD**, **Shaffer CL**, **Zaver H**, **Almqvist F**, **Skaar EP**, **Caprioli RM**, **Hadjifrangiskou M**. 2015. Adhesive Fiber Stratification in Uropathogenic Escherichia coli Biofilms Unveils Oxygen-Mediated Control of Type 1 Pili. PLoS Pathog **11**:e1004697.
51. **Mobley HLT**, **Warren JW**. 1996. Urinary Tract Infections: Molecular Pathogenesis and Clinical Management. ASM Press.
52. **Hooton TM**, **Stamm WE**. 1997. Diagnosis and treatment of uncomplicated urinary tract infection. Infect Dis Clin North Am **11**:551–581.
53. **Grabe M**, **Bjerklung-Johansen TE**, **Botto H**, **Cek M**, **Naber KG**, **Pickard RS**, **Tenke P**, **Wagenlehner F**, **Wullt B**. Guidelines on Urological Infections.
54. **Naber KG**, **Bergman B**, **Bishop MC**, **Bjerklund-Johansen TE**, **Botto H**, **Lobel B**, **Jinenez Cruz F**, **Selvaggi FP**, **Urinary Tract Infection (UTI) Working Group of the Health Care Office (HCO) of the European Association of Urology (EAU)**. 2001. EAU guidelines for the management of urinary and male genital tract infections. Urinary Tract Infection (UTI) Working Group of the Health Care Office (HCO) of the European Association of Urology (EAU). Eur Urol **40**:576–588.
55. **Taur Y**, **Smith MA**. 2007. Adherence to the Infectious Diseases Society of America Guidelines in the Treatment of Uncomplicated Urinary Tract Infection. Clin Infect Dis **44**:769–774.
56. **Nicolle L**, **Anderson PAM**, **Conly J**, **Mainprize TC**, **Meuser J**, **Nickel JC**, **Senikas VM**, **Zhanel GG**. 2006. Uncomplicated urinary tract infection in women. Can Fam Physician **52**:612–618.
57. **Rodrigues DF**, **Elimelech M**. 2009. Role of type 1 fimbriae and mannose in the development of Escherichia coli K12 biofilm: from initial cell adhesion to biofilm formation. Biofouling **25**:401–411.
58. **Reisner A**, **Krogfelt KA**, **Klein BM**, **Zechner EL**, **Molin S**. 2006. In Vitro Biofilm Formation of Commensal and Pathogenic Escherichia coli Strains: Impact of Environmental and Genetic Factors. J Bacteriol **188**:3572–3581.

59. **Danese PN**, **Pratt LA**, **Dove SL**, **Kolter R**. 2000. The outer membrane protein, Antigen 43, mediates cell-to-cell interactions within Escherichia coli biofilms. Mol Microbiol **37**:424–432.
60. **Kjærgaard K**, **Schembri MA**, **Hasman H**, **Klemm P**. 2000. Antigen 43 from Escherichia coli Induces Inter- and Intraspecies Cell Aggregation and Changes in Colony Morphology of Pseudomonas fluorescens. J Bacteriol **182**:4789–4796.
61. **Prigent-Combaret C**, **Prensier G**, **Le Thi TT**, **Vidal O**, **Lejeune P**, **Dorel C**. 2000. Developmental pathway for biofilm formation in curli-producing Escherichia coli strains: role of flagella, curli and colanic acid. Environ Microbiol **2**:450–464.
62. **Reisner A**, **Haagensen JAJ**, **Schembri MA**, **Zechner EL**, **Molin S**. 2003. Development and maturation of Escherichia coli K-12 biofilms. Mol Microbiol **48**:933–946.
63. **Ulett GC**, **Valle J**, **Beloin C**, **Sherlock O**, **Ghigo J-M**, **Schembri MA**. 2007. Functional Analysis of Antigen 43 in Uropathogenic Escherichia coli Reveals a Role in Long-Term Persistence in the Urinary Tract. Infect Immun **75**:3233–3244.
64. **Frank DN**, **Wilson SS**, **St. Amand AL**, **Pace NR**. 2009. Culture-Independent Microbiological Analysis of Foley Urinary Catheter Biofilms. PLoS ONE **4**:e7811.
65. **Buchanan K**, **Falkow S**, **Hull RA**, **Hull SI**. 1985. Frequency among Enterobacteriaceae of the DNA sequences encoding type 1 pili. J Bacteriol **162**:799–803.
66. **Johansson EMV**, **Crusz SA**, **Kolomiets E**, **Buts L**, **Kadam RU**, **Cacciarini M**, **Bartels K-M**, **Diggle SP**, **Cámara M**, **Williams P**, **Loris R**, **Nativi C**, **Rosenau F**, **Jaeger K-E**, **Darbre T**, **Reymond J-L**. 2008. Inhibition and Dispersion of Pseudomonas aeruginosa Biofilms by Glycopeptide Dendrimers Targeting the Fucose-Specific Lectin LecB. Chem Biol **15**:1249–1257.

5.6. Addition: Short REVIEW (in German)

“FimH-Antagonisten: eine neue Option für die Therapie von Harnwegsinfekten”

Beat Ernst, Anja Sigl

Schweizerisches Medizin Forum, December 2013

FORSCHUNG.CH

FimH-Antagonisten: eine neue Option für die Therapie von Harnwegsinfekten

Beat Ernst, Anja Sigl
Institut für Molekulare Pharmazie, Pharmazentrum der Universität Basel

Harnwegsinfekte (HWI) gehören weltweit zu den häufigsten Infektionen. Die Hälfte aller Frauen erleidet mindestens einmal im Leben einen unkomplizierten HWI, bei einem Viertel kommt es innerhalb von sechs Monaten zu einem Rezidiv [1, 2]. Von komplizierten HWI hingegen sind Frauen und Männer mit anatomischen Anomalitäten der Harnwege, Kathetern, Diabetes mellitus, Paraplegie oder Infektionen mit multiresistenten Bakterien gleichermassen betroffen [3, 4].

HWI werden mit Antibiotika behandelt. Deren häufiger Einsatz hat in den letzten Jahren zu einem alarmierenden Anstieg der Resistenzraten geführt. So lag im Jahr 2012 in der Schweiz die Resistenz von *E. coli* gegenüber dem häufig bei HWI eingesetzten Cotrimoxazol bei bereits 27,4% [5]. Neuartige Therapieansätze mit geringerem Resistenzpotential sind deshalb aus medizinischer Sicht dringend notwendig.

Unsere Forschungsgruppe untersucht die vielfältigen biologischen Funktionen und damit auch das therapeutische Potenzial komplexer Kohlenhydrate. Diese sind an zahllosen physiologischen und pathophysiologischen Prozessen beteiligt. Unter anderem spielen sie eine wichtige Rolle bei bakteriellen, viralen und mykotischen Infektionen, so auch bei Infektionen der Harnwege.

Ansatz der antiadhäsiven Therapie

Ursächlich für einen HWI ist das Aufsteigen von Bakterien über die Harnröhre in die Blase. In den meisten Fällen (>80%) handelt es sich bei den verursachenden Bakterien um uropathogene *Escherichia coli* (UPEC), die häufig aus der körpereigenen Darmflora stammen. Eine untergeordnete Rolle spielen *Staphylococcus saprophyticus, Klebsiella pneumoniae* oder *Proteus mirabilis* [1, 6].

In der Blase angekommen, heften sich die UPEC an Oberflächenstrukturen des Blasenurothels. Bei diesem initialen Schritt der Infektion spielen haarähnliche Fimbrien auf der Bakterienoberfläche, auch Typ-1-Pili genannt, eine Schlüsselrolle. An deren Spitze befindet sich ein Rezeptor, der für den Adhäsionsmechanismus verantwortlich ist. Dabei handelt es sich um das Protein FimH, das mit seiner Kohlenhydrat-erkennenden Domäne (carbohydrate recognition domain, CRD) die Zuckerstrukturen des Glykoproteins Uroplakin 1A an der luminalen Seite der Urothelzellen erkennt und daran bindet. Die Zuckerstrukturen sind Oligomere des Mannose-Typus.

Mit dieser Wechselwirkung erreichen die Bakterien zweierlei: Sie entgehen dem Ausschwemmen aus der Blase mit dem Urinfluss und können die Invasion der Urothelzellen und damit den Infektionszyklus initiieren. Einmal im Innern einer Urothelzelle angelangt, sind die UPEC mehrheitlich vor der Antibiotikatherapie, aber auch vor Angriffen des Immunsystems geschützt. Nach einer intrazellulären Replikationsphase, in der die Bakterien biofilmartige Strukturen ausbilden, können sie das Blasenurothel aufbrechen und einen neuen Infektionszyklus starten. Die Bakterien können aber auch in tiefer liegende Zellschichten vordringen und über längere Zeit latent bleiben. Damit erklären sich die häufig auftretenden Rezidive, die auf dieses schlummernde Infektionspotential zurückzuführen sind.

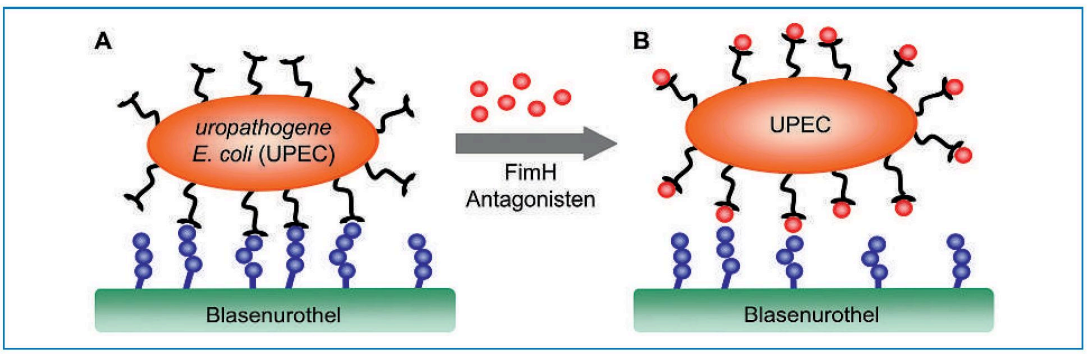

Abbildung 1
Hemmung der Adhäsion von UPEC an die Blasenurothel-Oberfläche.
A) Mit den Rezeptoren an der Spitze der Fimbrien (schwarz), den FimH, adhärieren die Bakterien an die Blasenurothelzellen.
B) Der FimH-Antagonist (rot) bindet an die bakteriellen Rezeptoren FimH, blockiert damit die Andockstellen und verhindert die Adhäsion der Bakterien an das Blasenurothel.

Die Autoren haben keine finanzielle Unterstützung und keine Interessenkonflikte im Zusammenhang mit diesem Beitrag deklariert.

Bereits in den 1970er Jahren wurde erkannt, dass Oligomannoside an FimH binden, damit den Rezeptor blockieren und folglich die Adhäsion von UPEC an Blasenurothelzellen verhindern können. Da jedoch natürlich vorkommende Glykane nur schwache Liganden sind und zudem unzureichende pharmakokinetische Eigenschaften aufweisen, ist ihr therapeutischer Einsatz nicht sinnvoll. Deshalb begannen wir mit der Suche nach Glykomimetika, das heisst niedermolekularen Verbindungen, welche die natürlichen Zuckerliganden imitieren, aber eine höhere Affinität zum bakteriellen Rezeptor FimH und verbesserte pharmakokinetische Eigenschaften aufweisen.

Der von uns verfolgte therapeutische Ansatz zielt also auf die Hemmung der Adhäsion an das Blasenurothel und somit den initialen Schritt des Infektionszyklus (Abb. 1 📷). Das soll mit einem Mimetikum erreicht werden, das den natürlichen Liganden imitiert und an dessen Stelle an FimH bindet. Damit kann die Wechselwirkung mit dem Blasenurothel verhindert und das Bakterium mit dem Urin ausgeschieden werden. Dieser Ansatz nutzt zudem den Vorteil, dass der Adhäsionsmechanismus über mehrere Bakterienklassen konserviert ist, was die therapeutische Anwendung nicht unwesentlich verbreitern könnte.

Ausserdem sind die Typ-1-Pili ein wichtiger Virulenzfaktor der Bakterien. UPEC mit defekten Typ-1-Pili sind viel schwächer virulent und bilden damit ein deutlich geringeres Infektionsrisiko. Schliesslich bietet die Behandlung mit FimH-Antagonisten einen weiteren wichtigen Vorteil, nämlich das zu erwartende geringe Resistenzpotential. Weil die Bakterien lediglich in ihrer Adhäsion an das Blasenurothel gehemmt werden, bleibt ein Selektionsdruck aus, der eine Voraussetzung für die Selektion von resistenten Mutanten darstellt.

Erfolge im Tiermodell

Ausgehend von D-Mannose konnten nach medizinisch-chemischen Optimierungsverfahren FimH-Antagonisten entwickelt werden, die sowohl eine hohe Affinität für FimH als auch gute pharmakokinetische Eigenschaften aufweisen. Einige können sogar zur oralen Applikation verwendet werden. Die besten Vertreter wurden in vivo in einem Infektionsmodell in der Maus validiert. Dabei zeigte sich, dass mit den besten Antagonisten die therapeutische Konzentration in der Blase nach einer Einmalgabe über acht Stunden aufrechterhalten werden kann und die Bakterienlast bis um das 1000-Fache reduziert wird [7]. Dieser Wert ist vergleichbar mit der antibiotischen Bakterienreduktion des bei HWI traditionell häufig angewandten Antibiotikums Ciprofloxazin [8]. Weil im menschlichen Körper vor allem im Immunsystem zahlreiche Mannose-Rezeptoren eine wichtige physiologische Rolle spielen, war es auch wichtig zu zeigen, dass unsere FimH-Antagonisten eine hohe Selektivität für den bakteriellen Rezeptor aufweisen [9].

Wie geht es weiter?

Dank dieser vielversprechenden Resultate wird zurzeit die präklinische Evaluierung der besten Kandidaten vorbereitet. Für einen späteren therapeutischen Einsatz bieten sich vor allem die Prävention, aber auch die Therapie – allenfalls auch in Kombination mit Antibiotika – der HWI an.

Korrespondenz:
Prof. Beat Ernst
Institut für Molekulare Pharmazie
Universität Basel
CH-4056 Basel
beat.ernst[at]unibas.ch

Literatur

1 Foxman, B. Epidemiology of urinary tract infections: incidence, morbidity, and economic costs. Am J Med. 2002;113:5–13.
2 Tarr P, Baumann K, Wallnöfer A, Zimmerli F, Maritz D, Burri U. Akute Harnwegsinfektionen, Teil 1: HWI in der Praxis. Schweiz Med Forum. 2013;13(23):467–71.
3 Pathophysiology of Complicated Urinary Tract Infections. 2013; http://emedicine.medscape.com/article/2039975-overview.
4 Tarr P, Baumann K, Wallnöfer A, Zimmerli F, Maritz D, Burri U, et al. Akute Harnwegsinfektionen, Teil 2: HWI im Spital sowie Alters- und Pflegeheim. Schweiz Med Forum. 2013;13(24):472–5.
5 Institut für Infektionskrankheiten, Universität Bern. Schweizerisches Zentrum für Antibiotikaresistenzen; www.anresis.ch.
6 Ronald A. The etiology of urinary tract infection: traditional and emerging pathogens. Am J Med. 2002;113:14–9.
7 Klein T, Abgottspon D,Wittwer M, Rabbani S, Herold J, Jiang X, et al. FimH Antagonists for the Oral Treatment of Urinary Tract Infections: From Design and Synthesis to in Vitro and in Vivo Evaluation. J Med Chem. 2010;53:8627–41.
8 Jiang X, Abgottspon D, Kleeb S, Rabbani S, Scharenberg M, Wittwer M, et al. Antiadhesion therapy for urinary tract infections – a balanced PK/PD profile proved to be key for success. J Med Chem. 2012;55:4700–13.
9 Scharenberg M, Schwardt O, Rabbani S, Ernst B. Target Selectivity of FimH Antagonists. J Med Chem. 2012;55:9810–6.

6. Conclusion

Conclusion

The increasing importance of new therapeutic options for the treatment of resistant bacteria thrives the development of new antibacterial agents with novel mode of actions. Thus, anti-adhesive therapies could be a valuable option, since they do not exert survival pressure and consequently do not promote resistance development. Bacterial lectins offer valuable targets for the development of anti-adhesives, as they mediate multiple interactions between the pathogen and host structures. Furthermore, anti-adhesives are natural sugars or derivatives thereof, hence, they should have a low immunogenic potential or should not cause adverse reactions.[234,235] However, the expression of multiple adhesins on a single bacterium might require a cocktail of anti-adhesives for an effective therapy.[234–236] Another difficulty is the phase variable expression of adhesins, which allows the bacteria to adapt and attach in different environmental conditions.[237] This might demand an exact understanding of the concentrations needed of every individual anti-adhesive molecules at the site of action, when applying an anti-adhesive cocktail.

To establish a basic knowledge on the PK/PD relationship of anti-adhesives, FimH antagonists were studied in this thesis. Both, their preventive and therapeutic effect within UTI were addressed. Thereby, it became clear that they offer a valuable preventive option, which work synergistically with antibiotics. They were active in mice and depleted bacterial loads by 2-3 Log_{10} CFU/ml in the bladder for several time spans of infection and in different treatment set-ups.

We could reveal that the MAC_{90} is an important value and represents the initial concentration needed in the bladder for a therapeutic effect. The most predictive PK/PD index for preventively applied FimH antagonists was the magnitude of the C_{max}/MAC_{90} ratio and how long this magnitude is maintained during infection. Treatment regimens should aim at increasing the C_{max} to keep up with replicating bacteria.

Furthermore, FimH antagonists prevented biofilm formation on catheter surfaces in concentrations as low as 6.25 µg/ml. Again, they were able to potentiate the antibiotic effect. In a next step, the effectivity of biofilm prevention should be assessed under flow conditions.

Conclusion

Although FimH antagonists have not been tested in humans yet, the therapeutic effect might be even higher than in mice, as humans do not have to face the challenge of 10^8 bacteria within a few seconds. Lower bacterial numbers will help to more easily reach the C_{max}/MAC_{90} ratio required for positive therapeutic outcome. Also, the most successful antagonist presented in this thesis (*para*-cyanobiphenyl α-D-mannopyranoside) resulted in urine concentrations over the MAC_{90} for 24 hours at a dose of 10 mg/kg and 1.25 mg/kg. Since mice have a faster metabolism than humans, urine concentrations and accumulation of the antagonist in humans might even be higher. However, inter-species statements concerning PK are not possible at this stage and would need further data.[238,239] Furthermore, the therapy with FimH antagonists could be combined with frequent liquid intake and urination, which could increase the therapeutic success.

Future investigations will have to solve the problem of the different affinity states of FimH and their influence upon the infection. Also, combining PapG with FimH antagonists seems a promising approach for clearing UTI.

7. References

(1) Foxman, B. Epidemiology of Urinary Tract Infections: Incidence, Morbidity, and Economic Costs. *Am. J. Med.* **2002**, *113* (1, Supplement 1), 5–13.

(2) Ronald, A. The Etiology of Urinary Tract Infection: Traditional and Emerging Pathogens. *Am. J. Med.* **2002**, *113* (1, Supplement 1), 14–19.

(3) Hooton, T. M.; Stamm, W. E. Diagnosis and Treatment of Uncomplicated Urinary Tract Infection. *Infect. Dis. Clin. North Am.* **1997**, *11* (3), 551–581.

(4) Russo, T. A.; Stapleton, A.; Wenderoth, S.; Hooton, T. M.; Stamm, W. E. Chromosomal Restriction Fragment Length Polymorphism Analysis of Escherichia Coli Strains Causing Recurrent Urinary Tract Infections in Young Women. *J. Infect. Dis.* **1995**, *172* (2), 440–445.

(5) Kärkkäinen, U. M.; Ikäheimo, R.; Katila, M. L.; Siitonen, A. Recurrence of Urinary Tract Infections in Adult Patients with Community-Acquired Pyelonephritis Caused by E. Coli: A 1-Year Follow-Up. *Scand. J. Infect. Dis.* **2000**, *32* (5), 495–499.

(6) Foxman, B.; Zhang, L.; Tallman, P.; Palin, K.; Rode, C.; Bloch, C.; Gillespie, B.; Marrs, C. F. Virulence Characteristics of Escherichia Coli Causing First Urinary Tract Infection Predict Risk of Second Infection. *J. Infect. Dis.* **1995**, *172* (6), 1536–1541.

(7) Foxman, B.; Barlow, R.; D'Arcy, H.; Gillespie, B.; Sobel, J. D. Urinary Tract Infection: Self-Reported Incidence and Associated Costs. *Ann. Epidemiol.* **2000**, *10* (8), 509–515.

(8) Ferry, S. A.; Holm, S. E.; Stenlund, H.; Lundholm, R.; Monsen, T. J. The Natural Course of Uncomplicated Lower Urinary Tract Infection in Women Illustrated by a Randomized Placebo Controlled Study. *Scand. J. Infect. Dis.* **2004**, *36* (4), 296–301.

(9) Fihn, S. D. Acute Uncomplicated Urinary Tract Infection in Women. *N. Engl. J. Med.* **2003**, *349* (3), 259–266.

(10) Melekos, M. D.; Naber, K. G. Complicated Urinary Tract Infections. *Int. J. Antimicrob. Agents* **2000**, *15* (4), 247–256.

(11) Raz, R.; Colodner, R.; Kunin, C. M. Who Are You—Staphylococcus Saprophyticus? *Clin. Infect. Dis.* **2005**, *40* (6), 896–898.

(12) Marrs, C. F.; Zhang, L.; Foxman, B. Escherichia Coli Mediated Urinary Tract Infections: Are There Distinct Uropathogenic E. Coli (UPEC) Pathotypes? *FEMS Microbiol. Lett.* **2005**, *252* (2), 183–190.

(13) Jones, C. H.; Pinkner, J. S.; Roth, R.; Heuser, J.; Nicholes, A. V.; Abraham, S. N.; Hultgren, S. J. FimH Adhesin of Type 1 Pili Is Assembled into a Fibrillar Tip Structure in the Enterobacteriaceae. *Proc. Natl. Acad. Sci. U. S. A.* **1995**, *92* (6), 2081–2085.

(14) Per Klemm; Mark Schembri. Type 1 Fimbriae, Curli, and Antigen 43: Adhesion, Colonization, and Biofilm Formation. **2004**, *EcoSal Plus*.

(15) Wright, K. J.; Seed, P. C.; Hultgren, S. J. Development of Intracellular Bacterial Communities of Uropathogenic Escherichia Coli Depends on Type 1 Pili. *Cell. Microbiol.* **2007**, *9* (9), 2230–2241.

(16) Wu, X. R.; Sun, T. T.; Medina, J. J. In Vitro Binding of Type 1-Fimbriated Escherichia Coli to Uroplakins Ia and Ib: Relation to Urinary Tract Infections. *Proc. Natl. Acad. Sci.* **1996**, *93* (18), 9630–9635.

(17) Ofek, I.; Hasty, D. L.; Abraham, S. N.; Sharon, N. Role of Bacterial Lectins in Urinary Tract Infections. Molecular Mechanisms for Diversification of Bacterial Surface Lectins. *Adv. Exp. Med. Biol.* **2000**, *485*, 183–192.

(18) Connell, I.; Agace, W.; Klemm, P.; Schembri, M.; Mărild, S.; Svanborg, C. Type 1 Fimbrial Expression Enhances Escherichia Coli Virulence for the Urinary Tract. *Proc. Natl. Acad. Sci. U. S. A.* **1996**, *93* (18), 9827–9832.

(19) Snyder, J. A.; Haugen, B. J.; Lockatell, C. V.; Maroncle, N.; Hagan, E. C.; Johnson, D. E.; Welch, R. A.; Mobley, H. L. T. Coordinate Expression of Fimbriae in Uropathogenic Escherichia Coli. *Infect. Immun.* **2005**, *73* (11), 7588–7596.

(20) Mulvey, M. A. Adhesion and Entry of Uropathogenic Escherichia Coli. *Cell. Microbiol.* **2002**, *4* (5), 257–271.

(21) Mobley, H. L. T.; Warren, J. W. *Urinary Tract Infections: Molecular Pathogenesis and Clinical Management*; ASM Press, 1996.

(22) Manning, S. D.; Zhang, L.; Foxman, B.; Spindler, A.; Tallman, P.; Marrs, C. F. Prevalence of Known P-Fimbrial G Alleles in Escherichia Coli and Identification of a New Adhesin Class. *Clin. Diagn. Lab. Immunol.* **2001**, *8* (3), 637–640.

(23) Strömberg, N.; Marklund, B. I.; Lund, B.; Ilver, D.; Hamers, A.; Gaastra, W.; Karlsson, K. A.; Normark, S. Host-Specificity of Uropathogenic Escherichia Coli Depends on Differences in Binding Specificity to Gal Alpha 1-4Gal-Containing Isoreceptors. *EMBO J.* **1990**, *9* (6), 2001–2010.

(24) Tseng, C.-C.; Wu, J.-J.; Liu, H.-L.; Sung, J.-M.; Huang, J.-J. Roles of Host and Bacterial Virulence Factors in the Development of Upper Urinary Tract Infection Caused by Escherichia Coli. *Am. J. Kidney Dis. Off. J. Natl. Kidney Found.* **2002**, *39* (4), 744–752.

(25) Tseng, C.-C.; Huang, J.-J.; Ko, W.-C.; Yan, J.-J.; Wu, J.-J. Decreased Predominance of PapG Class II Allele in Escherichia Coli Strains Isolated from Adults with Acute Pyelonephritis and Urinary Tract Abnormalities. *J. Urol.* **2001**, *166* (5), 1643–1646.

(26) Roberts, J. A.; Marklund, B. I.; Ilver, D.; Haslam, D.; Kaack, M. B.; Baskin, G.; Louis, M.; Möllby, R.; Winberg, J.; Normark, S. The Gal(alpha 1-4)Gal-Specific Tip Adhesin of Escherichia Coli P-Fimbriae Is Needed for Pyelonephritis to Occur in the Normal Urinary Tract. *Proc. Natl. Acad. Sci. U. S. A.* **1994**, *91* (25), 11889–11893.

(27) Roberts, J. A.; Kaack, M. B.; Baskin, G.; Chapman, M. R.; Hunstad, D. A.; Pinkner, J. S.; Hultgren, S. J. Antibody Responses and Protection from Pyelonephritis Following Vaccination with Purified Escherichia Coli PapDG Protein. *J. Urol.* **2004**, *171* (4), 1682–1685.

(28) Bergsten, G.; Samuelsson, M.; Wullt, B.; Leijonhufvud, I.; Fischer, H.; Svanborg, C. PapG-Dependent Adherence Breaks Mucosal Inertia and Triggers the Innate Host Response. *J. Infect. Dis.* **2004**, *189* (9), 1734–1742.

(29) Wullt, B.; Bergsten, G.; Connell, H.; Röllano, P.; Gebratsedik, N.; Hang, L.; Svanborg, C. P-Fimbriae Trigger Mucosal Responses to Escherichia Coli in the Human Urinary Tract. *Cell. Microbiol.* **2001**, *3* (4), 255–264.

(30) Wullt, B.; Bergsten, G.; Samuelsson, M.; Svanborg, C. The Role of P Fimbriae for Escherichia Coli Establishment and Mucosal Inflammation in the Human Urinary Tract. *Int. J. Antimicrob. Agents* **2002**, *19* (6), 522–538.

(31) Tamm, I.; Horsfall, F. L. Characterization and Separation of an Inhibitor of Viral Hemagglutination Present in Urine. *Exp. Biol. Med.* **1950**, *74* (1), 108–114.

(32) Serafini-Cessi, F.; Malagolini, N.; Cavallone, D. Tamm-Horsfall Glycoprotein: Biology and Clinical Relevance. *Am. J. Kidney Dis.* **2003**, *42* (4), 658–676.

(33) Pak, J.; Pu, Y.; Zhang, Z.-T.; Hasty, D. L.; Wu, X.-R. Tamm-Horsfall Protein Binds to Type 1 Fimbriated Escherichia Coli and Prevents E. Coli from

Binding to Uroplakin Ia and Ib Receptors. *J. Biol. Chem.* **2001**, *276* (13), 9924–9930.

(34) John R. Hoyer; Marcel W. Seiler. Pathophysiology of Tamm-Horsfall Protein. *Kidney Int* **1979**, *16* (3), 279–289.

(35) Satish Kumar; Andrew Muchmore. Tamm-Horsfall Protein—uromodulin (1950-1990). *Kidney Int* **1990**, *37* (6), 1395–1401.

(36) Bates, J. M.; Raffi, H. M.; Prasadan, K.; Mascarenhas, R.; Laszik, Z.; Maeda, N.; Hultgren, S. J.; Kumar, S. Tamm-Horsfall Protein Knockout Mice Are More Prone to Urinary Tract Infection Rapid Communication. *Kidney Int.* **2004**, *65* (3), 791–797.

(37) Stahlhut, S. G.; Struve, C.; Krogfelt, K. A.; Reisner, A. Biofilm Formation of Klebsiella Pneumoniae on Urethral Catheters Requires Either Type 1 or Type 3 Fimbriae. *Fems Immunol. Med. Microbiol.* **2012**, *65* (2), 350–359.

(38) Ong, C.-L. Y.; Ulett, G. C.; Mabbett, A. N.; Beatson, S. A.; Webb, R. I.; Monaghan, W.; Nimmo, G. R.; Looke, D. F.; McEwan, A. G.; Schembri, M. A. Identification of Type 3 Fimbriae in Uropathogenic Escherichia Coli Reveals a Role in Biofilm Formation. *J. Bacteriol.* **2008**, *190* (3), 1054–1063.

(39) Ulett, G. C.; Valle, J.; Beloin, C.; Sherlock, O.; Ghigo, J.-M.; Schembri, M. A. Functional Analysis of Antigen 43 in Uropathogenic Escherichia Coli Reveals a Role in Long-Term Persistence in the Urinary Tract. *Infect. Immun.* **2007**, *75* (7), 3233–3244.

(40) Old, D. C. Inhibition of the Interaction Between Fimbrial Haemagglutinins and Erythrocytes by D-Mannose and Other Carbohydrates. *J. Gen. Microbiol.* **1972**, *71* (1), 149–157.

(41) Ofek, I.; Mirelman, D.; Sharon, N. Adherence of Escherichia Coli to Human Mucosal Cells Mediated by Mannose Receptors. *Nature* **1977**, *265* (5595), 623–625.

(42) Firon, N.; Ofek, I.; Sharon, N. Interaction of Mannose-Containing Oligosaccharides with the Fimbrial Lectin of Escherichia Coli. *Biochem. Biophys. Res. Commun.* **1982**, *105* (4), 1426–1432.

(43) Neeser, J. R.; Koellreutter, B.; Wuersch, P. Oligomannoside-Type Glycopeptides Inhibiting Adhesion of Escherichia Coli Strains Mediated by Type 1 Pili: Preparation of Potent Inhibitors from Plant Glycoproteins. *Infect. Immun.* **1986**, *52* (2), 428–436.

(44) Eden, C. S.; Hansson, H. A. Escherichia Coli Pili as Possible Mediators of Attachment to Human Urinary Tract Epithelial Cells. *Infect. Immun.* **1978**, *21* (1), 229–237.

(45) Hagberg, L.; Jodal, U.; Korhonen, T. K.; Lidin-Janson, G.; Lindberg, U.; Edén, C. S. Adhesion, Hemagglutination, and Virulence of Escherichia Coli Causing Urinary Tract Infections. *Infect. Immun.* **1981**, *31* (2), 564–570.

(46) Freedman, L. R. Experimental Pyelonephritis. 13. On the Ability of Water Diuresis to Induce Susceptibility to E. Coli Bacteriuria in the Normal Rat. *Yale J. Biol. Med.* **1967**, *39* (4), 255–266.

(47) Aronson, M.; Medalia, O.; Schori, L.; Mirelman, D.; Sharon, N.; Ofek, I. Prevention of Colonization of the Urinary Tract of Mice with Escherichia Coli by Blocking of Bacterial Adherence with Methyl α-D-Mannopyranoside. *J. Infect. Dis.* **1979**, *139* (3), 329–332.

(48) Hagberg, L.; Engberg, I.; Freter, R.; Lam, J.; Olling, S.; Svanborg Eden, C. Ascending, Unobstructed Urinary Tract Infection in Mice Caused by Pyelonephritogenic Escherichia Coli of Human Origin. *Infect. Immun.* **1983**, *40* (1), 273–283.

(49) Iwahi, T.; Abe, Y.; Nakao, M.; Imada, A.; Tsuchiya, K. Role of Type 1 Fimbriae in the Pathogenesis of Ascending Urinary Tract Infection Induced by Escherichia Coli in Mice. *Infect. Immun.* **1983**, *39* (3), 1307–1315.

(50) Fujita, K.; Yamamoto, T.; Yokota, T.; Kitagawa, R. In Vitro Adherence of Type 1-Fimbriated Uropathogenic Escherichia Coli to Human Ureteral Mucosa. *Infect. Immun.* **1989**, *57* (8), 2574–2579.

(51) Hahn, E.; Wild, P.; Hermanns, U.; Sebbel, P.; Glockshuber, R.; Häner, M.; Taschner, N.; Burkhard, P.; Aebi, U.; Müller, S. A. Exploring the 3D Molecular Architecture of Escherichia Coli Type 1 Pili. *J. Mol. Biol.* **2002**, *323* (5), 845–857.

(52) Klemm, P.; Christiansen, G. Three Fim Genes Required for the Regulation of Length and Mediation of Adhesion of Escherichia Coli Type 1 Fimbriae. *Mol. Gen. Genet. MGG* **1987**, *208* (3), 439–445.

(53) Krogfelt, K. A.; Bergmans, H.; Klemm, P. Direct Evidence That the FimH Protein Is the Mannose-Specific Adhesin of Escherichia Coli Type 1 Fimbriae. *Infect. Immun.* **1990**, *58* (6), 1995–1998.

(54) Martinez, J. J.; Mulvey, M. A.; Schilling, J. D.; Pinkner, J. S.; Hultgren, S. J. Type 1 Pilus-Mediated Bacterial Invasion of Bladder Epithelial Cells. *EMBO J.* **2000**, *19* (12), 2803–2812.

(55) Struve, C.; Bojer, M.; Krogfelt, K. A. Characterization of Klebsiella Pneumoniae Type 1 Fimbriae by Detection of Phase Variation during Colonization and Infection and Impact on Virulence. *Infect. Immun.* **2008**, *76* (9), 4055–4065.

(56) Struve, C.; Krogfelt, K. A. In Vivo Detection of Escherichia Coli Type 1 Fimbrial Expression and Phase Variation during Experimental Urinary Tract Infection. *Microbiol. Read. Engl.* **1999**, *145 (Pt 10)*, 2683–2690.

(57) Schwan, W. R.; Lee, J. L.; Lenard, F. A.; Matthews, B. T.; Beck, M. T. Osmolarity and pH Growth Conditions Regulate Fim Gene Transcription and Type 1 Pilus Expression in Uropathogenic Escherichia Coli. *Infect. Immun.* **2002**, *70* (3), 1391–1402.

(58) Müller, C. M.; Åberg, A.; Straseviçiene, J.; Emődy, L.; Uhlin, B. E.; Balsalobre, C. Type 1 Fimbriae, a Colonization Factor of Uropathogenic Escherichia Coli, Are Controlled by the Metabolic Sensor CRP-cAMP. *PLoS Pathog* **2009**, *5* (2), e1000303.

(59) Gunther, N. W., 4th; Snyder, J. A.; Lockatell, V.; Blomfield, I.; Johnson, D. E.; Mobley, H. L. T. Assessment of Virulence of Uropathogenic Escherichia Coli Type 1 Fimbrial Mutants in Which the Invertible Element Is Phase-Locked on or off. *Infect. Immun.* **2002**, *70* (7), 3344–3354.

(60) Wu, X.-R.; Kong, X.-P.; Pellicer, A.; Kreibich, G.; Sun, T.-T. Uroplakins in Urothelial Biology, Function, and Disease. *Kidney Int.* **2009**, *75* (11), 1153–1165.

(61) Duncan, M. J.; Li, G.; Shin, J.-S.; Carson, J. L.; Abraham, S. N. Bacterial Penetration of Bladder Epithelium through Lipid Rafts. *J. Biol. Chem.* **2004**, *279* (18), 18944–18951.

(62) Mulvey, M. A.; Schilling, J. D.; Martinez, J. J.; Hultgren, S. J. Bad Bugs and Beleaguered Bladders: Interplay between Uropathogenic Escherichia Coli and Innate Host Defenses. *Proc. Natl. Acad. Sci.* **2000**, *97* (16), 8829–8835.

(63) Chen, Y.; Guo, X.; Deng, F.-M.; Liang, F.-X.; Sun, W.; Ren, M.; Izumi, T.; Sabatini, D. D.; Sun, T.-T.; Kreibich, G. Rab27b Is Associated with Fusiform

Vesicles and May Be Involved in Targeting Uroplakins to Urothelial Apical Membranes. *Proc. Natl. Acad. Sci.* **2003**, *100* (24), 14012–14017.

(64) Bishop, B. L.; Duncan, M. J.; Song, J.; Li, G.; Zaas, D.; Abraham, S. N. Cyclic AMP–regulated Exocytosis of Escherichia Coli from Infected Bladder Epithelial Cells. *Nat. Med.* **2007**, *13* (5), 625–630.

(65) Jorgensen, I.; Seed, P. C. How to Make It in the Urinary Tract: A Tutorial by Escherichia Coli. *PLoS Pathog* **2012**, *8* (10), e1002907.

(66) Song, J.; Abraham, S. N. TLR-Mediated Immune Responses in the Urinary Tract. *Curr. Opin. Microbiol.* **2008**, *11* (1), 66–73.

(67) Thumbikat, P.; Berry, R. E.; Zhou, G.; Billips, B. K.; Yaggie, R. E.; Zaichuk, T.; Sun, T.-T.; Schaeffer, A. J.; Klumpp, D. J. Bacteria-Induced Uroplakin Signaling Mediates Bladder Response to Infection. *PLoS Pathog* **2009**, *5* (5), e1000415.

(68) Eto, D. S.; Jones, T. A.; Sundsbak, J. L.; Mulvey, M. A. Integrin-Mediated Host Cell Invasion by Type 1–Piliated Uropathogenic Escherichia Coli. *PLoS Pathog* **2007**, *3* (7), e100.

(69) Martinez, J. J.; Hultgren, S. J. Requirement of Rho-Family GTPases in the Invasion of Type 1-Piliated Uropathogenic Escherichia Coli. *Cell. Microbiol.* **2002**, *4* (1), 19–28.

(70) Anderson, G. G.; Dodson, K. W.; Hooton, T. M.; Hultgren, S. J. Intracellular Bacterial Communities of Uropathogenic Escherichia Coli in Urinary Tract Pathogenesis. *Trends Microbiol.* **2004**, *12* (9), 424–430.

(71) Rosen, D. A.; Hooton, T. M.; Stamm, W. E.; Humphrey, P. A.; Hultgren, S. J. Detection of Intracellular Bacterial Communities in Human Urinary Tract Infection. *PLoS Med* **2007**, *4* (12), e329.

(72) Anderson, G. G.; Palermo, J. J.; Schilling, J. D.; Roth, R.; Heuser, J.; Hultgren, S. J. Intracellular Bacterial Biofilm-Like Pods in Urinary Tract Infections. *Science* **2003**, *301* (5629), 105–107.

(73) Bäckhed, F.; Söderhäll, M.; Ekman, P.; Normark, S.; Richter-Dahlfors, A. Induction of Innate Immune Responses by Escherichia Coli and Purified Lipopolysaccharide Correlate with Organ- and Cell-Specific Expression of Toll-like Receptors within the Human Urinary Tract. *Cell. Microbiol.* **2001**, *3* (3), 153–158.

(74) Song, J.; Bishop, B. L.; Li, G.; Duncan, M. J.; Abraham, S. N. TLR4 Initiated and cAMP Mediated Abrogation of Bacterial Invasion of the Bladder. *Cell Host Microbe* **2007**, *1* (4), 287–298.

(75) Poltorak, A.; He, X.; Smirnova, I.; Liu, M.-Y.; Huffel, C. V.; Du, X.; Birdwell, D.; Alejos, E.; Silva, M.; Galanos, C.; Freudenberg, M.; Ricciardi-Castagnoli, P.; Layton, B.; Beutler, B. Defective LPS Signaling in C3H/HeJ and C57BL/10ScCr Mice: Mutations in Tlr4 Gene. *Science* **1998**, *282* (5396), 2085–2088.

(76) Hedges, S.; Anderson, P.; Lidin-Janson, G.; Man, P. de; Svanborg, C. Interleukin-6 Response to Deliberate Colonization of the Human Urinary Tract with Gram-Negative Bacteria. *Infect. Immun.* **1991**, *59* (1), 421–427.

(77) Hunstad, D. A.; Justice, S. S. Intracellular Lifestyles and Immune Evasion Strategies of Uropathogenic Escherichia Coli. *Annu. Rev. Microbiol.* **2010**, *64*, 203–221.

(78) Samuelsson, P.; Hang, L.; Wullt, B.; Irjala, H.; Svanborg, C. Toll-Like Receptor 4 Expression and Cytokine Responses in the Human Urinary Tract Mucosa. *Infect. Immun.* **2004**, *72* (6), 3179–3186.

(79) Ashkar, A. A.; Mossman, K. L.; Coombes, B. K.; Gyles, C. L.; Mackenzie, R. FimH Adhesin of Type 1 Fimbriae Is a Potent Inducer of Innate Antimicrobial Responses Which Requires TLR4 and Type 1 Interferon Signalling. *PLoS Pathog* **2008**, *4* (12), e1000233.

(80) Mills, M.; Meysick, K. C.; O'Brien, A. D. Cytotoxic Necrotizing Factor Type 1 of Uropathogenic Escherichia Coli Kills Cultured Human Uroepithelial 5637 Cells by an Apoptotic Mechanism. *Infect. Immun.* **2000**, *68* (10), 5869–5880.

(81) Justice, S. S.; Hung, C.; Theriot, J. A.; Fletcher, D. A.; Anderson, G. G.; Footer, M. J.; Hultgren, S. J. Differentiation and Developmental Pathways of Uropathogenic Escherichia Coli in Urinary Tract Pathogenesis. *Proc. Natl. Acad. Sci. U. S. A.* **2004**, *101* (5), 1333–1338.

(82) Mulvey, M. A.; Schilling, J. D.; Hultgren, S. J. Establishment of a Persistent Escherichia Coli Reservoir during the Acute Phase of a Bladder Infection. *Infect. Immun.* **2001**, *69* (7), 4572–4579.

(83) Schwartz, D. J.; Chen, S. L.; Hultgren, S. J.; Seed, P. C. Population Dynamics and Niche Distribution of Uropathogenic Escherichia Coli during Acute and Chronic Urinary Tract Infection. *Infect. Immun.* **2011**, *79* (10), 4250–4259.

(84) Hannan, T. J.; Totsika, M.; Mansfield, K. J.; Moore, K. H.; Schembri, M. A.; Hultgren, S. J. Host–pathogen Checkpoints and Population Bottlenecks in Persistent and Intracellular Uropathogenic Escherichia Coli Bladder Infection. *FEMS Microbiol. Rev.* **2012**, *36* (3), 616–648.

(85) Andersen, T. E.; Khandige, S.; Madelung, M.; Brewer, J.; Kolmos, H. J.; Møller-Jensen, J. Escherichia Coli Uropathogenesis In Vitro: Invasion, Cellular Escape, and Secondary Infection Analyzed in a Human Bladder Cell Infection Model. *Infect. Immun.* **2012**, *80* (5), 1858–1867.

(86) Chen, S. L.; Hung, C. S.; Pinkner, J. S.; Walker, J. N.; Cusumano, C. K.; Li, Z.; Bouckaert, J.; Gordon, J. I.; Hultgren, S. J. Positive Selection Identifies an in Vivo Role for FimH during Urinary Tract Infection in Addition to Mannose Binding. *Proc. Natl. Acad. Sci.* **2009**, *106* (52), 22439–22444.

(87) Chen, S. L.; Hung, C.-S.; Xu, J.; Reigstad, C. S.; Magrini, V.; Sabo, A.; Blasiar, D.; Bieri, T.; Meyer, R. R.; Ozersky, P.; Armstrong, J. R.; Fulton, R. S.; Latreille, J. P.; Spieth, J.; Hooton, T. M.; Mardis, E. R.; Hultgren, S. J.; Gordon, J. I. Identification of Genes Subject to Positive Selection in Uropathogenic Strains of Escherichia Coli: A Comparative Genomics Approach. *Proc. Natl. Acad. Sci.* **2006**, *103* (15), 5977–5982.

(88) Garofalo, C. K.; Hooton, T. M.; Martin, S. M.; Stamm, W. E.; Palermo, J. J.; Gordon, J. I.; Hultgren, S. J. Escherichia Coli from Urine of Female Patients with Urinary Tract Infections Is Competent for Intracellular Bacterial Community Formation. *Infect. Immun.* **2007**, *75* (1), 52–60.

(89) Blango, M. G.; Mulvey, M. A. Persistence of Uropathogenic Escherichia Coli in the Face of Multiple Antibiotics. *Antimicrob. Agents Chemother.* **2010**, *54* (5), 1855–1863.

(90) Eto, D. S.; Sundsbak, J. L.; Mulvey, M. A. Actin-Gated Intracellular Growth and Resurgence of Uropathogenic Escherichia Coli. *Cell. Microbiol.* **2006**, *8* (4), 704–717.

(91) Romih, R.; Veranic, P.; Jezernik, K. Actin Filaments during Terminal Differentiation of Urothelial Cells in the Rat Urinary Bladder. *Histochem. Cell Biol.* **1999**, *112* (5), 375–380.

(92) Mysorekar, I. U.; Hultgren, S. J. Mechanisms of Uropathogenic Escherichia Coli Persistence and Eradication from the Urinary Tract. *Proc. Natl. Acad. Sci.* **2006**, *103* (38), 14170–14175.

(93) Taur, Y.; Smith, M. A. Adherence to the Infectious Diseases Society of America Guidelines in the Treatment of Uncomplicated Urinary Tract Infection. *Clin. Infect. Dis. Off. Publ. Infect. Dis. Soc. Am.* **2007**, *44* (6), 769–774.

(94) Savaria, F.; Zbinden, R.; Wüst, J.; Burnens, A.; Ledergerber, B.; Weber, R.; Kovari, H. Antibiotikaresistenzen von E.coli in Urinproben: Prävalenzdaten Dreier Laboratorien Im Raum Zürich von 1985 Bis 2010. *Praxis* **2012**, *101* (9), 573–579.

(95) National Guideline Clearinghouse | Urinary tract infection. http://www.guideline.gov/content.aspx?id=34419 (accessed Oct 21, 2013).

(96) Grabe, M.; Bjerklung-Johansen, T. E.; Botto, H.; Cek, M.; Naber, K. G.; Pickard, R. S.; Tenke, P.; Wagenlehner, F.; Wullt, B. Guidelines on Urological Infections. No. European Association of Urology 2013.

(97) Nicolle, L.; Anderson, P. A. M.; Conly, J.; Mainprize, T. C.; Meuser, J.; Nickel, J. C.; Senikas, V. M.; Zhanel, G. G. Uncomplicated Urinary Tract Infection in Women. *Can. Fam. Physician* **2006**, *52* (5), 612–618.

(98) Milo, G.; Katchman, E.; Paul, M.; Christiaens, T.; Baerheim, A.; Leibovici, L. Duration of Antibacterial Treatment for Uncomplicated Urinary Tract Infection in Women. In *Cochrane Database of Systematic Reviews*; John Wiley & Sons, Ltd, 1996.

(99) Butler, C. C.; Dunstan, F.; Heginbothom, M.; Mason, B.; Roberts, Z.; Hillier, S.; Howe, R.; Palmer, S.; Howard, A. Containing Antibiotic Resistance: Decreased Antibiotic-Resistant Coliform Urinary Tract Infections with Reduction in Antibiotic Prescribing by General Practices. *Br. J. Gen. Pract.* **2007**, *57* (543), 785–792.

(100) Ceran, N.; Mert, D.; Kocdogan, F. Y.; Erdem, I.; Adalati, R.; Ozyurek, S.; Goktas, P. A Randomized Comparative Study of Single-Dose Fosfomycin and 5-Day Ciprofloxacin in Female Patients with Uncomplicated Lower Urinary Tract Infections. *J. Infect. Chemother. Off. J. Jpn. Soc. Chemother.* **2010**, *16* (6), 424–430.

(101) Falagas, M. E.; Vouloumanou, E. K.; Togias, A. G.; Karadima, M.; Kapaskelis, A. M.; Rafailidis, P. I.; Athanasiou, S. Fosfomycin versus Other Antibiotics for the Treatment of Cystitis: A Meta-Analysis of Randomized Controlled Trials. *J. Antimicrob. Chemother.* **2010**, *65* (9), 1862–1877.

(102) PharmaWiki GmbH. PharmaWiki http://www.pharmawiki.ch/wiki/ (accessed Nov 4, 2013, Aug 25, 2015).

(103) Anderson, R.; Groundwater, P.; Todd, A.; Worsley, A. *Antibacterial Agents: Chemistry, Mode of Action, Mechanisms of Resistance and Clinical Applications*; John Wiley & Sons, 2012.

(104) Tu, Y.; McCalla, D. R. Effect of Activated Nitrofurans on DNA. *Biochim. Biophys. Acta BBA - Nucleic Acids Protein Synth.* **1975**, *402* (2), 142–149.

(105) Wang, Y.; Gray, J. P.; Mishin, V.; Heck, D. E.; Laskin, D. L.; Laskin, J. D. Role of Cytochrome P450 Reductase in Nitrofurantoin-Induced Redox Cycling and Cytotoxicity. *Free Radic. Biol. Med.* **2008**, *44* (6), 1169–1179.

(106) Backer, D. D.; Christiaens, T.; Heytens, S.; Sutter, A. D.; Stobberingh, E. E.; Verschraegen, G. Evolution of Bacterial Susceptibility Pattern of Escherichia Coli in Uncomplicated Urinary Tract Infections in a Country with High Antibiotic Consumption: A Comparison of Two Surveys with a 10 Year Interval. *J. Antimicrob. Chemother.* **2008**, *62* (2), 364–368.

(107) Rodríguez-Baño, J.; Navarro, M. D.; Romero, L.; Martínez-Martínez, L.; Muniain, M. A.; Perea, E. J.; Pérez-Cano, R.; Pascual, A. Epidemiology and Clinical Features of Infections Caused by Extended-Spectrum Beta-Lactamase-Producing Escherichia Coli in Nonhospitalized Patients. *J. Clin. Microbiol.* **2004**, *42* (3), 1089–1094.

(108) Tarr P., Baumann K, Wallnöfer A, Zimmerli F, Maritz D, Burri U, Egger M, Clerc O, Bernasconi E, Kovari H, Senn L. Akute Harnwegsinfektionen, Teil1: HWI in Der Praxis. *SMF-Schweiz. Med.-Forum* **2013**, No. 13(24), 467–471.

(109) Clearinghouse, T. N. N. K. and U. D. I. National Kidney and Urologic Diseases Information Clearinghouse Homepage http://kidney.niddk.nih.gov/ (accessed Aug 19, 2013).

(110) Narchi, H.; Al-Hamdani, M. Uropathogen Resistance to Antibiotic Prophylaxis in Urinary Tract Infections. *Microb. Drug Resist.* **2010**, *16* (2), 151–154.

(111) Goneau, L. W.; Hannan, T. J.; MacPhee, R. A.; Schwartz, D. J.; Macklaim, J. M.; Gloor, G. B.; Razvi, H.; Reid, G.; Hultgren, S. J.; Burton, J. P. Subinhibitory Antibiotic Therapy Alters Recurrent Urinary Tract Infection Pathogenesis through Modulation of Bacterial Virulence and Host Immunity. *mBio* **2015**, *6* (2), e00356–15.

(112) Jepson, R. G.; Williams, G.; Craig, J. C. Cranberries for Preventing Urinary Tract Infections. In *Cochrane Database of Systematic Reviews*; John Wiley & Sons, Ltd, 2013.

(113) Wang C; Fang C; Chen N; Liu, S; Yu, P; Wu, T; Chen, W; Lee, C. Cranberry-Containing Products for Prevention of Urinary Tract Infections in Susceptible Populations: A Systematic Review and Meta-Analysis of Randomized Controlled Trials. *Arch. Intern. Med.* **2012**, *172* (13), 988–996.

(114) Costerton, J. W.; Lewandowski, Z.; Caldwell, D. E.; Korber, D. R.; Lappin-Scott, H. M. Microbial Biofilms. *Annu. Rev. Microbiol.* **1995**, *49* (1), 711–745.

(115) Reisner, A.; Haagensen, J. A. J.; Schembri, M. A.; Zechner, E. L.; Molin, S. Development and Maturation of Escherichia Coli K-12 Biofilms. *Mol. Microbiol.* **2003**, *48* (4), 933–946.

(116) Flemming, H.-C.; Neu, T. R.; Wozniak, D. J. The EPS Matrix: The "House of Biofilm Cells." *J. Bacteriol.* **2007**, *189* (22), 7945–7947.

(117) Walters, M. C.; Roe, F.; Bugnicourt, A.; Franklin, M. J.; Stewart, P. S. Contributions of Antibiotic Penetration, Oxygen Limitation, and Low Metabolic Activity to Tolerance of Pseudomonas Aeruginosa Biofilms to Ciprofloxacin and Tobramycin. *Antimicrob. Agents Chemother.* **2003**, *47* (1), 317–323.

(118) Fux, C. A.; Costerton, J. W.; Stewart, P. S.; Stoodley, P. Survival Strategies of Infectious Biofilms. *Trends Microbiol.* **2005**, *13* (1), 34–40.

(119) Bjarnsholt, T.; Jensen, P. Ø.; Burmølle, M.; Hentzer, M.; Haagensen, J. A. J.; Hougen, H. P.; Calum, H.; Madsen, K. G.; Moser, C.; Molin, S.; Høiby, N.; Givskov, M. Pseudomonas Aeruginosa Tolerance to Tobramycin, Hydrogen Peroxide and Polymorphonuclear Leukocytes Is Quorum-Sensing Dependent. *Microbiology* **2005**, *151* (2), 373–383.

(120) Fexby, S.; Bjarnsholt, T.; Jensen, P. Ø.; Roos, V.; Høiby, N.; Givskov, M.; Klemm, P. Biological Trojan Horse: Antigen 43 Provides Specific Bacterial Uptake and Survival in Human Neutrophils. *Infect. Immun.* **2007**, *75* (1), 30–34.

(121) Bjarnsholt, T.; Kirketerp-Møller, K.; Jensen, P. Ø.; Madsen, K. G.; Phipps, R.; Krogfelt, K.; Høiby, N.; Givskov, M. Why Chronic Wounds Will Not Heal: A Novel Hypothesis. *Wound Repair Regen. Off. Publ. Wound Heal. Soc. Eur. Tissue Repair Soc.* **2008**, *16* (1), 2–10.

(122) Bjarnsholt, T.; Jensen, P. Ø.; Fiandaca, M. J.; Pedersen, J.; Hansen, C. R.; Andersen, C. B.; Pressler, T.; Givskov, M.; Høiby, N. Pseudomonas Aeruginosa Biofilms in the Respiratory Tract of Cystic Fibrosis Patients. *Pediatr. Pulmonol.* **2009**, *44* (6), 547–558.

(123) Kim, J.; Hahn, J.-S.; Franklin, M. J.; Stewart, P. S.; Yoon, J. Tolerance of Dormant and Active Cells in Pseudomonas Aeruginosa PA01 Biofilm to Antimicrobial Agents. *J. Antimicrob. Chemother.* **2009**, *63* (1), 129–135.

(124) Bjarnsholt, T.; Ciofu, O.; Molin, S.; Givskov, M.; Høiby, N. Applying Insights from Biofilm Biology to Drug Development — Can a New Approach Be Developed? *Nat. Rev. Drug Discov.* **2013**, *12* (10), 791–808.

(125) García-Castillo, M.; Morosini, M.-I.; Gálvez, M.; Baquero, F.; del Campo, R.; Meseguer, M.-A. Differences in Biofilm Development and Antibiotic Susceptibility among Clinical Ureaplasma Urealyticum and Ureaplasma Parvum Isolates. *J. Antimicrob. Chemother.* **2008**, *62* (5), 1027–1030.

(126) Molina, A.; Campo, R. D.; Máiz, L.; Morosini, M.-I.; Lamas, A.; Baquero, F.; Cantón, R. High Prevalence in Cystic Fibrosis Patients of Multiresistant Hospital-Acquired Methicillin-Resistant Staphylococcus Aureus ST228-SCCmecI Capable of Biofilm Formation. *J. Antimicrob. Chemother.* **2008**, *62* (5), 961–967.

(127) Cookson, A. L.; Cooley, W. A.; Woodward, M. J. The Role of Type 1 and Curli Fimbriae of Shiga Toxin-Producing Escherichia Coli in Adherence to Abiotic Surfaces. *Int. J. Med. Microbiol.* **2002**, *292* (3–4), 195–205.

(128) Harber, M. J.; Mackenzie, R.; Asscher, A. W. A Rapid Bioluminescence Method for Quantifying Bacterial Adhesion to Polystyrene. *J. Gen. Microbiol.* **1983**, *129* (3), 621–632.

(129) Pratt, L. A.; Kolter, R. Genetic Analysis of Escherichia Coli Biofilm Formation: Roles of Flagella, Motility, Chemotaxis and Type I Pili. *Mol. Microbiol.* **1998**, *30* (2), 285–293.

(130) Hasman, H.; Schembri, M. A.; Klemm, P. Antigen 43 and Type 1 Fimbriae Determine Colony Morphology of Escherichia Coli K-12. *J. Bacteriol.* **2000**, *182* (4), 1089–1095.

(131) De Oliveira-Garcia, D.; Dall'Agnol, M.; Rosales, M.; Azzuz, A. C. G. S.; Alcántara, N.; Martinez, M. B.; Girón, J. A. Fimbriae and Adherence of

Stenotrophomonas Maltophilia to Epithelial Cells and to Abiotic Surfaces. *Cell. Microbiol.* **2003**, *5* (9), 625–636.

(132) Blumer, C.; Kleefeld, A.; Lehnen, D.; Heintz, M.; Dobrindt, U.; Nagy, G.; Michaelis, K.; Emödy, L.; Polen, T.; Rachel, R.; Wendisch, V. F.; Unden, G. Regulation of Type 1 Fimbriae Synthesis and Biofilm Formation by the Transcriptional Regulator LrhA of Escherichia Coli. *Microbiology* **2005**, *151* (10), 3287–3298.

(133) Hung, C.; Zhou, Y.; Pinkner, J. S.; Dodson, K. W.; Crowley, J. R.; Heuser, J.; Chapman, M. R.; Hadjifrangiskou, M.; Henderson, J. P.; Hultgren, S. J. Escherichia Coli Biofilms Have an Organized and Complex Extracellular Matrix Structure. *mBio* **2013**, *4* (5), e00645–13.

(134) Schembri, M.; Ussery, D.; Workman, C.; Hasman, H.; Klemm, P. DNA Microarray Analysis of Fim Mutations in Escherichia Coli. *Mol. Genet. Genomics* **2002**, *267* (6), 721–729.

(135) Schembri, M. A.; Kjærgaard, K.; Klemm, P. Global Gene Expression in Escherichia Coli Biofilms. *Mol. Microbiol.* **2003**, *48* (1), 253–267.

(136) Hadjifrangiskou, M.; Gu, A. P.; Pinkner, J. S.; Kostakioti, M.; Zhang, E. W.; Greene, S. E.; Hultgren, S. J. Transposon Mutagenesis Identifies Uropathogenic Escherichia Coli Biofilm Factors. *J. Bacteriol.* **2012**, *194* (22), 6195–6205.

(137) Guiton, P. S.; Cusumano, C. K.; Kline, K. A.; Dodson, K. W.; Han, Z.; Janetka, J. W.; Henderson, J. P.; Caparon, M. G.; Hultgren, S. J. Combinatorial Small-Molecule Therapy Prevents Uropathogenic Escherichia Coli Catheter-Associated Urinary Tract Infections in Mice. *Antimicrob. Agents Chemother.* **2012**, *56* (9), 4738–4745.

(138) Reisner, A.; Maierl, M.; Jörger, M.; Krause, R.; Berger, D.; Haid, A.; Tesic, D.; Zechner, E. L. Type 1 Fimbriae Contribute to Catheter-Associated Urinary Tract Infections Caused by Escherichia Coli. *J. Bacteriol.* **2014**, *196* (5), 931–939.

(139) Rodrigues, D. F.; Elimelech, M. Role of Type 1 Fimbriae and Mannose in the Development of Escherichia Coli K12 Biofilm: From Initial Cell Adhesion to Biofilm Formation. *Biofouling* **2009**, *25* (5), 401–411.

(140) Olsén, A.; Jonsson, A.; Normark, S. Fibronectin Binding Mediated by a Novel Class of Surface Organelles on Escherichia Coll. *Nature* **1989**, *338* (6217), 652–655.

(141) Hatt, J. K.; Rather, P. N. Role of Bacterial Biofilms in Urinary Tract Infections. In *Bacterial Biofilms*; Romeo, T., Ed.; Current Topics in Microbiology and Immunology; Springer Berlin Heidelberg, 2008; pp 163–192.

(142) Prigent-Combaret, C.; Prensier, G.; Le Thi, T. T.; Vidal, O.; Lejeune, P.; Dorel, C. Developmental Pathway for Biofilm Formation in Curli-Producing Escherichia Coli Strains: Role of Flagella, Curli and Colanic Acid. *Environ. Microbiol.* **2000**, *2* (4), 450–464.

(143) Gualdi, L.; Tagliabue, L.; Landini, P. Biofilm Formation-Gene Expression Relay System in Escherichia Coli: Modulation of σS-Dependent Gene Expression by the CsgD Regulatory Protein via σS Protein Stabilization. *J. Bacteriol.* **2007**, *189* (22), 8034–8043.

(144) Chapman, M. R.; Robinson, L. S.; Pinkner, J. S.; Roth, R.; Heuser, J.; Hammar, M.; Normark, S.; Hultgren, S. J. Role of Escherichia Coli Curli Operons in Directing Amyloid Fiber Formation. *Science* **2002**, *295* (5556), 851–855.

(145) Cegelski, L.; Pinkner, J. S.; Hammer, N. D.; Cusumano, C. K.; Hung, C. S.; Chorell, E.; Åberg, V.; Walker, J. N.; Seed, P. C.; Almqvist, F.; Chapman, M. R.; Hultgren, S. J. Small-Molecule Inhibitors Target Escherichia Coli Amyloid Biogenesis and Biofilm Formation. *Nat. Chem. Biol.* **2009**, *5* (12), 913–919.

(146) Klemm, P.; Hjerrild, L.; Gjermansen, M.; Schembri, M. A. Structure-Function Analysis of the Self-Recognizing Antigen 43 Autotransporter Protein from Escherichia Coli. *Mol. Microbiol.* **2004**, *51* (1), 283–296.

(147) Kjærgaard, K.; Schembri, M. A.; Hasman, H.; Klemm, P. Antigen 43 from Escherichia Coli Induces Inter- and Intraspecies Cell Aggregation and Changes in Colony Morphology of Pseudomonas Fluorescens. *J. Bacteriol.* **2000**, *182* (17), 4789–4796.

(148) Danese, P. N.; Pratt, L. A.; Dove, S. L.; Kolter, R. The Outer Membrane Protein, Antigen 43, Mediates Cell-to-Cell Interactions within Escherichia Coli Biofilms. *Mol. Microbiol.* **2000**, *37* (2), 424–432.

(149) Hasman, H.; Chakraborty, T.; Klemm, P. Antigen-43-Mediated Autoaggregation ofEscherichia Coli Is Blocked by Fimbriation. *J. Bacteriol.* **1999**, *181* (16), 4834–4841.

(150) Kjærgaard, K.; Schembri, M. A.; Ramos, C.; Molin, S.; Klemm, P. Antigen 43 Facilitates Formation of Multispecies Biofilms. *Environ. Microbiol.* **2000**, *2* (6), 695–702.

(151) Kerchove, A. J. de; Elimelech, M. Impact of Alginate Conditioning Film on Deposition Kinetics of Motile and Nonmotile Pseudomonas Aeruginosa Strains. *Appl. Environ. Microbiol.* **2007**, *73* (16), 5227–5234.

(152) Kerchove, A. J. de; Elimelech, M. Bacterial Swimming Motility Enhances Cell Deposition and Surface Coverage. *Environ. Sci. Technol.* **2008**, *42* (12), 4371–4377.

(153) Burmølle, M.; Bahl, M. I.; Jensen, L. B.; Sørensen, S. J.; Hansen, L. H. Type 3 Fimbriae, Encoded by the Conjugative Plasmid pOLA52, Enhance Biofilm Formation and Transfer Frequencies in Enterobacteriaceae Strains. *Microbiology* **2008**, *154* (1), 187–195.

(154) Danese, P. N.; Pratt, L. A.; Kolter, R. Exopolysaccharide Production Is Required for Development of Escherichia Coli K-12 Biofilm Architecture. *J. Bacteriol.* **2000**, *182* (12), 3593–3596.

(155) McKenney, D.; Hübner, J.; Muller, E.; Wang, Y.; Goldmann, D. A.; Pier, G. B. The Ica Locus of Staphylococcus Epidermidis Encodes Production of the Capsular Polysaccharide/Adhesin. *Infect. Immun.* **1998**, *66* (10), 4711–4720.

(156) Tsuneda, S.; Aikawa, H.; Hayashi, H.; Yuasa, A.; Hirata, A. Extracellular Polymeric Substances Responsible for Bacterial Adhesion onto Solid Surface. *FEMS Microbiol. Lett.* **2003**, *223* (2), 287–292.

(157) Lindberg, L. E.; Holmbom, B. R.; Väisänen, O. M.; Weber, A. M.; Salkinoja-Salonen, M. S. Sugar Composition of Biofilms Produced by Paper Mill Bacteria. *Appl. Microbiol. Biotechnol.* **2001**, *55* (5), 638–643.

(158) Martinez, L. R.; Casadevall, A. Cryptococcus Neoformans Biofilm Formation Depends on Surface Support and Carbon Source and Reduces Fungal Cell Susceptibility to Heat, Cold, and UV Light. *Appl. Environ. Microbiol.* **2007**, *73* (14), 4592–4601.

(159) Ulett, G. C.; Mabbett, A. N.; Fung, K. C.; Webb, R. I.; Schembri, M. A. The Role of F9 Fimbriae of Uropathogenic Escherichia Coli in Biofilm Formation. *Microbiology* **2007**, *153* (7), 2321–2331.

(160) Schembri, M. A.; Dalsgaard, D.; Klemm, P. Capsule Shields the Function of Short Bacterial Adhesins. *J. Bacteriol.* **2004**, *186* (5), 1249–1257.

(161) Sherlock, O.; Schembri, M. A.; Reisner, A.; Klemm, P. Novel Roles for the AIDA Adhesin from Diarrheagenic Escherichia Coli: Cell Aggregation and Biofilm Formation. *J. Bacteriol.* **2004**, *186* (23), 8058–8065.

(162) Sherlock, O.; Vejborg, R. M.; Klemm, P. The TibA Adhesin/Invasin from Enterotoxigenic Escherichia Coli Is Self Recognizing and Induces Bacterial Aggregation and Biofilm Formation. *Infect. Immun.* **2005**, *73* (4), 1954–1963.

(163) Ulett, G. C.; Webb, R. I.; Schembri, M. A. Antigen-43-Mediated Autoaggregation Impairs Motility in Escherichia Coli. *Microbiology* **2006**, *152* (7), 2101–2110.

(164) Pesavento, C.; Becker, G.; Sommerfeldt, N.; Possling, A.; Tschowri, N.; Mehlis, A.; Hengge, R. Inverse Regulatory Coordination of Motility and Curli-Mediated Adhesion in Escherichia Coli. *Genes Dev.* **2008**, *22* (17), 2434–2446.

(165) Ogasawara, H.; Yamamoto, K.; Ishihama, A. Role of the Biofilm Master Regulator CsgD in Cross-Regulation between Biofilm Formation and Flagellar Synthesis. *J. Bacteriol.* **2011**, *193* (10), 2587–2597.

(166) Tambyah, P. A.; Maki, D. G. Catheter-Associated Urinary Tract Infection Is Rarely Symptomatic: A Prospective Study of 1,497 Catheterized Patients. *Arch. Intern. Med.* **2000**, *160* (5), 678–682.

(167) Warren, J. W. Catheter-Associated Urinary Tract Infections. *Int. J. Antimicrob. Agents* **2001**, *17* (4), 299–303.

(168) Frank, D. N.; Wilson, S. S.; St. Amand, A. L.; Pace, N. R. Culture-Independent Microbiological Analysis of Foley Urinary Catheter Biofilms. *PLoS ONE* **2009**, *4* (11), e7811.

(169) Barford, J. M. T.; Anson, K.; Hu, Y.; Coates, A. R. M. A Model of Catheter-Associated Urinary Tract Infection Initiated by Bacterial Contamination of the Catheter Tip. *BJU Int.* **2008**, *102* (1), 67–74.

(170) Macleod, S. M.; Stickler, D. J. Species Interactions in Mixed-Community Crystalline Biofilms on Urinary Catheters. *J. Med. Microbiol.* **2007**, *56* (11), 1549–1557.

(171) Nicolle, D. L. E. Catheter-Related Urinary Tract Infection. *Drugs Aging* **2005**, *22* (8), 627–639.

(172) Ferrières, L.; Hancock, V.; Klemm, P. Specific Selection for Virulent Urinary Tract Infectious Escherichia Coli Strains during Catheter-Associated Biofilm Formation. *FEMS Immunol. Med. Microbiol.* **2007**, *51* (1), 212–219.

(173) Roos, V.; Klemm, P. Global Gene Expression Profiling of the Asymptomatic Bacteriuria Escherichia Coli Strain 83972 in the Human Urinary Tract. *Infect. Immun.* **2006**, *74* (6), 3565–3575.

(174) Roos, V.; Nielsen, E. M.; Klemm, P. Asymptomatic Bacteriuria Escherichia Coli Strains: Adhesins, Growth and Competition. *FEMS Microbiol. Lett.* **2006**, *262* (1), 22–30.

(175) Roos, V.; Ulett, G. C.; Schembri, M. A.; Klemm, P. The Asymptomatic Bacteriuria Escherichia Coli Strain 83972 Outcompetes Uropathogenic E. Coli Strains in Human Urine. *Infect. Immun.* **2006**, *74* (1), 615–624.

(176) Cho, Y.-H.; Lee, S.-J.; Lee, J. y.; Kim, S. w.; Kwon, I. c.; Chung, S. y.; Yoon, M. s. Prophylactic Efficacy of a New Gentamicin-Releasing Urethral Catheter in Short-Term Catheterized Rabbits. *BJU Int.* **2001**, *87* (1), 104–109.

(177) O'Grady, N. P.; Alexander, M.; Dellinger, E. P.; Gerberding, J. L.; Heard, S. O.; Maki, D. G.; Masur, H.; McCormick, R. D.; Mermel, L. A.; Pearson, M. L.; Raad, I. I.; Randolph, A.; Weinstein, R. A. Guidelines for the Prevention of Intravascular Catheter–Related Infections. *Clin. Infect. Dis.* **2002**, *35* (11), 1281–1307.

(178) Gaonkar, T. A., PhD; Sampath, L. A., BA; Modak, S. M., PhD. Evaluation of the Antimicrobial Efficacy of Urinary Catheters Impregnated with Antiseptics in an In Vitro Urinary Tract Model •. *Infect. Control Hosp. Epidemiol.* **2003**, *24* (7), 506–513.

(179) Crnich, C. J.; Maki, D. G. Are Antimicrobial-Impregnated Catheters Effective? Don't Throw Out the Baby with the Bathwater. *Clin. Infect. Dis.* **2004**, *38* (9), 1287–1292.

(180) Johnson, J. R.; Kuskowski, M. A.; Wilt, T. J. Systematic Review: Antimicrobial Urinary Catheters to Prevent Catheter-Associated Urinary Tract Infection in Hospitalized Patients. *Ann. Intern. Med.* **2006**, *144* (2), 116–126.

(181) Berra, L.; Kolobow, T.; Laquerriere, P.; Pitts, B.; Bramati, S.; Pohlmann, J.; Marelli, C.; Panzeri, M.; Brambillasca, P.; Villa, F.; Baccarelli, A.; Bouthors, S.; Stelfox, H. T.; Bigatello, L. M.; Moss, J.; Pesenti, A. Internally Coated Endotracheal Tubes with Silver Sulfadiazine in Polyurethane to Prevent Bacterial Colonization: A Clinical Trial. *Intensive Care Med.* **2008**, *34* (6), 1030–1037.

(182) Kittinger, C.; Marth, E.; Windhager, R.; Weinberg, A. M.; Zarfel, G.; Baumert, R.; Felisch, S.; Kuehn, K.-D. Antimicrobial Activity of Gentamicin Palmitate against High Concentrations of Staphylococcus Aureus. *J. Mater. Sci. Mater. Med.* **2011**, *22* (6), 1447–1453.

(183) Siddiq, D. M.; Darouiche, R. O. New Strategies to Prevent Catheter-Associated Urinary Tract Infections. *Nat. Rev. Urol.* **2012**, *9* (6), 305–314.

(184) Langermann, S.; Palaszynski, S.; Barnhart, M.; Auguste, G.; Pinkner, J. S.; Burlein, J.; Barren, P.; Koenig, S.; Leath, S.; Jones, C. H.; Hultgren, S. J. Prevention of Mucosal Escherichia Coli Infection by FimH-Adhesin-Based Systemic Vaccination. *Science* **1997**, *276* (5312), 607–611.

(185) Han, Z.; Pinkner, J. S.; Ford, B.; Chorell, E.; Crowley, J. M.; Cusumano, C. K.; Campbell, S.; Henderson, J. P.; Hultgren, S. J.; Janetka, J. W. Lead Optimization Studies on FimH Antagonists: Discovery of Potent and Orally Bioavailable Ortho-Substituted Biphenyl Mannosides. *J. Med. Chem.* **2012**, *55* (8), 3945–3959.

(186) Cusumano, C. K.; Pinkner, J. S.; Han, Z.; Greene, S. E.; Ford, B. A.; Crowley, J. R.; Henderson, J. P.; Janetka, J. W.; Hultgren, S. J. Treatment and Prevention of Urinary Tract Infection with Orally Active FimH Inhibitors. *Sci. Transl. Med.* **2011**, *3* (109), 109ra115–109ra115.

(187) Totsika, M.; Kostakioti, M.; Hannan, T. J.; Upton, M.; Beatson, S. A.; Janetka, J. W.; Hultgren, S. J.; Schembri, M. A. A FimH Inhibitor Prevents Acute Bladder Infection and Treats Chronic Cystitis Caused by Multidrug-Resistant Uropathogenic Escherichia Coli ST131. *J. Infect. Dis.* **2013**, *208* (6), 921–928.

(188) Jiang, X.; Abgottspon, D.; Kleeb, S.; Rabbani, S.; Scharenberg, M.; Wittwer, M.; Haug, M.; Schwardt, O.; Ernst, B. Antiadhesion Therapy for Urinary Tract

Infections--a Balanced PK/PD Profile Proved to Be Key for Success. *J. Med. Chem.* **2012**, *55* (10), 4700–4713.

(189) Klein, T.; Abgottspon, D.; Wittwer, M.; Rabbani, S.; Herold, J.; Jiang, X.; Kleeb, S.; Lüthi, C.; Scharenberg, M.; Bezençon, J.; Gubler, E.; Pang, L.; Smiesko, M.; Cutting, B.; Schwardt, O.; Ernst, B. FimH Antagonists for the Oral Treatment of Urinary Tract Infections: From Design and Synthesis to in Vitro and in Vivo Evaluation. *J. Med. Chem.* **2010**, *53* (24), 8627–8641.

(190) Kleeb, S.; Pang, L.; Mayer, K.; Eris, D.; Sigl, A.; Preston, R. C.; Zihlmann, P.; Sharpe, T.; Jakob, R. P.; Abgottspon, D.; Hutter, A. S.; Scharenberg, M.; Jiang, X.; Navarra, G.; Rabbani, S.; Smiesko, M.; Lüdin, N.; Bezençon, J.; Schwardt, O.; Maier, T.; Ernst, B. FimH Antagonists: Bioisosteres To Improve the in Vitro and in Vivo PK/PD Profile. *J. Med. Chem.* **2015**, *58* (5), 2221–2239.

(191) Grabosch, C.; Hartmann, M.; Schmidt-Lassen, J.; Lindhorst, T. K. Squaric Acid Monoamide Mannosides as Ligands for the Bacterial Lectin FimH: Covalent Inhibition or Not? *ChemBioChem* **2011**, *12* (7), 1066–1074.

(192) Chandrasekaran, V.; Kolbe, K.; Beiroth, F.; Lindhorst, T. K. Synthesis and Testing of the First Azobenzene Mannobioside as Photoswitchable Ligand for the Bacterial Lectin FimH. *Beilstein J. Org. Chem.* **2013**, *9*, 223–233.

(193) Bouckaert, J.; Li, Z.; Xavier, C.; Almant, M.; Caveliers, V.; Lahoutte, T.; Weeks, S. D.; Kovensky, J.; Gouin, S. G. Heptyl α-D-Mannosides Grafted on a β-Cyclodextrin Core To Interfere with Escherichia Coli Adhesion: An In Vivo Multivalent Effect. *Chem. – Eur. J.* **2013**, *19* (24), 7847–7855.

(194) Papadopoulos, A.; Shiao, T. C.; Roy, R. Diazo Transfer and Click Chemistry in the Solid Phase Syntheses of Lysine-Based Glycodendrimers as Antagonists against Escherichia Coli FimH. *Mol. Pharm.* **2012**, *9* (3), 394–403.

(195) Sokurenko, E. V.; Courtney, H. S.; Maslow, J.; Siitonen, A.; Hasty, D. L. Quantitative Differences in Adhesiveness of Type 1 Fimbriated Escherichia Coli due to Structural Differences in fimH Genes. *J. Bacteriol.* **1995**, *177* (13), 3680–3686.

(196) Stahlhut, S. G.; Tchesnokova, V.; Struve, C.; Weissman, S. J.; Chattopadhyay, S.; Yakovenko, O.; Aprikian, P.; Sokurenko, E. V.; Krogfelt, K. A. Comparative Structure-Function Analysis of Mannose-Specific FimH

Adhesins from Klebsiella Pneumoniae and Escherichia Coli. *J. Bacteriol.* **2009**, *191* (21), 6592–6601.

(197) Sokurenko, E. V.; Chesnokova, V.; Doyle, R. J.; Hasty, D. L. Diversity of the Escherichia Coli Type 1 Fimbrial Lectin: Differentioal Binding to Mannosides and Uroeptihelial Cells. *J. Biol. Chem.* **1997**, *272* (28), 17880–17886.

(198) Aprikian, P.; Tchesnokova, V.; Kidd, B.; Yakovenko, O.; Yarov-Yarovoy, V.; Trinchina, E.; Vogel, V.; Thomas, W.; Sokurenko, E. Interdomain Interaction in the FimH Adhesin of Escherichia Coli Regulates the Affinity to Mannose. *J. Biol. Chem.* **2007**, *282* (32), 23437–23446.

(199) Rodriguez, V. B.; Kidd, B. A.; Interlandi, G.; Tchesnokova, V.; Sokurenko, E. V.; Thomas, W. E. Allosteric Coupling in the Bacterial Adhesive Protein FimH. *J. Biol. Chem.* **2013**, *288* (33), 24128–24139.

(200) Choudhury, D.; Thompson, A.; Stojanoff, V.; Langermann, S.; Pinkner, J.; Hultgren, S. J.; Knight, S. D. X-Ray Structure of the FimC-FimH Chaperone-Adhesin Complex from Uropathogenic Escherichia Coli. *Science* **1999**, *285* (5430), 1061–1066.

(201) Le Trong, I.; Aprikian, P.; Kidd, B. A.; Forero-Shelton, M.; Tchesnokova, V.; Rajagopal, P.; Rodriguez, V.; Interlandi, G.; Klevit, R.; Vogel, V.; Stenkamp, R. E.; Sokurenko, E. V.; Thomas, W. E. Structural Basis for Mechanical Force Regulation of the Adhesin FimH via Finger Trap-like β Sheet Twisting. *Cell* **2010**, *141* (4), 645–655.

(202) Dembo, M.; Torney, D. C.; Saxman, K.; Hammer, D. The Reaction-Limited Kinetics of Membrane-to-Surface Adhesion and Detachment. *Proc. R. Soc. Lond. B Biol. Sci.* **1988**, *234* (1274), 55–83.

(203) Isberg, R. R.; Barnes, P. Dancing with the Host: Flow-Dependent Bacterial Adhesion. *Cell* **2002**, *110* (1), 1–4.

(204) Aprikian, P.; Interlandi, G.; Kidd, B. A.; Le Trong, I.; Tchesnokova, V.; Yakovenko, O.; Whitfield, M. J.; Bullitt, E.; Stenkamp, R. E.; Thomas, W. E.; Sokurenko, E. V. The Bacterial Fimbrial Tip Acts as a Mechanical Force Sensor. *PLoS Biol* **2011**, *9* (5), e1000617.

(205) Schwartz, D. J.; Kalas, V.; Pinkner, J. S.; Chen, S. L.; Spaulding, C. N.; Dodson, K. W.; Hultgren, S. J. Positively Selected FimH Residues Enhance Virulence during Urinary Tract Infection by Altering FimH Conformation. *Proc. Natl. Acad. Sci.* **2013**, *110* (39), 15530–15537.

(206) Ernst, B.; Magnani, J. L. From Carbohydrate Leads to Glycomimetic Drugs. *Nat. Rev. Drug Discov.* **2009**, *8* (8), 661–677.

(207) Scharenberg, M.; Abgottspon, D.; Cicek, E.; Jiang, X.; Schwardt, O.; Rabbani, S.; Ernst, B. A Flow Cytometry-Based Assay for Screening FimH Antagonists. *ASSAY Drug Dev. Technol.* **2011**, *9* (5), 455–464.

(208) Szabados, F.; Kleine, B.; Anders, A.; Kaase, M.; Sakınç, T.; Schmitz, I.; Gatermann, S. Staphylococcus Saprophyticus ATCC 15305 Is Internalized into Human Urinary Bladder Carcinoma Cell Line 5637. *FEMS Microbiol. Lett.* **2008**, *285* (2), 163–169.

(209) Smith, Y. C.; Grande, K. K.; Rasmussen, S. B.; O'Brien, A. D. Novel Three-Dimensional Organoid Model for Evaluation of the Interaction of Uropathogenic Escherichia Coli with Terminally Differentiated Human Urothelial Cells. *Infect. Immun.* **2006**, *74* (1), 750–757.

(210) Schilling, J. D.; Mulvey, M. A.; Vincent, C. D.; Lorenz, R. G.; Hultgren, S. J. Bacterial Invasion Augments Epithelial Cytokine Responses to Escherichia Coli Through a Lipopolysaccharide-Dependent Mechanism. *J. Immunol.* **2001**, *166* (2), 1148–1155.

(211) Hvidberg, H.; Struve, C.; Krogfelt, K. A.; Christensen, N.; Rasmussen, S. N.; Frimodt-Møller, N. Development of a Long-Term Ascending Urinary Tract Infection Mouse Model for Antibiotic Treatment Studies. *Antimicrob. Agents Chemother.* **2000**, *44* (1), 156–163.

(212) O'Hanley, P.; Lark, D.; Falkow, S.; Schoolnik, G. Molecular Basis of Escherichia Coli Colonization of the Upper Urinary Tract in BALB/c Mice. Gal-Gal Pili Immunization Prevents Escherichia Coli Pyelonephritis in the BALB/c Mouse Model of Human Pyelonephritis. *J. Clin. Invest.* **1985**, *75* (2), 347–360.

(213) Lanne, B.; Olsson, B.-M.; Jovall, P.-; Öm, J.; Linder, H.; Marklund, B.-I.; Bergström, J.; Karlsson, K.-A. Glycoconjugate Receptors for P-Fimbriated Escherichia Coli in the Mouse AN ANIMAL MODEL OF URINARY TRACT INFECTION. *J. Biol. Chem.* **1995**, *270* (15), 9017–9025.

(214) Murawski, I. J.; Maina, R. W.; Malo, D.; Guay-Woodford, L. M.; Gros, P.; Fujiwara, M.; Morgan, K.; Gupta, I. R. The C3H/HeJ Inbred Mouse Is a Model of Vesico-Ureteric Reflux with a Susceptibility Locus on Chromosome 12. *Kidney Int.* **2010**, *78* (3), 269–278.

(215) Mobley, H. L. T.; Jarvis, K. G.; Elwood, J. P.; Whittle, D. I.; Lockatell, C. V.; Russell, R. G.; Johnson, D. E.; Donnenberg, M. S.; Warren, J. W. Isogenic P-Fimbrial Deletion Mutants of Pyelonephritogenic Escherichia Coli: The Role of α Gal(1–4)β Gal Binding in Virulence of a Wild-Type Strain. *Mol. Microbiol.* **1993**, *10* (1), 143–155.

(216) Johnson, J. R.; Brown, J. J. Defining Inoculation Conditions for the Mouse Model of Ascending Urinary Tract Infection That Avoid Immediate Vesicoureteral Reflux yet Produce Renal and Bladder Infection. *J. Infect. Dis.* **1996**, *173* (3), 746–749.

(217) Johnson, J. R. Reflux in the Mouse Model of Urinary Tract Infection. *Infect. Immun.* **1998**, *66* (12), 6063–6064.

(218) Christensen, G. D.; Simpson, W. A.; Younger, J. J.; Baddour, L. M.; Barrett, F. F.; Melton, D. M.; Beachey, E. H. Adherence of Coagulase-Negative Staphylococci to Plastic Tissue Culture Plates: A Quantitative Model for the Adherence of Staphylococci to Medical Devices. *J. Clin. Microbiol.* **1985**, *22* (6), 996–1006.

(219) O'Toole, G. A.; Pratt, L. A.; Watnick, P. I.; Newman, D. K.; Weaver, V. B.; Kolter, R. [6] Genetic Approaches to Study of Biofilms. In *Methods in Enzymology*; Doyle, R. J., Ed.; Biofilms; Academic Press, 1999; Vol. 310, pp 91–109.

(220) Li, X.; Yan, Z.; Xu, J. Quantitative Variation of Biofilms among Strains in Natural Populations of Candida Albicans. *Microbiology* **2003**, *149* (2), 353–362.

(221) Peeters, E.; Nelis, H. J.; Coenye, T. Comparison of Multiple Methods for Quantification of Microbial Biofilms Grown in Microtiter Plates. *J. Microbiol. Methods* **2008**, *72* (2), 157–165.

(222) Chavant, P.; Gaillard-Martinie, B.; Talon, R.; Hébraud, M.; Bernardi, T. A New Device for Rapid Evaluation of Biofilm Formation Potential by Bacteria. *J. Microbiol. Methods* **2007**, *68* (3), 605–612.

(223) Amidon, G. L.; Lennernäs, H.; Shah, V. P.; Crison, J. R. A Theoretical Basis for a Biopharmaceutic Drug Classification: The Correlation of in Vitro Drug Product Dissolution and in Vivo Bioavailability. *Pharm. Res.* **1995**, *12* (3), 413–420.

(224) Falcoz, C.; Jenkins, J. M.; Bye, C.; Hardman, T. C.; Kenney, K. B.; Studenberg, S.; Fuder, H.; Prince, W. T. Pharmacokinetics of GW433908, a Prodrug of Amprenavir, in Healthy Male Volunteers. *J. Clin. Pharmacol.* **2002**, *42* (8), 887–898.

(225) Stella, V. J.; Nti-Addae, K. W. Prodrug Strategies to Overcome Poor Water Solubility. *Adv. Drug Deliv. Rev.* **2007**, *59* (7), 677–694.

(226) Hung, C.-S.; Dodson, K. W.; Hultgren, S. J. A Murine Model of Urinary Tract Infection. *Nat. Protoc.* **2009**, *4* (8), 1230–1243.

(227) Cornaire, G.; Woodley, J.; Hermann, P.; Cloarec, A.; Arellano, C.; Houin, G. Impact of Excipients on the Absorption of P-Glycoprotein Substrates in Vitro and in Vivo. *Int. J. Pharm.* **2004**, *278* (1), 119–131.

(228) Yamagata, T.; Kusuhara, H.; Morishita, M.; Takayama, K.; Benameur, H.; Sugiyama, Y. Improvement of the Oral Drug Absorption of Topotecan through the Inhibition of Intestinal Xenobiotic Efflux Transporter, Breast Cancer Resistance Protein, by Excipients. *Drug Metab. Dispos.* **2007**, *35* (7), 1142–1148.

(229) Kisiela, D. I.; Rodriguez, V. B.; Tchesnokova, V.; Avagyan, H.; Aprikian, P.; Liu, Y.; Wu, X.-R.; Thomas, W. E.; Sokurenko, E. V. Conformational Inactivation Induces Immunogenicity of the Receptor-Binding Pocket of a Bacterial Adhesin. *Proc. Natl. Acad. Sci.* **2013**, *110* (47), 19089–19094.

(230) Hull, R. A.; Gill, R. E.; Hsu, P.; Minshew, B. H.; Falkow, S. Construction and Expression of Recombinant Plasmids Encoding Type 1 or D-Mannose-Resistant Pili from a Urinary Tract Infection Escherichia Coli Isolate. *Infect. Immun.* **1981**, *33* (3), 933–938.

(231) Mobley, H. L.; Green, D. M.; Trifillis, A. L.; Johnson, D. E.; Chippendale, G. R.; Lockatell, C. V.; Jones, B. D.; Warren, J. W. Pyelonephritogenic Escherichia Coli and Killing of Cultured Human Renal Proximal Tubular Epithelial Cells: Role of Hemolysin in Some Strains. *Infect. Immun.* **1990**, *58* (5), 1281–1289.

(232) Stahlhut, S. G.; Chattopadhyay, S.; Struve, C.; Weissman, S. J.; Aprikian, P.; Libby, S. J.; Fang, F. C.; Krogfelt, K. A.; Sokurenko, E. V. Population Variability of the FimH Type 1 Fimbrial Adhesin in Klebsiella Pneumoniae. *J. Bacteriol.* **2009**, *191* (6), 1941–1950.

(233) Weissman, S. J.; Chattopadhyay, S.; Aprikian, P.; Obata-Yasuoka, M.; Yarova-Yarovaya, Y.; Stapleton, A.; Ba-Thein, W.; Dykhuizen, D.; Johnson, J.

R.; Sokurenko, E. V. Clonal Analysis Reveals High Rate of Structural Mutations in Fimbrial Adhesins of Extraintestinal Pathogenic Escherichia Coli. *Mol. Microbiol.* **2006**, *59* (3), 975–988.

(234) Ofek, I.; Hasty, D. L.; Sharon, N. Anti-Adhesion Therapy of Bacterial Diseases: Prospects and Problems. *FEMS Immunol. Med. Microbiol.* **2003**, *38* (3), 181–191.

(235) Sharon, N.; Ofek, I. Safe as Mother's Milk: Carbohydrates as Future Anti-Adhesion Drugs for Bacterial Diseases. *Glycoconj. J.* **2000**, *17* (7-9), 659–664.

(236) Sharon, N. Carbohydrates as Future Anti-Adhesion Drugs for Infectious Diseases. *Biochim. Biophys. Acta BBA - Gen. Subj.* **2006**, *1760* (4), 527–537.

(237) Korea, C.-G.; Ghigo, J.-M.; Beloin, C. The Sweet Connection: Solving the Riddle of Multiple Sugar-Binding Fimbrial Adhesins in Escherichia Coli. *BioEssays* **2011**, *33* (4), 300–311.

(238) Huang, Q.; Riviere, J. E. The Application of Allometric Scaling Principles to Predict Pharmacokinetic Parameters across Species. *Expert Opin. Drug Metab. Toxicol.* **2014**, *10* (9), 1241–1253.

(239) Blanchard, O. L.; Smoliga, J. M. Translating Dosages from Animal Models to Human Clinical Trials—revisiting Body Surface Area Scaling. *FASEB J.* **2015**, *29* (5), 1629–1634.